THE STRUCTURE OF THE PROTEIN IN THE EGG CASE OF THE PRAYING MANTIS

Including a discussion of the X-ray diffraction techniques used.

With appendices on the analysis of the sequences of fibrous proteins.

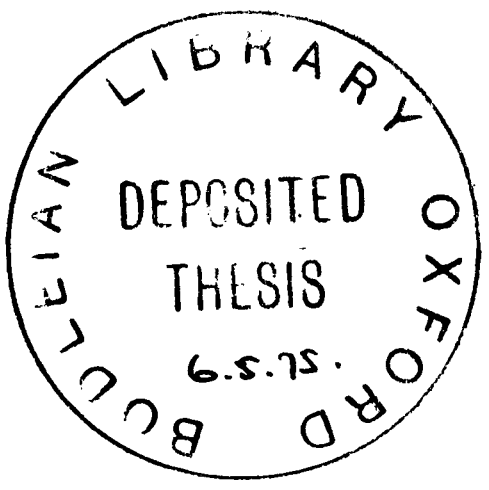

TO THE MEMORY OF MY FATHER

CONTENTS *

*Detailed contents are to be found before each Chapter and Appendix

FOREWORD

This thesis was undertaken in the Laboratory of Molecular Biophysics, Department of Zoology, University of Oxford while I was a student member of Balliol College. The contents are my own work except where it is stated otherwise.

This volume marks the culmination of the more organised phase of my education, so it is appropriate that it is dedicated to he who was the greatest source of encouragement during my school career - my father. He gave me the opportunities he was unable to have. It is fitting that the teachers of the Forest Grammar School, Berkshire, and the Department of Physics, University of Manchester, should be thanked for nurturing the seed of scientific interest. It was my enjoyment of biology lessons at school which led me to venture into biophysics, and my enjoyment of physics at Manchester which steered me towards research.

ACKNOWLEDGEMENTS

This thesis has been made possible by the cooperation of many people. I take this opportunity to thank them for all they have done.

The University, Balliol College, the Radcliffe Science Library and the Department of Zoology have been very cooperative during my stay in Oxford. Special thanks are due to Professor D.C. Phillips, who allowed me to work in his laboratory, the Laboratory of Molecular Biophysics, and to use the facilities therein. Members of the Laboratory of Molecular Biophysics and the Agricultural Research Council Unit were helpful at all times and gave me advice, encouragement and facilities.

Dr. A. Miller, my supervisor, provided advice, encouragement and training in experimental techniques. He painstakingly read through each draft of this thesis, making helpful suggestions. There are many references, most of them anonymous, to contributions made by others. These people are Dr. B.Brodsky-Doyle, Dr. P. Eagles, Dr. R.D.B.Fraser, Dr. D.W.L.Hukins, Mr.D.J.S.Hulmes, Mr. R.Kerr, Mrs. B.M.Luke, Dr. A.Miller,Dr. D.A.D.Parry, Dr.R.N.Pau, Mr. L.J.Stump and Dr. J.Woodhead-Galloway. Dr. P.C.J.Brunet and Dr. A.C.Neville informally discussed their work on related problems.

Advice, facilities and training in experimental techniques were given by Dr. A. Miller for X-ray diffraction, by Dr.L.N. Johnson and Mr. L.J.Stump for electron microscopy, and by Dr. P.A.M.Eagles and Dr. R.N.Pau for chemistry. Dr. P.C.J.Brunet, Mr. R.Kerr, Dr. R.Offord and Dr. C.D.Rodgers also helped with advice and facilities. Much of the apparatus used was built

by Mr. M. Pickford and Mr. J. Simms. Together with Dr. B. Brodsky-Doyle, Mr. T.McCabe, Mr. J.Marsh, Mr. M.Ritchert and Dr. C.D.Rodgers, they helped with technical advice and assistance, and manual labour.

Of invaluable assistance were Dr.W.Kenchington and his department, the Astbury Department of Biophysics, the University of Leeds, who sent me insects and egg cases on several occasions.

Mr.T.Allan prepared many photographs and Ms. V. Saunders typed the thesis.

The Medical Research Council supported me with a Research Studentship.

Thanks are given to the above mentioned people and many others who have contributed to my life, academic and otherwise, while at Oxford.

ABSTRACT

The thesis is mainly concerned with the structure of the protein in the egg case of the praying mantis. It continues the work of Rudall (1956), who showed that the protein was organised into lamellae and had an α-helical structure. He put forward two models: hexagonally packed α-helices, and two-stranded coiled coils arranged in layers. In the latter model, each coil is staggered from its neighbours by a quarter of the pitch, so as to allow optimum packing.

Sections on the X-ray diffraction camera, analysis of errors in reciprocal lattice coordinates, analysis of sequences of fibrous proteins, and unsuccessful structural studies on sequential polyheptapeptides are also included.

Lamellae may be removed from fresh egg cases, and ribbons from egg cases a few or more hours after production. Electron microscopy of negatively stained lamellae, positively stained lamellae and sectioned ribbons, and X-ray diffraction studies on the ribbons make it possible to postulate a model for the structure. The model is more detailed than Rudall's and has differences. It has layers of two-stranded α-helical coiled coils about 18Å thick packed in register to form 460Å thick lamellae about 1/um. x 10/um. The layers are perpendicular to those in Rudall's model. The lamellae pack into ribbons with considerable disorientation. Coiled coils within an 18Å thick layer probably pack in a way similar to that in the layers of Rudall's model with a stagger of 2.5 x the pitch and a rotation of 90° between adjacent coiled coils. Each coiled coil has chains about 730 Å long staggered by about 55 Å.

Coiled coils interact end to end with an overlap of about 40 Å, so as to leave gaps of about 15Å. The molecular length of 730 Å is consistent with the molecular weight of 53,000 estimated from SDS gel electrophoresis. The molecular axis is parallel to the principal shear plane in the lamella. Fibres of this protein drawn from the first order gland give an X-ray diffraction pattern indicating a very similar structure.

In the presence of water, uranyl acetate solution, neutralised phosphotungstic acid or a mixture of chlorobenzene and bromobenzene, the volume of the unit cell changes. X-ray diffraction evidence indicates that sliding occurs between coiled coils as the volume changes. The amount of lateral swelling is greater in the direction perpendicular to the surface of the lamella than in the direction parallel to it. Together with the different extents of the lattice in these directions, this is consistent with the model, which is different in these two directions.

A discussion is included on the literature relating to X-ray diffraction cameras using a Frank s mirror and a quartz crystal monochromator. To this has been added calculations concerning focal size, resolution and intensity of the X-ray beam. The results of these are embodied in a discussion of camera design. An appendix is devoted to a method of estimating standard errors of reciprocal lattice coordinates.

The analysis of the sequences of fibrous proteins and the statistical basis of this analysis are discussed in appendices. Preliminary calculations on tropomyosin have revealed periodicities which can be related to a 14 residue stagger between chains, in

agreement with Hodges et al (1973), and to the repeat of the actin helix. Hydrophobic residues and possibly positively charged residues are arranged in a pattern which, on the present limited data, appears to be important in interactions with actin. Residues generally considered to disrupt helical structures are arranged in a band coiling around the α-helix. A technique enabling the D stagger in collagen to be identified is described. This also gives information which suggests how hydrophobic interactions are important in defining the pitch of the collagen molecules and the interactions between them. Arguments based on this technique show how pairs of opposite charges lead to interactions consistent with a five-stranded microfibril.

There is also an appendix on attempts to produce oriented arrays of sequential polyheptapeptides, in order to obtain X-ray diffraction patterns. Another appendix describes how the colony of praying mantids was raised.

CHAPTER I

BACKGROUND TO THE PROBLEM

Chapter 1

Background to the problem

This chapter is not a complete review of fibrous proteins, but a brief guide to enable the reader to appreciate the thesis fully. Reference to the work by Fraser and MacRae (1973a) will not only give a more comprehensive account, but it will provide the most important references to other works. Seifter and Gallop (1966) and Cohen (1966) have also given interesting accounts. For other proteins, see the work by Dickerson and Geis (1969) and for other biopolymers, see the works of Yudkin and Offord (1971, 1973).

1.1 Biopolymers

There are three major classes of biological macromolecules: polynucleotides, polysaccharides and proteins. They are formed by condensation (that is by removal of water) from nucleotides, sugars and amino acids respectively. Polynucleotides are mainly concerned with the transfer of information and the control of protein synthesis. Food storage and the construction of structural tissue is a function of both proteins and polysaccharides, but only proteins are able to carry out sophisticated roles, such as those required of enzymes. Aggregates of lipids, the other major class of structural molecules, are the basis of several organelles, including most membranes.

1.1.1 Polysaccharides

Polysaccharides play an important role in food storage. In this role, they often exist in a branched form and possibly

do not have unique sequences of sugars, unlike polynucleotides and proteins, which have not been found in branched conformations. They are also used to construct complex structures. Their sequences, if regular, are generally rather simple, so they cannot be used as the sole component of sophisticated systems. They are the major component of some structural tissues, such as cellulose and chitin.

1.1.2 Proteins

Complex biological systems depend on protein for their structure and function. This is possible because there is a range of twenty naturally occurring amino acids which can be incorporated into a unique sequence. A protein of 150 residues can therefore have $20^{150} \simeq 10^{195}$ possible sequences, so it is generally possible to find one or more sequences among these that fulfil the required role extremely well. This property enables structural tissue, unlike polysaccharides, to be purpose built to fairly rigid specifications. It is also possible to construct molecules with very sophisticated modes of action, as is evident in the case of enzymes. Organelles, such as membranes, which are largely constructed of non-protein material, contain proteins to carry out the more sophisticated functions.

1.2 Structure and function of proteins

Most proteins can be classified as fibrous or globular, those with axial ratios (that is the ratio of the largest to the smallest overall dimension) less than five being

classified as globular and the rest as fibrous. Fibrous proteins make up the bulk of structural protein, whereas globular proteins are normally used in proteins with a specific non-structural role, such as enzymes.

It is interesting to consider muscle (see the review by Huxley, 1971), where the thick filaments are composed mainly of fibrous protein. In vertebrate muscle, the protein is myosin, which has a long rod-like portion in the filament and a globular head projecting from it. Possibly, the rod portion fulfils a structural role and the globular portion has an enzymic role, acting as a co-enzyme with actin in the hydrolysis of ATP. It may be thought that the long fibres of actin molecules perform a structural role even though actin is a globular protein close to 50 Å across in all directions. The presence of tropomyosin coiling around the actin filament makes it likely that this fibrous protein supplies the major tension bearing structure, whereas the actin has the enzymic role.

1.3.1. The collagens

Collagen is a very abundant protein, being the major protein component of most tension and pressure bearing tissues in vertebrates, as well as being present in many invertebrates. In humans, where collagen is the protein component of tendon and bone and is present as a large fraction of skin, the protein makes up to 20% of the dry weight of the body. The collagen molecule consists of three proline rich chains with glycine at every third position. It has also been suggested

that these triple helices aggregate into five-stranded ropes and such a rope has been referred to as a microfibril (Smith, 1968). X-ray evidence supports this (Miller and Wray, 1971) and suggests that these microfibrils would be arranged on a tetragonal lattice of side 38 Å (Miller and Parry, 1973). There are many varieties of collagen: a number of insects produce collagen-like silks, for example the gooseberry sawfly (Rudall, 1968).

1.3.2 β-sheet structures

The β-structures fall into two classes - the parallel-β and the cross-β structures. The parallel-β structures are constructed with polypeptide chains in parallel or antiparallel arrangement. Each chain is a 2₁ helix and is therefore approximately planar. These chains hydrogen bond into sheets, which pack so as to facilitate good side-chain packing. Random, parallel and antiparallel systems are believed to exist. Such structures are found in several synthetic polypeptides, such as β-poly-L-alanine and polyglycine I, as well as some naturally occurring materials, such as *Bombyx mori* and tussah silk. α-helical structures can often be converted to the β form by stretching under appropriate conditions. β structures are often coiled; feather keratin (Fraser et al., 1971) is an example of this.

Cross-β structures are exemplified in silk from the egg stalks of the green lacewing fly, *Chrysopa flava*. The X-ray pattern is very similar to that given by parallel-β structures, except that it is rotated through a right angle with respect

to the fibre axis. The polypeptide chain bends back on itself every five to nine residues (nine in *Chrysopa* silk) forming a ribbon. The ribbons hydrogen bond at the edges to form sheets which pack together.

1.3.3. α-helical structures

These structures, along with the collagen structures, were recognised by Astbury (Astbury, 1947; Astbury et al, 1948) as giving distinctive high-angle X-ray diffraction patterns. The α-helical class became known as the k-m-e-f class, since it contains keratin, myosin, epidermin and fibrinogen. The class can also be recognised by a high optical rotation at a wavelength of 220 nm., and by characteristic infra-red absorption bands.

These structures form a major part of biological organisms. Keratin is the protein of hair, horn and nail and forms a major part of mammalian skin (Fraser et al, 1972). The known structural proteins of muscle, paramyosin, the major part of the myosin molecule and tropomyosin are α-helical. Fibrinogen has only 30% helix and is thought to be globular units connected by helical filaments (Slayter, 1969). Paramyosin (Lowey, Kucera and Holtzer, 1963), tropomyosin (Tsao, Bailey and Adair, 1951) and the light meromyosin fragment of myosin (Holtzer, Lowey and Schuster, 1962) are rod-shaped molecules with an α-helix content in excess of 90%. α-helical proteins are widespread, examples being some insect silks (section 1.6) and whelk egg capsules (Flower, Geddes and Rudall, 1969).

X-ray and chemical evidence suggests that many α-helical proteins exist as two-stranded coiled-coils, which pack into

a lattice or rope structures. The close relationship between α and β-structures is shown by the ability of one to change to the other under appropriate conditions. The ease of the conversion in α-keratin suggests that the energy difference is small. It would be interesting to compare the sequence of the coiled β-structure, feather keratin, with that of an α-helical keratin fulfilling a similar function. This could provide information on how the sequence defines the structure.

1.3.4 Other fibrous proteins

There are many other fibrous proteins, but in general, their conformation has not been well characterised. References to many of them are given by Fraser and MacRae (1973a) and Seifter and Gallop (1966). Some are clearly aggregates of globular subunits, such as F-actin and TMV virus; for some, for example elastin and resilin, the best description is not clear and for others there is no generally accepted molecular model. Further discussion is beyond the scope of this thesis.

1.4 Theory of X-ray diffraction

Before more detailed analysis is given, it is important to give an account of X-ray diffraction which is sufficient to allow non-diffractionists to appreciate the problem. For a complete understanding, reference must be made to texts. There are good introductory texts on X-ray diffraction (Woolfson, 1970; Holmes and Blow, 1965) and accounts extending the theory to fibrous systems (Fraser and MacRae, 1973a; Dickerson, 1964; Wilson, 1966). More advanced ideas on diffraction are presented by Guinier (1963) and on diffraction from chain molecules by Vainshtein (1966).

1.4.1. General Theory

X-rays are scattered by lattices with regularly spaced points or atoms according to Bragg's Law (see Fig. 1.1). Constructive interference occurs when the path difference is an integral number of wavelengths and then

$$n\lambda = 2d\sin\theta \qquad (1.1)$$

The physical meaning of this is doubtful, but it is useful in practice. A three dimensional structure will scatter X-rays from a particular periodicity only when the incident ray is at particular angles of incidence on the lattice, so the specimen must be oriented for this. With the slightly disoriented specimens used in fibre work, it is normally possible to see many orders at the same time, each corresponding to an integral value of n. The 670 Å axial repeat in collagen is an example of this.

Reference is often made to a reciprocal lattice. This derives from the relationship

$$\underline{s} = h\,\underline{a}^* + k\,\underline{b}^* + l\,\underline{c}^*, \qquad (1.2)$$

which is mathematically equivalent to Bragg's Law. $\underline{s}$ is the scattering vector, $\underline{a}^*$, $\underline{b}^*$ and $\underline{c}^*$ define the reciprocal lattice and h, k and l are integers. If the specimen is oriented correctly, the reflection corresponding to particular values of these integers should occur. The angle is correct when the defined reciprocal lattice point falls on the Ewald sphere. (see standard texts).

Each repeating unit scatters X-rays in directions generally described by a continuous function. The form of

this function, which is closely related to the structure, determines the intensities of the reflections defined by the reciprocal lattice. Strong periodicities within each unit show themselves as intensity variations which are in accordance with Bragg's Law. The breadth of a reflection or modulation of intensity indicates the perfection and range of order in the structure producing it in a way analagous to scattering from a diffraction grating. The width of the reflection is close to the range of order as measured in reciprocal space, and it is therefore reciprocally related to that range.

Standard texts on optics show that a diffraction pattern is described by the Fourier transform of the diffractor. X-rays are scattered by electrons, so we find that (see, for example Woolfson, 1970).

$$F_{hkl} = V\int_{x=0}^{1}\int_{y=0}^{1}\int_{z=0}^{1} (xyz)\ \exp 2\pi i(hx+ky+lz)\,dx\,dy\,dz \quad (1.3)$$

where F_{hkl} is the scattered amplitude, V is the volume of the unit cell, x, y, z are the fractional coordinates of the sides of the unit cell, ρ is the electron density, and h,k,l are integer

1.4.2 Diffraction from helices

Cochran et al (1952) gave the theory of diffraction by helical structures and this was amplified by Klug et al (1958).

A continuous line helix gives a cross on a diffraction pattern when the incident beam is at right angles to the helix axis. The cross is centred where the unscattered beam strikes the film and the angle between the arms is determined by the radius and pitch of the helix. The lines of the cross

are close to being at right angles to the helix locus when the beam is incident at 90° to this line, owing to adjacent turns of the helix producing quasi-parallel lines acting as a grating. A helix of pitch P repeats at intervals of P, so intensity only occurs on lines (layer lines) at axial intervals of 1/P in reciprocal space. If scattering units, for example amino acid residues, occur at axial intervals of p along the axis, this is equivalent to a series of planes sampling the helix. By the convolution theorem (see texts on diffraction), the pattern from the helix is placed at each point where the planes scatter, so the helix pattern repeats at axial intervals of 1/p in reciprocal space. The true repeat of the structure may be infinite, but it can always be closely approximated to a finite one, as in α-keratin (Fraser and MacRae 1973 b).

Helices packed into a lattice give a diffraction pattern sampled by the points of the reciprocal lattice. Regular and irregular distortions (Vainshtein, 1966) and non-helical material cause complications. The small crystallites are usually disoriented with respect to each other and often randomly oriented about the helix axis. This superimposes several patterns, producing arcs, and brings extra reciprocal lattice points on to the Ewald sphere. Random staggers between helices sometimes occur, changing the pattern (Vainshtein, 1966).

1.5 α-helical proteins.

α-helical proteins have been discussed (Fraser and MacRae, 1973a; Fasman G.D., 1967).

1.5.1 The α-helix.

Pauling and Corey (1951) interpreted X-ray diffraction data obtained from poly-γ-methyl glutamate and poly-γ-benzyl-L-

glutamate (Bamford, Hanby and Happey, 1951) in terms of a hydrogen bonded helical structure with 3.6 residues per turn and an axial residue repeat of about 1.5 Å.. that is 18 residues and five turns in 27Å . This is the α-helix. Huggins (1952) showed that a right handed α-helix was more stable than a left handed one for L-amino acids, as borne out by a right handed α-helix in myoglobin (Kendrew et al 1960). Sugeta and Miyazawa (1967) computed atomic coordinates, and Parry and Suzuki (1969) calculated the coordinates of a standard helix of residue repeat 1.5 Å and residue rotation 100 degrees.

Studies on poly-L-alanine (Elliott, 1967; Brown and Trotter, 1956; Elliott and Malcolm, 1958; Arnott and Wonacott, 1966a,b; Arnott and Dover, 1967; Arnott, 1968) reveal a right handed α-helical structure with molecules randomly distributed between the parallel and anti-parallel orientations. It gives the X-ray diffraction reflections expected from an α-helix, notably the 1.5Å meridional reflection and the near meridional reflections on the 5.4Å layer line.

α-helical structures in synthetic polypeptides and globular proteins are tabulated (Fraser and MacRae, 1973a). The pitch and residue translation in the globular proteins listed is fairly constant. In fibrous polypeptides, the variation is greater and the mean distances are significantly shorter, indicating that coiling, twisting and tilting could be general phenomena, even in polypeptides considered to pack parallel. This is supported by the smaller differences in the unit twist than in the pitch.

1.5.2 Coiled-coil structures

The α-helix does not predict the X-ray diffraction patterns of proteins in the k-m-e-f class, where there are

strong meridional reflections at about 1.485 Å and about 5.15 Å. Many k-m-e-f proteins give similar diffraction patterns (Fraser et al, 1965).

Pauling and Corey (1953) and Crick (1952) independently proposed that α-keratin is based on a coiled-coil, since this predicted these two meridional reflections more closely. Crick (1953b) described the way two parallel helices would be able to fit together by interlocking the side chains so the mean centre to centre distance between groups is about 5Å. They can then coil around each other. The energy required to so coil an α-helix is probably very small (Crick, 1952; Parry and Suzuki, 1969).

Crick (1953b) gave the following likely values for a two strand rope, although they are likely to vary.

Turns of the major helix	$N_o=1$
Turns of the minor helix	$N_1=36$
Atoms in the set	$M=\frac{1}{2}x36x7=26$
Repeat distance	$C=126x1.5\cos 10^{\circ}$ Å$=186$Å
Radius of the major helix	$R_o=5.2$Å, say.

The proportion of non-polar (hydrophobic) groups in tropomyosin is lower than for globular proteins (Bailey, 1948). Non-polar groups are expected to occur between the chains, since by packing the hydrophobic side chains together, more hydrogen bonds form elsewhere, which is energetically preferable. The sequence (X-N-X-X-N-X-X) is to be expected, where N is a

non-polar residue and X is any residue. A sufficient length of tropomyosin has been sequenced to verify this (Hodges and Smillie, 1970, 1972 a,b; Hodges et al., 1973).

1.5.3 X-ray diffraction from a coiled coil

Fourier transforms of continuous and discontinuous coiled coils (Crick, 1953a; Lang, 1956; Ramachandran, 1960) are a good approximation, but they wrongly assume a constant line density for the continuous helix (Pardon, 1967). A method used for α-keratin requires only the atomic coordinates relative to the major helix for the repeating unit of seven residues, which is arranged on a simple helix (Fraser et al 1964). The general theory (Crick, 1953a) is not described here, but the applications are (Crick, 1953b).

The gradual major helix follows the axis of the α-helix. It has radius r_o, a repeat distance of P in the z direction (i.e. parallel to the coiled coil axis) and a pitch angle α given by $\tan \alpha = 2\pi r_o/P$. The minor helix approximates to the α-helix. r_1 is the distance of an atom from the minor helix axis. The structure has a repeat distance c in the z direction, the major helix making N_o turns and the minor helix N_1 turns relative to the major helix in that distance. M atoms are equally spaced along the coiled-coil locus in the repeat distance c. The cylindrical coordinates of reciprocal space are denoted by R, ψ and Z.

The Fourier transform $C(R,\psi,Z)$ is non-zero only on the layer lines (ℓ is the layer line number) since the structure is periodic in the z direction (the fibre axis). For a left-handed major helix and a right handed minor helix

$$C(R,\psi,Z) = C(R,\psi,\ell/c) = \Sigma\Sigma\Sigma_{pqs} J_p(2\pi R\, r_0) J_q(2\pi R r_1) J_s(2\pi(\ell/c) r_1 \sin\alpha) \cdot \exp i\,(p(\tfrac{1}{2}\pi-\psi)+q(\tfrac{1}{2}\pi+\psi)+s\pi) \quad (1.4)$$

subject to the condition that only terms for which

$$N_o p + (N_1 - N_o)\, q + N_1 s = \ell + m' M \quad (1.5)$$

are included, where p, q, s and m' can take any integer values, positive or negative.

$J_n(x)$ is very small for small x and large n, so Bessel functions of high order are usually unimportant. Consider terms for which p, q and s are small. The largest terms are normally those with two zero order Bessel functions, as follows:

p = q = s = m' = O : equatorial

q = s = m' = O, p small : near equatorial

p = q = m' = O s = 1 : 5.1Å meridional

p = q = s = O m' = 1 : 1.5Å meridional

p = s = m' = O q = 1 : 5Å meridional

Substituting the parameters for the two strand rope (section (1,5.2) in equation (1.5) gives

$$p + 35\, q + 36\, s = \ell + 126 m' \quad (1.6)$$

On the meridian, R = O and

$$C(O,O,\ell/c) = \Sigma_s J_s(2\pi(\ell/c)\, r_1 \sin\alpha) \exp(i\, s\, \pi) \quad (1.7)$$

subject to

$$36s = \ell + 126\, m' \quad (1.8)$$

Clearly, ℓ is a multiple of 18, so no meridional reflections

occur except at sub-multiples of 186/18 = 10.3Å (a consequence of the 18-fold rotation axis).

From equation (1.8):

(ℓ/18)	0	1	2	3	4	5	6	7	8	9	10
d(Å)	∞	10.3	5.17	3.45	2.59	2.07	1.72	1.48	1.29	1.15	1.03
s	0		1		2		3		4		5
		-3		-2		-1		0		1	

There are strong meridional reflections at 5.17Å and 1.48Å. The 5.17Å reflection is produced mainly by the side chains, where r_1 is large. At 1.48Å resolution, side chains, especially lysine, arginine and glutamic acid, which have high temperature factors (Kendrew, 1962), are normally disordered. The main chain contributes most to this reflection, except perhaps in crystalline structures with ordered side chains. At 10Å resolution, a side chain in water scatters much less than *in vacuo*, but beyond 5Å the effect is negligible, depending on small scale density fluctuations (Langridge et al 1960). Other reflections are predicted to be weak, except where side chains are highly ordered and $|s| \leqslant 2$.

Two helices related by a diad have a repeat distance of half the pitch of the major helix, so only even layer lines are present (Equivalent to (p-q) being even in equation 1.6).

On the equator, ℓ= 0 and s = 0, otherwise J_s becomes zero. The structure amplitude is

$$\sum_p \sum_q J_p(2\pi R r_o)\, J_q\,(2\pi R r_1) \qquad (1.9)$$

subject to

$$p + 35\,q = 126\,m' \qquad (1.10)$$

For small R, the only important term is for p = q = O. For higher R, terms such as p = 7, q = 7; p = -14, q = 4; p = -7, q = 11 may be important.

The near equatorial region corresponds to $p \neq 0$, $q = s = m' = 0$, so for a single coiled coil $C(R,\psi,\ell/c) = J_p(2\pi R r_o) . J_o(2\pi R r_1)$.

$$J_o(2\pi(\ell/c)\, r_1 \sin d) \exp i\, p\, (\tfrac{1}{2}\pi + \psi) \qquad (1.11)$$

subject to

$$N_o\, p = \ell \qquad (1.12)$$

Since $N_o = 1$, $p = \ell$. For small ℓ and r_1, and $r_o = 5.2$:

p	1	2	3	4
1/R(Å)	17.8	10.9	7.75	6.2
Θ degrees	5½	6½	7'	7½

$\tan \Theta = \ell/cR$ and the pitch angle is 10 degrees so the maxima occur at an angle from the equatorial direction of about two thirds of the pitch angle.

For a two strand rope, only even values of ℓ are present, so the first near equatorial is for $\ell = 2$. The broad maximum of J_2 gives an exact spacing, depending on neighbouring parts of the structure. The finite radius of the helix causes the intensities for $\ell = 4$ and higher to be low, since for $r_1 = 1.8$Å, $J_o(2\pi R\, r_1) = 0$ where $1/R = 4.5$Å.

The 5Å near meridionals for which $m' = 0$, s and q = 0 or 1 and p is small, and the reflections near the 1.5Å reflection for which $m' = 1$, $(s + q) = 0$, and p and q are small are important.

Distortions allow more reflections to appear as the unit cell increases in size. Packing into a lattice causes sampling by the discrete lattice reflections.

1.5.4. X-ray patterns

α-fibrous proteins, for example paramyosin, keratin, tropomyosin and myosin, give very similar X-ray diffraction patterns.

The unit cell is defined so that the c axis is parallel to the molecular axis.

1.5.4.1. Paramyosin

Low angle X-ray diffraction patterns obtained from paramyosin containing muscles show a series of meridional and near meridional reflections indexing on a two dimensional lattice.

A number of studies (Bear and Selby, 1956; Elliott, 1963, 1964; Elliott and Lowy, 1970) have found the c axis to be close to 720 Å and the angle β to be close to 90 degrees whether dry or wet. The a axis shrinks by about 20% when going from the wet to the dry state. The dry state dimensions for *Venus mercenaria* (250Å), *Crassostrea angulata* (330Å) and *Mytilus edulis* (420 Å) are in the ratio 3:4:5 and are multiples of about 82 Å in the dry state, equivalent to 106Å when wet.

The high angle pattern of the anterior byssus retractor of *M.edulis* in the wet state has a prominent meridional at 5.15 ± 0.06Å and off meridional maxima on the 5.25 Å layer line (Cohen and Holmes, 1963). The layer lines from the 720 Å repeat extend at least as far as 5Å for both living and dried muscle, the prominent reflection occurring on layer line 142, at 5.123 Å and 5.076 Å for living and dried muscle respectively.

A weak meridional arc occurs at 1.485 ± 0.005Å (Cohen and Holmes, 1963; Elliott et al, 1968) The spacing of the off equatorial layer line in the 10Å region is 89 ± 5Å (Cohen and Holmes, 1963), similar to the value for the opaque adductor of *C. comercialis* (Fraser et al.1965). *C.angulata* gives a value near 70Å, perhaps produced by an overlying interference function.

Native muscle from *M. edulis* gives a 20 Å equatorial interference maximum, and maxima occur on the near equatorial layer line for muscle soaked in acetone-water mixtures after drying (Cohen and Holmes, 1963), interpreted in terms of a body-centred tetragonal arrangement (Elliott et al 1968). The equatorial maximum corresponding to the lateral molecular separation varies from 17Å to 20Å as the mixture is varied (Elliott and Lowy, 1970). Half widths imply a coherent length of 150Å , much shorter than the molecule, suggesting that the pitch varies along the length (Cohen and Holmes (1963). The equatorial and near equatorial intensity corresponds better to a two-stranded coiled-coil than a three-stranded one (Cohen and Holmes, 1963). Fraser et al. (1965) considered the side chains and the background, obtaining a better fit, especially for the dry case.

1.5.4.2 α-keratin

The reciprocal spacings of porcupine quill α-keratin satisfy the selection rule

$$Z = m/h + n/P + s/P_d$$

where h = 67.1Å , P = 220Å, P_d = 235Å and m, n, and s are integers (Fraser and MacRae, 1973 b). In conjunction with the lateral distribution of intensity, this indicates that the microfibrils (observed in the electron microscope) in α-keratin have a helical structure with a 220Å pitch and a 67.1Å unit height

subject to a regular axial distortion of period 235Å. n must be a multiple of N where the microfibril has N-fold rotational symmetry (Klug, Crick and Wyckoff, 1958), so the off meridional intensity depends on terms of the type J_{kN}^2 $(2\pi Rr)$. Given a microfibril diameter of 36Å (Fraser et al , 1971) and lateral positions of off meridional reflections at 35 - 45 Å, N must be one.

Meridional reflections occur at spacings of 5.165Å and 1.485Å (Fraser et al 1964) Near equatorial spacings in α-keratin are in the range 70-85Å (Fraser et al, 1965). Two and three stranded coiled coils cannot be distinguished although a two stranded form is favoured because of the similarity between the diffraction patterns of α-keratin and paramyosin (Fraser et al 1965). A possibility not considered is that both two and three stranded coils are present.

1.5.4.3 Tropomyosin

Films prepared from tropomyosin give a meridional arc at 5.15Å, a diffuse equatorial reflection at 9.8Å (Astbury et al, 1948) and a meridional arc of spacing 1.49Å (Perutz, 1951a). Tropomyosin and paramyosin give similar patterns, so it was inferred that tropomyosin is a two-stranded coiled-coil (Fraser et al, 1965).

1.5.4.4. Myosin

Myosin gives a meridional reflection at a spacing of 1.50 Å (Perutz, 1951b). Light meromyosin fragments (the α-helical portion) have been oriented and give a high-angle α-pattern as well as meridionals and near meridionals indexing on an axial period of 430Å (Cohen and Szent-Györgyi, 1960; Szent-Györgyi et al, 1960). Both native and dried striated muscle

give a high angle α-pattern with a meridional arc at 5.15 Å and a diffuse equatorial reflection at 9.8Å (Astbury, 1947) presumably from myosin.

1.5.5. Chemical data

Chemical work provides information on molecular size and interactions from which inferences can be made about the native structure.

1.5.5.1. Paramyosin

Paramyosin has a molecular weight of about 200,000 (Lowey et al, 1963; McCubbin and Kay, 1968; Woods, 1969), but about half this in appropriate denaturing solvents (Olander et al. 1967; McCubbin and Kay, 1968; Weber and Osborn, 1969; Woods, 1969), suggesting that the molecule has two chains. Optical rotatory dispersion infers a very high α-helix content (Cohen and Szent-Györgyi, 1957, 1960; Simmons et al, 1961; Riddiford, 1966; Olander, 1971), consistent with the amino acid composition, in which it resembles tropomyosin and the rod portion of myosin. It has a high content of the α-helix favouring residues, glutamic acid, leucine and alanine, and a low content of the non-α-helix favouring residues, proline, glycine and cysteine (Finkelstein and Ptitsyn, 1971). Hydrodynamic and light scattering studies in solution (Lowey et al, 1963) indicate a length of 1330Å and an axial ratio of 64:1. Taken with the molecular weights and amino acid composition, this is strong evidence for a two-stranded coiled-coil.

1.5.5.2 Tropomyosin

The molecular weight of tropomyosin, as determined by hydrodynamic studies, is about 68,000 but in the presence of

denaturants and reducing agents the molecule dissociates into two chains of very similar weight and composition (Holtzer et al 1965; Woods, 1967). Optical rotatory dispersion in aqueous solution indicates an α-helix content nearly 100% (Cohen and Szent-Györgyi, 1957; McCubbin and Kay, 1969; Woods, 1969; Rainford and Rice, 1970).

Crick (1953b) predicted a sequence (X-N-X-X-N-X-X) for coiled coils, where N is a non-polar residue and X is any residue. This sequence has been found (Hodges and Smillie, 1970, 1972a,b; Hodges et al, 1973).

1.5.5.3. Myosin

The molecule has two chains that run side by side throughout a rod-like portion and end in a globular head (Lowey, 1971). Myosin has a molecular weight (M.W.) of 510,000. Two enzymic fractions of this, light meromyosin (M.W.140,000) and the S2 fragment of heavy meromyosin (M.W.62,000) have a very high helical content (Lowey et al , 1969). These fragments often occur together as the papain rod (M.W.220,000).

1.5.5.4. Keratin

Keratin contains many proteins, many forming the matrix surrounding the microfibrils. The low sulphur proteins form two groups, components 7 and 8 in the ratio of about 2:1 (Thompson and O'Donnell,1965) with molecular weights of about 53,000 and 45,000 (Jeffrey, 1972) and helix contents in solution of 56% and 62% (Crewther and Dowling, 1971). X-ray diffraction of oriented films of the low sulphur proteins gives an α-pattern (Happey, 1950). There is a suggestion that two chains of component 7 and one of 8

aggregate (Crewther et al 1968) to form a three strand rope, (Crewther et al., 1968; Crewther and Dowling, 1971). Provisional sequence work suggests helical and non-helical regions (O'Donnell, 1969; Corfield et al, 1968; Hosken et al, 1968).

1.5.6. Composition

α-fibrous proteins have similar compositions (Table 1.1). Approximately 2/7 of the residues are small hydrophobics, as predicted by Crick (1953b). Myosin is more polar than average and tropomyosin is more hydrophobic than average, reflecting differences in intermolecular interactions. The proportion of the helix disrupting residues, cysteine, glycine and proline (Finkelstein and Ptitsyn,1971) is small. The helical portions of the low sulphur proteins of keratin have a similar composition (Crewther and Dowling, 1971).

For globular proteins, Finkelstein & Ptitsyn (1971) found that α-helical regions had a significantly above average content of alanine, glutamic acid, leucine and histidine, and a significantly below average content of glycine, tyrosine, asparagine, serine, proline and cysteine.

1.5.7. Electron microscopy

1.5.7.1. Paramyosin

The thick paramyosin containing filaments in molluscan catch muscle are up to 60 μm long and 200-1600 Å in diameter (Hanson and Lowy, 1963). Treated and stained filaments show a two-dimensionally periodic structure (Hall et al, 1945; Hanson and Lowy, 1964a; Elliott and Lowy, 1970; Szent-Györgyi et al, 1971; Cohen et al, 1971a). Treatments revealing this structure may remove a surface layer of myosin. Hall et al (1945) found non-primitive cell dimensions of a = 193Å, c = 720Å and ß = 90 degrees, and

from the constancy of a, assumed they were flat ribbons, as is supported by the presence of enantiomorphic forms (also observed by Elliott, 1964; Elliott and Lowy, 1970; Cohen et al, 1971a). Cohen et al, (1971a) suggested that the filaments were helical but selective staining of the top surface occurred. Elliott (1971) shadowed both sides, obtaining an image giving the optical diffraction pattern expected for a helical structure. Elliott and Lowy (1970) observed an apparent change in the screw sense of a shadowed specimen accompanied by a change in a. A change in polarity without a change in screw sense has been observed (Cohen et al, 1971a). The a dimension varies widely; for filaments over 800Å in diameter, the a values were 200-400Å, but for smaller diameters, the upper limit was about 660Å, perhaps due to distortion at the outer surface of a layer bent into a cylinder (Elliott and Lowy, 1970). This suggests a two dimensional lattice of the type envisaged by Bear and Selby (1956) rolled into a spiral cylinder (Whittaker, 1955). However, no X-ray reflection corresponding to the intersheet spacing has been observed, nor has the edge of the sheet been seen in the electron microscope.

1.5.7.2. Keratin

The low sulphur proteins form microfibrils of 70Å diameter within a matrix of high sulphur proteins (Rogers, 1959). The microfibrils appear to be annular with a wall thickness of 20Å and high sulphur protein inside (Filshie and Rogers, 1961).

1.5.7.3. Tropomyosin

Rodlike particles of mean length 400Å believed to be individual tropomyosin molecules have been seen (Rowe, 1964; Ooi, and Fujime - Higashi, 1971).

1.5.7.4. Myosin

Hanson et al, (1971) isolated thick filaments from vertebrate striated muscle, These show the central M band about 495Å wide, flanked on either side by zones about 395Å wide, followed by ten repeats of a 420$^{+}_{-}$ 15Å period.

The form of the myosin containing filaments in vertebrate smooth muscle is not well established (Burnstock, 1970; Lowy et al, 1973). Lowy and Small (1970) say the filaments are ribbon-like, about 80Å thick, 200-1100Å wide and up to 30,000Å long. Other workers have generally observed filaments of diameter 150-200Å, apparently depending on the method of preparation. (Rice et al.,1971; Somlyo et al., 1971a,b; Cooke and Fay, 1972). The *in vivo* form is not known. In paramyosin containing smooth muscle, the myosin is believed to be located at the surface of the thick filaments (Hanson and Lowy, 1964b; Squire, 1971; Szent-Györgyi et al, 1971).

1.5.8. Artificial forms

Electron microscope studies of *in vitro* forms of paramyosin (Cohen et al, 1971a), tropomyosin (Cohen et al, 1971b) and myosin (Harrison et al, 1971; King and Young, 1972) have revealed banding patterns relating to molecular staggers. Molecular lengths can be estimated.

1.6. Silks

Fibrous proteins secreted by arthropods are normally classified as silks. Comprehensive reviews have been given by Lucas et al, (1958), Rudall (1962), Seifter and Gallop (1966), Lucas and Rudall (1968), Rudall and Kenchington (1971) and Fraser and MacRae (1973a).

1.6.1. Structures

Silk has been classified into six classes of β silks, one

cross-β class, one class of collagen-like and polyglycine-like silks and one class of α-helical silks (Warwicker, 1960; Lucas and Rudall, 1968; Rudall and Kenchington, 1971). The most complete list of silks and their structures is given by Fraser and MacRae (1973a). The different classes of parallel-β silks differ in structure and composition. The proportion of glycine present appears to be a crucial factor and varies from 45 residues per 100 in group 1 to 2.1 residues per hundred in group 6. (Rudall and Kenchington, 1971). Some silks have polyglycine I or II, or collagen structures (Rudall and Kenchington, 1971). The amino acid compositions are rich in glycine for polyglycine structures and more like that of collagen for collagen structures. (Lucas and Rudall, 1968; Rudall and Kenchington, 1971). α-helical silks have been found in a variety of arthropods. The silk of the green lace wing fly (*Chrysopa flava*) egg stalk was the first cross-β structure to be discovered (Geddes, A.J. et al, 1968). Rudall and Kenchington (1971) also discuss chitinous and cuticulin silks, but these contain little fibrous protein.

1.6.2. α-helical silks

The first α-helical silk to be so identified was the ootheca protein of praying mantids (Rudall 1956). Several are now known (Table 1.2). α-proteins generally have high contents of glutamic acid and lower glycine contents than is normal for silk. The amino-acid composition of purified mantis ribbons is compared with that of other silks and α-proteins in table 1.3.

Comparing the silk of *Arge ustulata*, which has some α-characteristics, with those which are α-fibroins, we see that glutamic acid and alanine are more important. However, the total number of acidic residues is closer to that in the α-fibroins and the quantity

of hydrophobics is not much greater. Lucas and Rudall (1968) compare this silk to two other Argid silks with a β structure.

	Ala	Glu (Res/100)
Digelansinus diversipes	38	36
Pachylota Audouini	36	36
Arge ustulata	41	33

Rudall and Kenchington (1971) regard the α-helical form in silk proteins as a consequence of a reduced glycine content and an increased content of acidic residues.

Aculeate Hymenopteran larvae silk gives α patterns with meridional arcs of spacing 5.1Å and 1.5Å. Atkins (1967) has studied the good pattern given by honey bee (*Apis mellifera*) larva silk. A meridional arc of spacing 5.06 ± 0.05Å and off meridional arcs, apparently on the same layer line, are obtained. Strong diffraction occurs on the equator at 9.4Å and on the 35Å layer line at a spacing of 8.4Å. The axial period is 280Å. A four-stranded coiled-coil model was fitted to the relative intensities and the positions of the equatorial and off-equatorial reflections, but it seems likely that other reasonable models could fit. Some indication that there may be a stable four chain unit was obtained by Flower and Kenchington (1967), who observed fibres 25Å in width under the electron microscope (They were produced by suspending the silk in 0.3M KCl). Shearing occurs during hardening of the silk. (Lucas and Rudall, 1968; Ramsden, 1938).

The wasp *Pseudopompilus humbolti, Dahlbom,* produced a silk with a good α pattern and a good α→β transformation with extensions of 90-100% in water at 70°C (Rudall, 1962).

The silk from the oothecae of *Aspidomorpha* beetles (Flower and Kenchington, 1967) produce X-ray patterns very like those of the praying mantis ootheca.

The silk from the flea *Xenopsylla cheopis* (Rudall and Kenchington, 1971) has an X-ray diffraction pattern much more like those of keratin and myosin than those of the *aculeate* silks.

1.7 Mantid Oothecal Protein

1.7.1. Egg-case production

Rudall (1956) considers three glands (Fig.1.1) to be important in the formation of the ootheca. The principle gland is a large set of parallel tubules each about 1 mm. in diameter and occupying much of the abdominal space (In *Sphodromantis membramacea* the tubules are about 1.5 mm. in diameter and could hardly be described as parallel (personal observation)). This gland, known as the main colleterial gland, the left colleterial gland or the first order gland, produces almost all of the substance of the ootheca. The gland tubules form a common duct opening into the genital atrium between the valvulae of the ovipositor. Just before this duct reaches the exterior, it is joined by the duct of a much smaller gland, the right colleterial gland (second order gland). There is also a gland which produces regular trapezium shaped crystals of calcium citrate enclosed in complex membranes (Parker and Rudall, 1955)

The left colleterial gland secretes numerous globules of protein up to 0.5 mm. in diameter (size estimated by Kenchington and Flower, 1969), a fluid serum and a pigment protein, which in different species may be dark or light brown, or greenish blue. When dark golden brown, this protein may occur as well-defined crystals, as in *Mantis religiosa* and *Paratenodera sinesis*, but it is usually

in solution. Shortly before laying, the protein globules are highly birefringent (Rudall, 1956; personal observation for *Sphodromantis membramacea*), but shortly after laying they are scarcely birefringent and much smaller. Each globule has a thin membrane surrounding it.

The function of the calcium citrate gland is uncertain, since Rudall (1956) found that normal egg cases were still produced after its removal. Kenchington and Flower (1969) found that protein globules dissected from the left gland form ribbons on treatment with calcium chloride solutions of 0.005M to 0.025 M. The ribbons are only 10 µm long and 2-3 µm wide, but they are otherwise identical to naturally occurring ribbons. Calcium citrate is sufficiently soluble to furnish these concentrations of calcium ions.

The right gland has an unknown function, but Stay and Roth (1962) have suggested that it supplies an essential chemical tanning, as in the cockroach ootheca (*Periplaneta* and *Blatta*) (Brunet and Kent, 1955) and a variety of other species (Stay and Roth, 1962).

In the production of the ootheca (Rudall, 1956) muscular action extrudes the contents of the colleterial glands. During extrusion, the globules lose their membranes and the contents become a viscous mass, which is moulded by the valvules into the fabric of the egg case.

Neville and Luke (1971) found that the spherulites in the left colleterial gland of both adult *Sphodromantis tenuidentata* and *Miomantis monacha* were formed of a continuous phase, whereas Kenchington and Flower (1969) working on *Sphodromantis centralis* found that the spherulites were composed of fibrils 0.05 - 0.1 µm. in diameter and Rudall (1956) found fibrils 0.2-0.5 µm. in diameter.

It seems likely that fibrils existed in the earlier preparations, but it is possible that conditions differed. Neville and Luke (1971) think that these fibrillar units are likely to be twin-coiled α-helices, but they observe a wide range of pitch. They also observe an irreversible denaturation at 55°C, which they attribute to the breakage of hydrogen bonds - a feature of α-helices.

Kenchington and Flower (1969) considered the spherulites to be constructed of sheets of fibrils, each sheet inclined at 18 degrees to the adjacent ones in a cholesteric arrangement. It is only possible to correlate a fixed 18 degrees with a wide range of pitch (Neville and Luke, 1971) if the fibril size varies.

Rudall (1956) and also Kenchington and Flower (1969) observe that just after laying there are many approximately cylindrical fibrils, which within 30 minutes change to ribbons 15 μm. long, 1-2 μm. wide and 200-300 Å thick. Rudall obtained the ribbons from the fresh egg case by limited treatment with dilute trypsin. At this stage, the ribbons are readily altered by heating in water, they dissolve in concentrated urea solution and are digested by trypsin, but, within hours, the ootheca dries, becomes browner and hardens; it is now completely resistant to boiling water, strong urea and tryptic digestion. Rudall (1956) observes that during ribbon formation the fibrils develop vacuoles and then flatten into ribbons.

1.7.2. Structure of the protein

1.7.2.1 Electron microscopy

Rudall (1956) examined the small ribbons formed after limited treatment of fresh egg case with trypsin. After staining with phosphotungstic acid (PTA), densely stained diagonal lines

were visible making an angle of about 20 degrees with the long edge of the ribbon. These striations, which also show after shadowing, are destroyed by longer treatment with trypsin. The proteolytic action of trypsin may aid PTA staining at certain sites (Rudall, 1962). At higher magnification, the striations appear as double rows of spots, each spot being 20-30Å in diameter (Rudall, 1962).

Millard and Rudall (1962) claimed that along each fibrous rod (which they considerered to be parallel to the striations) there was a staining centre every 33Å, although they only obtained this by dividing the period (400Å) by the number of staining centres (12). They relate this to the 6% arginine content of the ribbons. This is one residue in 22 and there are 22 residues in a 33Å length of an α-helix. On this basis, they conclude that the staining centres could be mainly arginine. A basic amino acid like arginine would be expected to be stained by PTA.

Rudall (1956) observed the main cleavage plane parallel to the ribbon axis and the minor one parallel to the diagonal lines.

1.7.2.2. X-ray diffraction

Rudall (1956) drew fibres from the globules in the left colleterial gland and also from material taken from the ovipositor. A diffuse X-ray pattern is produced with two well-marked features, namely arcs at 5.18Å and 1.5Å. There is equatorial scattering at 8.3Å and 14.5Å. Hexagonally packed rods 16.5Å in diameter were proposed to explain this.

Rudall (1956) found that ribbons with the X-ray beam parallel to the face and perpendicular to the long axis give X-ray diffraction patterns dominated by a set of row lines which are orders of

17.5 - 18.5Å. When the ribbon is rotated about the long axis to present the flat face to the beam, a pattern indicating an equatorial period of 31Å or 62Å is obtained. The meridional spacings at 5.18Å and 1.5Å remain.

On stretching the ribbons in cold or warm water, 100% extension was achieved, and X-ray patterns revealed a doubly oriented β-structure of axial periodicity 3.33Å with the hydrogen bonds perpendicular to the surface of the ribbon. The transformation was readily reversible. The axial period of 3.33Å and the period along the chain of 4.7Å gave strong, sharp reflections, whereas the chain separation period of about 9.8Å gave a weak, diffuse reflection.

More recent work suggests that the axial period of the ribbons is in excess of 480Å, based on two low-angle meridional reflections (Fraser and McRae, 1973a).

1.7.2.3. Models proposed

Rudall (1956) gave two interpretations. One considers straight α-helices packed hexagonally (fig.1.2). Taking cylinders of diameter 10.3Å, periods of 31Å and 17.8Å are readily obtained. The shading in his figure presumably indicates that there are two types of α-helices present, differing in sequence, twist, stagger or direction. The diagonal lines seen in the electron microscope are accounted for by postulating a superficial layer of fibrils superposed on the main parallel chains and making an angle of about 20 degrees with them. This could occur by fitting knobs into holes as suggested by Crick (1952). If the diagonal fibrils were also α-helices then they could give an axial period of 5.1Å.

Rudall states that there are several layer lines in the 5Å region, perhaps including a 5.4Å layer line.

This model does not fit well with the X-ray diffraction data. Projection of the structure on to the axis marked 31Å, then gives a periodicity of 31Å. Since the shaded and unshaded helices must be very similar, most of the intensity on the equator of the pattern obtained with the beam perpendicular to the face of the ribbon must fall on every sixth order of 31Å, which is not observed. For the same reason, most of the intensity not on the equator should fall on row lines corresponding to every third order of 31Å. The intensity is high near 10Å, but this is generally true for α- helical structures. With the thin edge of the ribbon towards the source, most of the intensity should fall on row lines which are orders of 17.8/2 = 8.9Å. Taking all α-helices as identical, and projecting the structure in fig. 1.2 on to a plane perpendicular to the paper and parallel to the axis marked 17.8Å, the structure repeats at intervals of 8.9Å . There is too much intensity on the odd orders of the 17.8Å for the structure to be consistent with it.

The other interpretation is based on two-stranded ropes of α-helices, which would give meridional reflections at 5.1Å and 1.5Å. If the diameter of each helix is 10.4Å and the pitch of the supercoil is 180-190Å, then these grooves will make an angle of about 20 degrees with the edge of the ribbons. The lateral period is 17.8Å and the inclination of the diagonal grooves is remarkably similar to the slope of the diagonal lines seen in the electron micrographs. Rudall notes that the grooves of the model are separated by about 30Å, while the true striations are separated by about 120Å, indicating an axial period of 360Å.

The tendency to cleave along diagonal lines suggests that they contain long fibrous elements. The method of packing the coiled coils is shown in fig. 1.3. A stagger between adjacent coiled coils of a quarter of the supercoil pitch allows optimum packing.

This model is in better agreement with the X-ray diffraction data. However, it is seen from fig. 1.3 that the true periods are 62Å and 35.6Å, twice the dimensions marked. If the structure is projected on to two planes perpendicular to the paper and parallel to the axes marked 31Å and 17.8Å, then these periods remain doubled. Weak row lines may occur on orders of 62Å but there is no sign of row lines on orders of 35.6Å. If the structure is projected on to the plane of the paper, the coiled coils become circularly symmetric, so orientation is no longer important. Projection of this structure on to the two axes gives periods of 31/2Å and 17.8/2 Å, so the equators for the two patterns should in one case have reflections as orders of 15.5Å and in the other as orders of 8.9Å.. This is not observed.

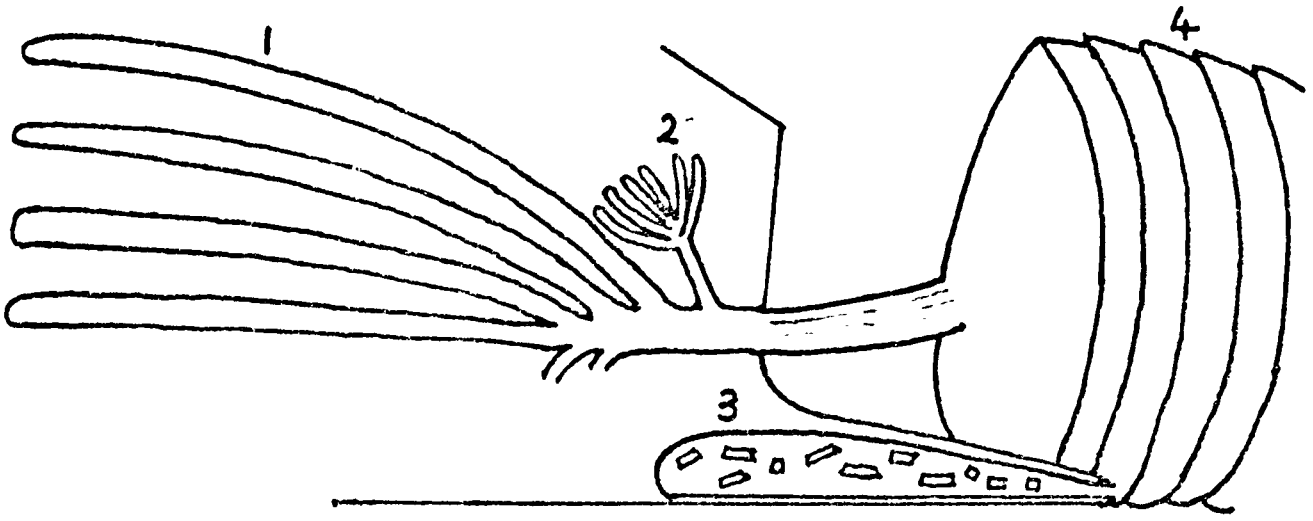

Fig.1.1 The glands which form the material of the ootheca in female mantids. 1, first order gland; 2, second order gland; 3, calcium citrate gland; 4 ootheca, (copied from Rudall, 1956).

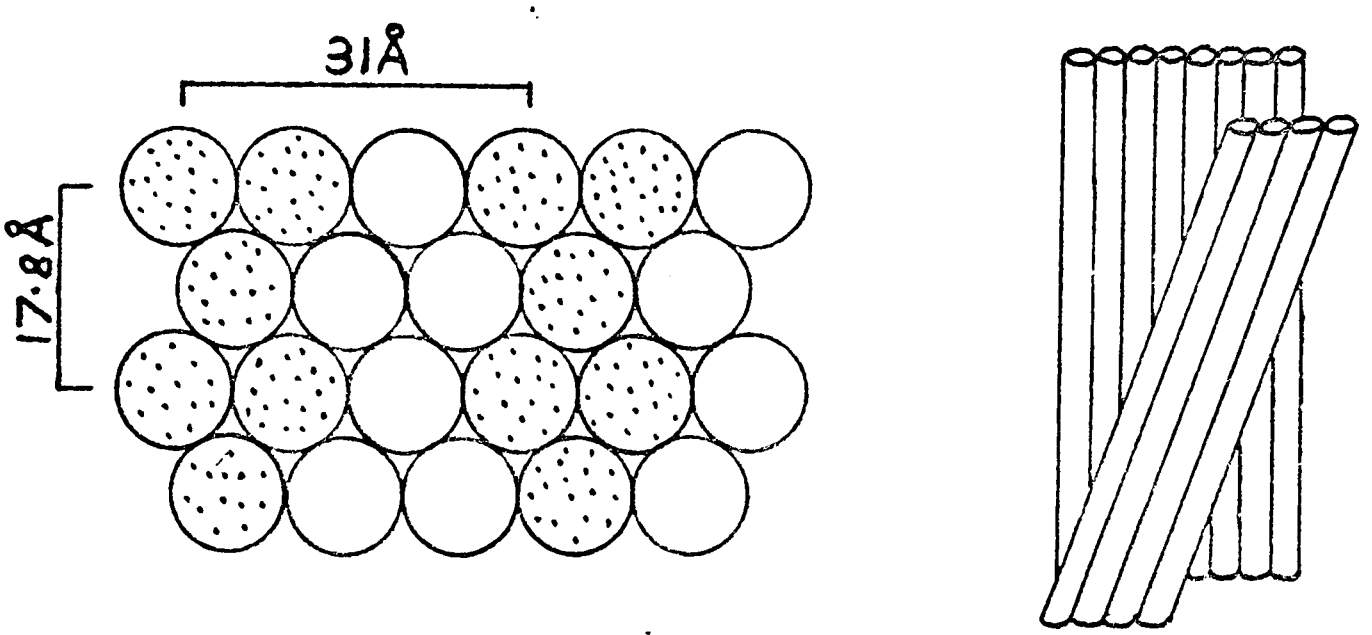

Fig. 1.2 A, hexagonal packing of straight α-helices of diameter 10.3Å; B, two superposed layers of α-helices inclined at about 20°. (Copied from Rudall, 1956)

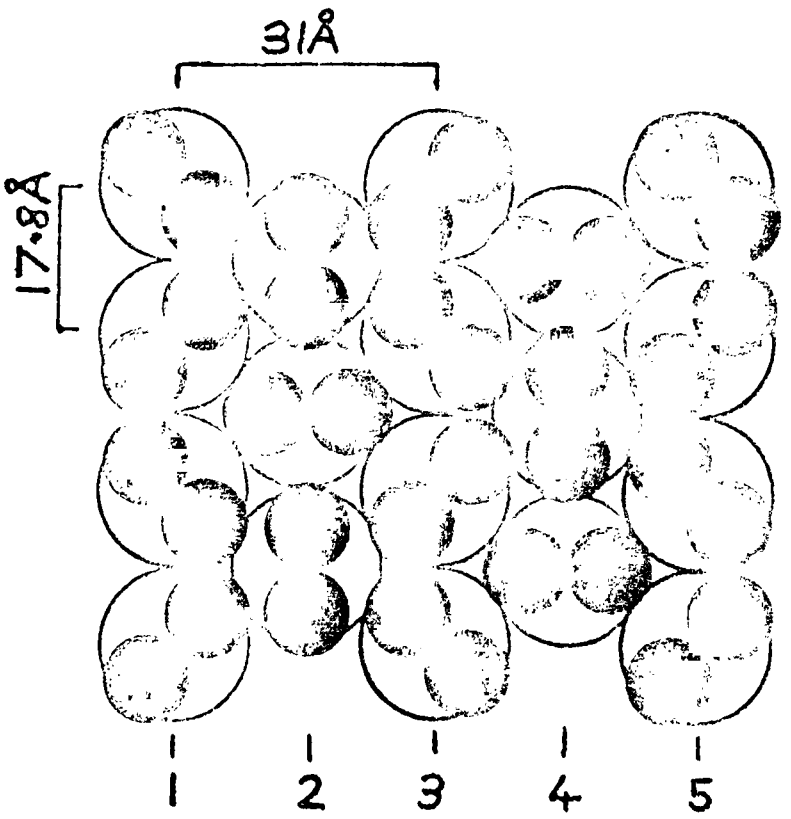

Fig. 1.3 Cross-section of five layers of α-helical coiled coils, the α-helix being 10.4Å in diameter. The lateral periodicities given are less than those in the photographs of 'wet' specimens. (Copied from Rudall, 1956).

TABLE 1.1

Amino acid compositions of α-helical proteins

Amino Acid	Residues /100			
	Myosin[a] -Papain rod fragment	Tropomyosin[b]	Paramyosin[c]	Average
Alanine	9.7	12.1	12.2	11.3
Arginine	6.4	4.8	9.8	7.0
Aspartic Acid	10.1	10.1	12.8	11.0
Glutamic acid	25.0	24.7	21.3	23.7
Glycine	2.3	1.3	2.0	1.9
Half cystine	0.5	1.0	0.6	0.7
Histidine	1.7	0.7	1.3	1.2
Isoleucine	4.1	3.8	3.3	3.7
Leucine	11.3	10.9	12.4	11.5
Lysine	12.2	13.2	6.9	10.8
Methionine	2.6	4.4	1.5	2.8
Phenylalanine	0.8	0.5	1.0	0.8
Proline	0	0.2	0.1	0.1
Serine	4.5	4.4	5.3	4.7
Theonine	4.3	2.7	4.5	3.8
Tyrosine	0.7	1.9	1.6	1.4
Valine	3.8	3.4	3.6	3.6
Ala+Leu+Ile+Val	28.9	30.2	31.5	30.2
Asp+Asn+Glu+Gln	35.1	34.8	34.1	34.7
Arg+His+Lys	20.3	18.7	18.0	19.0
Tyr+Met+Phe	4.1	6.8	4.1	5.0
Ser+Thr	8.8	7.1	8.8	8.5
Pro+Gly+½Cys	2.8	2.5	2.7	2.7

a Lowey et al. (1969)

b Rabbit skeletal (Hodges and Smillie, 1970)

c Rabbit skeletal (Huszar and Elzinger, 1971); small amounts of 3-methylhistidine also detected.

TABLE 1.2

Examples of α-helical silks.

Class, family or subfamily, genus, and species	Ref.[a]	X-ray classif-ication.	Content of selected residues res/100					
			Gly	Ala	Ser	Glu	Pro	Ref[a]
Apidae								
Apis mellifera	2	α(7)						
Bombus lucorum	2	α(7)						
Argidae								
Arge ustulata	1	β(6)+ α	2	41	8	33[b]	2	2
Mantidae								
Mantis (ootheca)	1	α	6	15	5	21	2	1
Pulicidae								
Xenopsylla cheopis	1	α						
Vespidae								
Vespa cabro	3	α						
Vespa sylvestris	3	α						
Pseudopompilus humbolti, Dahlbom	3	α						

a 1. Rudall and Kenchington (1971); 2. Lucas and Rudall (1968); 3 Rudall (1962).

b largely as glutamine.

TABLE 1.3

Comparison of the amino acid compositions of the mantis silk, other α-helical and partially α-helical silks and other α-helical proteins.

Residue	Mantis[a] ribbons	Arge[a,b] ustulata	4 species of α-fibroin[b] Vespidae & Apidae (Range)	α-helical myofibrillar proteins (Sec. 1.5.6.) (range)
Gly	5.5	2.1	4.6-6.5	1.3-2.3
Ala	14.7	40.9	16.1-36.7	9.7-12.2
Val	3.2	2.5	1.9-6.5	3.4-3.8
Leu	6.5	2.8	4.7-9.5	10.9-12.4
Ile	2.4	1.2	1.0-5.1	3.3-4.1
Ser	5.4	8.2	8.7-22.7	4.4-5.3
Thr	3.1	2.5	2.8-5.3	2.7-4.5
Asp+Asn	9.5	1.3	8.2-12.7	10.1-12.8
Glu+Gln	21.4	33.1	8.3-14.0	21.3-25.0
Lys	10.1	1.2	2.3-4.4	6.9-13.2
Arg	5.0	0.8	0.1-5.3	4.8-9.8
His	2.7	0.6	0.2-1.3	0.7-1.7
Tyr	3.8	1.0	0.1-2.5	0.7-1.9
Phe	1.9	-	0.1-2.2	0.5-1.0
Pro	1.9	1.7	1.3-3.1	0 -0.2
Met	-	0.1	-	1.5-4.4
½ Cys	-	-	-	.0.7
NH_3		(30.9)		-
Ala+Leu+Ile+Val	26.8	47.4		28.9-31.5
Asp+Asn+Glu+Gln	30.9	34.4		34.1-35.1
Arg+His+Lys	17.8	2.6		18.0-20.3
Tyr+Met+Phe	5.7	1.1		4.1-6.8
Ser+Thr	8.5	10.7		7.1-8.8
Pro+Gly+½Cys	7.4	3.8		2.5-2.8

a. M.M.Attwood's estimates (Rudall and Kenchington, 1971).

b. Lucas and Rudall (1968)

CHAPTER 2

X-RAY DIFFRACTION TECHNIQUES

CHAPTER 2

X-Ray Diffraction Techniques

2.1 Introduction

This chapter is concerned with the generation of X-rays and the X-ray optics used to obtain diffraction patterns from specimens. This is not intended to be a complete account of X-ray optics, but rather a description of those aspects required for an understanding of the system used for this work.

2.2 X-ray generation

This section only gives a brief outline of X-ray generation. An account of a variety of X-ray generators is given by Peiser, Rooksby and Wilson (1960). More specific information can be found in the manufacturer's manual. The discussion given here is intended to provide sufficient understanding of the generator to enable its role in the work to be understood.

2.2.1. The X-ray generator

X-rays were produced by an Elliott GX3 rotating anode X-ray generator. This utilises a water-cooled copper anode rotating at 3000 r.p.m. By distributing the heat produced by the electron beam around the 30 cm. circumference of the anode, a much higher power output can be obtained. Electrons are emitted by a tungsten filament and are accelerated towards the anode (see fig. 2.1). The copper focusing cup (bias cup) is set at a voltage with respect to the filament and is then able to focus electrons emitted by the filament into a horizontal line focus 200 μm high and appearing as a 200 μm

rectangle when viewed horizontally at $4\frac{1}{2}^{o}$ to the anode surface. The technique of viewing at a small angle gives an apparent increase in source brightness, because unlike visible light, which obeys the Lambert Cosine Law in emission, X-rays are emitted isotropically. At very small angles, surface roughness will decrease the intensity of emission. The focus is viewed through a beryllium window.

A 100 μm focusing cup can also be supplied with this equipment, but this is not necessarily an advantage. The reason for this is that with a 200 μm focus the generator can be operated at a beam power of 2 kW giving a power loading of 50 kW /mm^2, whereas with a 100 μm focus, the generator can only be operated at a power of ¾ kW, giving a power loading of 75 kW/mm^2. It is seen that for an increase in brightness of 50%, a decrease in power by a factor of four is suffered. One way of overcoming this would be to increase the speed of anode rotation, since the maximum permissible power is proportional to $\sqrt{w}$, where w is the rotational speed, but workers who have tried this find that the oil seal life is inversely proportional to w. These seals are fitted between the X-ray tube casing and the bearing sleeve which rotates with the anode. With the aid of oil lubrication, these seal the vacuum, so if there is a failure, oil enters the tube, carbonises and contaminates the system.

2.2.2. Operating the X-ray generator

Maintenance is basically the same as for any vacuum system associated with motors and electronics. Failure of water seals and oil seals occurs several times a year. An oil seal failure

contaminates the system, so it is necessary to clean the vacuum system completely every six to twelve months, and to clean in the vicinity of the anode whenever oil seals fail. Filaments fail after between 7 and 14 weeks' operation. Replacement of these is not easy as the quality of the focus is dependent on the filament position in the cup to a few tens of microns. The distance between the anode and the bias cup has a tolerance of ½ mm.

Before setting up X-ray cameras, the focus must be examined by putting a pinhole in the aperture outside the beryllium window. This selects a narrow beam leaving the anode at $4\frac{1}{2}^{o}$. Photographs of the focus can be taken at a magnification of ten by setting the film to pinhole distance at 40 cm, which is ten times the focus to pinhole distance. Optimally an image 2.2 mm square is obtained. The pinhole diameter is about 30 µm, which, at a magnification of ten, will add 11x30 µm = 330 µm to the image diameter. This indicates that a focus a little better than 200 µm could be obtained. Initially the voltage on the focusing cup is varied to produce the best focus.

For a correctly set filament with the focusing cup used, this occurred at 25% bias (equivalent to 125 V between the filament and the cup. The best bias is selected and the cathode is rotated until the best focus is again achieved. The tolerance on this setting is found to be one or two degrees. When this is done, it may be found necessary to make a further small adjustment to the bias.

The generator was often run at 40 kV, 50 mA, but experience showed that filament life and oil seal life were increased by running at 40 kV, 40 mA.

2.3 Outline of the X-ray camera

The camera system was similar to that used by Reedy, Holmes and Tregear (1965) and also Huxley and Brown (1967). The latter workers describe a number of properties of the camera. The quartz crytal monochromator was cut at an angle to the reflecting planes, which allowed the crystal to be placed closer to the source than the focus. Such a system was first used by Guinier (1946).

The elevation view of the camera is shown in Fig. 2.2. It shows the role of the Franks mirror in focusing. The Franks mirror is placed as far from the source as possible, but before the quartz crystal monochromator. Adjustments are made to the curvature of the mirror to give the best possible focus at F. As the system is very asymmetric, a source of size 200 μm is found to give a focus much larger than this. This focus is too large to give sufficient resolution, so its size is reduced by a horizontal collimating slit. The parasitic scatter from this slit and also from the monochromator is stopped by a guard slit, which the beam does not touch. The space between the specimen and the film is evacuated to prevent air scatter.

The plan view (fig. 2.3) shows the means of focusing in the horizontal direction. A quartz crystal monochromator accepts radiation in an angle of a few degrees from the source. The radiation scattered by the $10\bar{1}1$ planes, which is monochromatic, is focused at F. Collimating and guard slits perform the same function in this direction, except that the collimating slit does not touch the beam unless it is required to irradiate only a small part of the specimen. Radiation

scattered by the specimen comes to a focus on the cylindrical film.

The dimensions and properties of the camera will be described in later sections, but for the sake of comparison, I record here a brief summary of the observations of Huxley and Brown (1967). Most of their work was done using a 5 cm long, gold plated mirror centred 14 cm from the source, giving a focus 22 cm. from the crystal. They state that the perfection of focusing improves with length. At 2 m the focal size is less than 100 μm. The longer camera also gave cleaner pictures, because the non-Bragg scatter intensity falls approximately as the cube of the linear dimensions, whereas the intensity of the focus falls approximately as the square. They also used a 90 cm. camera giving 10,000 Å resolution and resolving the 1st order of the 640Å repeat in collagen. Their longest camera used a crystal cut at 7^{o} to the reflecting planes and placed 60 cm from the source. The specimen film distance was 186.5cm.

The following sections consider the separate parts of the camera in more detail.

2.4 Construction of the camera

Most of the equipment described in this section was made by our design engineer, Mr. M. Pickford. The exceptions were the guard slit, supplied by Beaudouin, the magnetic bases supplied by Eclipse, the monochromator turntable supplied by C.G.S, France, and the micromanipulator for the collimating slit.

2.4.1. The Franks mirror bender

The construction of the Franks mirror bender is in principle

very similar to that described by Franks (1958). It is primarily designed to bend the mirror into a cylindrical shape by applying equal couples at either end. The mirror itself was an optical flat of crown glass 6cm x 2cm x 0.4cm. This was sometimes plated with either gold or nickel.

The bender used is shown in sectional elevation in fig.2.4 and the end view is shown in fig. 2.5. The mirror is bent by screwing in the screw. This exerts a force at A which bends the spring, thus providing a lever. The force is transmitted via point B to point C where the brass block, F, exerts a downward force on the mirror. An upward force at D is exerted by the bar, so as to provide a couple acting at C and D. Point E is also force bearing. The five force bearing points must be kept very clean and so must block F to enable free movement. With the mirror placed symmetrically in the bender, equal couples are exerted at each end of the mirror. As the mirror is bent, the distance between the bars measured along the mirror increases. The mirror slides between points D and E against the frictional forces. This will change the shape of the mirror. If the optimum curvature is approached by increasing it, then the remaining forces are outward and the curvature of the mirror is then expected to be greater at the ends than in the centre. Owing to the thickness of the mirror, this is not a serious problem, but it must be considered. In the case of the quartz crystal monochromator, it is more serious. Neglecting the frictional forces and allowing the mirror to slide freely, it is seen that the mirror will minimise its energy by taking up the form of a cylinder.

I have introduced the frictional forces because no other worker pays them any attention and presumably they are thought to be insignificant. This is not so, as can be seen by considering the case when the mirror is displaced from being symmetrically placed in the bender to a position where the couples at each end are unequal. This has been done by a number of workers, using cameras where the mirror is closer to the source than the focus, Most of them are aiming to improve the focus by making the mirror approximate more closely to the optimum shape, which is generally considered to be an ellipse, and this will be discussed in a later section. Some workers claim that an asymmetrically placed mirror takes up the form of a cubic curve which can be made to approximate to the optimum curve, which is a logarithmic spiral (personal communication).

Our problem is the shape of the mirror in the asymmetric setting. Points to be considered are the possibility of rotation about point A in fig. 2.4, the size of the forces required to exert the couple and the radius of the curved mirror. The radius of the mirror will be shown later to be of the order of 100 m, and, for a mirror unable to slip over the bars, this corresponds to an increase in length of about 1 in 10^8. Considering that the forces required to exert the couple are not very small, as is apparent by the proportions of fig.2.6, slippage will be seriously inhibited.

Other workers have made calculations based on determining what line best fits the four points where the force is exerted. It is clear that the lowest order polynomial which passes through four points is a cubic. This argument is not valid, because energy is the appropriate criterion. It

is common knowledge that forces exerted on a rod at two points can produce a sinusoidal shape, which is a higher polynomial. Any standard text, such as that by Feynman, Leighton and Sands (1964), considers this. Another argument could be put forward suggesting that the bender determines the inclination and the position of the mirror at either end. This information can be fitted to a cubic polynomial, but not a quadratic. This argument can be objected to in the same way as the previous argument. Moreover, if slippage can occur, these criteria can be satisfied by a cylindrical surface. Even in this case, rotation about point A in fig. 2.4 could modify this.

As the problem has not been solved theoretically, it is fitting to say that the improvement in the focusing properties of the mirror that occur on placing the mirror asymmetrically in the bender indicates a change in the shape of the mirror towards the optimum shape; this shape is close to that of an ellipse.

2.4.2 The monochromator turntable

A simplified diagram is shown in fig. 2.7. The main feature is the rotating table which may be turned by hand and locked in position. Once locked, the table may be rotated by means of the fine rotational adjustment. Many turns of this gives a total movement at the table circumference of a fraction of a millimetre. It is very important that there is no slack in this, so this is taken up with a spring. On the source side of the table, there are slits which can be controlled in the vertical and the horizontal directions. The monochromator bender itself is placed on the table. It is clamped by a

very simple arrangement. Screws pass through a bar which passes over the top of the bender and into screw holes C and D. A cover fits over the bender and, with the aid of ridge A, radiation hazards are much reduced. A second cover, which can be rotated according to the direction of the exit beam, is placed over the first. This also had adjustable slits for the exit beam, but, as these were found to be difficult to use, they were not used in the horizontal direction. The horizontal slits at either end could be closed to about 2mm. and they were usually used at this setting. The entrant slits were helpful in aligning the table, but the main purpose was to prevent stray radiation passing through the system. The cylindrical projection shown enables a radiation-safe join to be made with the Franks mirror bender.

2.4.3. The monochromator crystal bender

A simplified diagram is shown in fig. 2.8. The quartz crystal is first placed in the bender and the position of block E is adjusted with the screw shown. The screw shown can slide freely in part F, which is fixed to the frame of the bender. When this has been done, force is exerted at A by tightening the screw. The spring bends, providing a lever action, and transmits the force via three stainless steel balls, marked B, to the bars. These bars exert a force on the crystal at C. This is matched by an upward force at D providing a couple to bend the crystal. The separation between the upper bars is 3.89 cm. and that between the lower bars is 3.81 cm.

The problem of the resulting shape of the crystal is similar to that in the Franks mirror. Here however, the crystal is bent to a radius which sometimes is as small as 50cm., although 100 cm is more normal, so the crystal will almost certainly slide between the bars. If it increased in length without sliding then in order to produce a cylindrical surface an increase in length of 1 in 10^4 would be required. It is probable that the crystal slides, but not enough to take up a perfect cylindrical shape. The beams produced by the crystal indicate that the crystal is very close to the optimum shape. If the crystal position is approached from the underbent situation, a distortion similar to that shown in fig. 2.9 could occur. If the correct position is approached from the other direction, the distortions that are possible are quite intriguing. When the curvature of the crystal is varied about

the correct position, the changes in the beam produced could indicate the presence of distortions. The situation shown in fig. 2.9 could be as close to the optimum shape as is the cylindrical surface.

A serious problem with the bender was its sensitivity to changes of temperature. This could be due to thermal expansion or changes in the elastic properties of the spring and the quartz crystal. The problems of thermal expansion could be overcome by constructing the bender out of materials with a lower coefficient of thermal expansion. A worker has been reported as suggesting that a quartz crystal should be used as a spring (personal communication). This is a very good suggestion, since the balance between the spring and the crystal would no longer be temperature sensitive.

It is sometimes found that crystals require some time to become stable even when the temperature is steady. This could be caused by the crystal slipping between the bars or by the relaxation of frictional forces in the horizontal position adjustment of the crystal. A colleague has suggested a better system which is shown in fig. 2.10. This has the advantage of using Teflon sliding on brass, which is better than brass on brass, and applying an equal frictional force at either end of the crystal.

2.4.4. The Collimating System

The collimating slit is shown in fig. 2.11. The edges were made from tantalum and could be set at various separations up to 500 μm. The design is such that parasitic scatter is minimised.

It is important that the edges are not damaged, since this increases parasitic scatter. Owing to the soft nature of tantalum, each edge was cleaned with lens tissue until no dirt could be seen at a magnification of fifty. Any particle causes parasitic scatter. In the horizontal direction, collimation was provided by two pieces of lead with edges cut in the same way as the tantalum edges. The slit itself was mounted so as to have fine vertical and horizontal adjustments and it was placed as close as possible to the monochromator.

The guard slit, which was made by Beaudouin, was constructed in a similar way. The differences being that both the horizontal and the vertical slits were made of steel, and each of the horizontal sides of the slit had independent, very fine adjustments. The adjustment of the slit width in the horizontal direction was performed by sliding the edge in and out. The guard slit was placed as close as possible to the specimen.

2.4.5. The Evacuated Film Chamber

This chamber is important in this camera, because the specimen cell and the backstop assembly are attached to it. The apparatus is shown in figs. 2.12, 2.13 and 2.14. It is necessary to evacuate the space before the film to prevent air scatter, which can seriously darken the film in the region within about 15Å.

Fig. 2.13 shows the cylindrical chamber. A cylindrical film holder slides into this, so as to be easily removed. Focusing of the scattered radiation requires that the specimen be placed on the same cylinder as the film. The front plate is easily removeable to enable different plates, capable of use with larger specimen cells, to be put in its place. The mylar window is used because it is not a strong absorber of X-rays. At the

rear of the camera is a hole used for the purposes of alignment. There is also a fine two way adjustment within the camera. This holds a frame which supports a mylar strip, upon which is glued a lead backstop. Lead back stops were cut from sheet lead. Experience has shown that scatter of X-rays from the backstop on to the film is a serious problem. To prevent this, the backstop was cupped in the direction shown. Simple geometry shows that it is also necessary to curve the backstop slightly in the other direction. Backstop diameters of 1 or 2 mm were generally used although 5 mm was more normal when the camera was tilted for high angle reflections.

Fig. 2.12. shows the front view of the camera and is basically self-explanatory. The specimen cell support has a fine adjustment in which the slack is taken up by a spring. The specimen cell is easily removeable from this mount. The steel ball shown is directly beneath the specimen. Adjustment of the screws at the rear of the camera shown in fig. 2.14 will rotate the assembly about the specimen. If the beam is passing along the centre of the table, the central part of the table need only be slid back until the beam is again focused upon the film. The problems with this are that the backstop moves with the assembly and certain angles cannot be set without moving the table as a whole. This tilting is necessary to produce diffraction from small repeats along the length of the specimen.

2.4.6. Specimen cells.

A number of specimen cells were used. The first, shown in Fig. 2.15, was constructed from brass. It was designed to support

fibres glued between the pins at various humidities determined by a flow of air through the cell. The distance between the pins could be varied so that specimens could be put under tension. For ease of mounting, the inner part slid into the outer part. The holes marked on the diagram are to allow the passage of air. For a well controlled humidity, it is necessary to bubble air against a counter current of solution in a column filled with glass helices to maximise the contact area. (A colleague; personal communication). He also reports that air above a solution needs to be left overnight before equilibrium is reached. In my experiments, air was bubbled through water which was sufficient to make the specimen dripping wet.

The second specimen cell, shown in fig. 2.16, was constructed of perspex. The specimen was clamped in the method shown with the force being supplied by the springs. Tension could be supplied by altering the distance between the clamps with adjustments A and B. To allow easy mounting of the specimen, the front of the cell could be removed. The cell was normally used with some solution inside to keep the air at a desired humidity. It could also be used with totally immersed specimens, and the windows could be screwed very close to the specimen to allow this. The two tubes shown allow air or solution to be passed through the cell. These were normally kept sealed. Bar C joined the two clamps together, and enabled specimens to be rotated about their axis.

2,5 Theory of the Franks Mirror

The best treatment of the Franks mirror is given by Franks (1955), who describes X-ray diffraction cameras using one mirror and two mirrors.

2.5.1. Reflection of X-rays

The content of this section is mainly a summary of work presented by Witz (1969). The refractive index of a substance for X-rays is less than unity by a few parts per million (Darwin, 1914; James, 1948) :

$$n = 1 - \delta = 1 - \frac{e^2 \lambda^2}{2\pi mc^2} N f(0) = 1 - 2.72 \times 10^{10} \frac{f(0)}{A} \rho\lambda^2 \qquad (2.1)$$

where λ(cm) is the wavelength of the X-rays; ρ ($g.cm^{-3}$) is the density of the substance; A (g) is the atomic weight of the scattering atoms; f(0) is the number of electrons per atom effectively scattering in the forward direction (i.e. allowance being made for the dispersion correction). As a first approximation f(0) = Z, the atomic number of the substance.

X-rays are therefore reflected from a plane surface at glancing angles smaller than the critical angle θ_c (Compton, 1923):

$$\theta_c = \sqrt{2\delta} = 2.33 \times 10^5 \lambda \sqrt{\frac{\rho f(0)}{A}} \qquad (2.2)$$

θ_c is of the order of a fraction of a degree. For CuKα and nickel $\theta_c = 6.9 \times 10^{-3}$ rad. = 2.3'. This gives

$$\theta_c \propto \lambda \qquad (2.3)$$

Since θ_c is proportional to λ, short wavelengths present in the incident beam are eliminated by confining the glancing incidence to angles close to θ_c: the CuKβ line and the peak of the white radiation (which occurs at about 0.5Å for an operating voltage of 40 kV) are not reflected on a mirror set at an angle $\theta = 0.9 \times \theta_c$ since λ(CuKβ) = 0.9λ (CuKα). In practice, the region close to θ = 0 cannot be used, since not only is the reflected intensity low, but the reflected beam is too close to the incident beam to be separated from it.

Near the critical angle absorption in the mirror causes a decrease of the reflectivity. Prins (1928); (see also James, (1948)) calculated the reflectivity curve $R(\Theta)$ assuming Fresnel's laws to apply to X-rays, with a complex index of refraction.

$$n = 1 - \delta = 1 - \alpha - i\,\beta \qquad (2.4)$$

where α is given by equation (2.1) and $\beta = \mu_o \lambda/4\pi$ takes into account the linear absorption coefficient. (This can be found in any standard text e.g. Bleaney and Bleaney (1965)). Fig. 2.17 gives the reflectivity curves for nickel and gold films deposited by evaporation and reflecting CuKα radiation. In equation (2.1) ρ measures the density of the film, which can be different from the bulk material. Kiessig (1931) measured the density of nickel films and Rieser (1957) the density of copper films; they found them to be 10% below the corresponding values of the bulk material. The same correction is applied to the density of the gold film in fig. 2.17.

The reflectivity is not only less than unity at $\Theta < \Theta_c$, but has appreciable values at angles larger than Θ_c. This lack of sharpness of the limit of reflection makes a mirror less efficient as a monochromator. As can be seen from table 2.1, the sharpness is much greater for glass than for either gold or nickel. Table 2.1 also shows the calculated ratios of the reflectivities for the CuKβ and CuKα radiations for different mirrors set at the critical single Θ_c (CuKα): the resolution depends on $\frac{\partial R}{\partial \Theta}$ at Θ_c and on $\Delta\Theta = \Theta_c$ (CuKα) $- \Theta_c$ (CuKβ).

Witz (1969) states that the total energy reflected by a mirror is approximately proportional to $\Theta_c\, R(\Theta_c)$. This is not generally the case, as will be seen later, but this is a reasonable

index for comparison and it is obeyed precisely in the special case of a point source at the centre of a logarithmic spiral on which the mirror is placed.

It is also seen from fig. 2.17, that the distribution of intensity across the reflected beam is given by $R(\theta)$, if the X-ray source is a fine line parallel to the reflecting plane. Some indication of this non-uniformity is given by the value of $\frac{\partial R}{\partial \theta}$ at $\theta = \theta_c$: the smaller the absorption, the steeper the slope of $R(\theta)$ at $\theta = \theta_c$; the sharper the cut-off and the higher the reflectivity at $\theta < \theta_c$. Witz (1969) says that the best material for a mirror has an absorption discontinuity at a wavelength slightly shorter than that of the reflected radiation, such as nickel for Cukα. . This is true where uniformity is a requirement.

Since the angle of incidence is small, any imperfection of the reflecting surface causes scattering of the X-rays and variations in the intensity of the reflected beam. The problem has been studied by Ehrenberg (1949), who showed that irregularities as small as 10Å in the flatness of the reflector can scatter X-rays. In practice the beam is fairly uniform to within 10%, but the width of the beam is larger than predicted by the geometry. Even a finger print on the mirror causes a detectable deterioration in the usefulness of the mirror (a colleague; personal communication). The topographic changes caused by touching the surface can be detected using X-ray reflectometry. (Franks, 1973).

Scattering is not the only problem with imperfect surfaces; interference is also serious, and the following description

of this was given by Franks (1973). The path difference introduced by an irregularity of height h_x on the reflector surface is 2 h_x sin i, where i is the glancing angle of incidence. The equivalent path difference for visible light at normal incidence is $2h_L$. For the scatter to be acceptably low, the path difference must be less than some fraction of the wavelength. For light, $2h_L$ must be less than $\lambda_{L/f}$, where λ_L is is the light wavelength and f is normally taken to be 4, 8, 10 or 20 depending on the application. For X-rays, 2 h_x sin i must be less than $\lambda_{x/f}$ where λ_x is the X-ray wavelength. For $\lambda_x = 1.5\text{Å}$, i = 25 min, and $\lambda_L = 5000\text{Å}$, $h_{x/h_L} = \frac{1}{25}$ and 2 h_x sin i = 103Å. Monitoring facilities for such surfaces are being set up at the National Physical Laboratory (Lindsey,1973).

2.5.2 The symmetric Franks camera

The best account is that given by Franks (1955) in which he discusses cameras with both one mirror and two mirrors;

he aims to bend the mirror into a cylinder as a good approximation of the optimum shape, an ellipse. The last paragraph of this section, summarises some of the information from this paper. This approximation is best when the source and the focus are equidistant from the mirror.

The ellipse is seen to be the best shape by considering fig. 2.18 and applying a well known theorem in elementary geometry; all angles subtended by the foci of the ellipse at a point on the ellipse have a bisector which is perpendicular to the tangent at that point. The source S and the focus F are considered as the foci of an ellipse. It is seen that a

a point source of light at S in a reflecting ellipsoid will produce a point focus at F. In our case, we are considering the less efficient elliptical cylinder, with a very high eccentricity to keep the grazing angle of incidence below θ_c. A high eccentricity also makes the mirror shape closer to that of an ellipse.

It is seen that the grazing angle of incidence is not a constant along the mirror. This is particularly true when the length of the mirror is within an order of magnitude of the major axis of the ellipse. Under these conditions the elliptical shape is not the one that maximises the intensity. Another factor which must be considered is the source size : for large sources, an ellipse neither maximises the intensity nor produces the best focus. These problems have not been discussed, because they are not serious problems for a symmetric camera, but they will be discussed later for the asymmetric case.

Franks (1955) states that the intensity at the focus is proportional to the specific loading and the height of the source, and the greatest intensity was obtained when the nearest edge of the mirror was less than 1 cm. from the source. The maximum low angle resolution for a mirror 20 cm. from both the focus and the source is about 800 Å for a 4 cm mirror, but nearly 5000 Å for a 1 cm. mirror. The intensity decreases rapidly with the camera length and also with the mirror length, for the case of constant resolution. The maximum low angle resolution for the camera with the mirror 20 cm. from both the source and the focus occurs at a specimen film distance of 4 cm.

2.5.3 The mirror position in the bender

It has been suggested that positioning the mirror asymetrically in the bender gives a better approximation to the ellipse. Experiments with gold plated mirrors did not indicate any improvement. When glass and nickel mirrors were available, a colleague suggested trying the experiment again. When the mirror was moved in the bender about 0.6 mm towards the source, a great improvement was noticed for glass and an improvement was noticed for nickel. These experiments were done with a 200μm source and a total camera length of 50 cm with the mirror between 10 cm. and 15 cm. from the source. The experiment with glass was done by colleagues and that with nickel was done jointly by a colleague and myself; all workers agreed. This experiment was also carried out with glass, a 100 μm source, a mirror to focus separation of about 80 cm. and the mirror as close to the source as before; a similar improvement was noted for an approximately equal movement. The best estimate of the mirror displacement is 600μm; it does not escape my notice that the bar separation at one end would be 1800 μm compared with 600 μm at the other - a ratio of 3 to 1. In all these experiments there was intensity over a couple of mm. with a focused image in the centre. Only with glass did this image become a fine, well-defined line.

The bender aims to give the mirror a cylindrical shape when the mirror is placed symmetrically. As the improvement when glass was used was so significant, assume the shape is elliptical for the purpose of demonstrating the factors determining the camera geometry.

2.5.4. The focus of the mirror

I have not given a complete treatment here. This is not worthwhile until the precise shape of the mirror is known and better data are available for the variation of reflectivity with the grazing angle of incidence. When these are known, it will be a straightforward matter to provide a full treatment. For the purpose of illustrating the principles, I have considered an elliptical geometry which is by far the simplest.

Firstly consider the elliptical geometry shown in fig. 2.19. For an element, $\delta\ell$, of the mirror distance D from the focus and distance d from the source, given that the height of the source is s and that of the focus is f, we see that the size of the focus is given by

$$f = \frac{Ds}{d} \qquad (2.5)$$

In the cameras used, the mirror was always placed very asymmetrically, so that the focal size had to be reduced by collimation. Under these circumstances, consider the focal height after collimation to be F; then the height of the source used is S where

$$S = \frac{dF}{D} \quad (\text{if } \frac{F}{s} < \frac{D}{d}) \qquad (2.6)$$

For a mirror of length ℓ centred at this position, the height of the source used by one end is given as

$$S_1 = \frac{(d-\frac{\ell}{2})\ F}{D + \frac{\ell}{2}} \qquad (2.7)$$

and that used by the other end is given by

$$S_2 = \frac{(d+\frac{\ell}{2})F}{D - \frac{\ell}{2}} \qquad (2.8)$$

If $\ell \ll d$, it is reasonable to approximate the height for the whole mirror by

$$S^1 = \tfrac{1}{2}(S_1 + S_2) = \frac{(Dd + \frac{\ell^2}{4})F}{D^2 - \frac{\ell^2}{4}}$$

If $\ell << d$, this becomes

$$S^1 \simeq \frac{dF}{D} \qquad (2.9)$$

which is identical to (2.6) and is the approximation we shall use. For cases where $\ell \not\ll d$, it can be noted that a source the size of S_2 can be effectively used. In practice for a common case where $d = 2.5\ell$, the useful source size is about 1.2.S, but as the outer parts of the source are only used by part of the mirror, it would be preferable to sacrifice some size for increased brightness.

It is seen that for constant values of d, F and D in cameras of the dimensions commonly used , the power received by the mirror is dependent on the brightness of the source, rather than the size. Now it is approximately true for an anode limited by its ability to lose heat that

$$B \propto \frac{1}{\sqrt{s}} \qquad (2.10)$$

It would therefore be sensible to aim to reduce the size of the focus until s = S. If the source size is fixed, the intensity at the focus can be increased, but by a lesser amount, by increasing d until $\frac{d}{D} = \frac{s}{f}$. The total intensity is proportional to S in equation (2.6). Now it is normally the case that D is fixed by

other requirements of the camera. In this case the fraction, E, of the incident radiation that is reflected is given by

$$E \propto d \qquad (2.11)$$

Now the incident energy depends on the angle subtended by the mirror at the source and this varies inversely with d. The increase in reflected energy comes from the mirror being in a position where the curvature of the ellipse is small. It is then possible to set the mirror in a shape that deviates little from the optimum. If the beam is not limited by the size of the monochromator crystal and if monochromators supplying varying degrees of asymmetry are available, the best position for the mirror is that which gives $\frac{d}{D} = \frac{s}{f}$. Increasing the length of the mirror would also increase the intensity of the focus, but if this makes it harder to attain the optimum shape, the gains will be smaller than expected. If it is possible to place the mirror in a more symmetric position, this could be overcome.

It is interesting to consider the effect of using nickel, gold or glass. Experience suggests that glass is the best. This is partly because, owing to the small grazing angle of incidence on the mirror, the mirror subtends a smaller angle at the source. It is clear that, for the small angles concerned, the curvature of the mirror is proportional to this angle. As the initial planar geometry and a circular geometry both tend towards an elliptical geometry as the curvature decreases, glass more closely imitates the optimum shape. The decnease in the angle of incidence would be expected to lead to a decrease in the intensity produced in a strictly proportional manner. This is not the case, seeing glass not only has a higher reflectivity than nickel or gold, but it maintains this with little fall

before the critical angle is reached. There is a decrease in the reflected intensity, but less than might be expected.

This would not alone make glass better than gold or nickel, Another loss of energy with gold or nickel is parasitic scatter from the obviously less perfect surface. This can be observed with a fluorescent screen. The death knell for this plated surface is that it rapidly deteriorates in the X-ray beam - visibly so after a few months.

The answer lies in a material that is sufficiently dense to allow a high grazing angle of incidence yet has a high reflectivity and a high quality surface. With the advantages of gold and nickel, without lower reflectivities, parasitic scatter and deterioration with time, a more intense beam could be produced, hopefully by a factor of two. This problem may already be solved. A colleague reports that some groups, including his own, are using double extra flint glass with a high lead oxide content for the mirrors of standard Franks cameras (Franks, 1955).

It is useful to consider a typical camera geometry. A camera that has been set up has the monochromator centred 20cm. from the source and the focus 30cm. from this. The mirror is about 12½cm. from the source giving a value of $\frac{D}{d}$ of 4. The focal size is 240 μm leading to the height of source being used to be 60μm.

Care must be taken when using such an argument until the deviations from ellipticity are quantified. Such deviations would be likely to increase the size of the source that could be effectively used. Possibly it could be as large as 100 μm. Another factor is that the gain in intensity produced by moving a mirror to the point where $s/f = d/D$ is less; owing to

deviations in the geometry, not all of the mirror is then effectively using all of the source.

It has been suggested that a logarithmic spiral is the best shape for a Franks mirror, since it is then possible to illuminate the whole mirror at a grazing angle of incidence of θ_c (personal communication). This is not true and not merely because the maximum of the reflectivity curve is at an angle below θ_c , but because the mirror needs a very large source to use it effectively. This can be shown. In the case of reflecting crystals, de Wolff has carried out some calculations (de Wolff 1950; Wilsdorf, 1951). With a source to crystal distance of 110 mm, a crystal to focus distance of 220 mm, and an angular aperture of 3^{o}, the focal size is 20 μm and the X-ray tube focus required is 330 μm. If this is done with a mirror, there would be a similar result. If the same is done with the source, rather than the focus, as the origin of the spiral, only a small part of the source and the potential power could be used. This part of the power which can be used is the same as that part which can be used with the source at the origin, since each part of the source is only effectively used by a part of the mirror. Another factor which diminishes the usefulness of the logarithmic spiral is that the angle subtended by the source at the mirror is very small. In the

case of the camera dimensions mentioned, where the effective source height was 60 μm, the effective source subtends an angle of 5×10^{-4} rad. at the mirror. This means that the reflectivity is always close to the maximum value, even for nickel, where the reflectivity curve is strongly peaked, so there is not much gain that can be made. The worst imaginable system would be to use a logarithmic spiral with the source at the focus; this maximises the energy lost through collimation.

I conclude this section with a description of how the optimum geometry may be discovered. It is general, but all the illustrations refer to an elliptical geometry. The arguments start from equation (2.5).

The angle subtended by $\delta\ell$ at the source is $\delta\sigma$ and the angle that a line joining a point on the source to the element makes with the element is θ. For nickel, the mirror will be set so that radiation is incident on the mirror at angles a little below θ_c. (see fig. 2.17). This is done so as to maximise the reflected intensity from the mirror for the part of the source used. (In practice, the intensity would be maximised for the whole source and the brightest part would be selected by collimation; neglecting the problems of monochromatisation, this is effectively the same for a source of uniform brightness). It is seen that the power incident upon the mirror for an element δS of the source is given by

$$\delta P_i \propto \delta\sigma\,\delta S \qquad (2.12)$$

Now

$$\delta\sigma = \frac{\theta\delta\ell}{d} \qquad (2.13)$$

$$\delta P_i \propto \frac{\theta\,\delta\ell\,\delta S}{d} \qquad (2.14)$$

If we now extend this to consider a mirror of length L centred at distance d from the source, we obtain

$$\delta P_i \propto \frac{\theta \delta \ell}{d + \ell} \delta S \qquad (2.15)$$

where ℓ is the position of the element $\delta\ell$ measured from the centre of the mirror away from the source. The total incident energy is given by

$$P_i \propto \int_{-\frac{L}{2}}^{\frac{L}{2}} \int_{0}^{s} \frac{\theta(S,\ell)\, d\ell\, dS}{d + \ell} \qquad (2.16)$$

where the coordinates O and S are the edges of the effective source with O being defined as the edge nearest the plane approximating most closely to the mirror. θ (S,ℓ) depends on the material used, as this affects the grazing angle of incidence. For nickel it approximates to

$$\theta \simeq 5 \times 10^{-4} + \frac{S}{d + \ell} \qquad (2.17)$$

The total reflected energy is given by

$$P_r \propto \int_{-\frac{L}{2}}^{\frac{L}{2}} \int_{0}^{s} \frac{R(\theta)\ \theta(S,\ell)\, d\ell\, dS}{d + \ell} \qquad (2.18)$$

where R (θ) is the function given in fig. 2.17.

It is seen from equation '2.17) that the mirror is considered to be planar. This is a reasonable approximation

especially when D is large, but if the geometry is to be optimised, a better expression must be used. As a very simple example, consider the elliptical geometry of fig.2.18.

Considering the geometry of fig. 2.18. it can be easily shown that if a>>b, then the foci are a distance $b^2/2a$ from the extremities of the ellipse. For the ellipse,

$$\frac{x^2}{a^2} + \frac{y^2}{b^2} = 1 \qquad (2.19)$$

we can show that $$\frac{dy}{dx} = \frac{-b^2 x}{a^2 y} \qquad (2.20)$$

Noting that all angles of incidence are small; for a point distance $d + \ell$ from the source, the angle of incidence on an elliptical mirror is given by

$$\theta = \frac{dy}{dx} - \frac{y}{d+\ell} \qquad (2.21)$$

$$= \frac{-b^2 d + b^4/_2 a + a b^2}{a^2 y}$$

$$\therefore \theta \simeq \frac{b^2(a - d)}{a^2 y} - \frac{y}{d} \qquad (2.22)$$

Using the relationships

$$y = \frac{b}{a}\sqrt{a^2 - x^2} \qquad (2.23)$$

and

$$x = d + \frac{b^2}{2a} - a \qquad (2.24)$$

the relationship for θ can be deduced. It is, however, likely that numerical methods will need to be invoked to solve equation (2.18) since the functional form of $R(\theta)$ is not simple. The optimum geometry is then found by the simultaneous minimisation of (2.18) for all the variables. In the case of elliptical geometry, S could be set as $\frac{dF}{D}$ and F and D could be treated as constants while the system is minimised with respect to b and d. Allowance must be made for the case f = F. A further factor

needs to be included within the integral of (2.18). This allows for the fact that increasing the source to crystal separation decreases the angle subtended by the crystal at the source, and hence decreases the intensity. This function M, has a number of variables. The final form is

$$P_r = K \int_{-\frac{L}{2}}^{\frac{L}{2}} \int_{0}^{S} \frac{M\ R\ (\Theta)\ \ \Theta\ (S,\ell\ )\ d\ell\, d\ S}{d + \ell} \qquad (2.25)$$

where K is a constant.

2.5.5 The mirror as a monochromator

It was seen in section 2.5.1 that the mirror can act as a monochromator. This is a useful property, since the scattering of non-Kα radiation from the monochromator crystal is a serious problem.

Consider the well known argument repeated by Witz (1969). Since $\Theta_c \propto \lambda$ and λ(Cu Kβ) = 0.9λ (CuK α), it is necessary to set the mirror at an angle $\Theta = 0.9 \times \Theta_c$.

This argument in our situation means that the source must subtend an angle less than $0.1 \times \Theta_c$ at the mirror, that is an angle less than 1.4' for glass which is about 4×10^{-4} rad. For a mirror 12 cm. from the source, a source size of 50μm is required. This is even smaller than the effective source for the elliptical geometry shown, resulting in only some of the Cu(Kβ) being removed. Most of the white radiation, however will not be scattered.

2.6 Theory of the crystal monochromator

2.6.1 Principles of crystal monochromators

The following argument is very similar to that presented by

Witz (1969).

Consider the example illustrated in fig. 2.20: a plane crystal slab is set to reflect the radiation of wave-length λ emitted by a point source S. Only a narrow region of the crystal, limited by the circular intersections of the plane and the cones of apex S, axis SN normal to the crystal and half angles $\frac{\pi}{2} - \theta$ and $\pi/2 - \theta - \pi$ will reflect the radiation, and the divergence of the reflected beam is equal to the width η of the rocking (or reflection)curve of the crystal radiation of a different wavelength λ' and Bragg angle θ' will be reflected by another region. The crystal can be used as a monochromator only if the two regions do not overlap, and this condition sets an upper limit to η :

$$\eta < | \theta - \theta ' | \qquad (2.26)$$

Since X-ray sources have a finite size SS', the condition applies to the sum $\eta+\alpha$, where α is the angular width of the source determined from the reflecting region of the crystal:

$$\eta + \alpha < | \theta - \theta' | \qquad (2.27)$$

This condition is set by the need for one part of the crystal not to reflect the different wavelengths. If the Kα doublet is to be resolved into its components, $\eta+\alpha$ is limited to $\Delta\theta = \theta ' (K\alpha_2) - \theta (K\alpha_2) = (\lambda ' - \lambda) \lambda^{-1} \tan \theta$. For a given monochromator material, $\Delta \theta$ is a constant for Kα wavelengths between 0.5Å and 2.5Å and Bragg angles smaller than $\theta = 30^{o}$ (Sandström, 1957): for (101) quartz, $\Delta\theta = 6 \times 10^{-4}$ rad. Some examples of $\Delta\theta$ are given in table 2.2.

Considering that the size of the focus achieved is about 50 µm, it would be reasonable to sacrifice some of the fineness of focusing in order to increase the intensity. This is also

discussed by Witz (1969) and the argument (abridged) is reproduced below. My comments are in parentheses.

A distinction must be made between the height of the rocking curve, the reflectivity, and its area, the integrated intensity. The intensity of the reflected beam is proportional to the latter only if the angular width of the source is larger than the mosaic spread η. (This is the case with the cameras used). If the source is small ($\alpha << \eta$) the intensity is determined by the reflectivity.

Renninger(1956) calculated the integrated intensities R_m and R_p for the mosaic (ideally imperfect) and perfect states of some crystals mechanically suitable as monochromators: the area of the rocking curve is measured in radians in Darwin's formula, since the variable of integration is the angle of incidence (James, 1948). It will be seen from Table 2 that mosaic spreads close to $\eta = 5 \times 10^{-4}$ rad, which are necessary for α doublet resolution, are of the order of, or smaller than, the values of R_m, and are only a small multiple of the width $0.75R_p$ (James, 1948) of the rocking curve for the perfect state. (It is seen that quartz is suitable even in the mosaic state.)

Extinction is therefore the predominant factor determining the shape and area of the rocking curve (For a comprehensive account of this see James (1948), and for a comrehensible account, see Woolfson (1970)). Bacon and Lowde (1948) calculated the rocking curves for crystals having negligible primary extinction, and a Gaussian mosaic spread of standard deviation $\bar{\eta}$. They found the reflectivity to vary by a factor 3 if $R_m/\bar{\eta}$ increases from 1 to 20. If absorption is negligible, the height is unity over the range η and the area is η . This

behaviour is very similar to that of the integrated intensity R_p for the perfect state which varies only by a factor 2 as R_m varies by a factor 20, for the reflections examined by Renninger (1956).

For quartz crystals and $CuK\alpha_1$ radiation, reflectivities as high as 25% (Fournet, 1951) or 50% (measured by H.Huxley; reported by Witz (1969)) have been measured, although a curved quartz crystal does not reflect more than 7% of the $CuK\alpha_1$ component of the incident beam emitted by a semi-microfocus X-ray tube (Witz, 1969), the loss of intensity is entirely caused by the geometry of the incident beam which fits only approximately that of the object caustic of the curved monochromator crystal (Fournet, 1951). Here ends the account adapted from Witz. (1969)

The surface of the monochromator is very critical. If consideration is given to section 2.5.1, it is seen that the effect of a surface irregularity increases with the grazing angle of incidence. It is possible to provide quartz with what is known as a corona finish, but the advantage of this must be considered together with the changes in the rocking curve. Sakisaka (1930) found that the effect of the same surface treatment given to different crystals varied widely. For quartz, grinding with fine emery poweder increases both the height and the width of the rocking curve - the height by about 30% and the integrated intensity by a factor of two or three; this gain is caused by the surface being broken up enough for primary extinction to become negligible. Quartz plates polished, as ours are, to optical transparency, gave the same integrated intensity as etched ones. (Sakisaka (1927, 1930)).

Some interesting work was done by White (1950). Bending quartz

crystals induces strain which increases the ability of a crystal to diffract by up to over 20 times in integrated intensity. The value gradually increases from the value for the perfect state. This is of interest to our case although knowledge of the reversibility and magnitude of the effect is required.

Polarisation at the monochromator does not cause a serious loss of intensity, but it must be considered in accurate intensity measurements (Witz. 1969). The spectral composition of the reflected beam is pure, since the higher harmonics of $CuK\alpha_1$ are eliminated at the Franks mirror along with the white radiation at short wavelengths.

2.6.2 Curved crystal monochromators

A complete account is not given here. This is partly because Johann (1931) has given a lucid, rigorous and comprehensive account of the subject. Johansson (1933) produced an excellent account in which he extended the work to crystals which were first ground to a radius of 2R and then bent to a radius of 2R giving the surface a radius of R. I have given a semi-qualitative account which should enable the basic principles to be understood.

In the following, the absorption is considered to be sufficientl high in the region of $\lambda(CuK\alpha)$ for only the surface to be considered. This is a reasonable approximation, but see White (1950).

The crystal is bent to a shape which is closely cylindrical. Ideally for a point source, the crystal would be bent to a logarithmic spiral with the source as the origin, such that radiation is incident along the whole length at the same angle.

This is the system of de Wolff (1950) in reverse. This crystal would have to have a relatively small angular aperture to maintain a small focal image. As it is, we do not have a point source, so we can use a larger part of the source. The system by de Wolff (1950) required a source size of 330 μm to produce a size at the focus of 20 μm. This system will transmit the same amount of energy as the one where the source and focus are interchanged, assuming a constant source brightness. Moreover, using a 330 μm source makes it impossible to separate CuKα_1 and CuK α_2 for the camera dimensions given by de Wolff. The system with the source at the origin of the spiral has one advantage over a cylindrical crystal, and that is that the angular aperture is not limited by the rocking curve.

The crystals used were cut at an angle to the surface. For specimen film distances of less than 30 cm., a 3° cut was used and for longer distances a 6° cut. The reason for doing this is to increase the intensity of the beam at the focus without changing the separation of the crystal and focus. This was first done by Guinier (1946). Guinier's initial work was carried out with the following values: 2R = 500 mm, $\alpha = 7^{\circ}$, SC = 55cm and CP = 170 mm, where 2R is the radius of the bent crystal, α is the angle the surface makes with the reflecting planes, SC is the source to crystal distance and CP is the crystal to focus distance. Guinier also compared the Johann arrangement (i.e. a bent plane crystal) with the Johansson arrangement (a bent curved crystal) for a value R = 600 mm; he found the Johansson arrangement allowed an angular aperture of about 3° compared with 1.5° for the Johann arrangement. There

was an increase in intensity at the focus by a factor of 2.2 and the focus was nearly as fine.

A description of the principles of this system was given by Guinier et al (1955). A diagram illustrating the principle is given in fig. 2.21. The dotted lines added indicate how Guinier must have arrived at his relationship.

$$\frac{SC}{CF} = \frac{\sin(\theta - \sigma)}{\sin(\theta + \sigma)} \qquad (2.28)$$

where the symbols are defined in the diagram.

It was stated that the asymmetric cut of the crystal was useful in increasing the intensity at the focus, and this can be shown by simple geometry. CF is the dimension that is fixed by the need for resolution of the X-ray pattern, so we consider it to be a constant. Using the symbols from fig. 2.21

$$SC.\alpha = \ell \sin(\theta - \sigma)$$

$$CF.\alpha = \ell \sin(\theta + \sigma)$$

It is necessary to maximise α. If ℓ is fixed, this is done by making σ as large as possible; values up to 10 degrees have been used, which is close to the upper limit of θ, which is 13^{o} 21' for the quartz planes used. It is seen that increasing the length of the crystal also increases the intensity. This is limited by the need for the crystal to be short enough for radiation to be incident at very nearly the same angle along its length. If this is not satisfied, not all of the crystal would be reflecting and in a more serious situation $K\alpha_2$ would be reflected.

2.6.3 Focusing geometries

This section is an abridged version of part of the work

published by Witz (1969). My comments are in parentheses or otherwise referenced.

The geometrical aberrations define the size of the focal image and that of the effective source. Where the crystal is cut at an angle σ to the reflecting planes, the X-rays from this source strike the monochromator surface at an angle within the interval $(\theta - \sigma, \theta - \sigma + \eta)$.

Fig. 2.22 shows the geometry for the surface reflection (Johann, 1931) arrangement. The plane of the figure is perpendicular to the crystal bent to a radius R; the incident and reflected beams are tangents to the source caustic circle of radius $R \sin(\phi + \sigma)$ and to the object caustic circle of radius $R \sin(\phi - \sigma)$ respectively. Both circles are concentric with the crystal circle. For a narrow region of the crystal centred at C, the focal circle of diameter OC = R, tangential at C to the crystal circle, intersects the caustics at the source S and the focus F: $SC = R \cos(\phi + \sigma)$ and $CF = R \cos(\phi - \sigma)$; $\phi = \pi/2 - \theta$. Also notice in the figure that M is very close to the focal circle: $\hat{MFC} = \hat{MSC} = \omega$: the angular apertures of the incident and reflected beams are both equal to the corresponding aperture of the crystal and they do not vary with the angle σ if the radius R of the crystal remains constant. This is equivalent to my deduction in the last section that, for a constant CF, ω is maximised by maximising σ.

The effective width of the source in the Johann arrangement, measured along OS perpendicular to the source to crystal distance SC, is determined as follows: $\Delta_1 S = \frac{1}{2} R\omega^2 \cos(\theta - \sigma)$ corresponds to the geometrical aberration shown in fig. 2.22. The reflection curve contributes $\Delta_2 S = \eta . CS$. A further increase is caused

by the finite width $\Delta\lambda$ of the characteristic line reflected by the crystal, and the correlative thickness of the caustic: $\Delta_3 S = R\Delta\lambda/\lambda \sin(\phi - \sigma) \tan\theta$. The effective width of the X-ray tube focus for a beam of convergence 2ω is given by

$$\Delta S_e = \overline{SC}\left[\eta + \frac{\omega^2}{2}\cot(\theta - \sigma) + \frac{\Delta\lambda}{\lambda}\tan\theta\right] \qquad (2.29)$$

For a perfect quartz crystal reflecting $CuK\alpha_1$ on the (101) planes, $\theta = 13^{\circ}21'$ and $\eta = 3.2 \times 10^{-5}$ rad. Compton & Allison (1935) give $\Delta\lambda$ as 5.8×10^{-4} Å. For the camera dimensions used for much of my work, where, as stated before, $\overline{SC}$ = 200 mm and $\overline{CF}$ = 300 mm, ΔS_e is about 50 µm. It is seen that the source size required increases as the value of σ increases and increases proportionally with $\overline{SC}$. The width of the focal spot, measured along OF perpendicular to CF can be obtained in the same way:

$$\Delta F_e = \overline{CF}\left[\eta + \frac{\omega^2}{2}\cot(\theta+\sigma) + \frac{\Delta\lambda}{\lambda}\tan\theta\right] \qquad (2.30)$$

For the camera measured this is 60 µm, which is also the width measured at the film. This also indicates that the crystal geometry is very closely cylindrical. When narrower beams were used, 40 µm, was measured.

One point not mentioned by Witz (1969) is the restrictions imposed by the need to resolve $K\alpha_1$ and $K\alpha_2$. If ω is increased, a larger source must be provided, so that radiation is incident on the whole crystal at grazing angles of incidence between θ and $\theta + \eta$. After a certain point this allows α_2 to appear. Using the following figures from Compton and Allison (1935)

Wavelength $CuK\alpha_2$ = 1.544 Å
Wavelength $CuK\alpha_1$ = 1.540 Å
Width at half maximum for $CuK\alpha_2$ = 7.7×10^{-4} Å
Width at half maximum for $CuK\alpha_1$ = 5.8×10^{-4} Å

We find that the angular separation of $K\alpha_1$ and $K\alpha_2$ at the crystal is 5.9×10^{-4} rad. To allow for the line width, it is reasonable to set an upper limit of 6×10^{-4} rad. to the angular range accepted by the crystal. Again using the same camera dimensions it is found that the maximum permissible aperture corresponds to a source size of 100 μm. With larger sources, the effective source must be so positioned on the total source that the $CuK\alpha_2$ does not appear.

2.6.4 Parasitic Scatter from the Monochromator

This is a serious problem which can be overcome in two ways. Fournet used two crystals such that the focus of one was the source for the other (Guinier, 1955). In this case the second crystal was supplied with monochromatic radiation and the parasitic scatter was limited to within ten minutes of the main beam. In our case, partial monochromatisation was supplied by the Franks mirror and the area affected was reduced by guard slits. The method of using guard slits was also adopted by Guinier (1955).

2.7 Collimation

This section is similar in many ways to a discussion given by Guinier (1955), but as it was derived independently and contains differences, he cannot accept responsibility for it. I have considered the collimation in the Franks mirror direction in the first sub-section, and in the second, the collimation in the other direction is considered.

2.7.1. Collimation in the vertical direction

The beam from the crystal is relatively narrow in the vertical direction defined by the Franks mirror and it is about 7mm wide in the horizontal direction on leaving the crystal. Vertically the beam may be either divergent or convergent, depending on the asymmetry of the Franks mirror position; in any case, it is almost a parallel beam. The system is shown diagrammatically in fig. 2.23. The collimating slit reduces the size of the beam to a size generally between 100 μm and 300 μm, and the guard slit is set so that the beam just misses it; the relative dimensions of the two slits are, of course, dependent on the degree of convergence or divergence of the beam. However, parasitic scatter from the first slit and also from the crystal is defined by XA and YB. As the parasitic scatter from the crystal is very strong, the region AB cannot be used for data collection, especially for weakly diffracting specimens. This distance y is found by simple geometry to be

$$y = \frac{D}{d} (w + x) + x \qquad (2.31)$$

Given that D = d, s = 11cm, w = 200 μm and x = =40 μm, we obtain

$$y = 2 (w + x) - w$$

$$= w + 2x$$

$$= 700 \ \mu m.$$

This corresponds to a largest resolvable spacing of 470 Å. In practice, allowing for a clear resolution between the reflection and the focus, 235Å would be more reasonable and this corresponds well with practice. Even this limit is difficult to obtain, owing to the problems associated with back-stop construction. It is necessary to cup the backstop to prevent the beam scattering from

the backstop on to the film; the parts of the film closer to the front than the sheet lead back-stop are the most vulnerable. The smallest back-stops successfully used, blanked out the centre of the film to 300 Å and often for ease of construction, back-stops over 2mm across were used, which masked the film out to 150 Å. The back-stop problem is technically soluble. At higher angles a 200 μm focus is adequate for resolution in exeess of 400 Å, 200 μm corresponding to a separation of 825 Å.

2.7.2. Collimation in the horizontal direction

In the horizontal direction there is a strongly convergent beam, so collimation is more difficult. This system is shown in fig. 2.24. The collimating slit normally just touches the beam and only when a narrower beam is required is it adjusted so as to just miss the beam. Parasitic scatter from the crystal and the collimating slit is defined by the dotted lines. This is a good approximation when the collimating slit does not cut the beam and it is precise when it does so by more than a small amount. The region affected by parasitic scatter is given by the relationship

$$r = \frac{D}{d} (p + q) + q. \qquad (2.32)$$

which is analogous to (2.31).

When beams that are highly convergent are used, this normally results in scatter out to about 30 Å, although figures around 70Å to 100 Å were commonly obtained using narrow beams. It is possible to use the outer part of the streak for data collection, since this is produced by a small part of the monochromator, whereas the centre of the pattern, collects parasitic scatter from

the whole crystal.

It is easy to see that reducing the beam width by means of a variable slit placed near the source would be a more effective means of controlling the width of the beam; it would commonly decrease the area affected by parasitic scatter by about 20 per cent, since d is effectively increased. For a collimating slit placed 5 cm from the centre of the crystal and for d = D = 10 cm, the length of the parasitic scatter streak is decreased by a third by collimating before the crystal. Parasitic scatter is also decreased by decreasing the amount of non-useful (e.g. non Kα) radiation incident upon it; this could in part be achieved by slits adjustable vertically placed near the source.

2.8 Focusing of the diffraction pattern

In the vertical direction the beam is defined by the collimating slits. There is no focusing, just a defocusing caused by striking the film at an angle. For a beam with a vertical component of angular deviation at the specimen of ε, the focus is broadened by a factor of sec ε, for a specimen of insignificant size.

In the horizontal direction, the scattered radiation focuses on the cylindrical film as shown in fig. 2.25; this is a standard technique (Guinier, 1955). The convergence of the scattered beam cannot be changed at the specimen, so the reason for using cylindrical geometry becomes obvious, since an arc of a circle subtends equal angles at all points on that circle outside the arc itself.

There are three factors that would increase the size of the focus at the film: the specimen size, the angle of incidence

that the beam makes with the film and the effect of the specimen not following the cylinder. Bending specimens around the circle makes a significant improvement at high angles. The effect of specimen size is illustrated in fig. 2.26. The treatment given is illustrative and refers to the total width at the focus, not the standard deviation. It is seen that the increase of the width of the focus, f_s, is d sin (γ+ β)/sin.β so that

$$f_s = d(\sin \gamma \cot \beta + \cos \gamma) \qquad (2.33)$$

This is often an important factor. If d = 0.5mm and $\gamma = \beta = 30^o$, $f_s \simeq 650$ μm, which is an order of magnitude higher than the focal size obtained with a specimen of infinitesimal size. It also illustrates the need to use small specimens for high angle work.

The effect of the specimen curvature would not be expected to be large. The major problems are that for highly oriented specimens, not all of the specimen would be scattering X-rays, and for specimens with large unit cells, unwanted reciprocal lattice points make their contribution to the pattern. It is seen that working with a disoriented specimen with a large unit cell verges on the impossible. The problems mentioned could be corrected by giving the specimen a radius of curvature equal to twice that of the focusing cylinder. This would also half the deviation of the specimen from the cylinder. Another way of improving matters is to decrease the convergence of the beam. The improvement with curved specimens needs an explanation so one is given below. As the angle of scattering is a constant, the maximum widening of the beam is caused by scattering from the

specimen at the point where it deviates most from the cylinder. From fig. 2.27 it is seen that the increase in focal width, f_c, produced by the specimen not being curved is t sin $(\gamma + \beta)/\sin \beta$. The distance t is found to be $R - R \cos \sigma \simeq \frac{R\sigma^2}{2}$ so

$$f_c = \frac{R\sigma^2}{2} \quad (\sin \gamma \cot \beta + \cos \gamma) \qquad (2.34)$$

If R = 5 cm and $\sigma = 2 \times 10^{-2}$ rad, this gives $f_c \simeq 13$ μm, which is a small effect. This suggests that this factor is small except at very high angles and high beam convergence. The latter explanation is reasonable. The effect of the factor is to give the specimen an effective width, d_e, given by

$$d_e = d + \frac{R\,\sigma^2}{2} \qquad (2.35)$$

Another quantity f_b must be defined as the width of the unscattered beam as measured on a plane at the focus and at right angles to the beam. From fig. 2.27 it is seen that the beam makes an angle $\pi/2 - \gamma$ with the film. This increases the width of the focus by a factor of sec γ.

The final focal width f is given by

$$f = (f_b + f_c + f_s) \sec \gamma \qquad (2.36)$$

f_c is generally small, f_s dominates at high angles, especially for thick specimens, and f_s dominates at low angles. A surprising fact is that, after taking into account specimen absorption, the specific intensity at high angles, particularly below 2 Å, is maximised by specimens of less than 100 μm thickness. The optimum value is obtained by evaluating

$$\frac{\partial}{\partial d} \left\{ \frac{d}{f} e^{-k\,d} \right\}$$

where the factor $e^{-k\,d}$ takes account of the specimen absorption.

$e^{-k\,d}$ approximates to 1 - kd in this example.

2.9 Camera design

This section is a summary of some results from earlier sections. It is primarily designed to enable those who have faith in the derivations to build a good camera system.

2.9.1. Maximising the intensity

In earlier sections it was discovered that the position of the Franks mirror in the camera had only a small effect on the intensity in the conditions of asymmetry prevailing. It was found that moving the crystal towards the source did have a significant effect on intensity. The best situation was with the Franks mirror very close to the source so as to allow the crystal to be placed very close to the source. Different camera lengths can then be provided by choosing crystals with varying angles between the surface and the reflecting planes. Reduction of parasitic scatter was found (theoretically) to be brought about by fixing a two-way adjustable slit between the mirror and the source; this is especially apparent when it is necessary to reduce the width of the beam. Concentration on working out a method to make the Franks mirror more precisely elliptical would also be worthwhile.

On these bases, I suggest a source to the centre of the mirror distance, SM, of 7 cm. and a source to the centre of the crystal distance SC, of 14cm. These are about as short as these distances can be conveniently made. Even though a maximum beam divergence of 3×10^{-2} rad. can be achieved (Guinier, 1946), it

was shown that it is advantageous to restrict this to about 2×10^{-2} rad. These two figures would require Franks mirror slit widths of about 2.7 mm. and 1.8 mm. respectively. If slits are interposed between the mirror and the source, a standard 3 mm. would be more than adequate.

Another factor to be considered is the quartz crystal. The length is such that the maximum beam convergence is not used. With a 3^{o} crystal 14 cm. from the source, an angle of convergence of 2.2×10^{-2} rad. is possible, but with higher angles of cut, the convergence is below the optimum range. As most of the work was done with a 3^{o} crystal, this was not of great concern, but it is useful to consider how to solve the problem for higher angles. It seems reasonable to give the bars bending the crystal extra support, so that a central part about 1mm. wide can be largely filed away, as in the Franks mirror. It is simple to see the effect of bars of thickness h holding a crystal of cut σ with a bar separation of d. The useful length of the crystal becomes $d - h (\cot (\theta-\sigma) + \cot (\theta + \sigma))$, where $\theta = 13^{o}21'$. Reducing the bar thickness by half, as in the Franks mirror, allows a convergence angle of 2×10^{-2} rad. to be used with crystals cut at angles as high as 6^{o}. To extend this to 10^{o}, either the angle of convergence must be decreased, or the crystal must be doubled in total length and the bender increased in size.

Assuming that air absorption is not serious and for a fixed mirror position, the intensity at the focus is simply dependent on the angle of convergence; this can be maximised by using a suitably long crystal as close as possible to the source. This means that, providing air absorption can be reduced, fairly short

specimen-film distances can be used with long crystal to focus distances, allowing good control of parasitic scatter. This argument is not as simple as it may appear if only part of the source is effectively used (section 2.6), as is true except for fine-focus X-ray generators. In this case, moving the crystal closer to the source reduces the fraction of the source used, cancelling other benefits.

Clearly, intensity increases with the source brightness.

2.9.2. Other considerations

Other considerations are concerned with maximising both low and high angle resolution. The low angle region is masked by parasitic scatter. For the best elimination of this, the distance between the two slits should be large compared with the distance between the guard slit and the film; for my work, it was found convenient to make these distances equal - for an 11 cm. specimen to film distance, a 30 cm crystal to focus distance allows the slits to be 14 cm and 28 cm from the focus. It must be borne in mind that the Franks mirror often produces a diverging beam, resulting in a loss of intensity as the crystal to focus distance is increased.

The resolution is also dependent on the specimen to film distance. More surprisingly, if resolution only in the direction defined by the crystal is considered, the shortest exposure times do not correspond to the maximum angle of convergence and making the specimen film distance large enough to resolve the reflections. Using equation (2.30) this is maximised by setting:

$$\frac{\partial}{\partial \omega} \left(\frac{\omega}{\Delta F_e}\right) = 0 \qquad (2.37)$$

This gives

$$\omega = \frac{2\eta \frac{\Delta\lambda}{\lambda} \tan \theta}{\cot (\theta + \omega)} \qquad (2.38)$$

which is about 0.35° for $\omega = 3^{\circ}$.

Generally it is required to maximise the intensity rather than the resolution, as the resolution is more often limited by the mirror focusing and collimation.

There are other reasons for using smaller angles of convergence. Highly oriented specimens cannot usefully use high angles, and large unit cells and small specimens require smaller angles.

It is interesting to examine the asymmetry of the camera. A 3° crystal would allow a crystal to focus distance of 21 cm. This would be most suitable for specimen film distances of 6 cm. or less; this allows the guard slit to be placed at least as close to the film as to the collimating slit. A 6° crystal would allow a crystal to focus distance of 35 cm which is ideal for specimen film distances up to 13 cm. Beyond 7° a larger crystal and a different bender design are advisable; air absorption between the two slits also becomes a problem. However, having solved these problems and placed a 10° crystal 16 cm from the source, a crystal to focus distance of 110 cm is obtained. Because the parasitic scatter is not focused, it is often possible to use a specimen film distance of a metre and not use a guard slit. The relative intensity of the focused to the unfocused radiation increases with the specimen film distance. If parasitic

scatter needs to be removed, a specimen film distance as high as 50 cm. could be used.

2.10. Setting up the camera

Much of the material in this section was taught to me by A. Miller. To avoid taking undue credit and to cater for those who prefer experience to youth, an account of both the methods of myself and a colleague is given. Techniques I have developed are all simple, so it is likely that workers elsewhere have used some of them.

Before setting up the camera, pressure bearing points in the benders should be cleaned, care being taken not to touch the mirror and crystal surfaces.

2.10.1. The Franks mirror

Before setting the mirror, a length of tubing should be fixed to the X-ray tube window so as to allow a beam to be taken off the anode at an angle of about 4.5^{o}. The generator is then put on to low power for setting the mirror. The brass guard is fitted over the end of the mirror bender. This fits over the tube leading from the X-ray window. Care is taken that it is fitted such that the mirror is still free moving and such that room is left for the mirror to be placed asymmetrically in the bender, setting the bars as in fig. 2.28. I prefer to set the mirror at an initial angle of $4\frac{1}{2}^{o}$ but a colleague prefers to find the angle by rotating the mirror until the beam produced is at its maximum intensity. The mirror is adjusted heightwise and horizontally until the widest bright beam can be seen on a fluorescent screen

placed near the mirror. Rotation is not normally necessary, but this is easily checked by sliding the bars in and out one at a time; the widest beam should correspond to both bars being completely inserted. The technique preferred by a colleague consists in finding the widest beam without recourse to moving the bars.

When the mirror is in position, X-ray shielding is put in position and the fluorescent screen is placed in a position near where the intended focus is to be. The bar nearest the source is then rotated to the position shown in fig. 2.29. On moving the mirror bender up and down in the vertical direction, two beams appear on the screen, the lower one being the reflected beam and the upper one being the beam passing the mirror. The separation is made as great as possible before the intensity of the reflected beam drops noticeably; this is more easily done with a glass mirror than with a nickel or a gold mirror. When this has been done the bar nearest the source is rotated until the upper beam disappears leaving the reflected beam at its original intensity; the way this happens is shown in fig. 2.30. The mirror is put in a number of positions for testing the quality of the focus. The final position is normally displaced 0.5 mm. towards the source. Experiments with asymmetrically placed mirrors were carried out by a colleague before I used the technique. For each position tried, the curvature of the mirror is adjusted to give the best possible focus on the fluorescent screen.

It should not be expected that a fine focus should be produced, especially for highly asymmetric mirror positions. The

surface is also very important - only with glass could a fine line be produced and this was superimposed upon about 2 mm. of background. With nickel and gold it is not easy to decide on the best focus.

2.10.2. The monochromator crystal

Sections 2.4.2 and 2.4.3 describe the monochromator bender and its supporting turntable. With reference to these sections and with the aid of a microscope, the crystal can be placed symmetrically in the bender.

There are two approaches to setting the monochromator turntable in position: that of a colleague rests heavily on examining the beam reflected from the crystal and adjusting the table position until the best beam is obtained; my method which I describe, concentrates more on aligning the table before the crystal is bent.

The monochromator table is adjusted in height until the cylindrical lip on the source side fits into a brass cover on the Franks mirror, giving a radiation free fit. The structure supporting the slits on the side of the table nearest the source allows the table to be placed squarely against the Franks mirror, care being taken that the brass cover on the mirror is not pushed tightly against it, as this inhibits movement of the mirror. The horizontal slit on the table is made as narrow as possible - about 2mm. - and the height is adjusted until the beam passes through the centre. It is important that the beam passes along the diameter of the turntable. This is easily brought about by closing the slit plates from either side

until the aperture matches the width of the beam. From the position of the slits, it is seen whether or not the beam is passing over the centre of the table, and horizontal adjustments must be made until the beam does. It is easy to carry out these procedures using a fluorescent screen. The beam is then checked to see if it indeed does pass over the centre of the table.

The crystal bender is then taken and placed in the centre of the table. It is viewed from above and placed so that the surface of the crystal is parallel to the beam and lies along a diameter of the table. This can be checked in part by viewing the beam passing by the crystal; this will be less than half the normal width since the bending bars are obstructing the beam and half of the beam is not passing in front of the crystal at all. Small rotations of the table should have the effect of making the beam narrower; if the opposite is the case, the crystal is not parallel to the beam. The bender is now clamped to the table. Tests are carried out at this stage to see if the crystal is at the right height; only a small adjustment should be required.

It is often not certain whether the crystal is the right way round in the bender, even though the crystals are often marked to indicate it. Under these circumstances bending the crystal does not produce a widening reflected beam. This is a good indication of this, but especially for a 3^{o} crystal placed a good distance from the source, this can fail. In this case, the asymmetry of the camera is only 1.5, so reversing the positions of the source and the focus requires the crystal to be bent 1.5 times as much as normal. If the source to crystal distance is not too small, this could be done without breaking

the crystal and a focus would be produced $1.5^2 = 2.25$ times as close to the crystal as expected. Owing to the brittleness of the crystal, the following method has been adopted.

A fluorescent screen is placed close to the crystal so as to receive both the main and the reflected beams. The crystal is first rotated so that the bar farthest from the source cuts off most of the remaining main beam. The power is then switched to at least 20 KV 20mA with a 200 μm source and the room is completely darkened. Turning the turntable by hand will eventually produce the reflected Kα beam as a small point of light on the screen. The screen is then placed farther from the source and the positions of the main and reflected beams are are marked on the screen. Now the angles made by the crystal with the incident and reflected beams are measured. The grazing angle of incidence should be $(\theta - \sigma)$ where θ is 13° 21' for quartz 1C$\bar{1}$1 planes and σ is the angle of cut of the crystal, and the grazing angle of reflection is $(\theta + \sigma)$. If the reverse is the case, the crystal is the wrong way round and the bender must be turned over.

The crystal must now be bent. The method employed is basically that received from a colleague, although tests have been developed which check to see if the crystal has been overbent; these tests enable the crystal to be bent with more confience. The method received consists in watching the reflected beam widen as the crystal is bent. Eventually a uniform, symmetric beam is produced, and separation of α_1 and α_2 is achieved by observing the beam near the crystal. My method is described in detail.

The fluorescent screen is placed near the crystal at an angle such that the image of the beam is magnified about five times. The crystal is rotated by hand until the beam is seen as a fine point and the table is locked so as to allow rotation with the fine adjustment. As the crystal is rotated the fine point moves across the screen. The distance between the point where the beam appears on the screen and the point where it disappears corresponds to the length of the beam for which we are aiming. As the crystal is bent, the beam widens and since radiation is incident on the crystal at a smaller range of angles, the beam moves more quickly across the screen. If the bender is rotated such that the angle of incidence increases, the point of reflection moves from the end of the crystal nearest the source to that nearest the focus. This results in the beam moving across the screen towards the line of the incident beam. If the reverse is true, the crystal is overbent. The crystal is bent until the beam on the screen becomes wider. At this point the beam fills all of its original track and rotating the crystal through it causes it to appear briefly and then disappear. The beam should not be striking the bending bars. This can be checked by moving the crystal a small amount across the beam while looking for the shadow of the bars on a fluorescent screen. The crystal is returned to its original position unless the beam is striking a bar. In this case, the earlier procedure in setting the crystal and turntable should be repeated.

Now fine adjustments are carried out.A technique employed by a colleague consists in adjusting the crystal about the final beam until symmetry is achieved. As the crystal is rotated such

that the angle of incidence is decreased, the bright beam in the centre splits into equal parts which move towards the outside. When these have nearly disappeared, another brighter image appears in the centre and fills the original beam width, with a certain amount of non-uniformity. Continued rotation causes this to split into two parts as did the other. The first beam is α_2 and the second beam is α_1. It seems clear that this method consists of setting the angle of incidence correctly at the two ends of the crystal.

A good method is to set the crystal very close to the correct setting by aiming to set it for the region between α_1 and α_2. This is done by placing a fluorescent screen at the focus at an angle to the beam and then rotating the crystal unti α_1 and α_2 are of equal intensity. A piece of lead is taken and moved in front of the crystal to ascertain whether the α_2 is incident on the source end or the focus end of the crystal. As the α_2 corresponds to a greater deviation, it also corresponds to a greater angle of incidence on the crystal. The crystal is then bent or unbent until α_1 and α_2 are reflected weakly from both ends of the crystal. Now only an extremely fine adjustment is necessary. The aim is to obtain a uniform bright beam that corresponds to the presence of no α_2 in the beam, as determined by a fluorescent screen at the focus and one placed near the crystal. Eventually the beam is such that rotation of the crystal through the correct position causes the beam to appear and disappear and no α_2 is in the beam. It has been found that approaching the correct position from the underbent position often gives a better beam; this is probably due to distortions in the crystal. It would be expected that if higher beam

convergences were used, a less perfect beam would be produced and in that case, setting the two ends of the crystal for the same angle of incidence could be the best possible. After this, the covers are put on the table in such a way that the beam is not obstructed.

A crystal set in this way is stable in a temperature controlled environment, although small movements are common in the first few days after setting up. Small adjustments can be made by observing the beam leaving the crystal and bringing it back to the original position by a fine adjustment of the curvature.

2.10.3. The rest of the camera

The equipment used is described in section 2.4.4.,5, and 6. Firstly the table is set so that the beam passes along the central line. The evacuated chamber is placed on the table so that the position can be refined by aligning the beam with the centre of the mylar window and the centre of the alignment hole. This requires adjusting the position and height of the three legs of the table. The central part of the table slides back and forth. This is adjusted positionally, using a fluorescent screen, so that the focus corresponds closely to the film position. The final adjustment is carried out with a film in the camera. A through focal series can be taken, through brass for absorption, as the position is adjusted; the setting corresponding to the finest focus is selected.

The focus is now refined by putting a screen at the focus at an angle to the beam. The Franks mirror curvature is given

a fine adjustment to increase the intensity of the focus at the brightest point.

The collimating slit is set to the desired height and the width in the horizontal direction is chosen so as to either just miss the beam or to cut it. The horizontal adjustment, being a more recent development is provided by pieces of lead. The adjustments are best carried out with the aid of a microscope. The slit is then adjusted, by means of the fine adjustment available and the beam passing through it is examined with a fluorescent screen. By moving the slit up and down through the beam, it is possible to check that the slit is horizontal. Using a Geiger counter, the slit is placed as close to the crystal as possible in such a way that the intensity is maximised.

The guard slit is then positioned as close as is convenient to the specimen position. Starting with the slits wide apart and the beam passing between them, the slits are closed down until they just touch the beam. The slits can then be adjusted until the beam is just missing them. With practice the slit sides can be placed about 10 μm from the beam, but the system is not designed so that this is done easily. The slits in the horizontal direction must be adjusted by sliding them in and out so that they just miss the beam. This is difficult to do, since the camera was not fitted with adjustments to screw the slits in and out, but after a number of attempts, the slit edge can be placed very close to the beam. It is easier to adjust the horizontal position of the whole guard slit assembly to bring one side near the beam; then only one slit edge needs to be set.

The specimen is now mounted in a cell and this is supported on the front of the camera in the mount provided. For a long

well oriented specimen such as collagen, the specimen is positioned, by means of the fine vertical adjustments, such that it reduces the intensity of the beam, as measured with a Geiger counter. At low angles the maximum intensity is achieved by cutting the intensity by a factor of e (2.718) (This can very easily be proved), but at high angles, this is not the case and not just because of the longer path length of the X-rays through the specimen. (See section 2.9). For high resolution it is found that smaller specimens are better, especially at high angles. For very thin specimens and for specimens with only a small ordered area, a brass window needs to be constructed just before the specimen. This is necessary since the specimen cannot be aligned by absorption. In the case of a small specimen, in the absence of adjustments on the specimen cell, the table position is given a fine adjustment to position the beam in the chosen part of the specimen. The size of the ordered area must be borne in mind when choosing the dimensions of the collimating slit. The height adjustment is carried out to position the beam in the predetermined area.

The back stop is set by adjusting its vertical and horizontal position until the beam is striking the centre. For an untilted camera this is done with a Geiger counter, in which case it is easy to count the turns of the key between the two edges and place the beam in the centre. In the tilted case, a fluorescent screen must be used.

If a tilted camera is required, the camera is tilted after setting the specimen height, unless a window and fluorescent screen are used. This may require moving the whole table.

One or more films are enclosed in black paper and slid into

the film holder, which is then slid into the evacuated chamber. The camera is finally sealed and evacuated. A short exposure is enough to check that all is well, after which the film is changed and a longer exposure is carried out.

TABLE 2.1

Numerical data for mirrors Taken from Witz (1969)

	θ_c	$R(\theta_c)$	$\frac{\partial R}{\partial \theta}$ at θ_c	$\theta_c R(\theta_c)$	$\frac{R(CuK\beta)}{R(CuK\alpha)}$ at $\theta_c(K\alpha)$
Crown glass	14'	0.73	100	100	0.048
Nickel	23'	0.65	72	150	0.021
Gold	32'	0.45	40	140	0.13

Radiation: CuKα
Columns 3 and 4 in arbitrary units

θ, angle of incidence; θ_c the critical angle; R, reflectivity.

TABLE 2.2

Integrated intensities. Taken from Witz (1969)

	R_m	R_p	$s\theta(K\alpha_2-K\alpha_1)$
(200) LiF	9.1×10^{-4}	0.32×10^{-4}	10.3×10^{-4}
(101) quartz	4.3×10^{-4}	0.44×10^{-4}	5.9×10^{-4}
(002) graphite	62.5×10^{-4}	0.52×10^{-4}	5.8×10^{-4}

Radiation: CuKα

R_m and R_p taken from Renninger (1956)

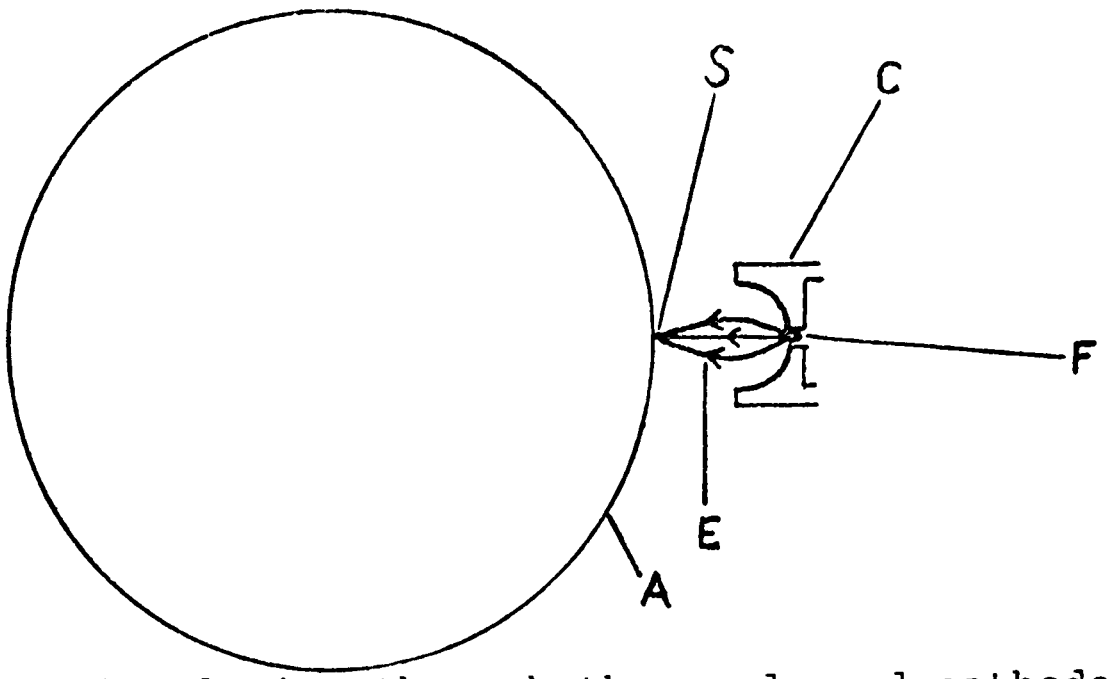

Fig. 2.1 Sectional view through the anode and cathode of the generator. A, anode; C, focusing cup; E, electron path; F,filament; S, X-ray source.

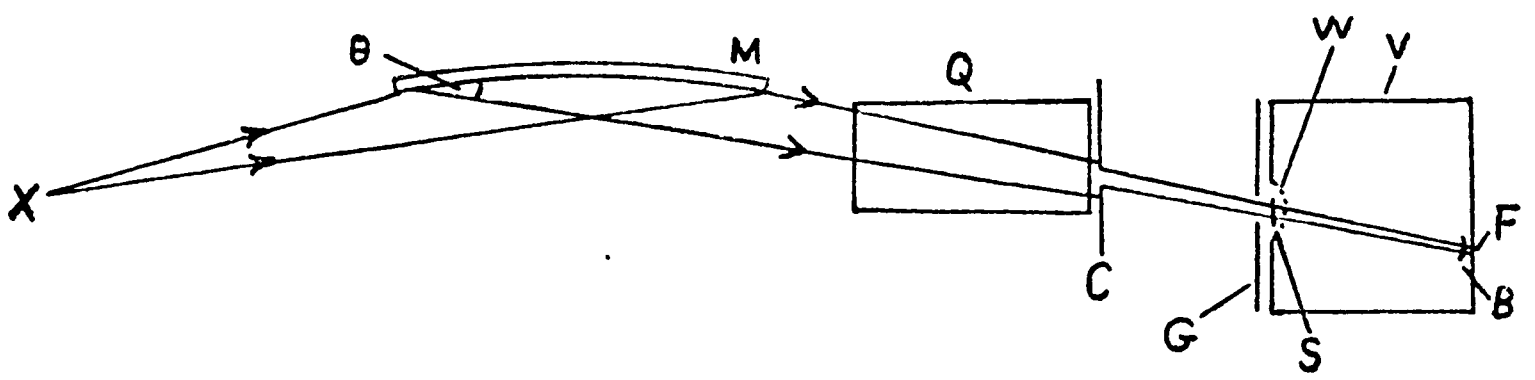

Fig. 2.2 Elevation view of the X-ray camera. For clarity, it is not to scale. In practice $\theta < 0.5^{o}$. Fig. 2.3 is closer to scale at about half actual size. The symbols are as for fig. 2.3.

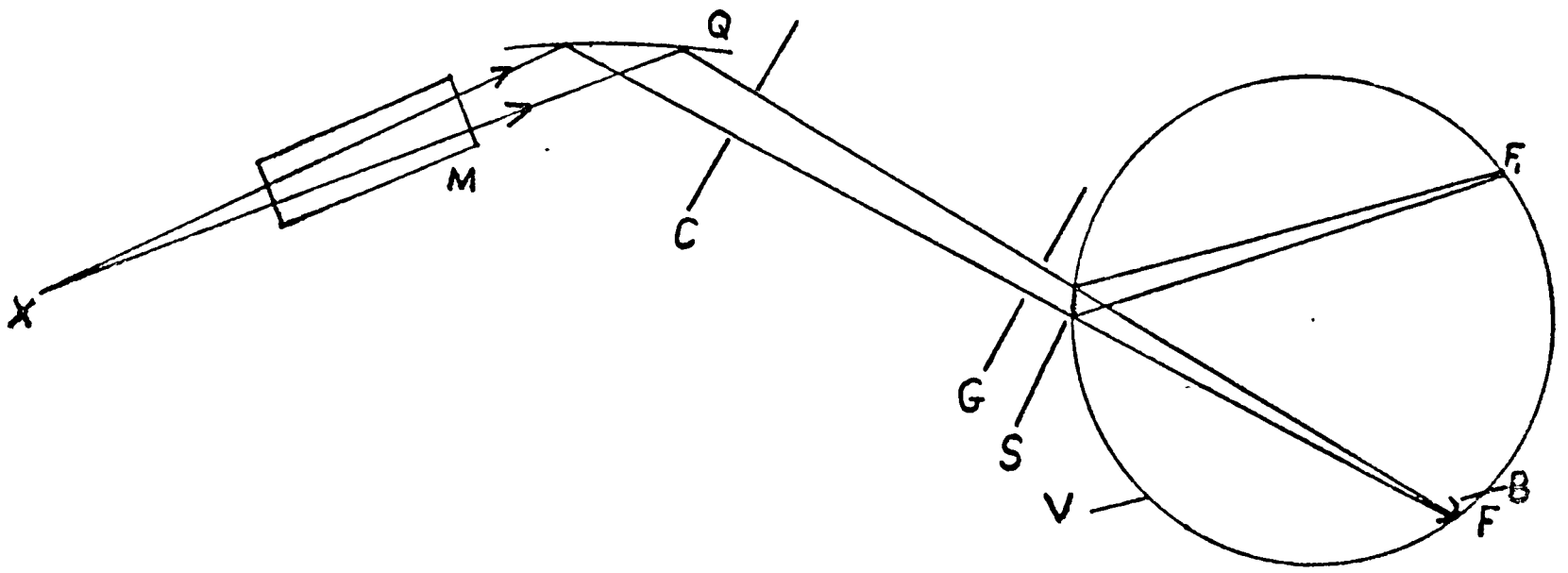

Fig. 2.3 Plan view of the X-ray camera. B, beam stop; C,collimating slit; F, focus of X-rays; F, focus of diffracted X-rays; G, guard slit; M, Frank s mirror; Q, quartz crystal monochromator; S, specimen; V, evacuated chamber; W, mylar window; X, source of X-rays.

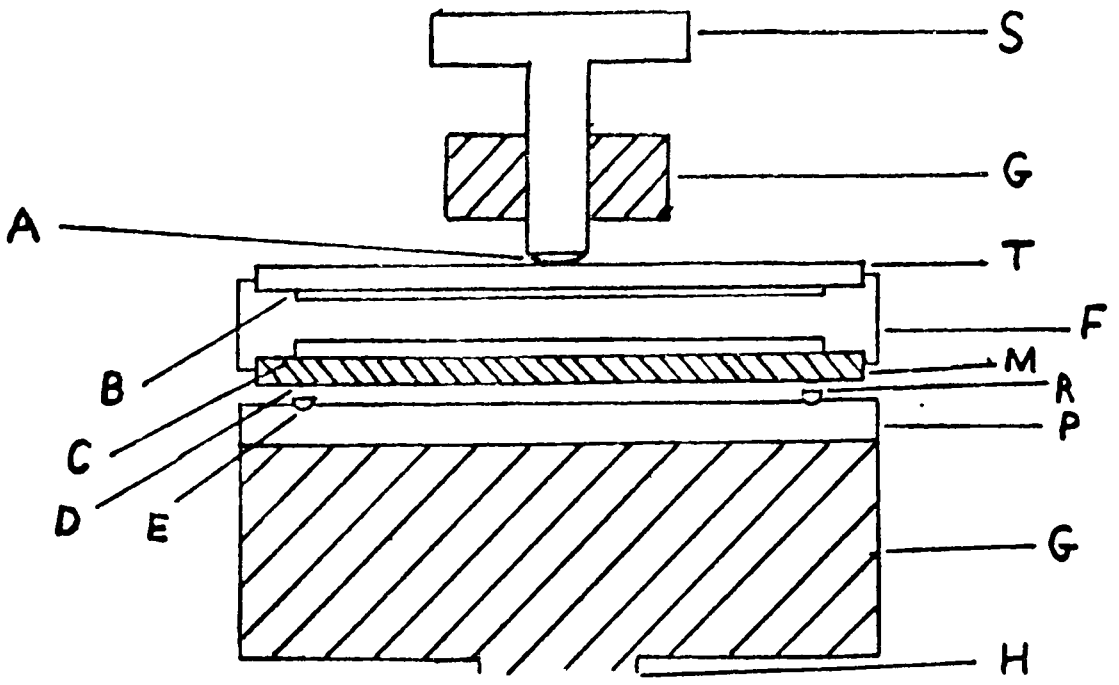

Fig. 2.4 Sectional front elevation of the Frank s mirror bender (actual size). Symbols as for Fig. 2.6

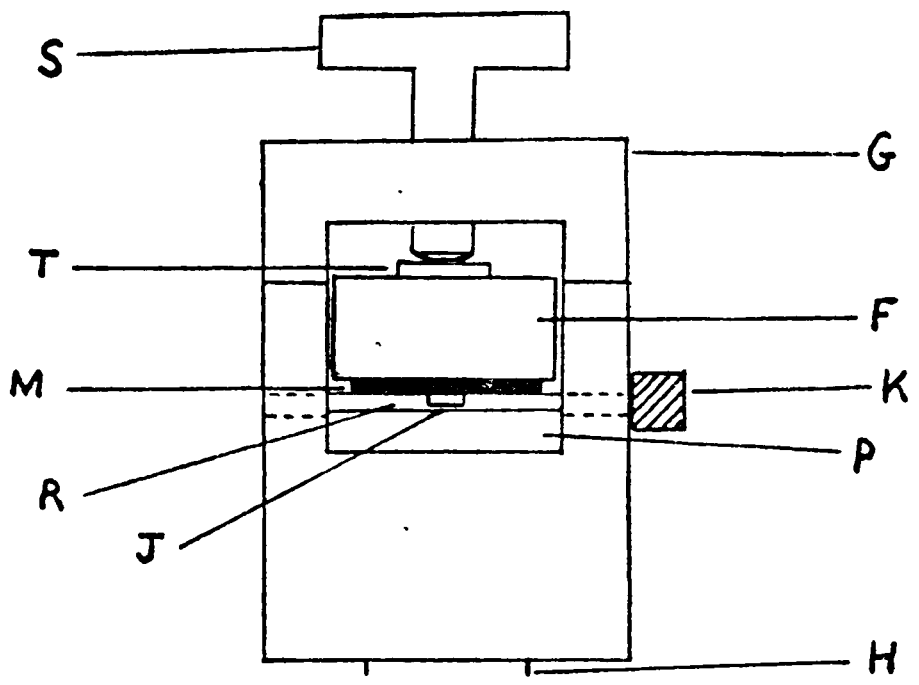

Fig. 2.5 End elevation of the Frank s mirror bender. (actual size). Symbols as for Fig. 2.6

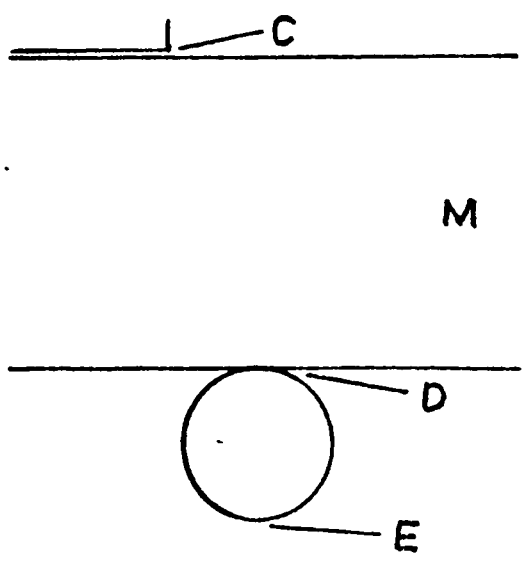

Fig. 2.6 Enlargement (7.5X) of part of fig. 2.4 for a mirror placed symmetrically in the bender. A,B,C,D,E, force bearing points; F, brass block; G, frame of the bender; H, attachment to fit a magnetic base; J, slit 1/8 in. wide X 3/64in. deep; K, screw for turning the bar; M, Frank s mirror; P, brass; R, bars 3/32 in. in diameter; S, bending screw; T, steel spring.

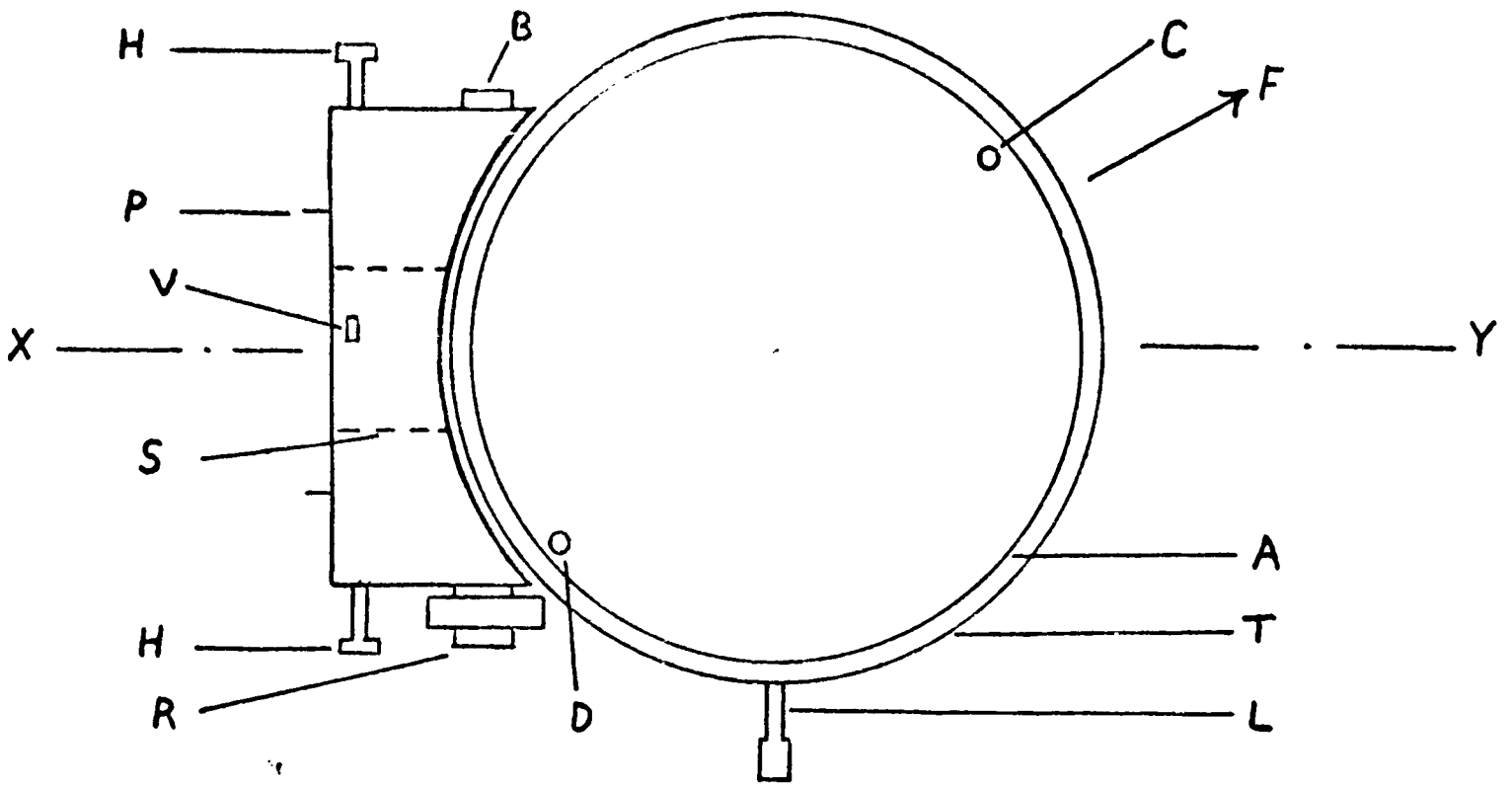

Fig. 2.7 Simplified plan view of the monochromator turntable. A, ridge; B, spring adjustment; C and D, holes for screws; F, focus of X-ray camera; H, horizontal slit adjustment; L, locking screw; P, cylindrical projection; R, fine rotational adjustment; S, aperture defined by slits; T, rotating table; V, vertical slit adjustment; XY, centre line and direction of entrant beam.

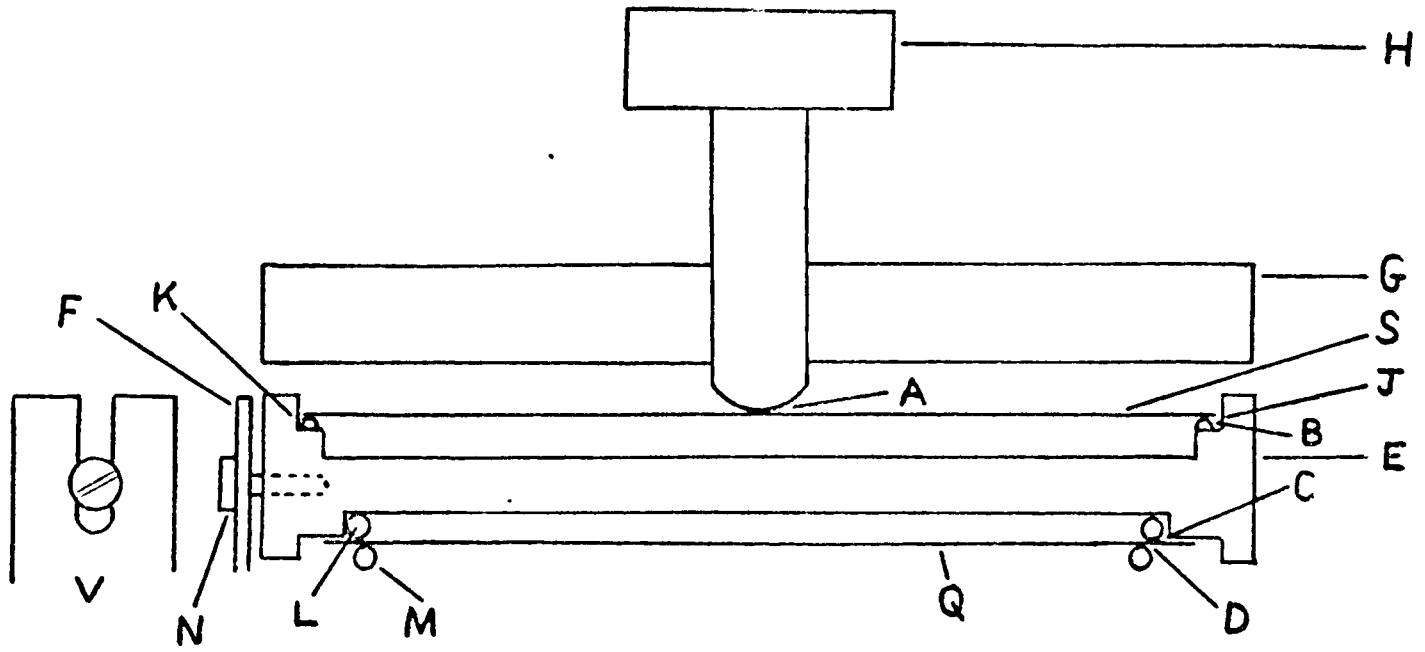

Fig. 2.8 Simplified sectional plan of the quartz crystal bender (twice full scale). A,B,C and D, force bearing points; E, brass block; F, brass plate; G, frame of bender; H, bending screw; J, steel ball; K, 2 steel balls; L and M, 1/16 in. diameter bars- M fixed to the frame of the bender; N, screw; Q, quartz crystal monochromator; S, steel spring; V, end elevation of F.

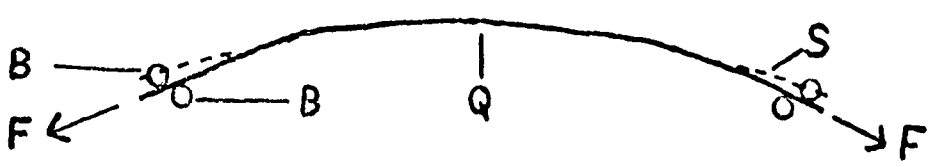

Fig.2.9 A possible distortion of the monochromator crystal (greatly exaggerated). B, bars; F, frictional forces; Q, quartz crystal monochromator; S, a cylindrical shape.

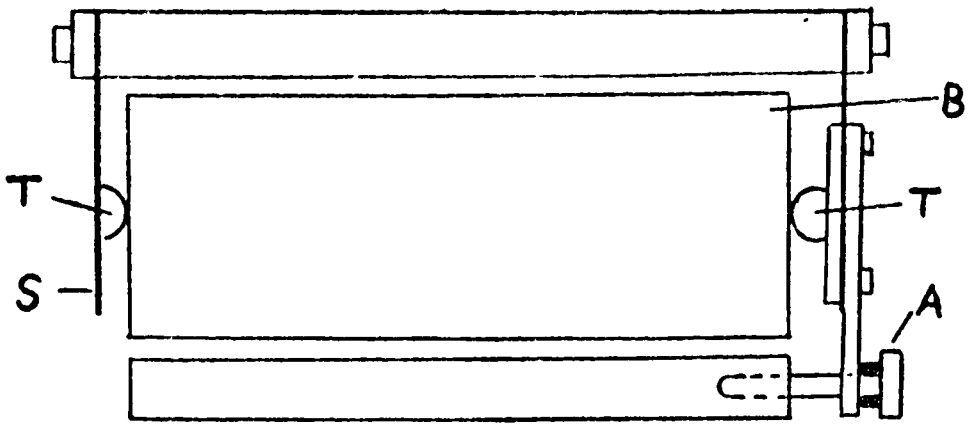

Fig. 2.10. An improved horizontal adjustment for the quartz crystal. A, adjustment screw; B, brass block; S, metal strip (spring); T, teflon.

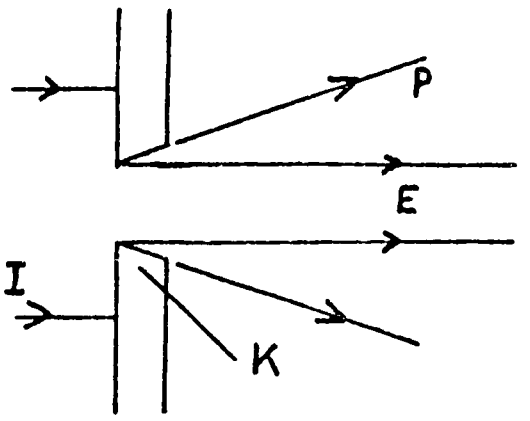

Fig. 2.11. The collimating slit. E, exit beam I, incident beam; K, tantalum knife edge; P, parasitic scatter.

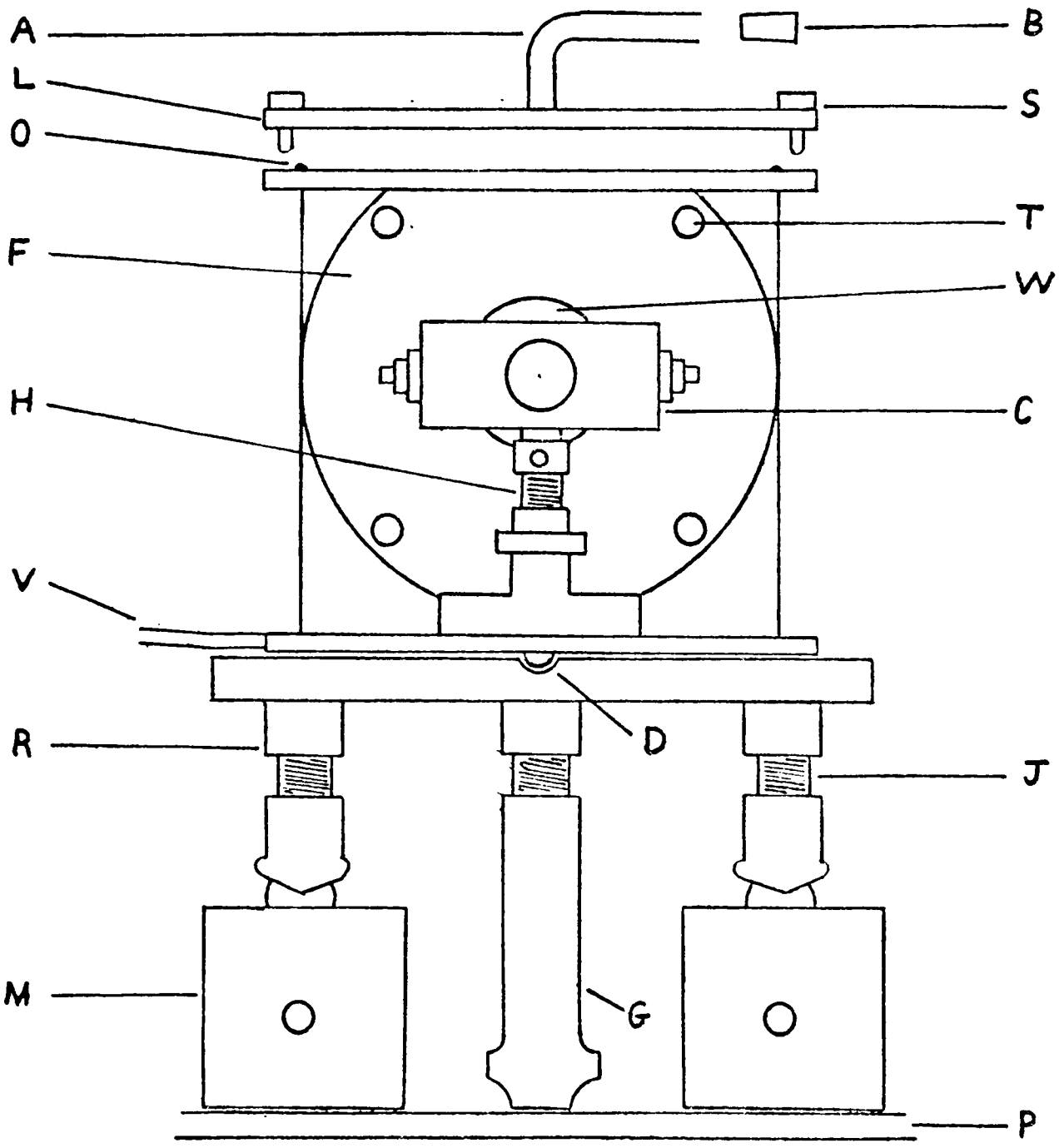

Fig. 2.12. The evacuated film chamber.
A, air inlet pipe; B, bung; C, specimen cell; D, locating steel ball; F, front plate; G, front leg; H, specimen cell height adjustment; J, height adjustment; L, lid; M, magnetic base; O, 'O' ring; P, steel plate; R, rear leg; S, 3 screws; T, 4 screws; V, evacuation pipe; W, mylar window.

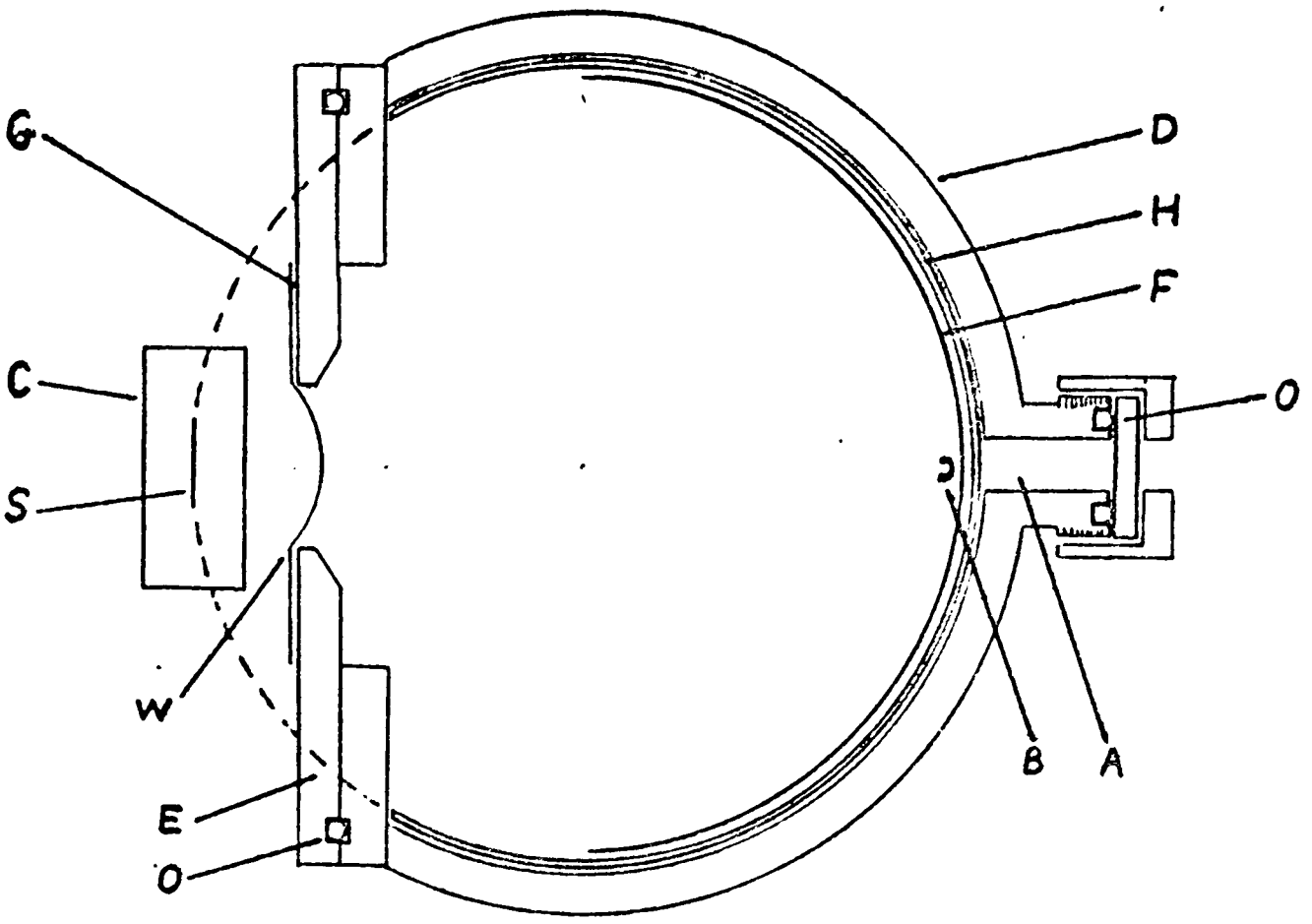

Fig. 2.13. Sectional plan of the evacuated chamber.
A, alignment hole; B, lead backstop supported on mylar, one thou. thick; C, specimen cell; D, cylindrical chamber; E, front plate; F, film in black paper; G, araldite glue; H, film holder; O, 'O' ring seal; S, specimen; W, mylar window, one thou. thick.

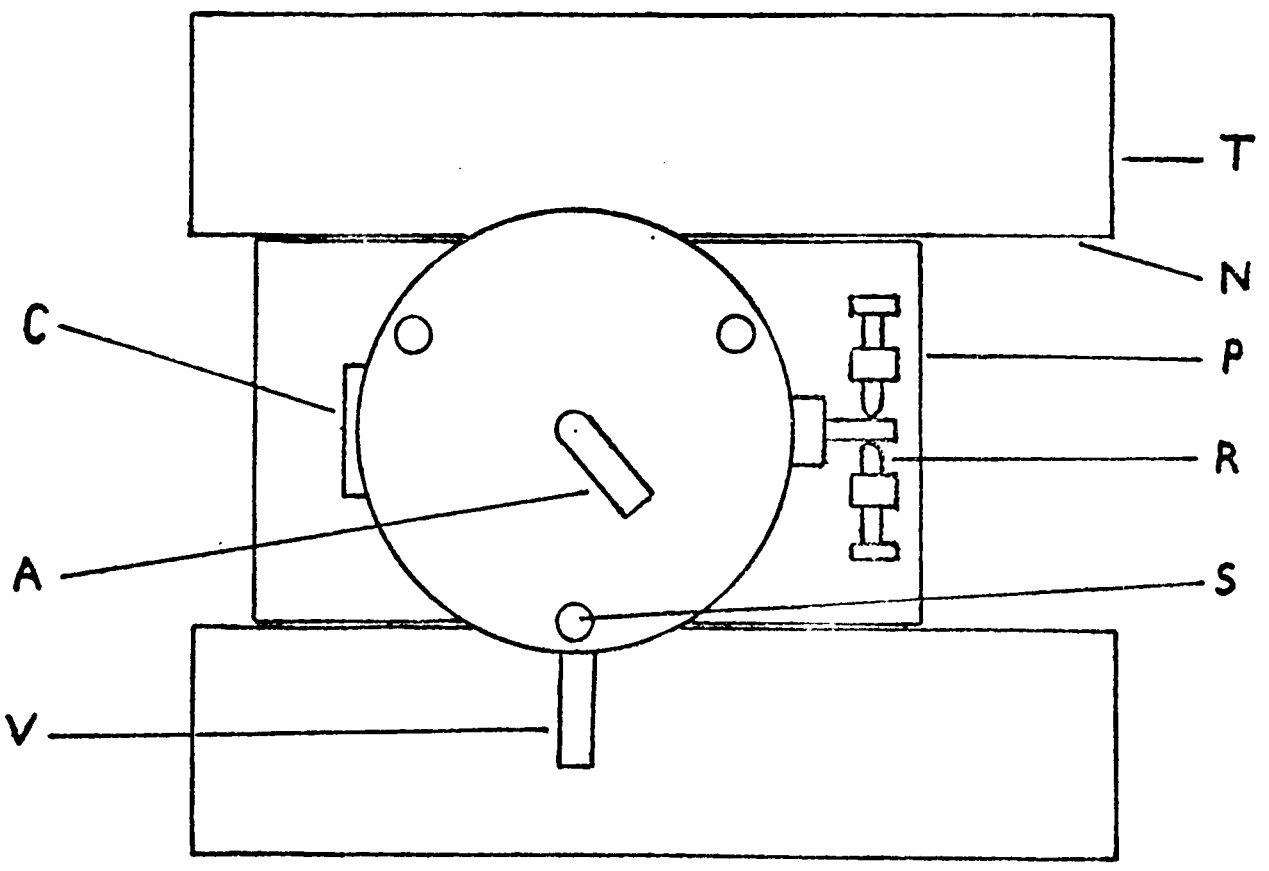

Fig. 2.14. Plan of the evacuated chamber and its support table.
A, air inlet; C, specimen cell; N, nylon slides; P, table - sliding part; R, adjustment screw; S, 3 screws; T, table; V, evacuation pipe.

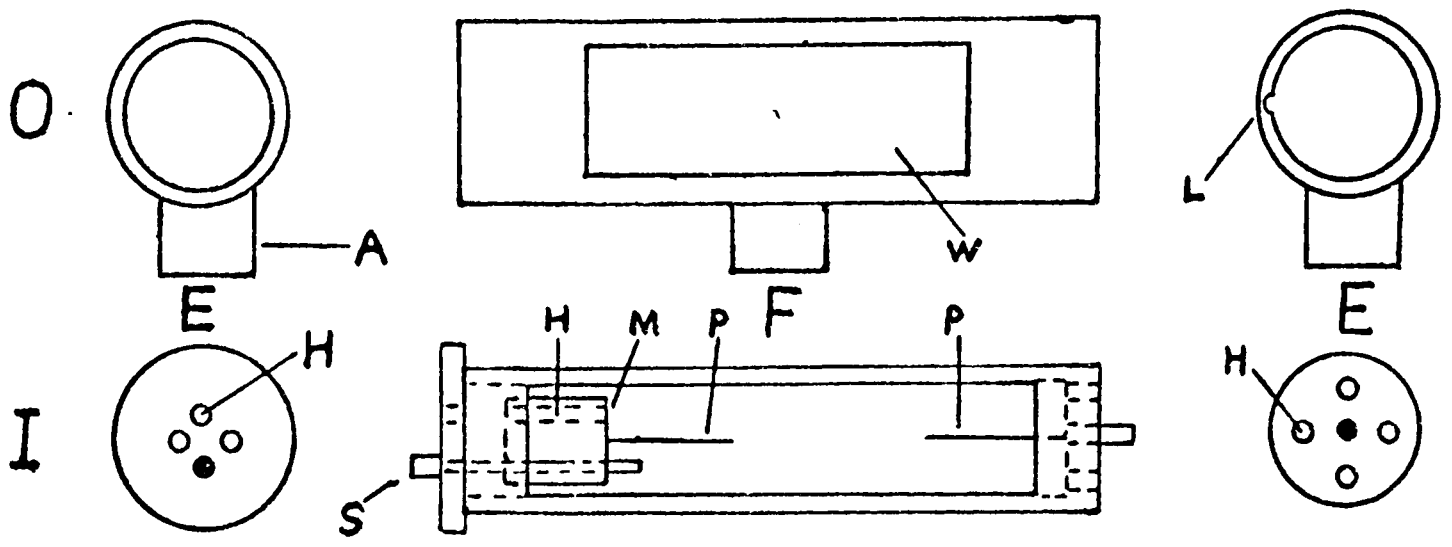

Fig. 2.15. A specimen cell designed for fibres in a controlled atmosphere.
A, attachment for support; E, end elevations; F, front elevation; I, inner part; L, slot for locating pin; M, moveable support; O, outer part; P, pins; S, screw for moving M and P; W, mylar window.

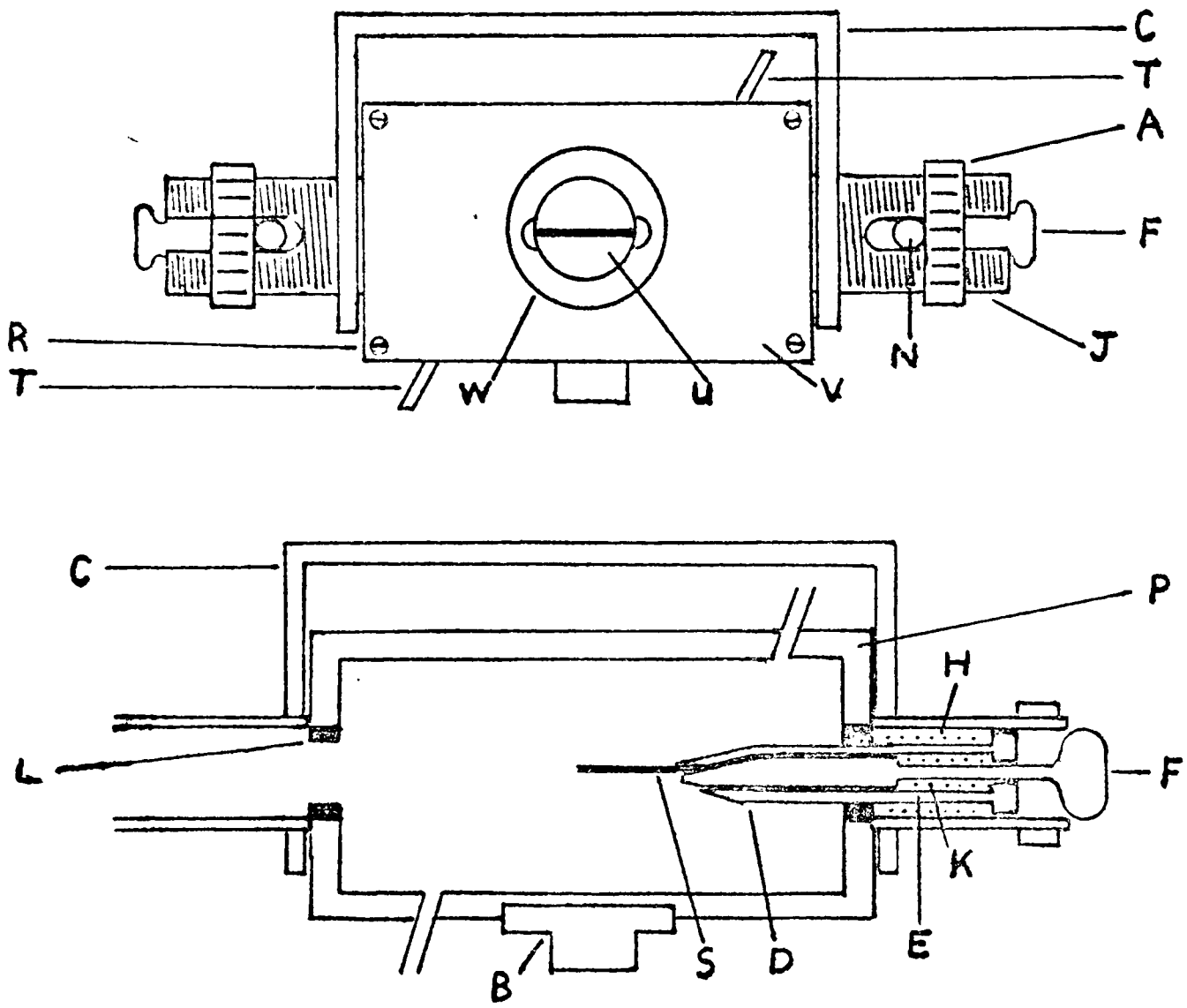

Fig. 2.16. Front view and section of a cell for specimens in a controlled atmosphere or immersed. For clarity, one clamp is removed from the section. A, screw-in adjustments pushing on N; B, attachment for support; C, metal bar; D, clamp; E, outer part of D; F, inner part of D - pull to release the clamp; H, spring keeping E against N; K, spring for pushing F against E; L, leak-proof seal; M, slot for N; N, metal rod attached to E; P, perspex cell; R, 4 screws; S, specimen; T, tube; U, mylar; V, removeable front; W, screw-in window.

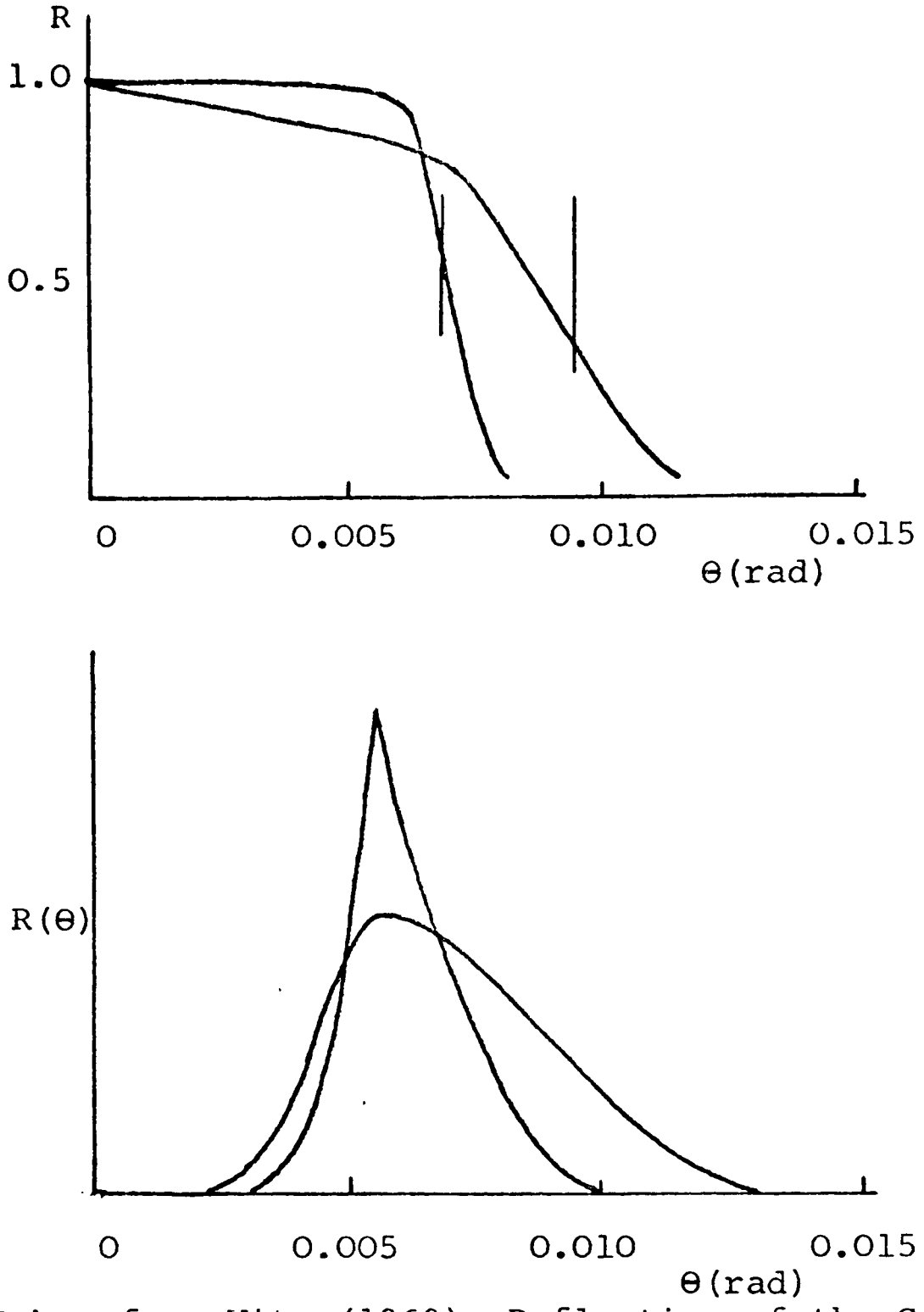

Fig. 2.17 Taken from Witz (1969). Reflection of the CuKα radiation from plane nickel and gold plated mirrors. Calculated reflectivities (top) and observed intensity distributions with a semi-microfocus X-ray tube (1mm X 0.1mm source).

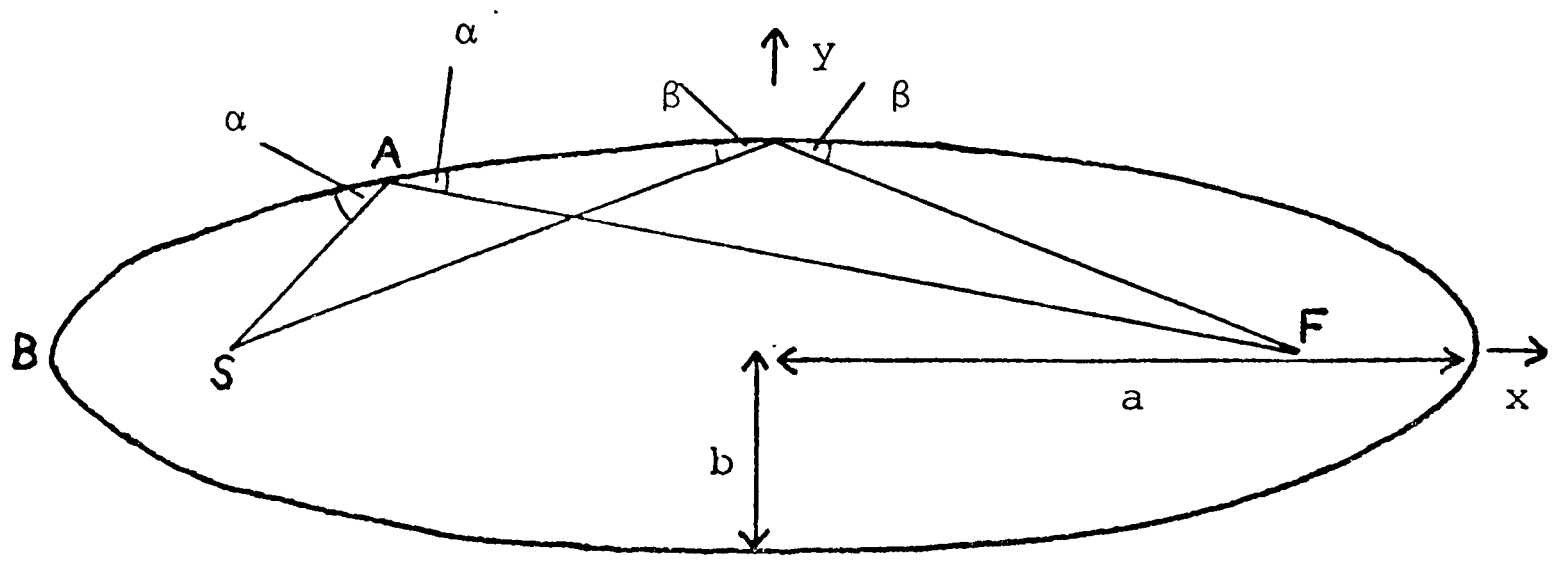

Fig. 2.18 The optimum reflection geometry for a Frank s mirror. Exaggerated in the y direction. All angles of incidence are less than 30'. BS = $b^2/2a$, if a >> b. S, source; F, focus. S & F are the foci of the ellipse.

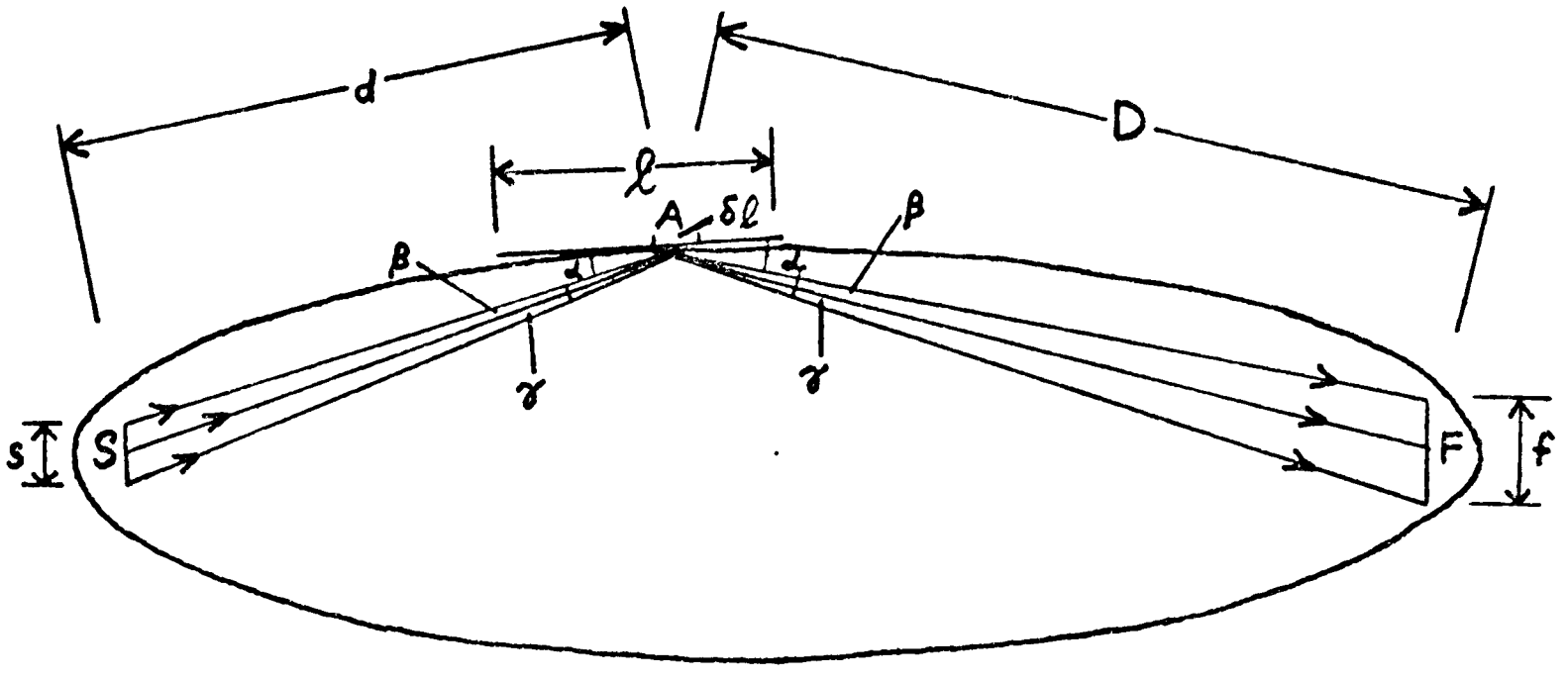

Fig. 2.19. Elliptical geometry for an asymmetrically placed Frank s mirror with a source of a finite size (all angles of incidence are less than 30'). A, Frank s mirror; F, focus; S, source.

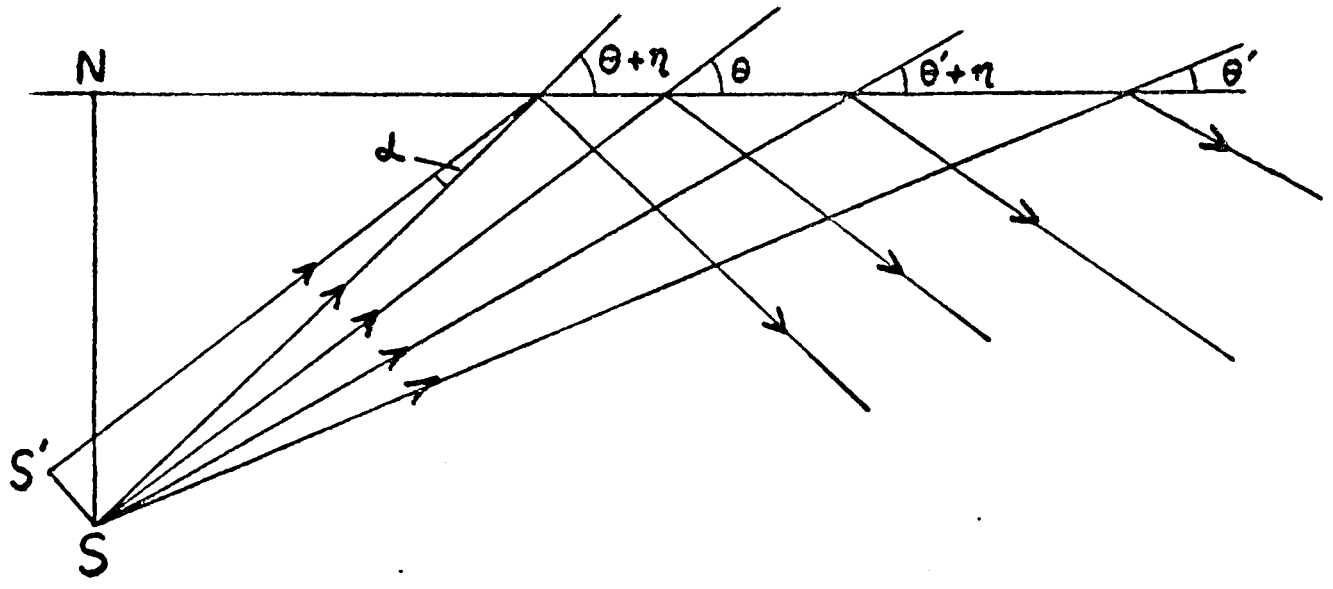

Fig. 2.20. Reflection of X-rays from a plane monochromator. (From Witz (1969))

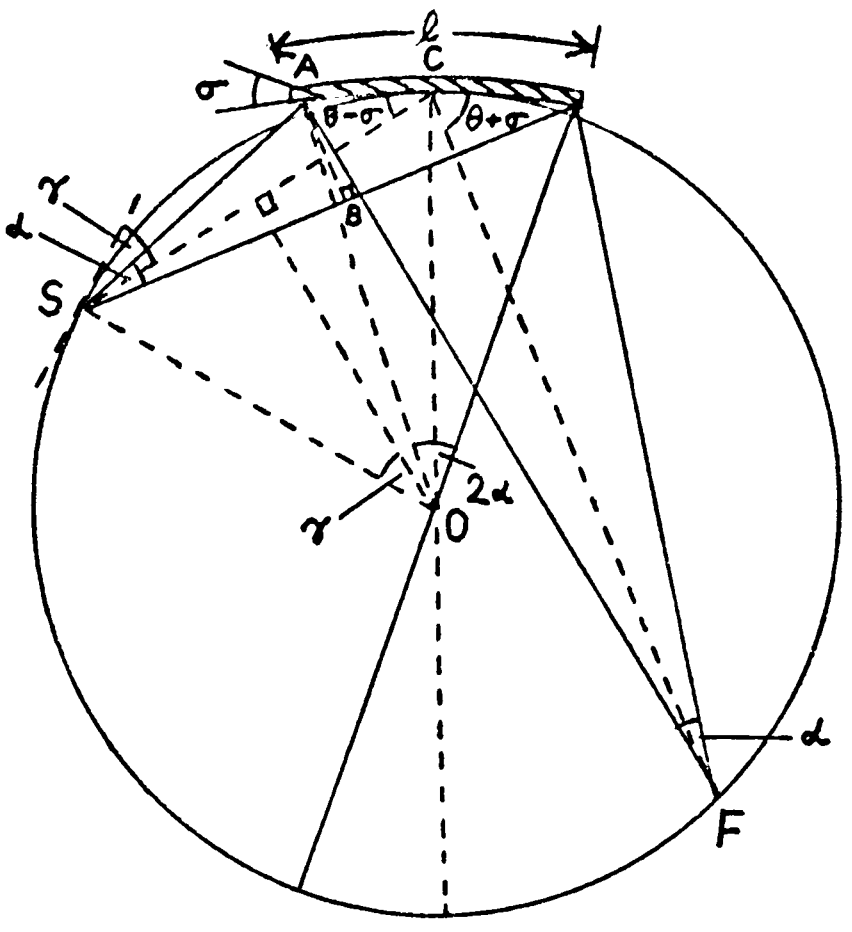

Fig. 2.21 Asymmetrical bent crystal monochromator. The diagram is from Guinier (1955). Dotted lines have been added to make clear the derivation of the mathematical formulae. SC = d; CF = D; AB ≃ ℓsin (θ -σ); sin γ = d/2R; AO = SO = CO = FO = R.

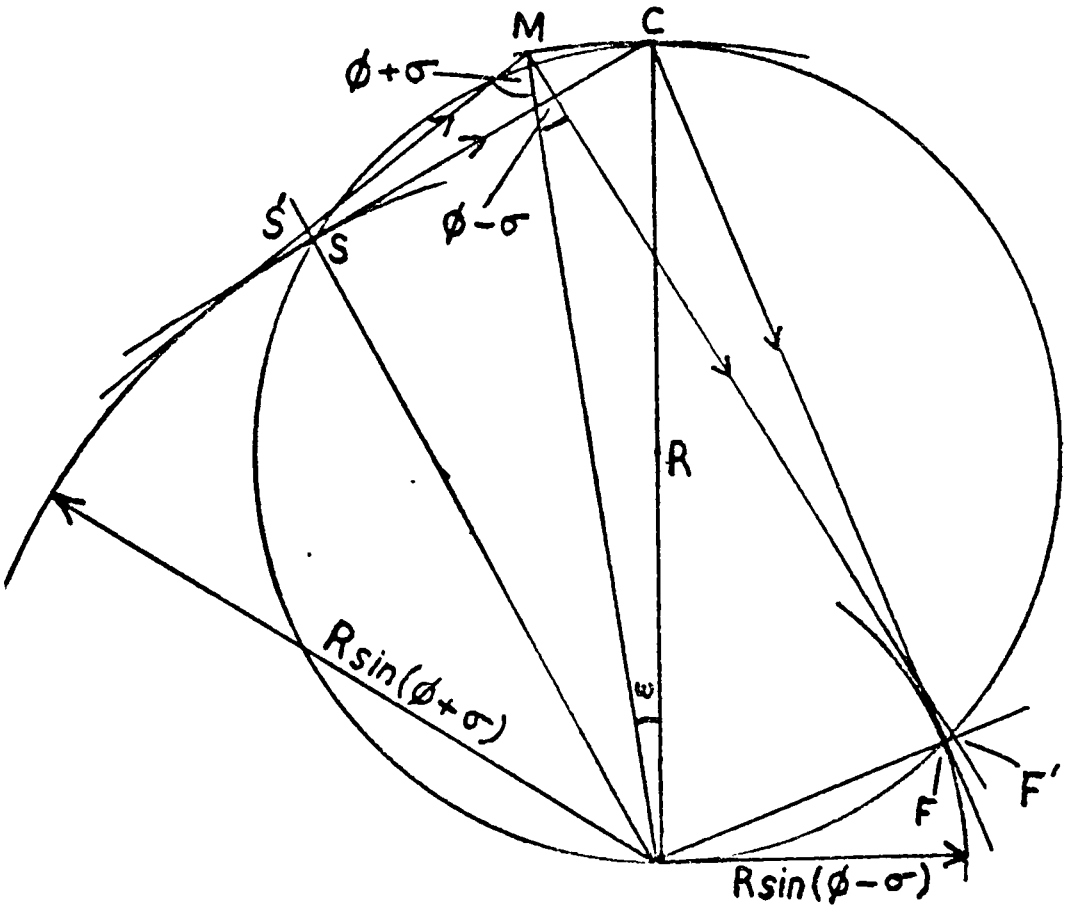

Figure 2.22 Curved crystal monochromator - the Johann system (Johann, 1931). Diagram from Witz (1969).

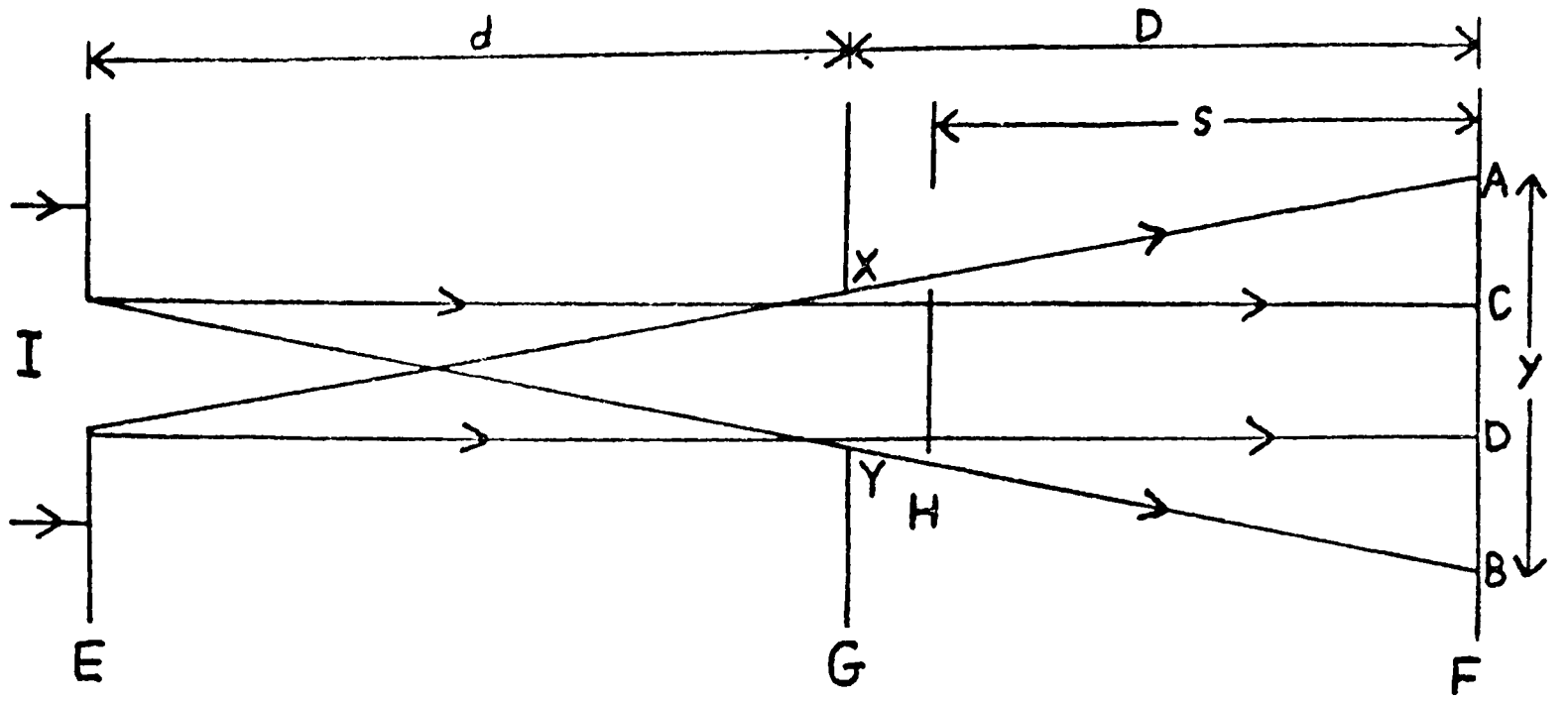

Fig. 2.23. Elevation view of the collimating system.
AB, range of parasitic scatter; CD, main beam; E, collimating slit; F, film; G, guard slit; H, specimen; I, beam from the monochromator; XY = x.

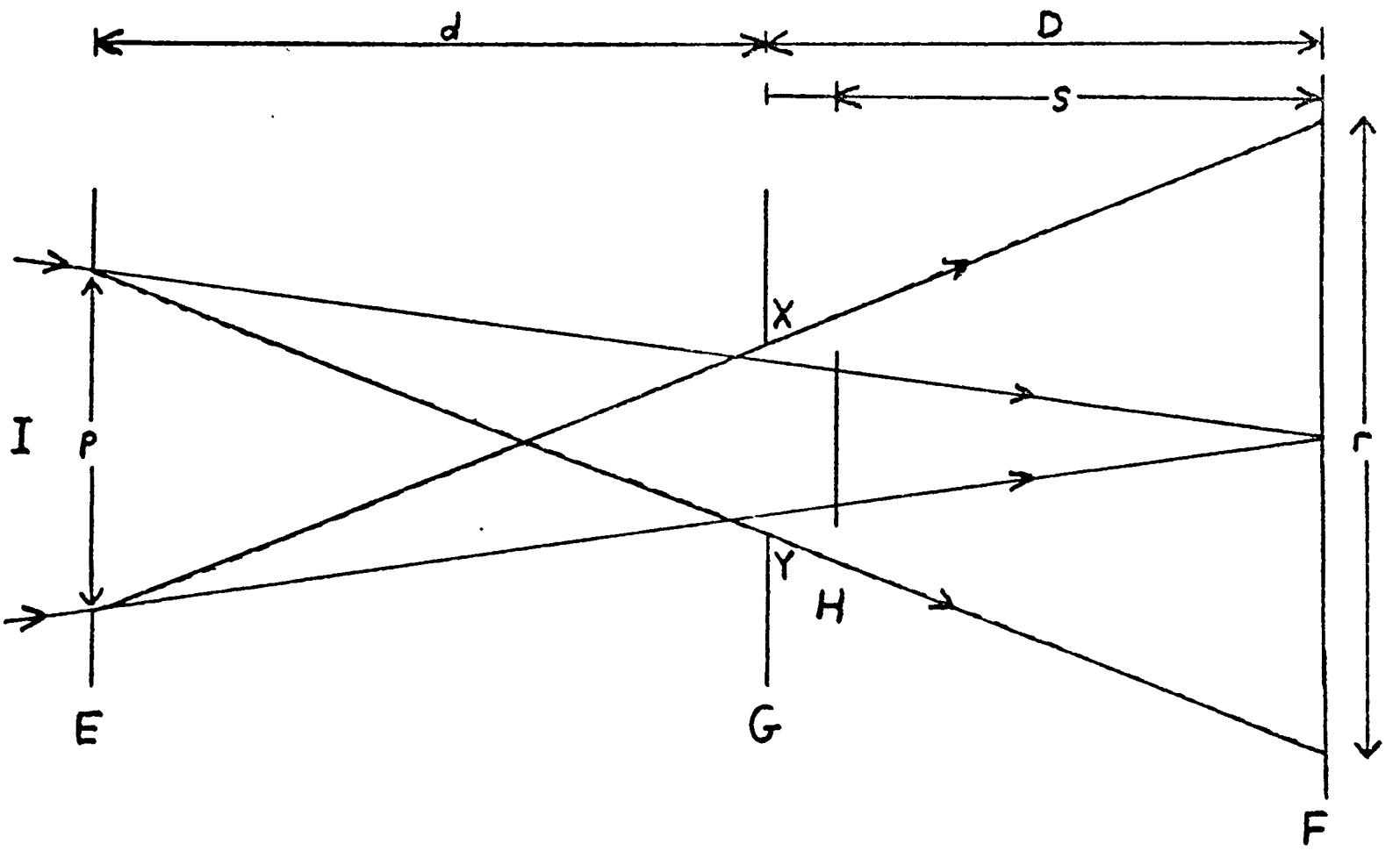

Fig. 2.24 Plan view of the collimating system.
E, collimating slit; F, film; G, guard slit; H, specimen; I, beam from the monochromator; XY = p.

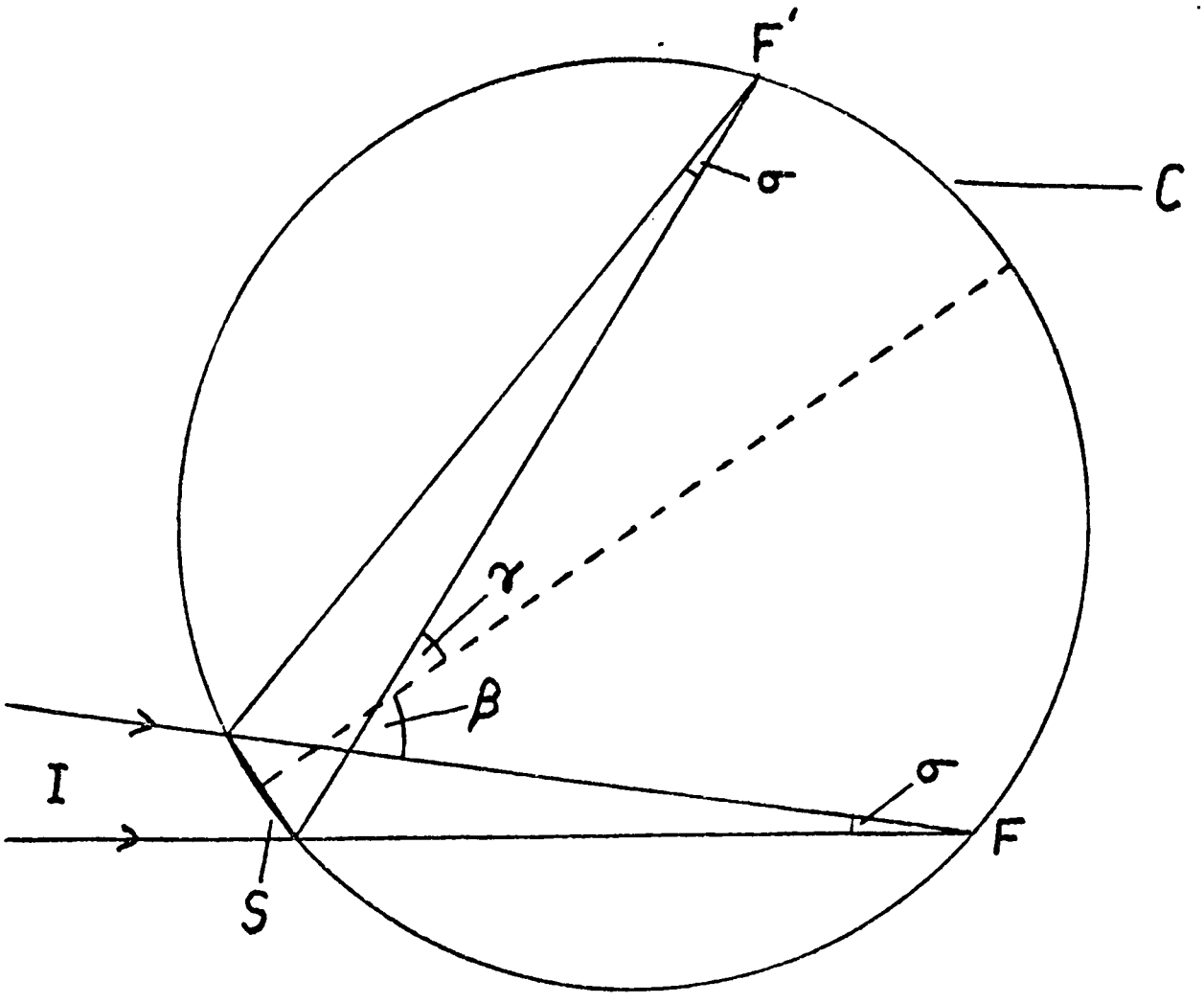

Fig. 2.25 Representation of focusing.
C, focusing cylinder; F, focus of main beam; F', focus of scattered beam; I, beam from the monochromator; S, specimen.

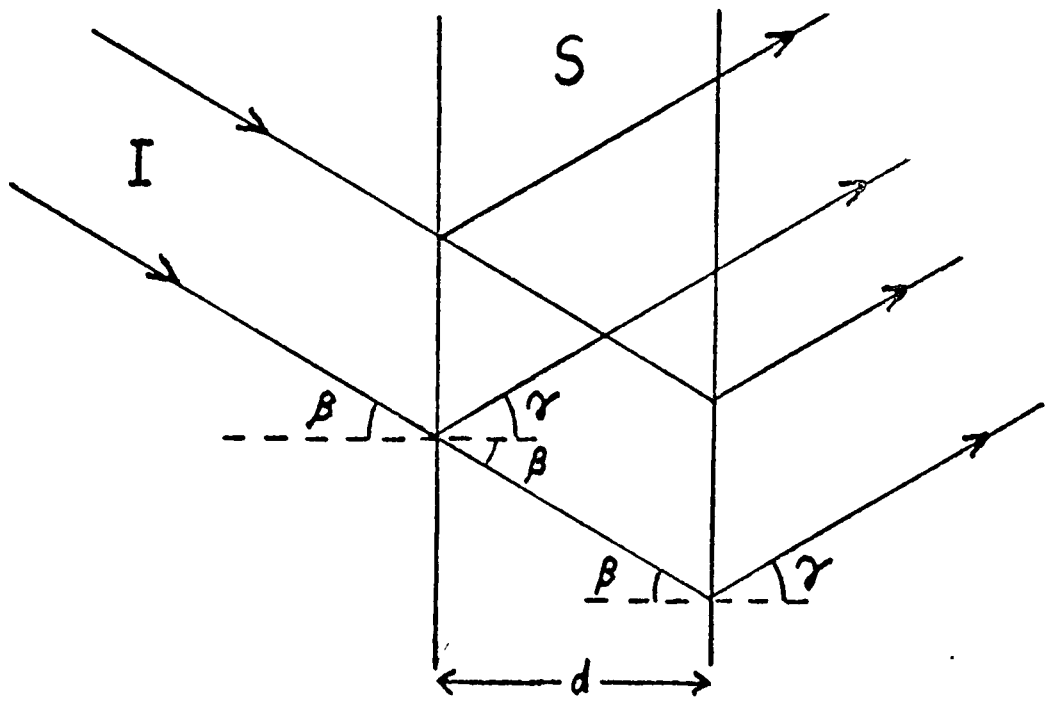

Fig. 2.26 Illustration of how specimen thickness affects the focal size.
I, beam from monochromator; S, specimen.

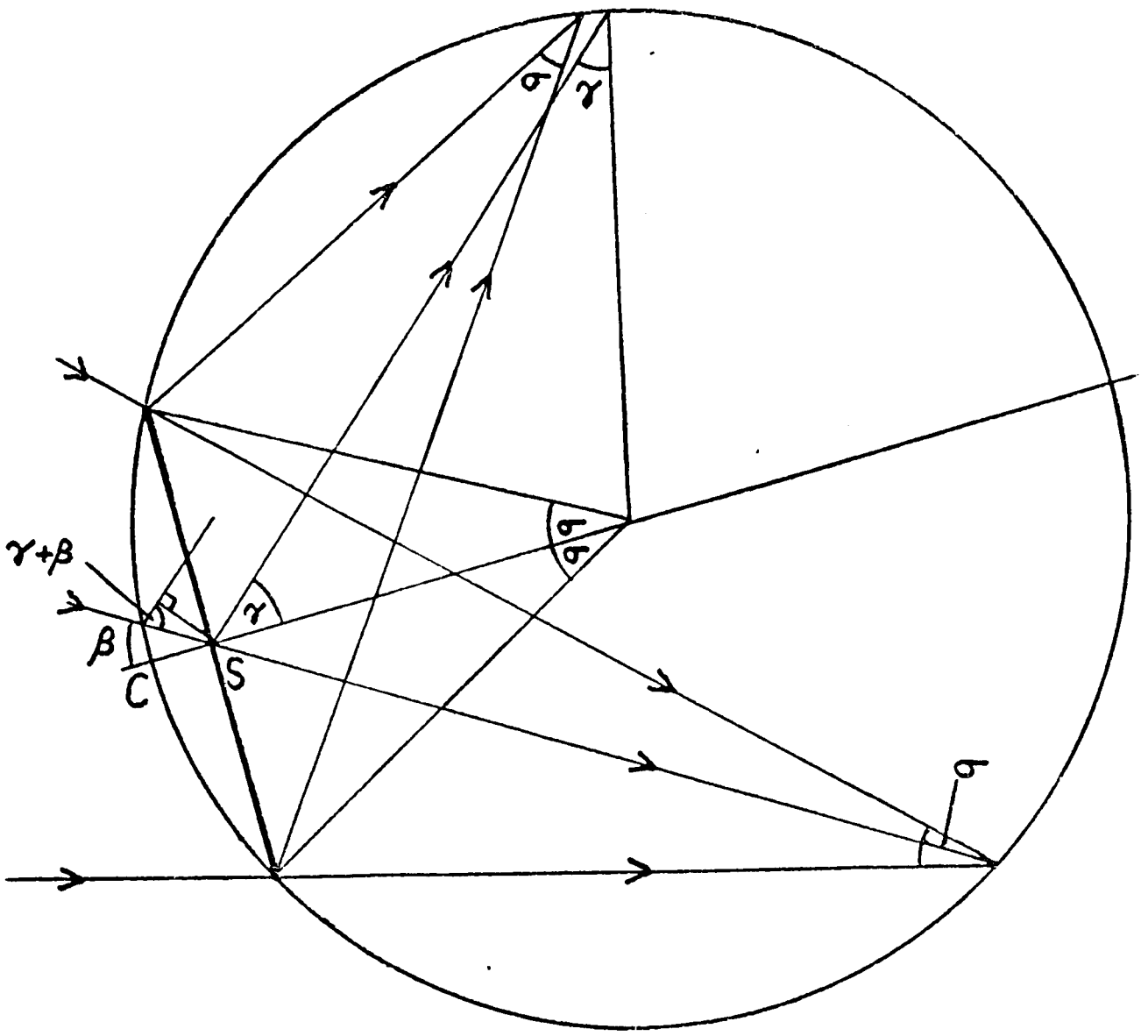

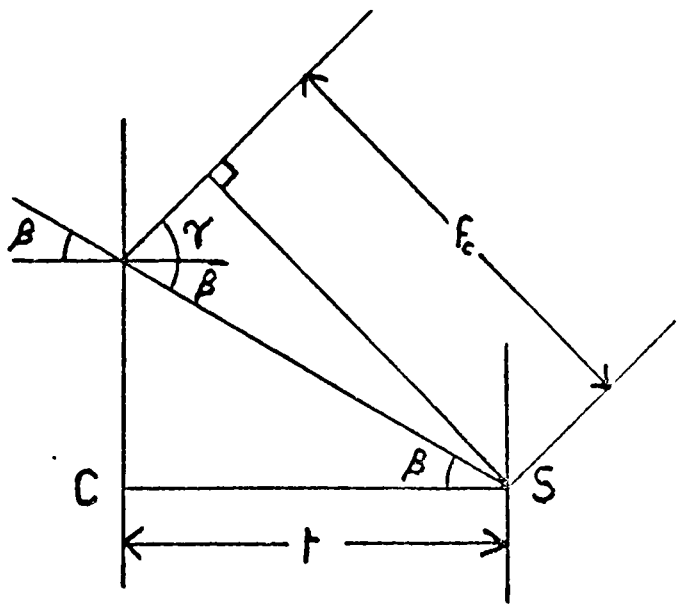

Fig. 2.27 Illustration of the effect of specimen curvature on the size of the focus with part of the diagram enlarged (bottom). Point S is the centre of the specimen.

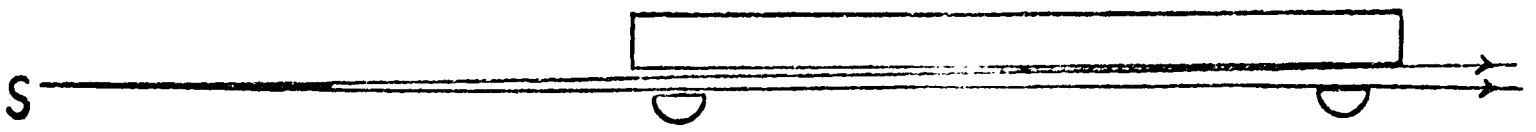

Fig. 2.28 Section through the Frank s mirror before commencing adjustment.

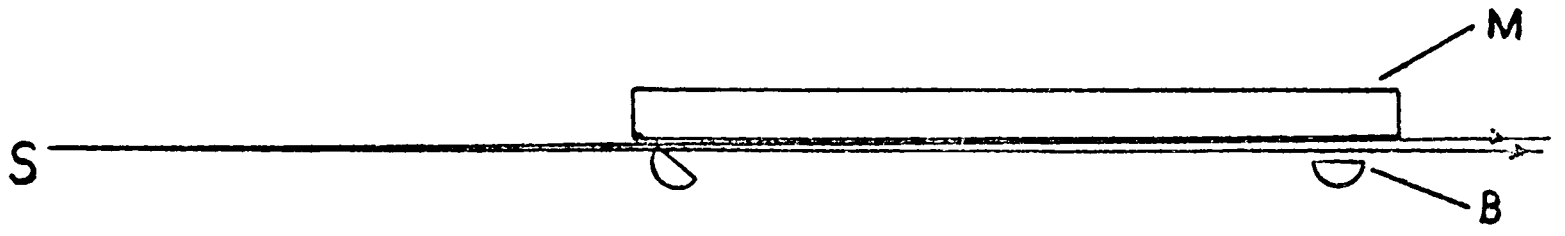

Fig. 2.29 Section through the Frank s mirror after the first adjustment.

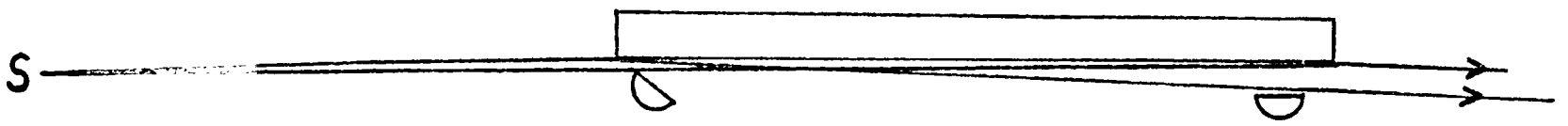

Fig.2.30 Section after the final adjustment.

Figs. 2.28-2.30 Adjustment of the bars of the Frank s mirror bender. B, bars; M, Frank s mirror; S, source of X-rays.

CHAPTER 3

CHEMICAL WORK

CHAPTER 3

Chemical Work

3.1 Preparations by R. Pau

Some preliminary work was done by R. Pau using Sphodromantis tenuidentata.

The outer protein was removed from a freshly laid egg case and put with a few ml. of distilled water. The protein was washed by repeated sonication, centrifugation and suspension in water and stored in suspension at 4°C. It was used for measurements of molecular weights and amino acid compositions. Later work on this is reported in section 3.4.

3.2 Separation of the protein

Later experiments were carried out using S. membramacea.

The egg case was taken immediately after completion and the soft white protein was removed as before. Separation of the insoluble lamellae was achieved by sonication, centrifugation and suspension in water repeated three times, keeping the temperature at 4°C. Early preparations were stored suspended in water at 4°C, but after about a week they began to smell. Components of different molecular weights were separated by SDS gel electrophoresis. Many components were found to be present, so it was suspected that bacteria had caused some chains to break down. Storage in liquid nitrogen was also tried, but after thawing, the protein proved difficult to dissolve in urea solutions, indicating that cross-linking had already occurred. This was overcome by storing the protein in 8M urea with a little β-mecapto-ethanol added to prevent oxidation of S-H groups. The solution was green.

The soluble material left after centrifugation during separation

was precipitated using ammonium sulphate. Most of the green colouring matter appeared to be fixed to this component. The remaining solution of ammonium sulphate and unprecipitated matter was left at 4°C. After a few weeks, an emerald green precipitate had formed.

3.3 Chemical investigations

A carboxy methyl cellulose (CMC) column was formed. The CMC was washed with normal sodium hydroxide for four minutes, washed thoroughly with water, washed with normal sulphuric acid for four minutes and washed again with water. This was equilibrated with a solution containing 6M urea and 10 mM phosphate (the sodium salts) at pH 5.8 and packed into a column.

The solution of lamellae dissolved in 8M urea was dialysed against the solution used to equilibrate the CMC with one crystal (about 10^{-6} c.c.) of chlorobutanol added to deter bacteria. The resulting solution was pippetted on to the column. Protein was clearly fixed to the CMC as evidenced by the green colouring matter attached to the protein.

All solutions of salts used were made up using the buffer used for equilibration. After initial washing of the column with the buffer, the concentration of sodium chloride was slowly increased from zero to 1M. The solution leaving the column was passed through a meter measuring UV absorption and collected at 50 drops per tube. The UV absorption indicated that no significant quantity of protein left the column at concentrations of sodium chloride above 0.5M. Finally, 1M ammonium sulphate solution was passed through the column. No further protein was removed. Protein corresponding to the two major peaks in the UV absorption was collected, dialysed thoroughly against water at 4°C and

freeze dried. One peak corresponded to a 0M sodium chloride concentration and the other to 0.2M.

Samples of the water insoluble and water soluble components of the egg case were compared with the two major fractions derived from the CMC column using SDS gel electrophoresis. Both fractions from the column contained components of different molecular weights. The dominant component from the water insoluble lamellae had a molecular weight around 50-55000, but all samples showed this band to some extent. As both fractions from the column showed several bands, it was decided that this technique was unsuitable. When further material became available, it was separated and stored.

3.4 Further investigations by R. Pau

These investigations are currently being undertaken, but the results are not yet available. It is hoped to determine accurate molecular weights and amino-acid compositions of the major components of the lamellae.

3.5 Polymorphic forms

Polymorphic forms of the protein could yield useful information. Protein dissolved in 8M urea was dialysed at $4^{o}C$ against a solution of urea which was changed in small steps from 8M to about 2.6M. The solution was buffered initially with 50 mM tris, but the concentration was decreased as the urea solution was diluted. Some solutions contained either magnesium or calcium chloride at a 1mM concentration. At about 2.6M, precipitates formed. The structures formed were apparently crystalline in the presence of magnesium ions at pH 8.5.

Bacteria destroyed the structure before it became possible to examine them in the electron microscope.

It was decided to repeat the experiment, extending the work to include other values of pH and phosphate buffers. No suitable material became available for this.

3.6 Density measurements

To help choose a model for the protein structure, density measurements were made. Lamellae were pelleted in the centrifuge and dehydrated by immersion in ethanol for several days. The pellet was then transferred to a mixture of chlorobenzene and alcohol, keeping air from the pellet, and finally into chlorobenzene. The two steps allow the pellet to be dense enough to remain immersed at all times. Bromobenzene was gradually added over two weeks, maintaining the pellet at the same density as the solution. When the density of the pellet had stabilised, the density of the solution was determined. It was found that the density of the lamellae was 1.338 gm./c.c. when immersed in a mixture of chlorobenzene and bromobenzene of the same density at $24.4^{o}C$.

It was hoped that the protein structure would become dehydrated and collapse. The new unit cell size estimated by X-ray methods would then allow the density in the natural state to be determined. Measurements of the unit cell dimensions suggest that much of the water was replaced by the solution. A smaller unit cell size could be obtained by treating material with air dried over silica gel, lending support to this hypothesis.

CHAPTER 4

ELECTRON MICROSCOPY

CHAPTER 4

Electron Microscopy

4.1 The Work of P. Eagles and R. Pau

4.1.1 Specimen preparation

Protein was removed from a freshly laid egg case produced by Sphodromantis tenuidentata. After brief treatment with trypsin, the lamellae making up the protein were separated by sonication to prevent cross-linking, the soluble components were removed by repeated sonication, centrifugation and resuspension in fresh water.

4.1.2 Embedded lamellae

Lamellae were embedded sectioned and stained with potassium permanganate and lead citrate. An electron micrograph obtained is shown in plate 4.1. It is not possible to say whether the lamellae have a constant thickness, since they are sectioned at a range of angles, but they are possibly all about 400 Å thick. A banding of period about 166 Å is seen on some of the lamellae.

4.1.3 Negatively stained lamellae

Lamellae were placed on carbon coated grids and stained briefly with 0.5% uranyl acetate solution. Electron micrographs obtained are shown in plates 4.2-4.4. A micrograph gives the optical diffraction pattern shown in plate 4.5. A mask was constructed to filter out light not confined to the lattice of points and the pattern was reconstructed to produce an image, as shown in plate 4.6. An image produced by five superimpositions of a selected area of a micrograph is shown in plate 4.7.

The contrast in this plate is the negative of that in plates 4.5 and 4.6, so the stain is represented by white areas. The dimensions of the lattice determined from this are similar to those marked in fig. 4.1. The figure defines the cell sides a and c. b is perpendicular to the paper as will be seen later. The dimensions of the lattice determined from plate 4.7 are $c = 87$ Å, $a = 133$ Å and $\beta = 98^{\circ}$. The striations separated by 30 Å were also noted.

4.2 Further work

4.2.1 Specimen preparation

A freshly laid egg-case produced by S. membranacea was taken and the lamellae were separated by sonication, centrifugation and resuspension in fresh water three times. Trypsin was not used for most of the work, although it did produce a cleaner preparation with a lesser tendency to form clumps of lamellae. The suspension was placed on electron microscope grids. Some of the grids were treated with 0.1% trypsin solution for between three and ten minutes and this was then washed off. It had little effect.

4.2.2 Negatively stained lamellae

It was found that 3% uranyl acetate solution was a suitable stain. Increasing the time of staining from a few seconds to two minutes increased the contrast, but otherwise had little effect. The micrograph obtained was identical to that obtained using S. tenuidentata.

4.2.3 Positively stained lamellae

The best positive staining was obtained by staining for an hour or more with 0.1% uranyl acetate solution. Good results were also obtained with 0.1% phosphotungstic acid followed by 0.1% uranyl acetate. If phosphotungstic acid was used alone, fine details were not visible and if it was first neutralised with sodium hydroxide, eventhe major striations could not be seen.

Plate 4.8 shows a lamella stained with 0.1% uranyl acetate solution. The striations separated by 30 Å are more dominant than with negative staining. Plate 4.9 is rather unusual. The treatment was identical, but the 133 Å striations are scarcely visible, whereas the 30 Å striations are clearly visible.

4.3 Negatively stained lamellae

The observations described here were derived from the micrographs and images described in section 4.1.

4.3.1 The pattern obtained

This is drawn in fig. 4.1. In practice there were variations in distances measured. Angles generally had a range of about 3° and distances had a range of between 5% and 10% of the mean value. This could in part be due to experimental errors in calibrating the microscopes at different magnifications. However, variations in the structure were probably produced by molecular sliding. Where distances cannot be averaged over many repeats, variations in staining cause variations in measurements. The measurements used here were obtained from plate 4.7. This is typical, although the 94 Å cell dimension is about

3 Å greater than average.

The striations spaced at 133 Å intervals are composed of short lines about 80Å long at an angle of about 15° to the striations and spaced at intervals of 94Å along each striation. The structure of each line appears to vary, but most commonly is three equally spaced centres of stain. Variations are probably caused by irregularities of staining. The staining centres are about 20 Å in diameter.

In addition to the major striations, there are less pronounced striations at an angle of about 19 degrees to the major striations and separated from each other by about 30 Å. Further striations, showing as indistinct lateral bands about 40 Å wide, occur along the direction AB and separated by 80 Å.

The features described above can be seen on both selected areas of micrographs and also on images produced by superimposition. They are arranged on a unit cell having sides of 94 Å and 133 Å at an angle of 82°. This cell agrees with optical diffraction from the micrograph.

On some micrographs, the image of the lamella appears to change. On close inspection of images produced by reconstruction or superimposition, such as plate 4.6, it is seen that the staining is different in these regions. It is seen that the central spot in the line of three disappears in the second type of pattern. It could be that positive staining is dominant in these areas, in which case the central spot would normally be a gap. The greater complexity of these regions could indicate positive staining. Some areas of plate 4.6 show the central spot as absent, but only the other two spots are present, one more intense than the other, suggesting a direction to the structures present.

From the image, they should be parallel. Reconstructions such as plate 4.6 should be treated with caution, since artifacts produced by the technique may occur.

4.3.2 Shear planes

Inspection of plates 4.3 and 4.4 reveals two sets of shear planes. One runs along the major striations. This is visible in two places on plate 4.3. It is seen that small filaments often cross these striations. The most common shear planes are found approximately parallel to the fine striations. Measurements of seven shears give the mean angle between the shear and the major striation as $21^{o}2' \pm 15'$, significantly greater than the 19^{o} for the minor striations. Plate 4.4 shows fine filaments free from the main matrix running along the shears. These filaments are less than 20A in diameter and are never free of the matrix for more than 600 Å. Both shear planes contain evidence that the filaments are continuous across the major striations. In plate 4.3 there appears to be one per group of three spots, that is one per minor striation giving a separation of 30Å.

4.4 Positively stained lamellae

Lamellae from S. membræmacea positively stained with 0.1% uranyl acetate solution gave very similar micrographs. The major striations were still present, though the minor striations were more dominant than before. Examination of plate 4.8 shows that three spots are often visible, but sometimes the central one is less intense. One of the two outer spots is often more intense, indicating that the structures present are not centrosymmetric. There are indications that the groups of three spots are parallel rather than anti-parallel but the quality of the

micrograph makes this uncertain. Plate 4.8 is an example where the angle of the cell is 79° rather than 82°. The 133 Å side is marked by lines of limited staining, perhaps apolar, running between the groups of three spots. This plate also shows lamellae with different faces uppermost overlapping. It is seen from the non-overlapping regions that they are oriented hands in such a way as to leave the minor striations approximately parallel. The angle between the two sets of major striations is about 30°.

Plate 4.9 shows a structure given the same treatment. It is identical except that the major striations are very weak. The 30 Å striations are very clear.

4.5 Sectioned material

4.5.1 Specimen preparation

Ribbons were removed from the egg case of S. tenuidentata. It was decided to fix, embed, section and stain the material, so Mrs. B.M. Luke did this and took micrographs. The specimens were fixed in osmium tetroxide and stained with uranyl acetate and lead citrate.

4.5.2 Micrographs obtained

Plate 4.10 shows a section approximately at right angles to the plane of the lamellae. They have a thickness of about 400 Å with tapered ends and the packing is only approximately regular. Plate 4.11 is a section in the plane of a lamella, revealing the major striations seen in the sonicated lamellae. Plate 4.12 is a section taken at a small angle to this plane, indicating that the major striations are continuous through the thickness of a lamella.

Sections like that shown in plate 4.10 often contain lamellae showing transverse banding patterns, as shown in plates 4.13-4.16. The most distinctive pattern is the myosin-like pattern as in plates 4.15 and 4.16 and as drawn in fig. 4.2. The term myosin-like refers to the appearance; the structure is unlike that of myosin. The repeat is about 140 Å and contains two strong bands followed by three weak ones. The distance between bands is 39 Å between strong ones and 26 Å elsewhere. Uniform banding patterns are also found, 30 Å being the most common spacing. 20 Å, 51 Å and 90 Å have also been seen. The five repeats measured are multiples of 10 Å.

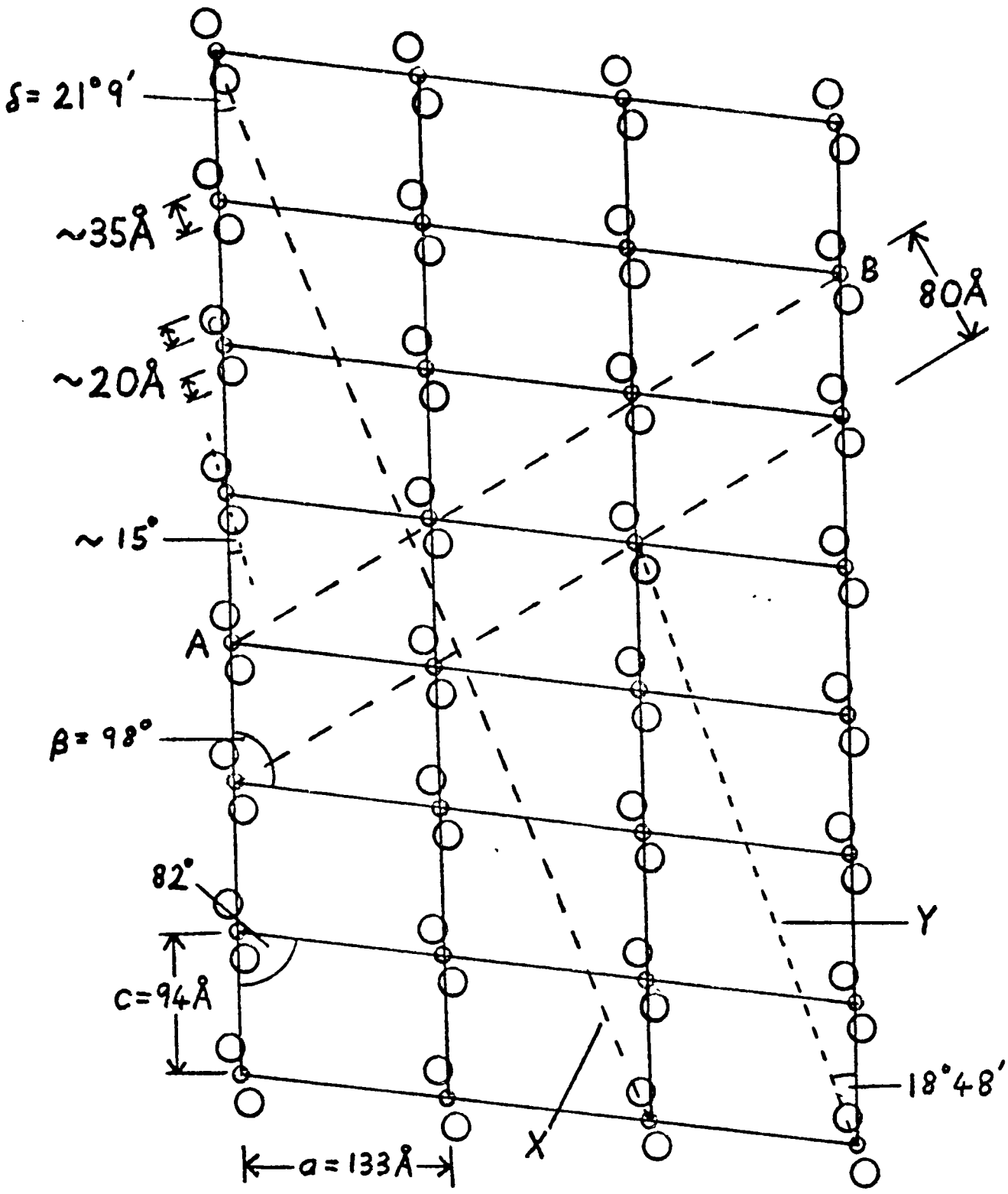

Fig. 4.1. Pattern derived from micrographs of lamellae negatively stained with uranyl acetate. The unit cell dimensions are from Plate 4.7. X, line of shear plane - δ was estimated as $21^{\circ}2' \pm 15'$ shear planes; Y, approximate line of minor striation- AB line of lateral bands; AB = 457 Å.

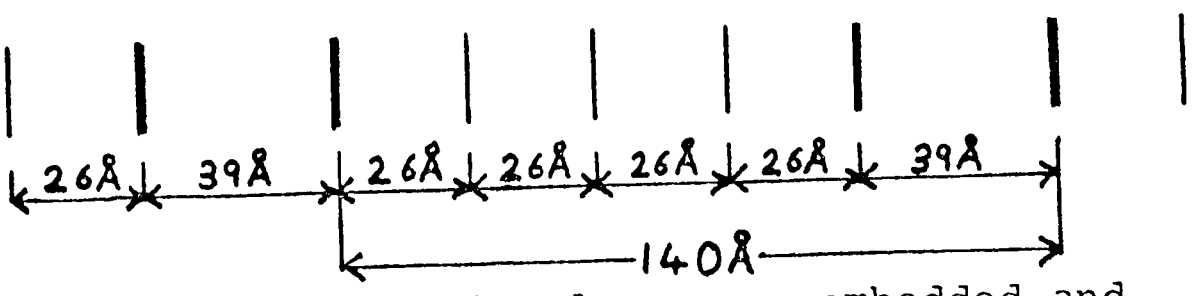

Fig.4.2 A transverse banding found on some embedded and sectioned lamellae. The estimated distances of 26Å and 39Å are approximate.

PLATES 4.1 - 4.16

Electron micrographs of sonicated lamellae and sectioned ribbons from the egg case of *Sphodromantis tenuidentata* were taken by Dr. P.A.M.Eagles (plates 4.1-4.5) and Mrs. B.M. Luke (plates 4.10-4.16) using the AEI801A electron microscope. Electron micrographs of sonicated lamellae from the egg case of *S.membramacea* were taken by the author with the assistance of Mr. L.J. Stump using the AEI801A electron microscope (plate 4.8) and by the author using the Hitachi HU11E electron microscope (plate 4.9). Optical diffraction, reconstruction and superimposition (plates 4.5-4.7) are the work of Dr. P.A.M. Eagles and Dr. R.N.Pau.

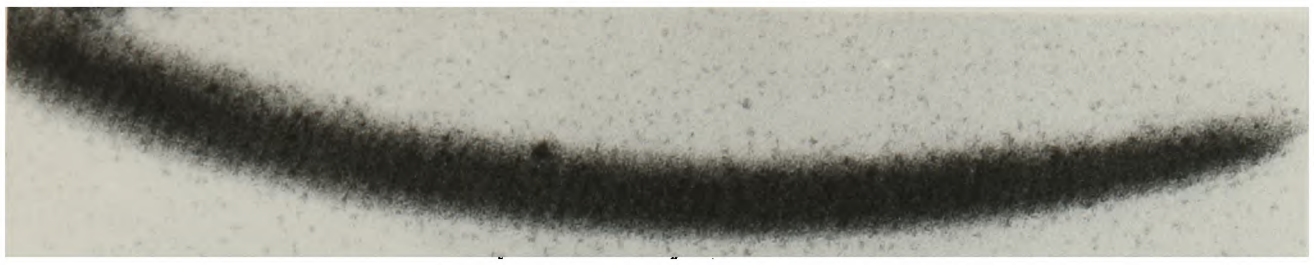

Plate 4.1 Embedded lamellae from *S.tenuidentata* showing bands spaced by 166Å . Stain: potassium permanganate and lead citrate. Magnification of plate: 63,000. Magnification of print: 125,000. (By P.A.M.Eagles).

Plate 4.2 Sonicated lamellae from *S.tenuidentata* negatively stained with 0.5% uranyl acetate solution. Magnification of plate: 2,600. Magnification of print: 5,000 (By P.A.M.Eagles).

Plate 4.3. Sonicated lamella negatively stained with 0.5% uranyl acetate solution.
Magnification of plate: 63,000. Magnification of print: 350,000 (By P.A.M.Eagles).

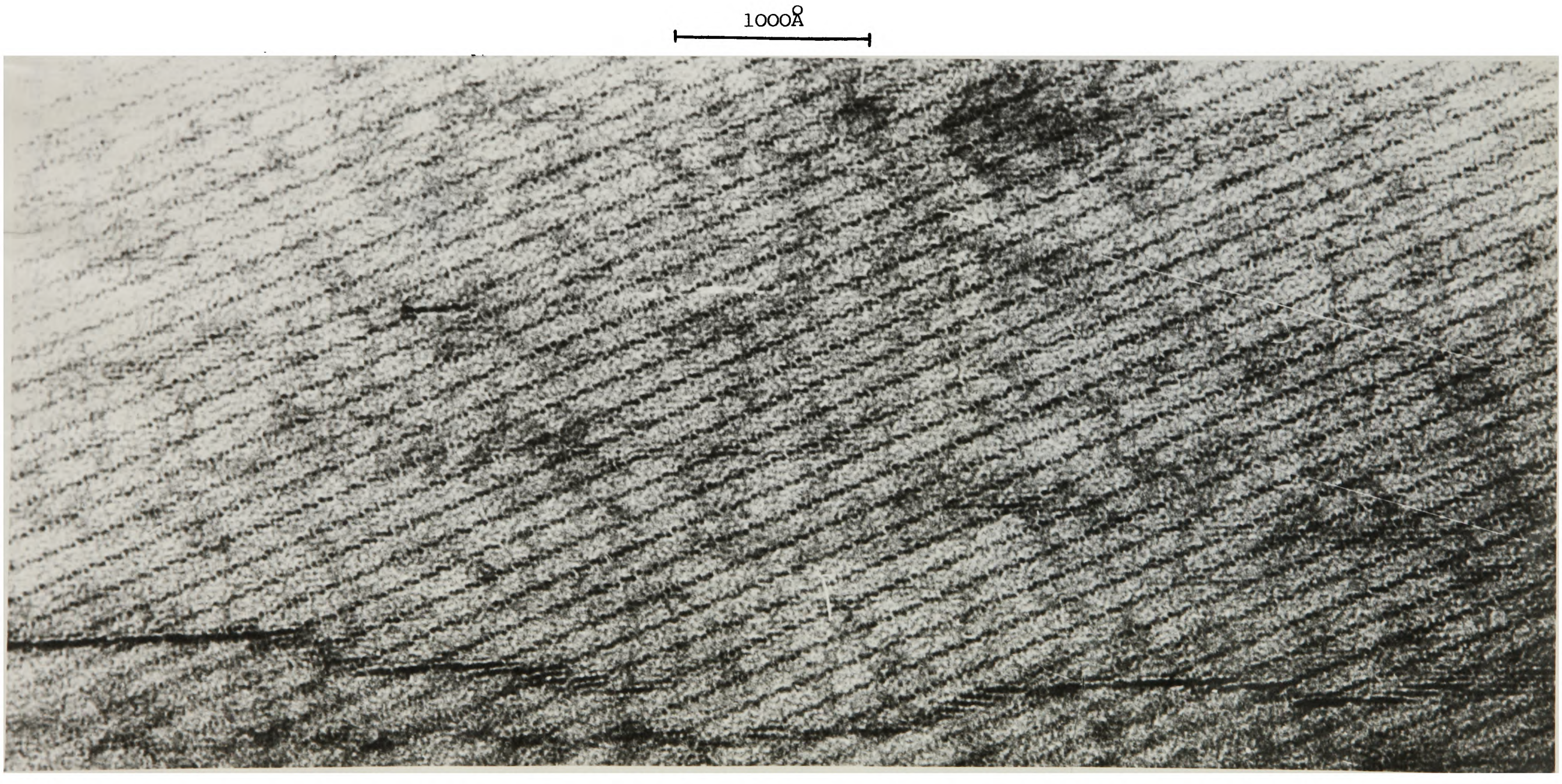

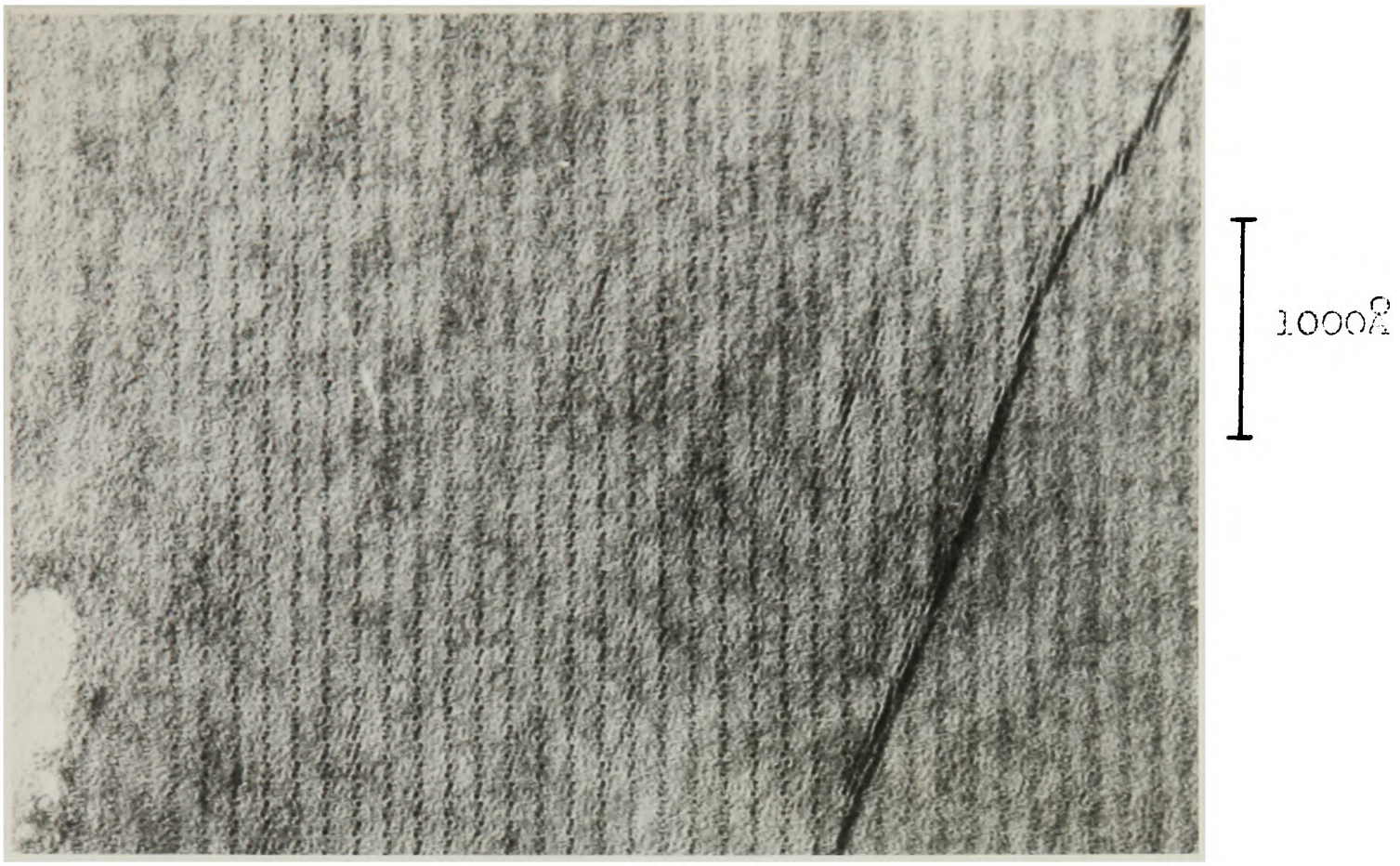

Plate 4.4 Sonicated lamella from *S.tenuidentata* negatively stained with 0.5% uranyl acetate solution. Magnification of plate: 63,000. Magnification of print: 250,000. (By P.A.M.Eagles).

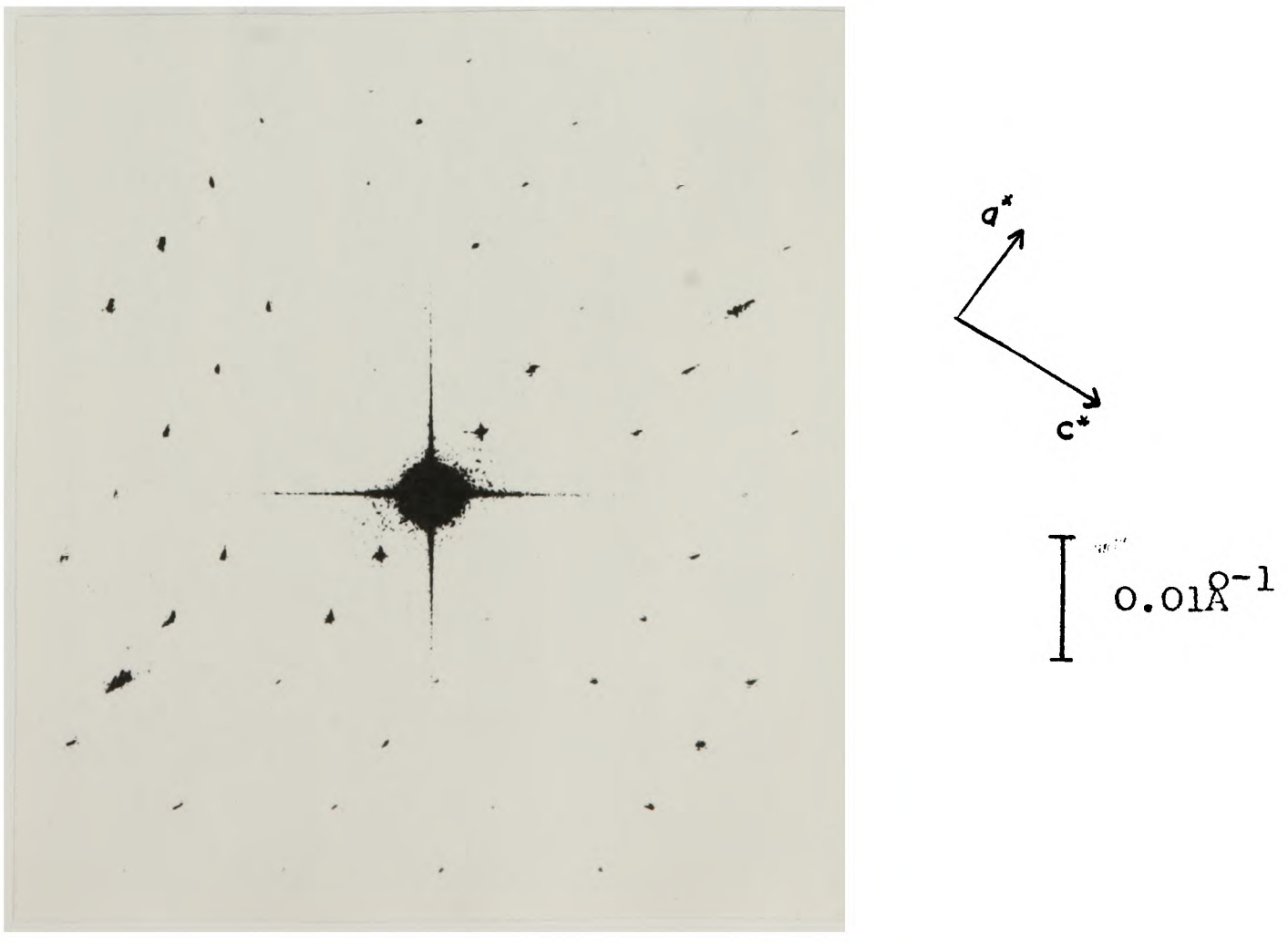

Plate 4.5 Optical diffraction pattern of a selected area from a micrograph like plate 4.3. (By P.A.M.Eagles and R.N.Pau).

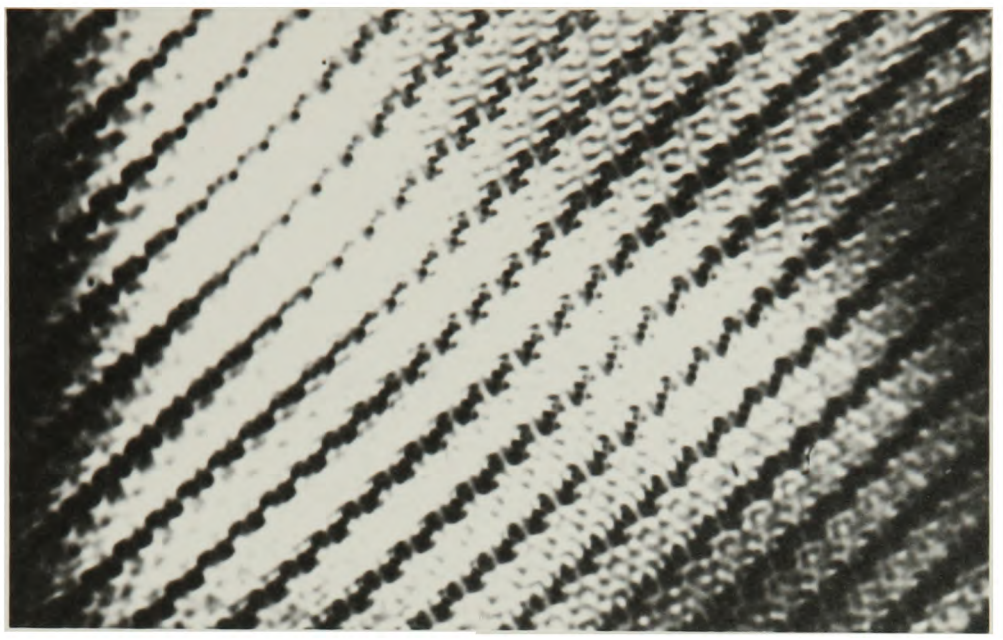

100Å

Plate 4.6 Image produced by optical reconstruction of a selected area of a micrograph like plate 4.3, showing an apparent change of structure. Magnification: 500,000. (By P.A.M.Eagles andR.N.Pau).

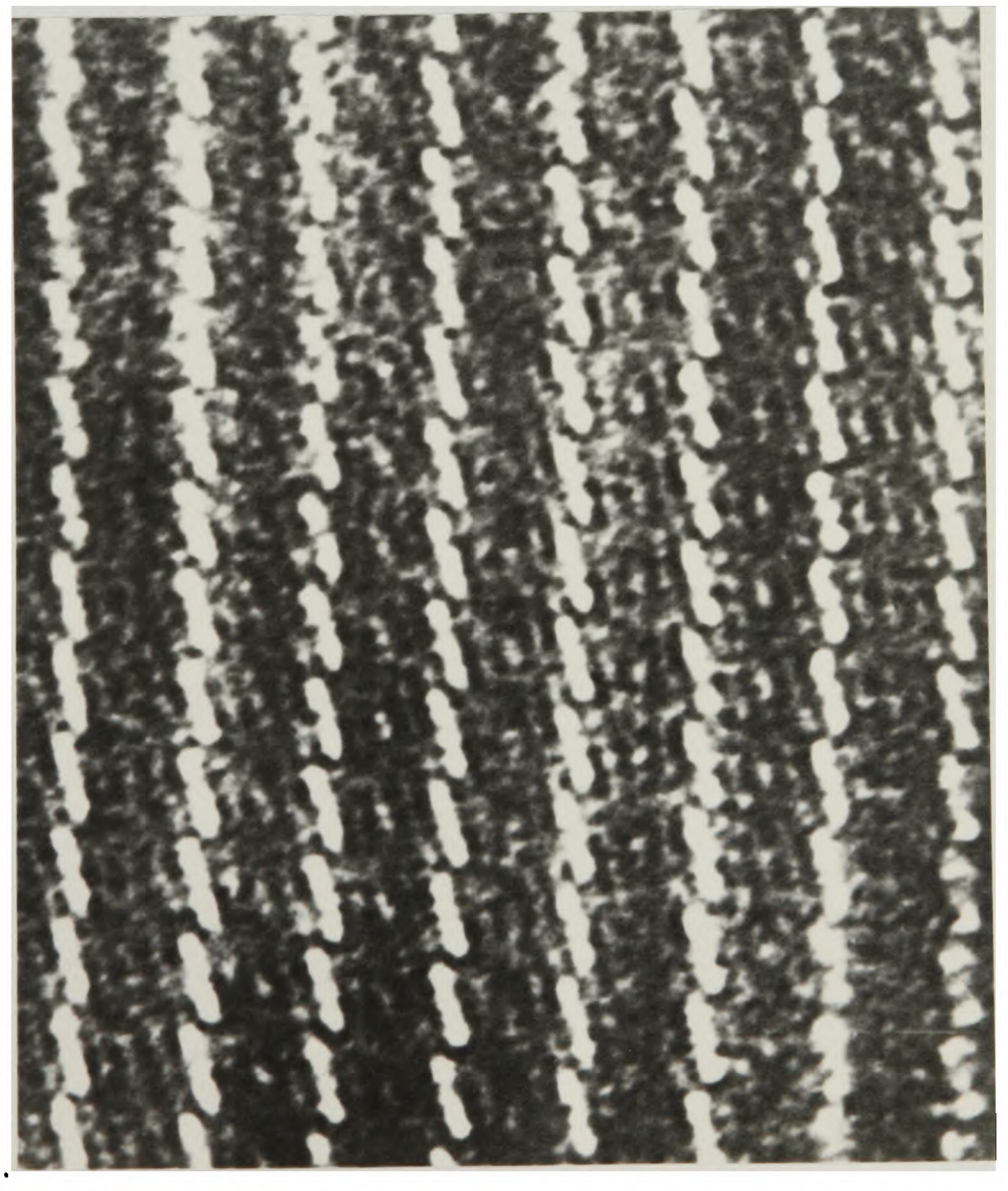

100Å

Plate 4.7 Image produced by five superimpositions of a selected area of a micrograph, like plate 4.3. Magnification: 1,000,000. The stain is white. (By P.A.M.Eagles and R.N.Pau).

Plate 4.8 Sonicated lamella from *S.membramacea* positively stained with 0.1% uranyl acetate solution. Two orientations of the major striations are seen. Magnification of plate: 100,000. Magnification of print: 350,000. (By L.J.Stump and the author).

Plate 4.9 Sonicated lamella from *S.membramacea* positively stained with 0.1% uranyl acetate solution, showing the more closely spaced striations as the dominant feature. Magnification of plate: 100,000. Magnification of print: 330,000. (By the author)

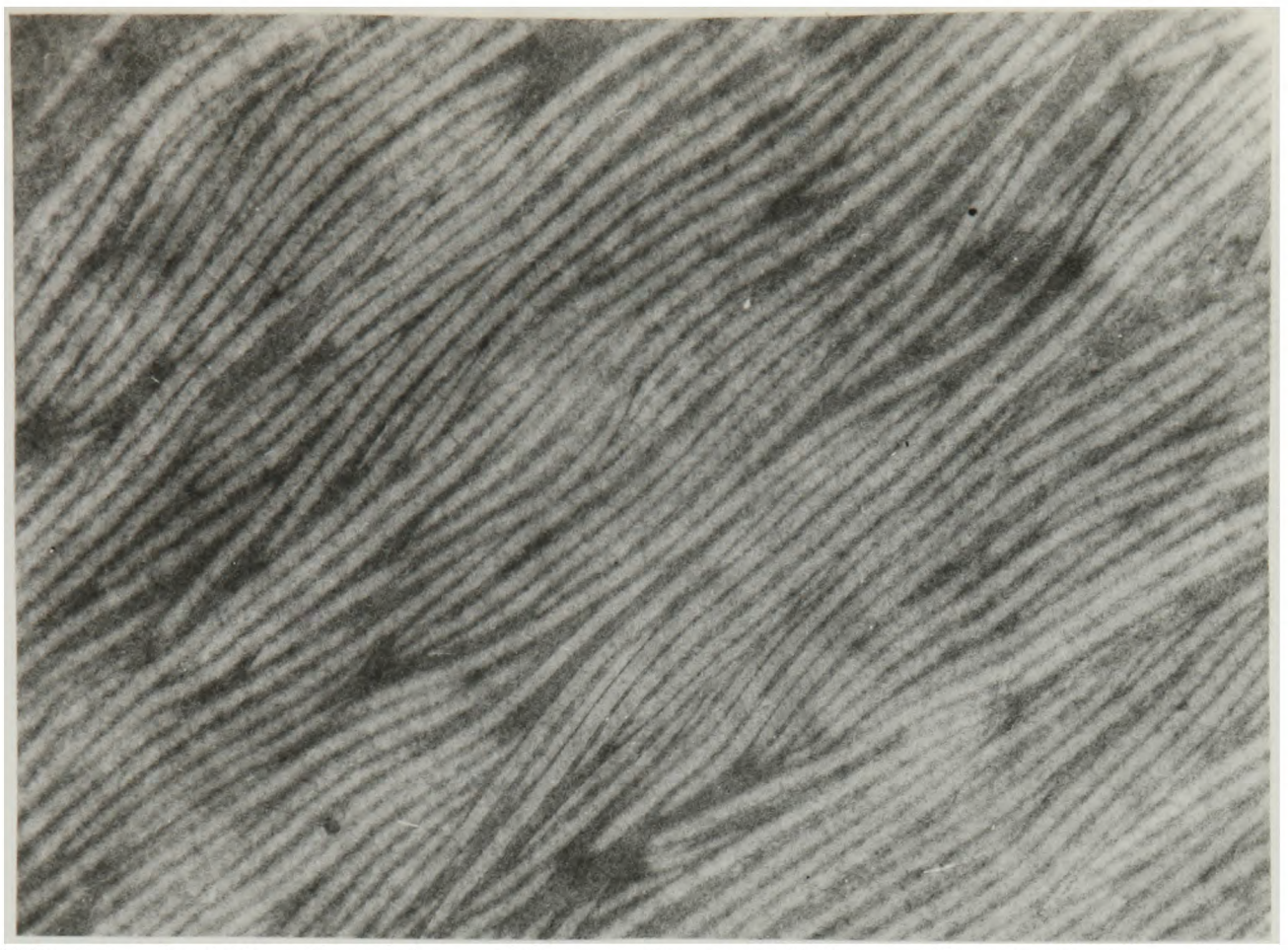

Plate 4.10 Section through a ribbon from *S.tenuidentata* approximately perpendicular to the lamellae surfaces, showing packing of 400 Å thick lamellae. Stain: uranyl acetate and lead citrate. Magnification of plate: 43,000. Magnification of print: 70,000. (By B.M.Luke).

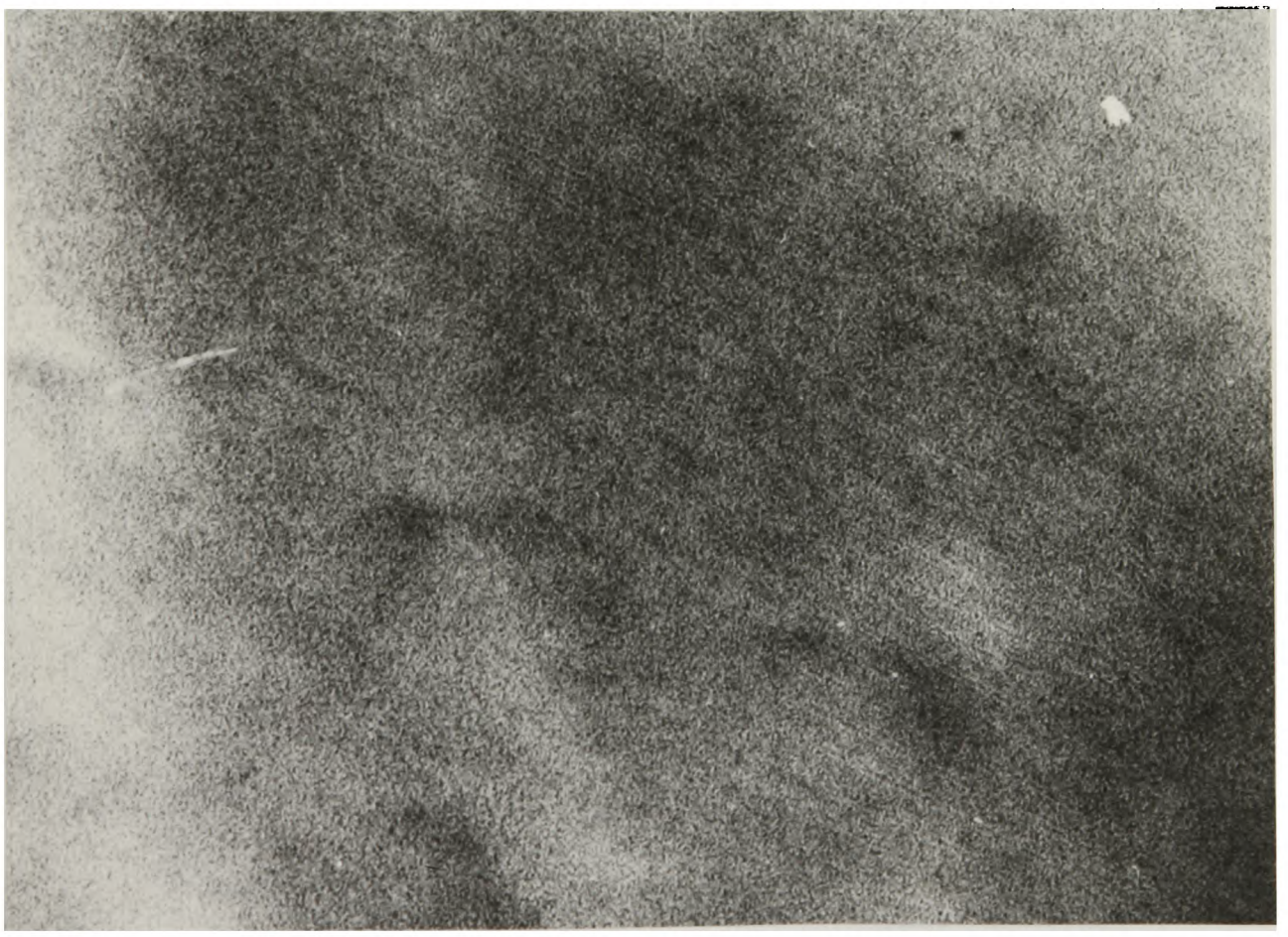

Plate 4.11 Sectioned ribbon from *S.tenuidentata* stained with uranyl acetate and lead citrate, showing the major striations Magnification of plate: 67,000. Magnification of print: 200,000. (By B.M.Luke).

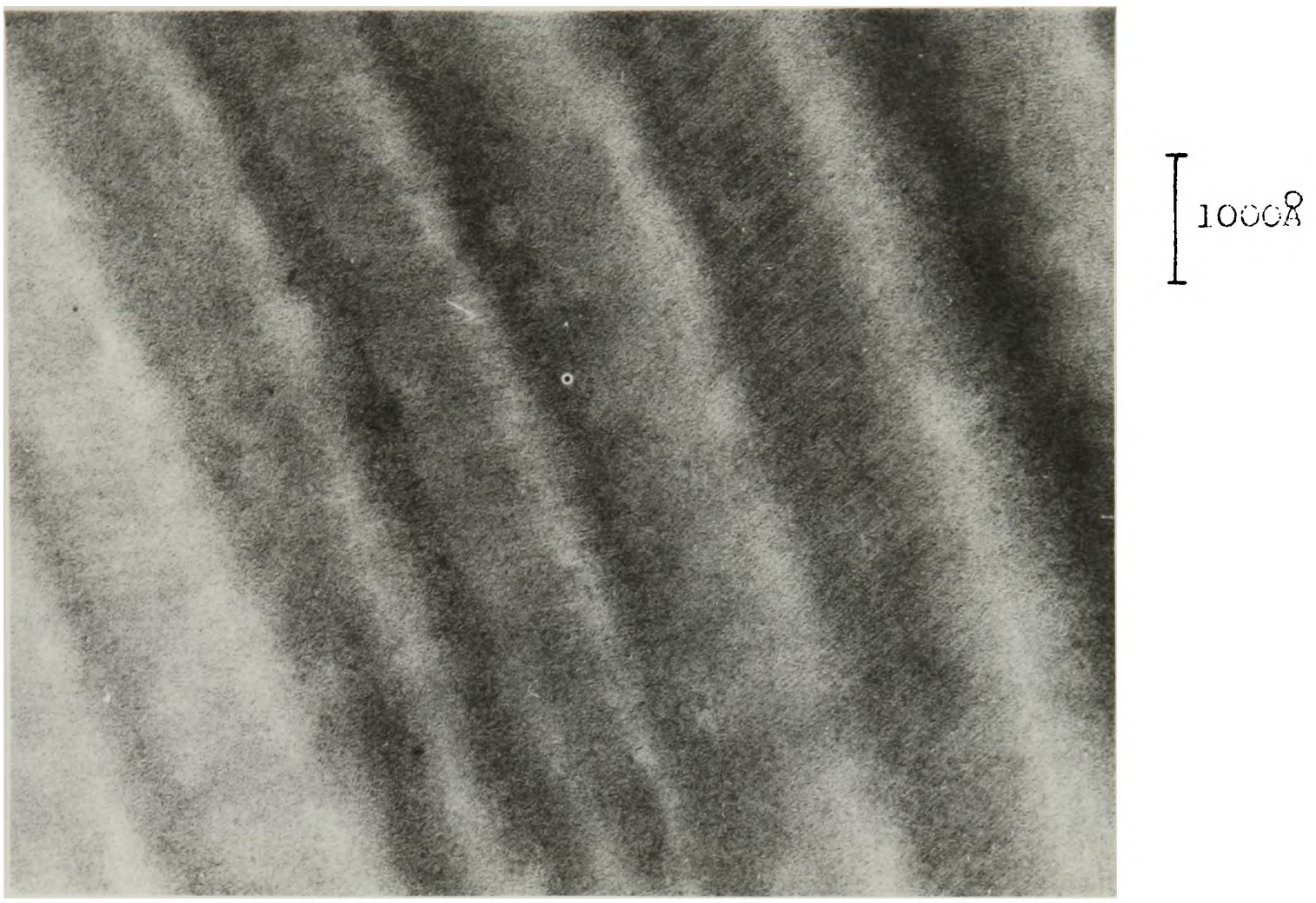

Plate 4.12 Sectioned ribbon from *S.tenuidentata* stained with uranyl acetate and lead citrate. The section, taken at an angle through several lamellae, shows that the major striations are continuous across a lamella. Magnification of plate: 67,000. Magnification of print: 145,000. (By B.M.Luke).

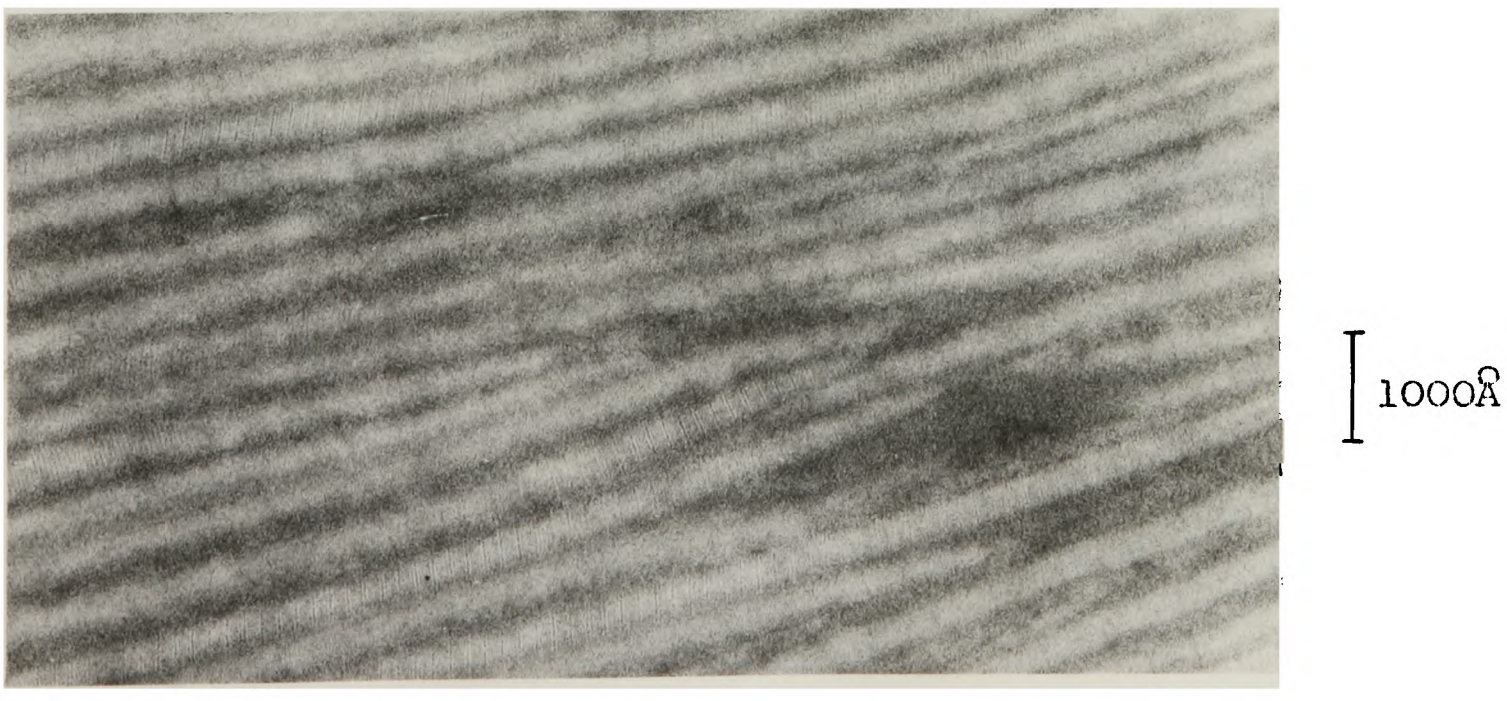

Plate 4.13 Sectioned ribbon from *S.tenuidentata* stained with uranyl acetate and lead citrate, showing several different patterns of transverse banding. Magnification of plate: 67,000. Magnification of print: 110,000. (By B.M.Luke).

Plate 4.14. Section through a ribbon from *S.tenuidentata* approximately perpendicular to lamellae surfaces, showing a regular 90Å transverse banding. Stain: uranyl acetate and lead citrate. Magnification of plate: 43,000. Magnification of print : 83,000. (By B.M.Luke).

Plate 4.15 Section through a ribbon from *S.tenuidentata* approximtely perpendicular to the lamellae surfaces, showing a regular 30Å banding and also the pattern referred to as 'myosin-like'. Stain: uranyl acetate and lead citrate. Magnification of plate: 67,000. Magnification of print: 200,000. (By B.M.Luke).

Plate 4.16 Section through a ribbon from *S.tenuidentata* approximately perpendicular to the lamellae surfaces, showing the pattern referred to as 'myosin-like' and drawn in Fig.4.2. Stain: uranyl acetate and lead citrate. Magnification of plate: 67,000 . Magnification of print: 140,000 .(By B.M.Luke).

CHAPTER 5

X-RAY DIFFRACTION

5.I Studies on the Gland Contents

5.I.I Removal of Gland Tubules

5.I.2 Physical Properties

5.I.3 Specimen Preparation

5.I.4 X-Ray Patterns

5.I.4.I The Equatorial Pattern

5.I.4.2 The Meridional and Near Meridional Pattern

5.I.4.2.I Low and Medium Angle Reflections

5.I.4.2.2 The 5Å Region

5.1.4.2.3 High angle reflections

5.I.4.3 The Near Equatorial Pattern

5.I.5 Intact Gland Tubules

5.2 Studies on the Egg Case Ribbons

5.2.I Removal of Ribbons

5.2.2 Low Angle X-Ray Diffraction

5.2.3 Nomenclature

5.2.4 Medium Angle Diffraction Patterns of Ribbons from S.tenuidentata

5.2.4.I With the Beam Parallel to the Ribbon Surface

5.2.4.2 With the Beam Perpendicular to the Ribbon Surface

5.2.4.3 Polymorphic Forms

5.2.4.4 High Angle Pattern

5.2.4.5 Range of Order

5.2.4.6 Lipid

5.2.5 Intensities

5.2.6 Ribbon from the Egg Case of S.Membranacea

5.2.7 Stained Specimens from S.Membranacea

5.2.7.I Phosphotungstic Acid Stained Specimens

CHAPTER 5

X-Ray Diffraction

This chapter describes the results obtained by X-ray diffraction and some of the physical properties of the materials examined. The data given are those used in the arguments, the complete data being given in Appendix II.

5.1 Studies of the gland contents

These were carried out on a female mantid of species Sphodromantis membramacea, as shown in plate 5.1.

5.1.1 Removal of gland tubules

The insect was first anaesthetised with chloroform. Access to the gland was obtained by cutting along the mid-ventral line from the ovipositor to the thorax. The gland, filling about half the abdomen, contains green tubules about 1 mm. in diameter and is as described in chapter 1. A number of aqueous solutions, including water, were tried as preservatives of the gland during dissection, but all caused rapid coagulation of the contents, so the cuticle was kept in place as long as possible. A one or two centimetre length of gland tubule could easily be removed by pulling it free with forceps. After two or three hours, the whole gland hardened.

Only about one insect in five was found to provide suitable material for experiments. Age appeared to be a factor, young insects having a small gland and older insects having a gland with degenerating tubules.

5.1.2 Physical properties

As the gland contents hardened after a short time, these experiments were performed jointly with R. Kerr.

It was hoped to be able to preserve the gland contents. A range of concentrations of sodium chloride, calcium chloride and mixtures of both in aqueous solution all produced coagulation of the gland contents. Varying the pH had little effect, nor did the removal of calcium ions with EGTA, or the removal of both calcium and magnesium ions with EDTA. The blood of the insect itself, which forms a green jelly on contact with the air, was the best anti-coagulant. Glycerol also prevented coagulation until hardening occurred after several hours.

A punctured tubule was placed under glycerol. Observation between crossed polars showed high birefringence and good extinction for the material flowing from the orifice, indicating that flow orients the material. When left under glycerol for a few hours, spherulites were obtained similar to but smaller than those produced by Neville (Neville and Luke, 1971).

5.1.3 Specimen preparation

A gland tubule was held with two pairs of forceps and stretched gently. The outer wall of the tubule broke and sometimes left a thin filament of the contents between the two parts. Each severed end closes to leave a small orifice through which a thin fibre may be pulled. As the two parts are drawn apart, the tubule contents flow out. The fibre dries a few centimetres from where it is produced, but by then it has been stretched to about twice its original length. Fibres can only be drawn at about

one centimetre per second. Below this speed, the fibre is stretched less and sometimes dries so as to seal the orifice. Above this speed it breaks, allowing the undried portion to shrink. Fibres up to 30 cm. in length have been drawn. It is likely that flow orientation is much more important than orientation by stretching.

The fibres produced were between 10 μm and 30 μm in diameter, highly birefringent and gave almost perfect extinction between crossed polars. After a few weeks, the fibres gain a mosaic appearance and show less extinction. This happens overnight at 100% relative humidity. Fibres were held under tension at 100% relative humidity in an attempt to increase the orientation and crystallinity, but the decrease in extinction and the loss of fibres through breakage indicated that such experiments could result in the loss of the material. When water made contact with the fibres, they became soft, white and fluffy. X-ray patterns obtained after a few weeks, when extinction is poor, showed that orientation was still good and the pattern had changed little. A photograph of fibres a month after pulling is shown in plate 5.3. This was taken between crossed polars and shows the high degree of birefringence.

The fibres were brittle, elastic, and stretched very little, presenting problems for mounting. A U-shaped support with a V filed in each arm was used after removal of the sharp edges. A small clamp was placed on each end of the fibre, which was then rested over the support and glued into position with a solution of cellulose nitrate in acetone. The fibre could then be cut, leaving a length of fibre glued to the support. Several hundred fibres were mounted one at a time, so as to form a bundle.

5.1.4 X-Ray patterns

The bundle of fibres was exposed under room conditions with a cylindrical film and a specimen film distance of 11.07 cm. (calibrated using aluminium powder). Plates 5.6-5.8 show the X-ray patterns obtained when the fibre axis is at right angles to the beam and when it is tilted from this position by 8.5° and 31° respectively. The patterns reveal a highly oriented structure with limited crystallinity.

5.1.4.1 The equatorial pattern

The equatorial pattern is very similar to that obtained from α-keratin (Fraser et al., 1964). Most of the intensity is in the slowly varying background, presumably from material with little crystallinity. Superimposed on the background are three broad maxima which index on a tetragonal unit cell. Closer inspection reveals splitting of reflections. Owing to the varying background, it is difficult to ascertain the true position of a reflection. To overcome this, an equatorial densitometer trace was obtained using the Joyce-Loebl densitometer (fig. 5.1). The background was estimated and subtracted, leaving a profile of the reflections. It was seen that the eye estimated the position of a reflection as being at a point where the specific intensity was higher than it was at the peak position indicated by the trace. For the purposes of estimating the unit cell, it was considered that the separations between reflections were best estimated for reflections of similar intensity on a uniformly varying background. Positions were considered to be estimated well where the background was uniform. As the eye integrates over the whole reflection, it was taken to give a better indication of positions

than the densitometer. The measurements and indexing obtained are given in table 5.2. A quasi-tetragonal cell of sides 16.8 ± 0.5 Å and 15.4 ± 0.5 Å was considered to fit the data.

Not only were reflections split to make the unit cell only approximately tetragonal, but there were many very weak reflections whose positions could not be estimated accurately, perhaps relating to higher levels of organisation.

At low angles, there was a very weak broad shadow at about 30 Å and a weak equatorial streak out to about 50 Å. This streak had indications of maxima on a repeat of the order of 250 Å, but the pattern is not well resolved here.

5.1.4.2 The meridional and near meridional pattern

5.1.4.2.1 Low and medium angle reflections

There is a weak pattern on and near the meridian. It was not easy to determine which reflections were meridionals, owing to the prohibitive exposure time required to obtain a good pattern, but meridional components could be estimated. The meridional pattern corresponding to spacings less than 70 Å is not visible, but layer lines streak out to about 50 Å in the near equatorial region, allowing measurements to be made. All reflections streak along the layer lines. A peak in the overall transform occurs at the 17 Å reflection which is almost certainly on the meridian. The strongest layer lines occur at 163 Å, 78.5 Å, 53.3 Å and 17.08 Å.

The measurements and indexing are tabulated in table 5.3, which also includes standard errors for each reflection (See appendix I for the method of estimation). The standard errors are based on estimates of systematic

errors and considerations of random errors. The standard errors assume a normal distribution of measurements, but as the eye tends to select certain areas in a reflection, the distribution is not normal. The error is, therefore, only an indication and probably an underestimate of the true error.

The quality of the pattern makes unambiguous indexing difficult. It can be indexed on a cell of 490 $\pm$ 6Å, 1435 $\pm$ 8Å or 1944 $\pm$ 10Å. The standard deviation between observed and calculated values of reciprocal spacings would be expected to decrease proportionally with the increase in the proposed unit cell size, if there was no relation between the proposed and true cells. The true cell should be marked by an appreciable minimum in the standard deviation, as is the 1435Å unit cell. If the poorly indexed reflection at 395Å, which is difficult to measure owing to the proximity of the equatorial streak, is overlooked, then the 1435Å cell is by far the best. For sharp, strong reflections it is possible to index a pattern on such a large cell with a high confidence. In this case, the quality of the pattern makes this estimate uncertain. The cell size is almost certainly very large.

There are modulations in intensity of the near meridional reflections. It is difficult to obtain a good estimate, but the intensity is low in the region of 26Å and increases in both directions from here. The 17Å and 10Å regions are peaks in the modulation. The minima appear to be orders of about 26Å. However, these minima are apparently not of zero intensity.

5.1.4.2.2 The 5Å region

The transform reaches a maximum in the 5Å region (plate 5.7)

which is dominated by the strong meridional reflection at 5.18 ± 0.05Å. A number of weak reflections which are meridional or near meridional occur. Table 5.4 shows that they occur at separations corresponding to a repeat of 122Å. They can be fitted to a 490 Å cell as the 91st, 95th, 99th, 103rd and 107th layer lines. If the spacings are indeed regular, they would correspond to every 16th order on a cell of 1944Å, or to every 12th order on a cell of 1435Å, but indexing is beyond the quality of the data.

Broad maxima also occur with an equatorial component of 10.2Å and an axial one of 4.9Å.

5.1.4.2.3 High angle reflections

The high angle region (plate 5.8) is dominated by the strong meridional at 1.49 ± 0.01Å. The reflections in this region are broad with half widths of 0.02Å^{-1}. This suggests that the regular structures producing them extend for only 50Å. All reflections are very weak except for the one mentioned and a weak, broad reflection at 1.14Å, just within the limit of observation. The reflections are so weak that it is impossible to say whether or not they are meridional. The measurements are recorded in table 5.5.

5.1.4.3 The near equatorial pattern

Layer lines, which are strongest in the 10Å region, sample the row lines. Their positions are affected by the varying background, but they are consistent with being the first four orders of 82 ± 5Å, which is one sixth of 490Å or one eighteenth of 1435Å (**Table 5.6**).

5.1.5 Intact gland tubules

An X-ray diffraction pattern was obtained from an air hardened intact

tubule. A broad meridional arc extending through about a right angle was obtained near 5.1 Å. There was some preferential orientation along the tubule. This reflection probably comes from the same protein as that drawn into fibres.

5.2 Studies on the egg case ribbons

The rest of this chapter deals with studies carried out on ribbons removed from the hardened egg case.

5.2.1 Removal of ribbons

Egg cases were removed from the cages after they had turned brown. This occurs a few hours after laying. Cases used were between a few days and six months old. Plate 5.2 shows egg cases from Sphodromantis membramacea on the left and egg cases from S. tenuidentata on the right. The former is about 4 cm x 1.5 cm and the latter is about 2.5 cm x 1 cm. Both have layers of sheet and ribbon like protein encapsulating an inner region of regularly arranged eggs. S. tenuidentata has a layer of protein several millimetres thick which can be torn into sheets or ribbons. S. membramacea has a layer less than 0.5 mm thick, which is easily divided into ribbons.

The outer layer of protein is removed and moistened with distilled water. It is convenient to tear the protein apart with two pairs of forceps whilst examining it between crossed polars at a magnification of 6 or 12. It is possible to break down the material by shearing along the few lines along which it readily shears. Finally a ribbon about 15 mm x 0.5 mm x 0.1 mm is obtained. Such a ribbon removed from S. membramacea is shown in plate 5.4. It is seen that the birefringence colours vary greatly

across the specimen. About a dozen egg cases from S. tenuidentata were examined. Each egg case provides thousands of ribbons. Occasionally these can be broken down to give a unit which shows good extinction, but usually they become too small to use before this stage is reached. There is variation between egg cases. One case produced several ribbons showing areas which were deep blue between crossed polars and gave much better extinction. The largest of these areas was over 2 mm long and is shown in plate 5.5. Work on egg cases of S. membramacea suggested that they might produce better specimens than those produced by S. tenuidentata, but an exhaustive search was not carried out. Only one ribbon had a sufficiently large area of good extinction to obtain diffraction patterns from this area alone.

5.2.2 Low angle X-ray diffraction

X-ray diffraction patterns of ribbons from S. tenuidentata were obtained using specimen film distances of about 65 cm. With the flat face of the ribbon towards the source, no strong features were visible within the meridional arcs at 82Å. Weak features would not have shown owing to the long exposures required. Difficulties in handling the limited supply of good material and the difficulty of determining the molecular axis accurately made stacked specimens impracticable.

With the specimen mounted with the thin edge towards the source, strong equatorial reflections appeared, the intensity decreasing rapidly with increasing distance from the centre. The data for a ribbon dried under room conditions were collected. Those corresponding to spacings greater than 120Å were collected using a 64.7 cm. specimen to film distance, the rest being collected using a 17.50 specimen film distance. These

equatorials correspond to the first seven orders of 455 $\pm$ 3Å (Table 5.7). Plate 5.9 shows a pattern obtained from a specimen held over water.

5.2.3 Nomenclature

The three perpendicular directions in the ribbon are parallel to the a, b and c axes. The c axis is parallel to the ribbon axis. The a axis is in the plane of the ribbon and the b axis is at right angles to it. When reference is made to the primitive unit cell, the sides are designated as in fig. 4.1. ζ and ξ are the meridional and equatorial components of reciprocal space.

5.2.4 Medium angle diffraction patterns of S. tenuidentata

5.2.4.1 With the beam parallel to the ribbon surface

Specimens from the egg case of S. tenuidentata were supported horizontally with the X-ray beam at right angles to the ribbon axis and parallel to the ribbon surface. Patterns were obtained at room temperature (22°C) at 100% relative humidity, room conditions and over silica gel. Little change in the overall appearance of the pattern occurred as humidity was varied, but unit cell dimensions changed. There were small variations between specimens under the same conditions.

Plates 5.10 and 5.11 were patterns obtained at 100% relative humidity and at room conditions respectively. Plates 5.12 and 5.13 were obtained at room conditions and over silica gel respectively four months later. It is seen that the deterioration in the quality over this time was small. The specimen in plate 5.12 was tilted about its axis by 3° in order to bring reflections on the a axis on to the Ewald sphere. Little change was noted. This could be due to a substantial volume of reciprocal space

contributing to this reflection combined with the effects of disorientation. It is seen that specimens at 100% relative humidity have three reflections - an equatorial and a near equatorial pair - on the same layer line. As the humidity is decreased, a reflection outside the equatorial increases in intensity until it is as strong as the others over silica gel. It is the next reflection on the 450Å lattice. The meridional data are given in table 6.7.

The pattern is dominated by strong row lines corresponding to a repeat of about 18Å. These are most intense on the equator and in regions corresponding to spacings between 4Å and 5Å. Weaker row lines also occur indexing on a repeat of about 450Å. The axial repeat appears to increase at increasing resolution. 991Å fits quite well, but reflections on odd orders are weak or absent, so for most purposes a repeat of 495Å may be considered to describe the structure. The true unit cell with the fibre axis as one edge may be very large and it may change with conditions. For a full understanding, reference must be made to the primitive unit cell as in chapter 6, but it is useful to take the unit cell as 495Å while describing the data. The data are recorded in table 5.9. Data for meridional patterns are given in tables 6.5-6.7.

The 18Å repeat distance was estimated using the first and second order equatorial reflections. Between four and six orders appeared, depending on the camera geometry, the second being the strongest. It was considered that higher orders would not give accurate values without tilting the specimen. However, inclusion of all the orders made no significant difference (table 5.8). The values estimated were 18.6Å, 17.9Å and 17.5Å for material at 100% relative humidity, at room conditions and over silica gel respectively.

The axial repeat was estimated using reflections both on and off the meridian out to about 8Å. It varied little as humidity changed, being 495 ± 2Å, 494 ± 2Å and 492 ± 2Å at 100% relative humidity, at room conditions and over silica gel respectively. It was sometimes found that intensity moved to the neighbouring reciprocal lattice point, but the overall intensity distribution was the same. Small intensity variations were also found between specimens observed under the same conditions. The medium angle reflections are tabulated in table 5.9. Meridional data compiled from two similar patterns are tabulated in table 6.5.

The equatorial period is more difficult to ascertain, since reflections are not sharp equatorially. The low angle pattern gave a value of 455 ± 3Å for material under room conditions. The medium angle pattern gives periods of 485 ± 3Å, 462 ± 3Å and 452 ± 3Å for material at 100% relative humidity, room conditions and over silica gel respectively. The reflections are grouped close to the 18Å row lines.

Axial sampling on the 18Å row line was found with up to eleven orders of 82Å or one sixth of 495Å. Sampling of about 460Å equatorially can be seen within each reflection in the 18Å equatorial and near equatorial region. Axial sampling in the 9Å row line was usually hidden by disorientation, but one measurement was possible and gave an axial component of 73Å. The range of measurements was from 54Å to 82Å, so 82Å could be the true value, but lower values are more likely. Measurements of sampling in different parts of the pattern, including the 5Å region, gave a range of 80Å to 85Å.

5.2.4.2 With the beam perpendicular to the ribbon surface

Patterns were obtained with the beam perpendicular to the ribbon

surface. The pattern changed little as conditions changed but the unit cell became bigger. Plates 5.14 and 5.15 show the pattern obtained under room conditions and over silica gel respectively.

It is seen that the pattern is both more complex and more greatly arced than that obtained with the thin edge towards the source. The meridional pattern is the same but the rest of the pattern is different. The major modulation in the equatorial intensity has a period of 33.0 $\pm$ 0.6Å for a ribbon kept at 100% humidity. This period decreases as the humidity is decreased, becoming 32.1Å at room conditions and 30.6Å over silica gel.

The equatorial period is uncertain and could vary. At 100% relative humidity a period of 927 $\pm$ 6Å gave the best indexing. Most reflections occur on a lattice of 463Å, but some strong ones require a lattice of 309Å. The data displayed in table 5.10 indicates that the indexing is not the whole story. However, it is a useful approximation and helps in the presentation of the data. It is seen that 463Å is 14 x 33Å which can be related to the structure as seen in chapter 6. The equatorial period becomes 899 $\pm$ 6Å at room conditions and 859 $\pm$ 6Å over silica gel.

Table 5.10 reveals that the first odd order meridional occurs on the 35th layer line and this is very weak. As the layer line number increases, so does the intensity falling on odd numbered layer lines. Odd numbered layer lines of low orders have intensity only beyond the 20th row line. It is seen that a 495Å unit cell describes the low resolution structure.

The line of greatest intensity in the equatorial direction is often at about 88° to the line of greatest intensity in the meridional direction. There are possible reasons for this (See chapter 6).

5.2.4.3 Polymorphic forms

With the flat face of the ribbon towards the beam, different patterns were sometimes obtained. One such pattern is shown in plates 5.16 and 5.17. It was obtained from the specimen shown in plate 5.5. These patterns were normally obtained from areas less than 1 mm across. Larger areas sometimes gave patterns showing the presence of both types of structure in the same specimen under the same conditions.

The pattern is essentially identical to the other except that low and medium angle meridional reflections are rotated to a line at about 18^{o} to the fibre axis. The spacings remain the same, whereas the meridional components necessarily change. The patterns in the equatorial and $5\mathring{A}$ regions are the same for the two patterns.

The degree of arcing in certain meridional reflections suggests that any of the specimens examined may contain structures producing these reflections at angles other than about 0 degrees and 18 degrees to the meridian. This and the possibility of reflections overlapping due to this effect and disorientation makes intensity estimation very difficult.

5.2.4.4 High angle pattern

There is an intense pattern in the $5\mathring{A}$ region, as shown in plate 5.18. The meridional pattern is not simple, but specimens tilted by 8.5 degrees give a strong reflection at $5.12 \pm 0.02\mathring{A}$.

With the beam striking the face of the ribbon, disoriented patterns are produced which are difficult to interpret, but with the beam striking the thin edge, the pattern is less disoriented. The $5\mathring{A}$ region is sampled by the $18\mathring{A}$ row lines, which are themselves sampled axially by a period of about $85\mathring{A}$ (about one sixth of $495\mathring{A}$).

at higher angles there are no strong features, the strongest being the very weak meridional at 1.485 ± 0.005Å, which is sampled by several orders of about 500Å (measurement is difficult), presumably corresponding to the 495Å unit cell.

5.2.4.5 Range of order

From the widths of reflections, the size of the crystallites was estimated assuming the material was a mosaic of perfect crystals. In practice the widths come from a number of effects, in particular short range imperfections. The widths estimated corresponded to about 450Å in the b direction, 1000Å in the a direction and a distance at least of the order of 10,000Å axially.

The irregularity of specimen shape made precise estimates difficult, since broadening due to the non-zero specimen size could only be estimated approximately.

5.2.4.6 Lipid

Some specimens had a substantial amount of lipid producing a ring at about 45Å. Plate 5.19 shows an X-ray diffraction pattern of a ribbon held with the flat face towards the beam. The intense lipid ring almost totally disappeared if the specimen was soaked in acetone for 10 minutes. With the thin edge towards the beam, the ring was concentrated on the equator and it was sampled by the 450Å lattice giving spacings of 46.4Å and 41.5Å under room conditions.

5.2.5 Intensities

The intensity distribution is very similar for different specimens, but

the intensity for particular reflections often changes. Table 5.11 shows the extent of such changes for strong meridionals under the three different degrees of humidity used.

Arcing and overlapping reflections made intensities difficult to estimate. The intensities were estimated from a densitometer trace, taking account of the disorientation. Since the disorientation is high and the focal size small, integrated intensities were found by multiplying the specific intensity by the layer line number. The intensities of the meridional reflections were corrected for the Lorentz and polarization factors (Guinier, 1963) and finally normalised to give a total intensity of 1000 up to and including the 64th layer line. These intensities are recorded in table 5.12 for two specimens supported with the thin edge towards the beam under room conditions. It is seen that the intensity is a maximum in both cases close to the 46th layer line. Only one of the two specimens, however, has a high intensity on the 32nd layer line.

At high intensities, densitometer readings become non-linear. To avoid errors from this, intensities on the backing film were compared with those on the front film. For very intense regions, the appropriate corrections were made.

Table 5.13 gives similar intensities estimated from a pattern obtained from a specimen oriented with the flat face towards the beam.

5.2.6 Ribbons from the egg case of S. membranacea

The X-ray diffraction patterns obtained were almost identical to those obtained from specimens from the other species. Plates 5.20 and 5.21 show patterns obtained with the thin edge towards the beam at 100% relative humidity and with the flat face towards the beam at room conditions. The disorientation present is normal except where an exhaustive

search has been made for a good specimen, as was done for S. tenuidentata.

There was no significant change in the unit cell dimensions. The changes were of the kind found between different specimens of S. tenuidentata. The greatest change was that the strong 82Å meridional was replaced by a weak one at 100Å. In S. tenuidentata this reflection occurred in only one specimen which was observed flat on at 100% relative humidity. In this case it was accompanied by a strong 82Å reflection. It must be remembered that this appeared with the specimen oriented edge on for a specimen with a large degree of disorientation, as revealed by the pattern obtained with the flat face towards the beam.

5.2.7 Stained specimens from S. membramacea

Staining specimens for a few days had little effect, so the specimens used were soaked for three months. The effects of stain were not pronounced, especially when phosphotungstic acid was used. Uranyl acetate had a greater effect. The staining solutions used were 2% phosphotungstic acid (PTA) neutralised with sodium hydroxide and 0.5% uranyl acetate. The ribbons were removed from the solutions, the excess solution was removed, and they were allowed to dry under room conditions before being X-rayed.

5.2.7.1 PTA stained specimens

These specimens were little changed by the stain and the unit cell dimensions were unchanged. Insufficient exposure time was available to examine small changes. The diffraction patterns obtained for the specimen with the thin edge towards the source and with the flat face

towards the source are shown in plates 5.22 and 5.23 respectively.

5.2.7.2 Uranyl acetate stained specimens

5.2.7.2.1 Very low angle reflections

With the flat face towards the beam at a specimen film distance of 17.5 cm., the region between 100Å and 200Å was investigated. This region had revealed no reflections with any other treatment, but two pairs of strong reflections were observed with uranyl acetate. These reflections can be seen in plate 5.24. They are arcs on lines 21.5 degrees to the equator, the lines crossing at the centre of the pattern. The spacing is 147Å. The meridional and equatorial components are 402Å and 158Å. The unit cell estimated as for earlier patterns is given by the higher angle pattern as 990Å axially and 923Å equatorially. It cannot definitely be said that the true value of the 402Å estimate is not 495Å, but this seems unlikely for a strong well defined reflection such as this. The arcing should not produce such a large error. Reflections can occur in positions other than expected if they are sampling a rapidly varying transform, but this requires the reflection to correspond to a substantial volume of reciprocal space for an individual crystallite within the ribbon. This appears not to be the case. We must conclude that even though a 495Å cell describes the meridional pattern quite well, this is unlikely to be a true cell. This dilemma is resolved in chapter 6.

There is an additional weak reflection whose measurement is rendered difficult by the parasitic scatter from the monochromator. It occurs at a spacing of approximately 165Å and is of the order of 15° from the meridian.

5.2.7.2.2 The medium angle pattern

The medium angle pattern is shown in plates 5.25, 5.26, 5.27 and 5.28. The first three being determined with the flat face towards the beam. As there was substantial background at low angles, three plates are given to enable all features to be seen. Plate 5.28 shows the pattern obtained when the thin edge is towards the beam.

The unit cell dimensions increased in the two equatorial directions from 899Å to 923Å in the a direction and from 462Å to 493Å in the b direction. These values are close to those for an untreated specimen at 100% relative humidity (927Å and 485Å).

The meridional pattern (tables 5.14 and 6.4) has a 40Å modulation in intensity. The 41.2Å meridional becomes very strong, whereas it is weak or absent for untreated S. tenuidentata and medium for S. membramacea.

With the beam parallel to the ribbon surface, the 18Å equatorial region increases in intensity, whereas the 9Å region decreases in intensity. The spacings of these reflections become 19.0Å and 9.45Å.

With the beam perpendicular to the face of the ribbon, three equatorial reflections are seen to have been enhanced by the treatment. These occur at 29.7Å, 33.5Å and 36.8Å, They can be indexed on 923Å, as the 25th, 28th and 31st orders, but it is seen that they closely fit the 8th, 9th and 10th orders of 297Å.

5.2.8 Specimens from S. membramacea treated with chlorobenzene and bromobenzene

A specimen was soaked in a mixture of chlorobenzene and bromobenzene (specific gravity 1.33) for two weeks. The X-ray diffraction

patterns of the treated specimens are given in plates 5.29 and 5.30 for the specimen positioned with the flat face and the thin edge respectively towards the beam. The patterns were almost identical to those obtained from untreated specimens. The unit cell size was intermediate between those of specimens under room conditions and over silica gel, the equatorial components being 883Å and 457Å.

It is noticed that weak meridionals occur on both the 10th (99Å) and 12th (82Å) layer lines in the specimens observed. There is also an increase in intensity falling on the 18th layer line away from the meridian. The row lines of the 18Å repeat are sharper than normal. The meridional data are recorded in table 6.10.

5.2.9 Meridional modulations in intensity

It is immediately apparent that the patterns decrease in intensity beyond 15Å, and beyond 8Å they fade to nothing before appearing again in the 5Å region. Only approximate measurements can be made, but the first minimum occurs between 13.1Å and 9.5Å for untreated specimens. Measurements on patterns from specimens treated with a mixture of chlorobenzene and bromobenzene suggest a minimum in the range 14.3Å to 10.7Å. A uranyl acetate treated specimen gave a pattern indicating that the minimum occurs at 12.1Å or less. All these values are consistent with the range 10.7Å to 12.1Å.

TABLE 5.1

List of intensities in order as used in this chapter:

vvs	very, very strong
vs	very strong
s	strong
ms	medium strong
m	medium
mw	medium weak
w	weak
vw	very weak
vvw	very, very weak.

TABLES 5.2 - 5.6 relate to fibres drawn from the gland.

TABLE 5.2

Equatorial spacings Observed spacings Å			Indexing	Calc. spacings Å
Main maxima	Determined using a densitometer	Finer Structure		
15.6	18.6	16.31	01	16.80
		14.95	10	15.44
10.7	10.9	10.92	11	11.34
	8.4	8.40	02	8.40
8.3	7.8	7.96	20	7.72

The cell sides are 16.8 ± 0.5Å and 15.4 ± 0.5Å

TABLE 5.3

Meridional and near meridional reflections

Observed spacing Å	Standard error Å		Notes	Indexing on 489.5Å Layer line number	Indexing on 489.5Å Calc. spac.	Indexing on 1435Å Lay. line number	Indexing on 1435Å Calc. spac.	Indexing on 1944Å Lay. line number	Indexing on 1944Å Calc. spac.
395	26	w	sharp	1	490	4	359	5	389
234	9	w	sharp	2	245	6	239	8	243
163	3	m		3	163	9	159	12	162
129	2	w	sharp	4	122	11	130	15	190
102	2	w	sharp	5	98	14	102	19	102
78.4	1.5	m		6	81.6	18	79.7	25	77.8
53.3	0.3	mw	blurred	9	54.4	27	53.1	36	54.0
41.4	0.4	w		12	40.8	35	41.0	47	41.4
33.3	0.2	vvw		15	32.6	43	33.4		
30.4	0.2	vw		16	30.6	47	30.5	64	30.4
26.0	0.2	mw		19	25.8	55	26.1	75	25.9
23.9	0.2	mw		20	24.5	60	23.9	81	24.0
21.22	0.10	mw		23	21.28	68	21.10	92	21.13
19.10	0.09	mw		26	18.83	75	19.13	102	19.06
17.08	0.08	m		29	16.86	84	17.08	113	17.20
16.38	0.09	mw	blurred	30	16.35	88	16.31		
14.26	0.08	vw		34	14.40	101	14.21		
13.01	0.07	vw		38	12.88	110	13.05		
11.09	0.06	w		44	11.12	129	11.12		
10.81	0.06	w	blurred	45	10.88	133	10.79		
9.82	0.07	w	broad	50	9.79	146	9.83		
9.08	0.06	vw		54	9.06	158	9.08		
8.62	0.07	vw		57	8.59	166	8.64		

TABLE 5.4

Meridionals or near meridionals in the 5Å region.

Observed spacing	Intensity	Fitted to a 489.5A° cell Index	Calc.spac.
5.38	w	91	5.379
5.18	s(meridional)	95	5.153
4.95	w	99	4.944
4.78	w	103	4.752
4.57	vw	107	4.576

The accuracy of measurement does not permit fitting to the 1435Å cell.

TABLE 5.5

Meridionals and near meridionals between 4Å and 1.1Å

Observed spacing Å	Intensity	description
3.20	vw	
3.06	vw	
2.49	vw	
2.13	vw	
1.93	vw	
1.65	vw	
1.49	s	meridional
1.37	vw	
1.30	vw	
1.18	vw	
1.17	vw	
1.14	w	very broad

TABLE 5.6

Layer lines sampling the row lines in the 10Å region.

Observed spacing Å	Intensity	Orders of 82Å
70.0	s	82.0
39.9	vw	41.0
30.1	w	27.3
21.7	vw	20.5

The spacings fit orders of 82 $\pm$ 5Å.
1/6 of the axial period is 81.7Å

TABLE 5.7

Low angle equiatorials for a ribbon at room conditions with its thin edge towards the source.

Observed spacing	Intensity	Order	Calculated spacing
Obtained with (505	vvs	1	455
64.7cm specim.(249	vs	2	238
film distance (153	ms	3	152
With 17.50 cm.(116	mw	4	114
specimen film (89	vvw	5	91
distance (73	vvvw	6	76
(64	vvvw	7	65

TABLE 5.8

Main equatorial row lines for a ribbon from *S.tenuidentata* at various humidities with the thin edge towards the beam.

100% R.H.			Room conditions			Over silica gel		
Order	spacing Å		Order	Spacing Å		Order	Spacing Å	
	Obs.	Calc.		Obs.	Calc.		Obs.	Calc.
1	18.31	18.6		17.70	17.9		17.39	17.5
2	9.33	9.3		9.00	8.95		8.80	8.75
3	6.19	6.2		6.01	5.97		5.87	5.83
4	4.64	4.65		4.50	4.48		4.42	4.38
5	3.73	3.72		3.62	3.58			
Period	18.6 ± 0.1Å			17.9±0.1Å			17.5± 0.1Å	

TABLE 5.9

Medium angle reflections for a ribbon from *S.tenuidentata* at room conditions with the thin edge towards the source.

* - reflections that fit poorly.

ζ Å^{-1} x 10^6		ξ Å^{-1} x 10^6		intensity	ℓ	k
Obs	Calc.	Obs.	Calc.			
0	0	859	866	w	0	4
0	0	1118	1082	w	0	5
0	0	1363	1299	w	0	6
0	0	1561	1515	w	0	7
0	0	2156	2165	w	0	10
0	0	2408	2381	w	0	11
0	0	2554	2598	w	0	12
0	0	2910	2814	w	0	13*
0	0	4856	4763	w	0	22*
0	0	5094	5196	w	0	24*
0	0	5514	5412	w	0	25*
0	0	5665	5629	s	0	26
0	0	6052	6062	s	0	28
0	0	6947	6928	m	0	32
0	0	7182	7144	w	0	33
0	0	7658	7577	w	0	35*
0	0	7874	7793	w	0	36*
1080	1113	500	433	w	11	2
1231	1214	0	0	s	12	0
1289	1316	5638	5629	s	13	26
1613	1619	501	433	vw	16	2
1922	1923	539	433	w	19	2*
2183	2226	4403	4330	w	22	30*
2195	2226	3926	3897	w	22	18
2220	2226	0	0	s	22	0
2507	2530	5505	5412	w	25	25*
2712	2732	1316	1299	vw	27	6
2833	2834	255	216	vw	28	1
3273	3238	0	0	s	32*	0
3446	3441	0	0	s	34	0

cont'd.

TABLE 5.9. cont'd.

3703	3744	0	0	w	37*	0
3753	3744	5553	5629	w	37	26*
4057	4048	0	0	w	40	0
4309	4352	0	0	s	43*	0
4656	4655	0	0	s	46	0
4930	4959	579	649	vw	49	3
4945	4959	285	216	w	49	1
5247	5262	454	433	vw	52	2
5310	5262	0	0	vw	52*	0
5414	5465	0	0	vw	54*	0
5474	5465	652	649	w	54	3
5516	5566	0	0	w	55*	0
5679	5667	0	0	w	56	0
5903	5870	0	0	w	58	0
5972	5971	3842	3897	w	59	18
6154	6173	5499	5412	w	61	25*
6174	6173	0	0	w	61	0
6370	6376	2444	2381	w	63	11
6533	6579	0	0	w	65*	0
6700	6679	1608	1515	w	66	7*
6787	6780	5647	5629	w	67	26
6791	6780	835	866	w	67	4
6833	6882	384	433	w	68*	2
6842	6882	0	0	w	68*	0
7113	7084	0	0	w	70	0
7533	7489	0	0	w	74*	0
7560	7590	0	0	w	75	0
7696	7691	0	0	w	76	0
7735	7691	0	0	w	76	0
8368	8400	828	866	w	83	4
8387	8400	0	0	w	83	0

TABLE 5.10

Data obtained from a ribbon from *S.tenuidentata* at 100% relative humidity with the beam perpendicular to the ribbon surface.

* Reflections that index poorly.

ζ Å $^{-1}$x10^6		ξ Å $^{-1}$x10^6				
Obs.	Calc.	Obs.	Calc.	Intensity	ℓ	h
0	0	2256	2266	mw	0	21
0	0	3377	3345	w	0	31
0	0	5739	5719	s	0	53
0	0	6044	6042	vw	0	56
0	0	6367	6366	s	0	59
505	505	2256	2266	mw	5	21
516	505	2886	2913	vw	5	27
583	605	1602	1618	mw	6	15
792	807	392	432	w	8	4*
822	807	986	971	s	8	9
942	908	5899	5934	w	9*	55*
1035	1009	0	0	w	10	0
1197	1211	0	0	s	12	0
1503	1514	3012	3021	w	15	28
1851	1816	4910	4963	w	18*	46*
2017	2018	2739	2698	w	20	25*
2187	2220	0	0	vs	22	0
2310	2321	2517	2482	w	23	23
2916	2926	517	539	w	29	5
3028	3027	1098	1079	mw	30	10
3256	3229	0	0	w	32	0
3402	3431	0	0	vs	34	0
3511	3532	0	0	vw	35	0
3870	3834	1062	1079	s	38*	10
4051	4036	0	0	s	40	0
4092	4137	1395	1403	s	41*	13
4432	4440	0	0	vw	44	0
4626	4641	0	0	vs	46	0
4727	4742	0	0	vw	47	0
4778	4742	1234	1187	mw	47*	11*
4921	4944	0	0	mw	49	0
5072	5045	1354	1403	mw	50	13*
5345	5348	727	755	mw	53	7
5345	5348	996	971	mw	53	9
5483	5448	0	0	vw	54*	0
5628	5650	0	0	mw	56	0
5857	5852	0	0	m	58	0
6045	6054	1159	1187	m	60	11
6128	6155	0	0	m	61	0
6391	6357	1519	1511	m	63	14
6569	6559	0	0	m	65	0

TABLE 5.11

Changes in strong meridionals. (*S.Tenuidentata)*

Approx. Space. Å	Layer Line	100% R.H. $Å^{-1}$ X10^6 Obs.	Calc.	int,	Room Conditions $Å^{-1}$ X10^6 Obs.	Calc.	int.	Over silica gel $Å^{-1}$ X 10^6 Obs.	Calc.	int.
41.2	12	1232	1208	s	1235	1214	s	1270	1219	s
22.5	22	2204	2220	s	2213	2226	s	2232	2235	s
15.4	32	3252	3229	w	3245	3238	ms	3264	3251	s
14.5	34	3430	3431	s	3448	3441	s	3404	3454	ms
13.4	37	absent			3685	3744	mw	3745	3759	m
12.4	40	4048	4036	ms	4055	4048	w	absent		
11.8	42	absent			absent			4237*	4267	mw
11.5	43	4338	4339	m	4304	4352	s	4338*	4369	ms
10.7	46	4650	4641	s	4637	4655	s	4665	4674	s
8.5	58	5857	5852	m	5883	5870	mw	5884	5893	m
8.1	61	6128	6155	m	6172	6173	mw	6196	6198	w
	64	absent			6496	6477	w/ms	absent		
7.6	65	6569	6559	m	absent			6594	6604	w

*not present together.

TABLE 5.12

Meridional intensities found from 2 patterns from *S.tenuidentata* obtained with the beam parallel to the ribbon surface. The intensities are corrected for Lorentz and polarisation factors.

Specimen one.

Layer line	12	22	32	34	36	42	46	53	58	61	64
Intensity	34	70	45	48	21	141	216	155	68	71	131

Specimen two.

Layer Line	12	22	32	34	37	40	46	49	54	56	58	61	64	68	70
Intensity	25	38	218	95	27	21	333	25	29	32	32	58	64	72	56

TABLE 5.13

Equatorial intensities found with the beam perpendicular to the ribbon surface, *(S.tenuidentata)* .

Row Line	21	27	32	53	58	63	74	85	88	97	112	122
Integrated Intensity.	112	149	96	457	1076	63	717	1445	276	1736	1286	1401

TABLE 5.14

Meridional pattern. Specimen of *S. membramacea* treated with uranyl acetate.

Intensity	$3\text{Å}^{-1} \times 10^6$	1/3 Å
w	2206	45.33
vs	2455	40.73
w	2763	36.20
mw	3181	31.44
mw	3430	29.15
vw	3760	26.60
m	4089	24.45
ms	4258	23.49
s*	4609	21.69
m*	6447	15.49

*Some weak reflections occur between these two reflections.

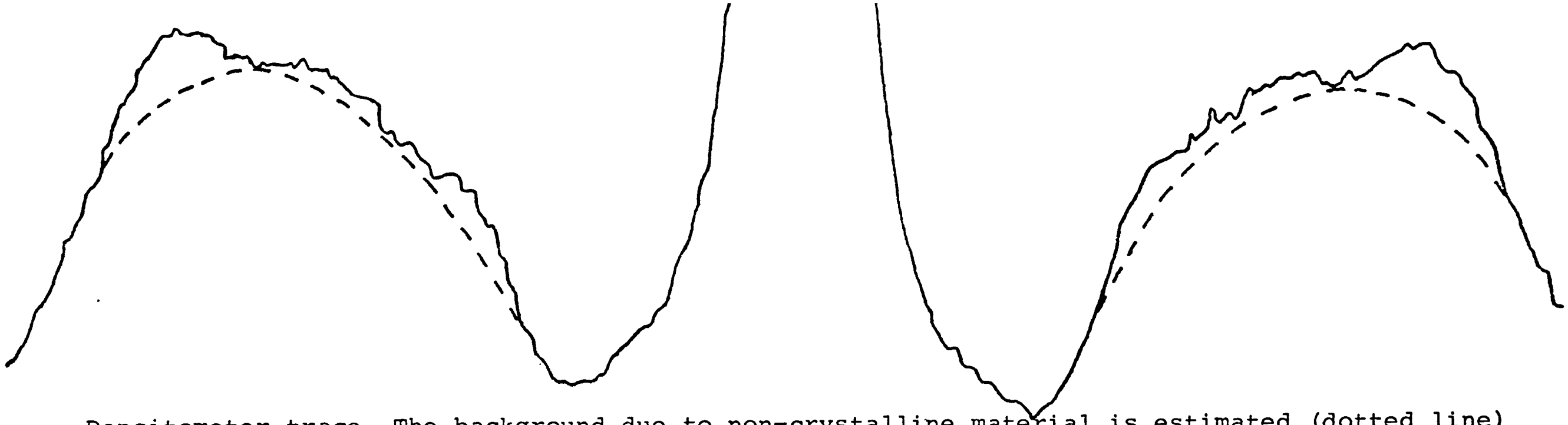

Densitometer trace. The background due to non-crystalline material is estimated (dotted line).

Trace after subtraction of the background.

Fig. 5.1 Densitometer trace along the equator of an X-ray diffraction pattern of fibres drawn from the left colleterial gland of *S.membramacea*. The typical α-helical profile is seen with reflections superimposed upon it.

PLATES 5.1 - 5.30

The X-ray diffraction patterns were obtained using the equipment described in Chapter 2. Unless specified otherwise, the specimen to film distance is 11cm. and a cylindrical film is used. The fibre axis is usually at right angles to the X-ray beam and perpendicular to the axis of the cylindrical film. The exceptions are most of the tilted specimens which are tilted from this position in the plane containing the fibre axis and the X-ray beam. Other tilted specimens are rotated about the fibre axis so as to explore the equatorial plane. Scattering from the mylar windows produces rings in the 8Å region. The scales marked are only approximately correct in the high angle equatorial region - a property of the camera geometry.

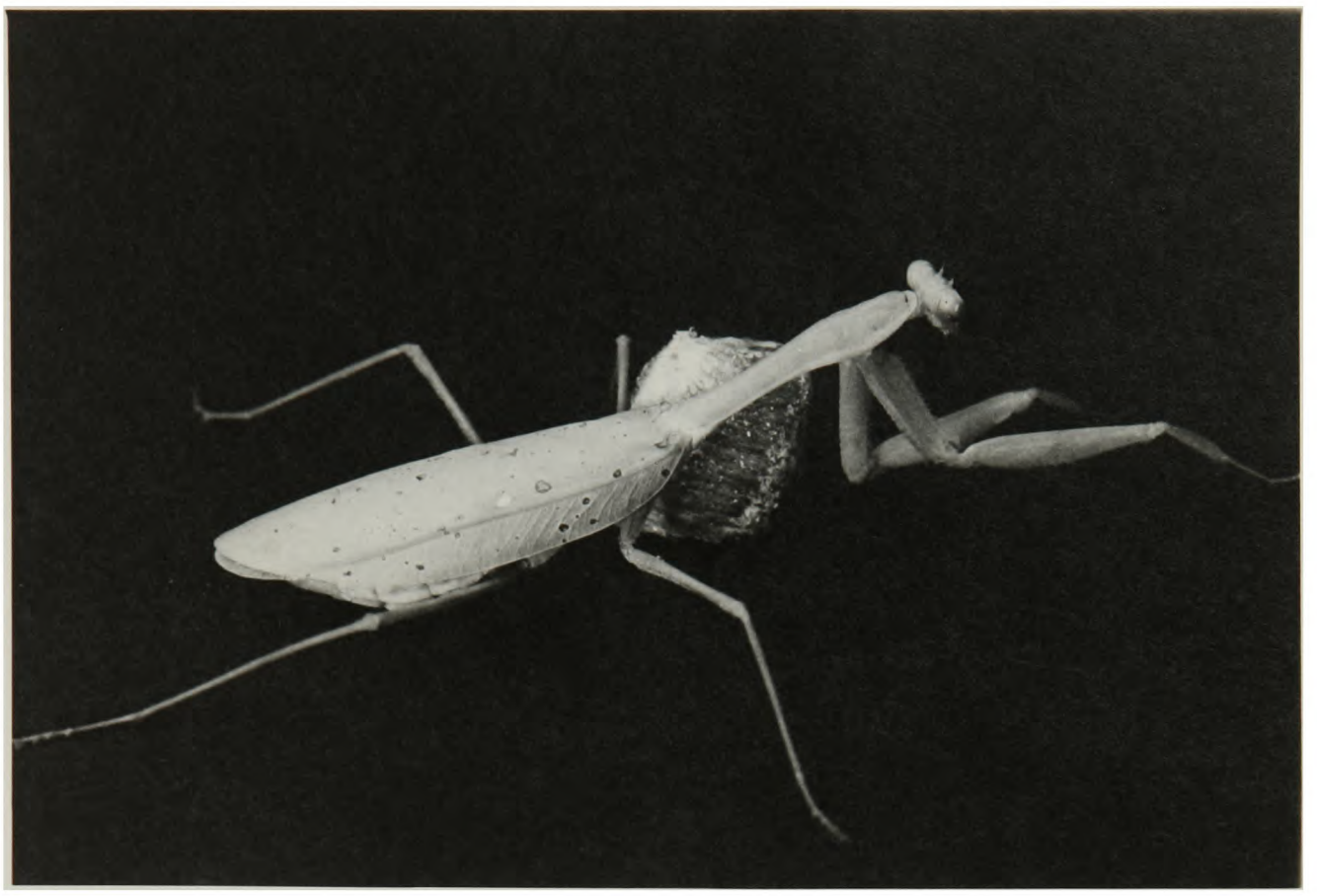

Plate 5.1 Adult female mantid of species *Sphodromantis membramacea*, together with an egg case. (About 2/3 life size).

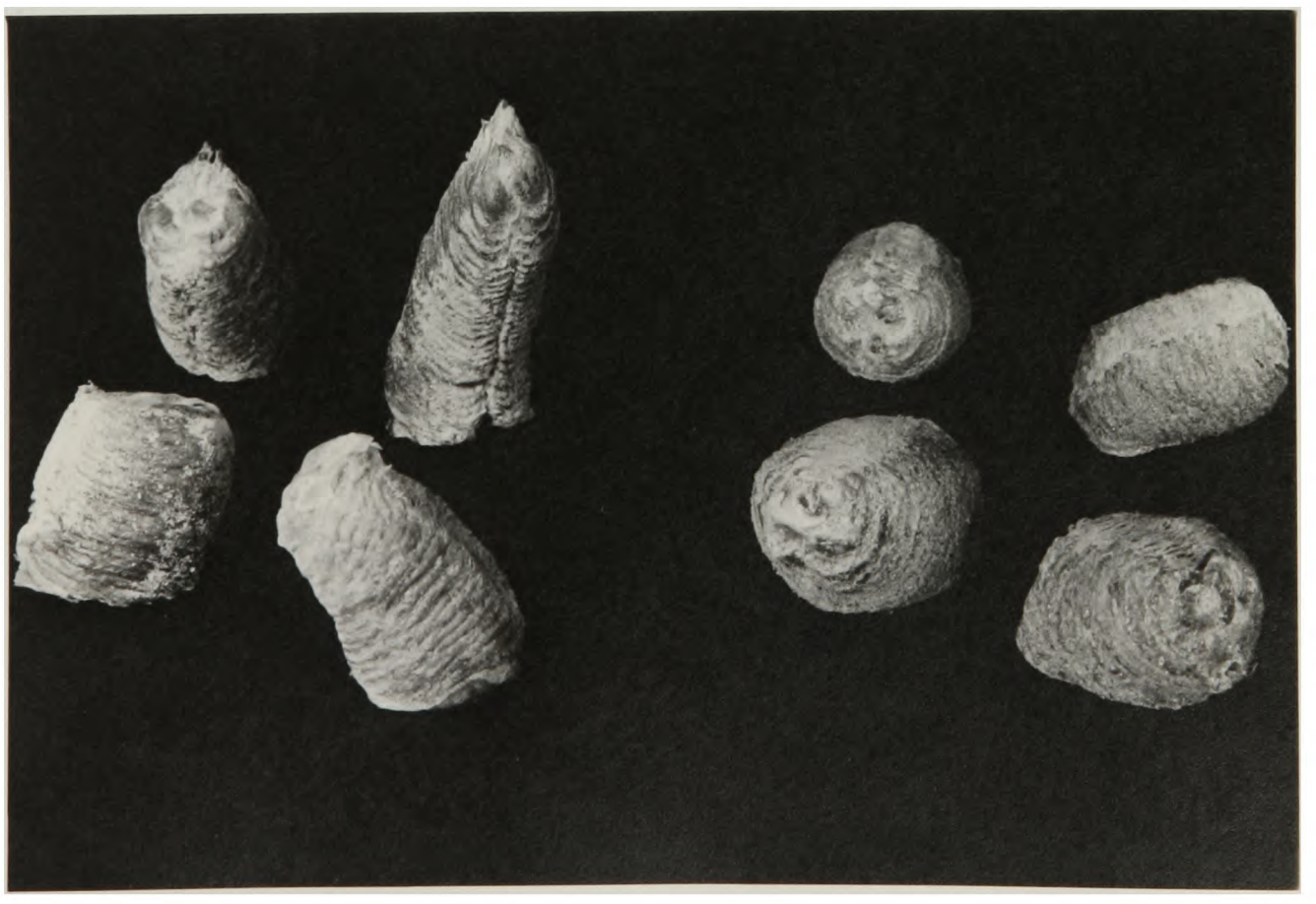

Plate 5.2 Egg cases from *Sphodromantis membramacea* (left) and *S.tenuidentata* (right). (Life size).

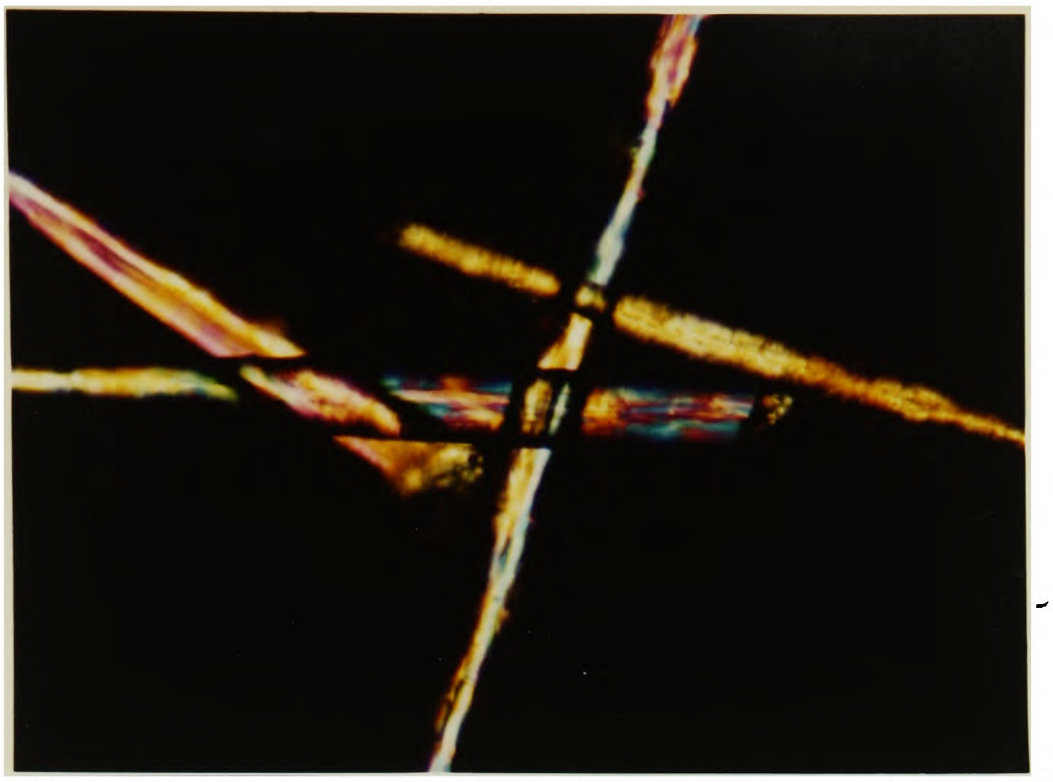

Plate 5.3 Fibres drawn from the left colleterial gland of *S.membramacea* photographed between crossed polars at a magnification of 100.

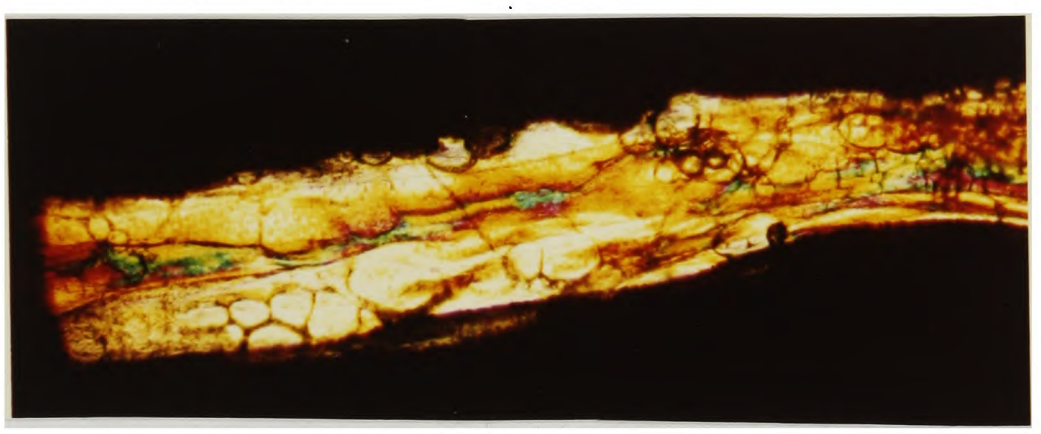

Plate 5.4 A ribbon from the egg case of *S.membramacea* photographed between crossed polars at a magnification of 20.

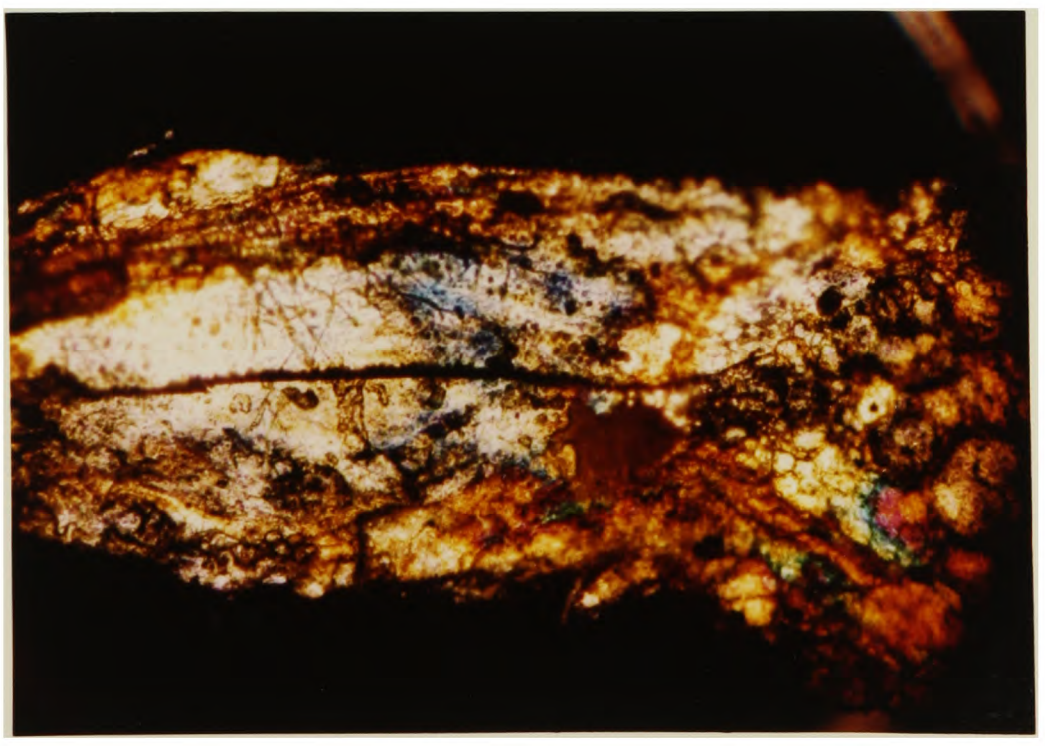

Plate 5.5 A well oriented area (coloured blue) in a ribbon from the egg case of *S.tenuidentata* photographed between crossed polars at a magnification of 50.

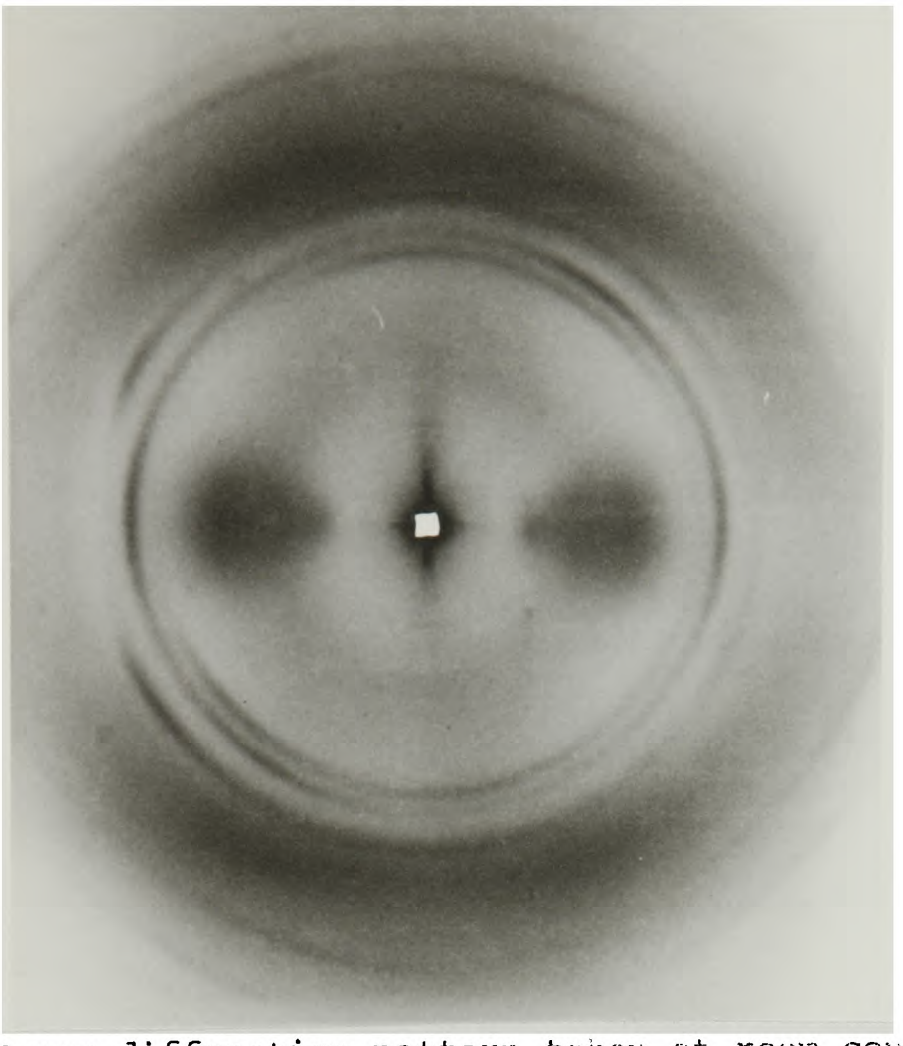

Plate 5.6 X-ray diffraction pattern taken at room conditions of fibres drawn from the left colleterial gland of *S.membranacea* 6 day exposure.

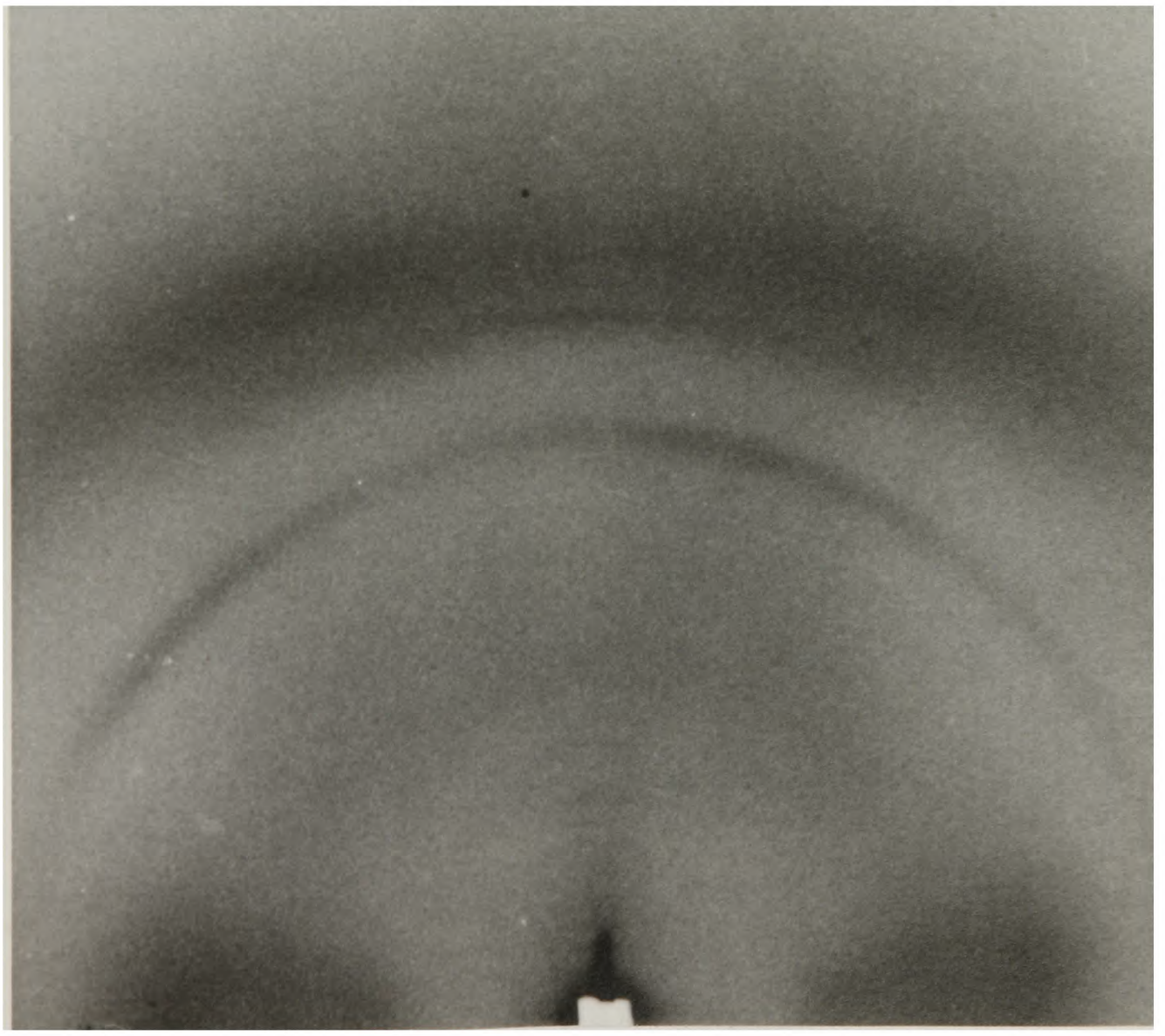

Plate 5.7 X-ray diffraction pattern taken at room conditions of fibres drawn from the left colleterial gland. The fibres are tilted by 8.5° to show the 5.12Å reflection. 3 day exposure.

Plate 5.8 X-ray diffraction pattern taken at room conditions of fibres drawn from the left colleterial gland of *S.membranacea*. The fibres are tilted by 31° to show the 1.49Å reflection. 7 day exposure.

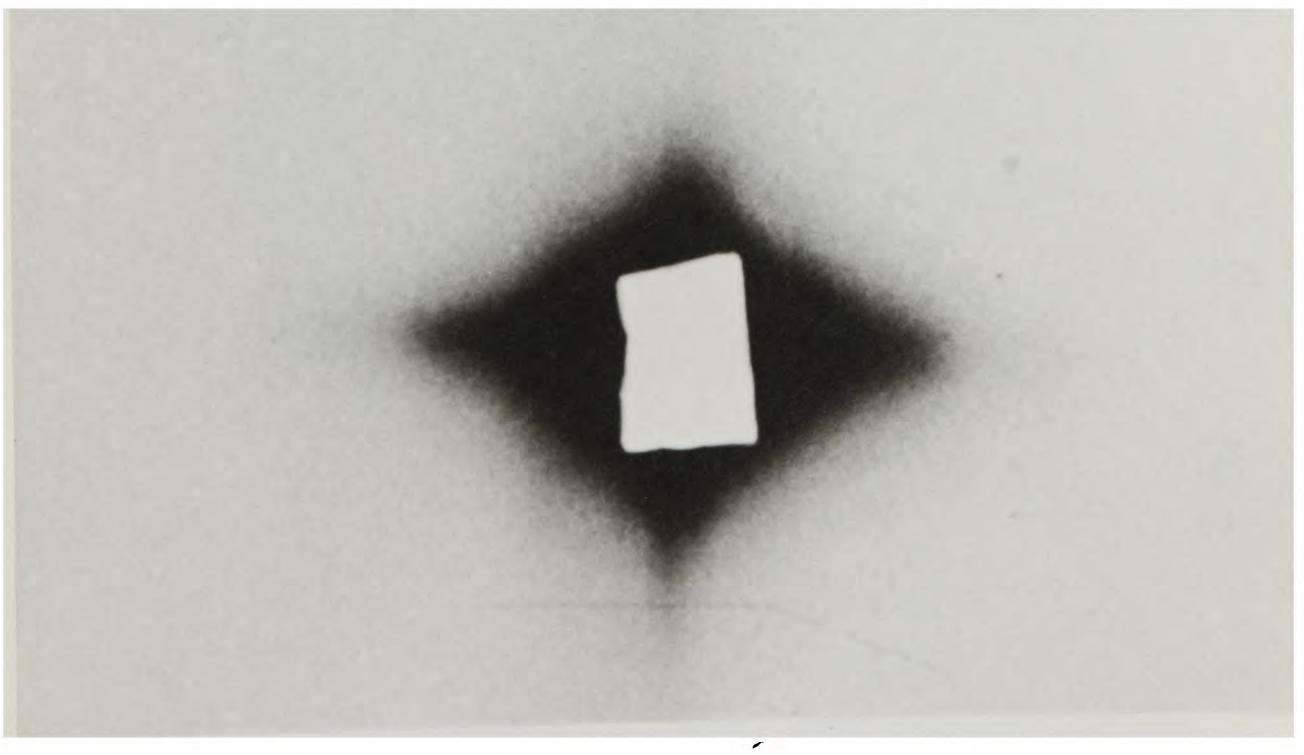

Plate 5.9 X-ray diffraction pattern taken at high humidity of a ribbon from the egg case of *S.tenuidentata*. The specimen is under slight tension and it is supported with the beam in the plane of the ribbon. Flat film. 64.7cm specimen to film distance. 66 hr. exposure.

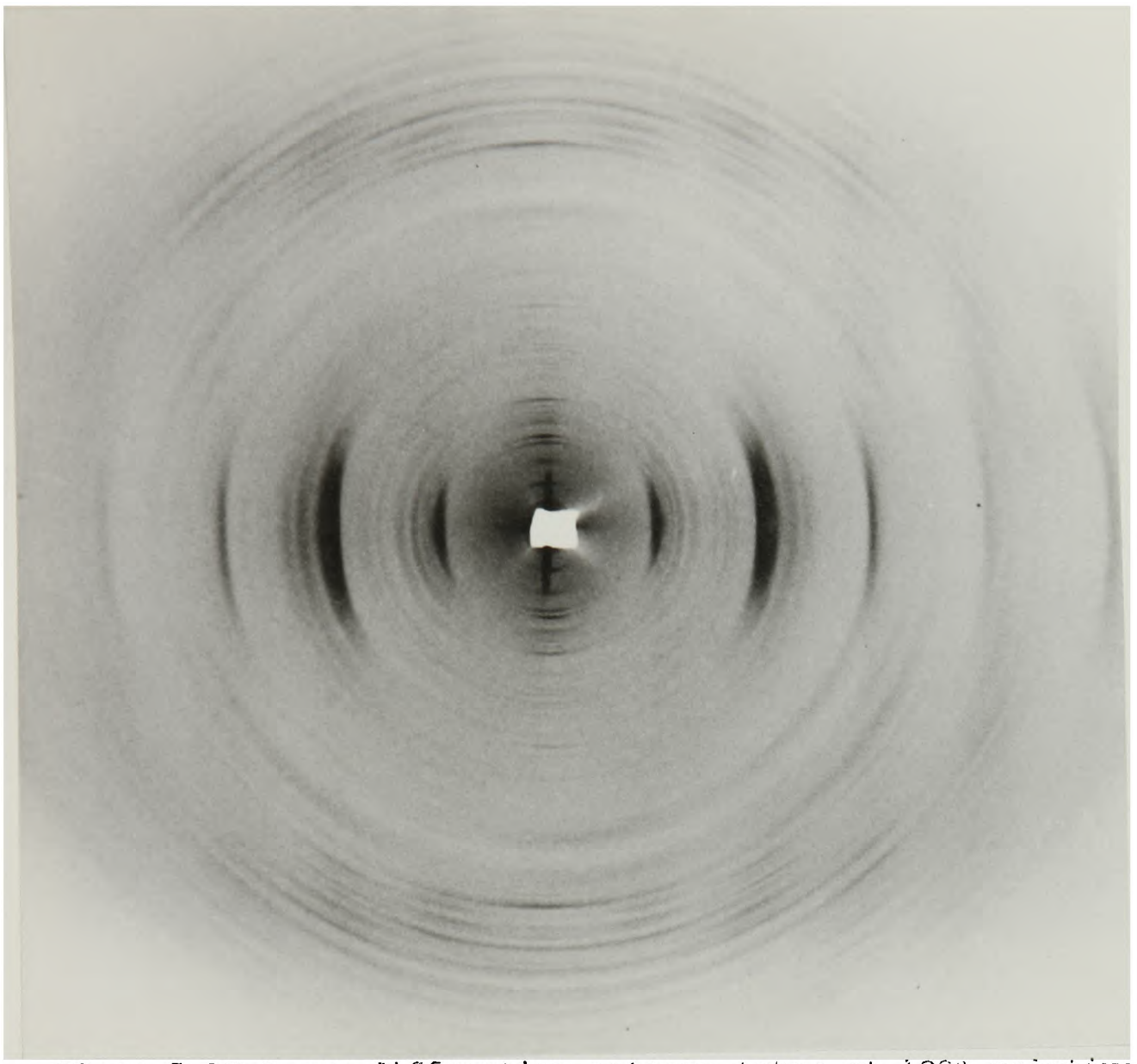

Plate 5.10 X-ray diffraction pattern taken at 100% relative humidity of a ribbon from *S.tenuidentata* with the beam in the plane of the ribbon. 5 day exposure.

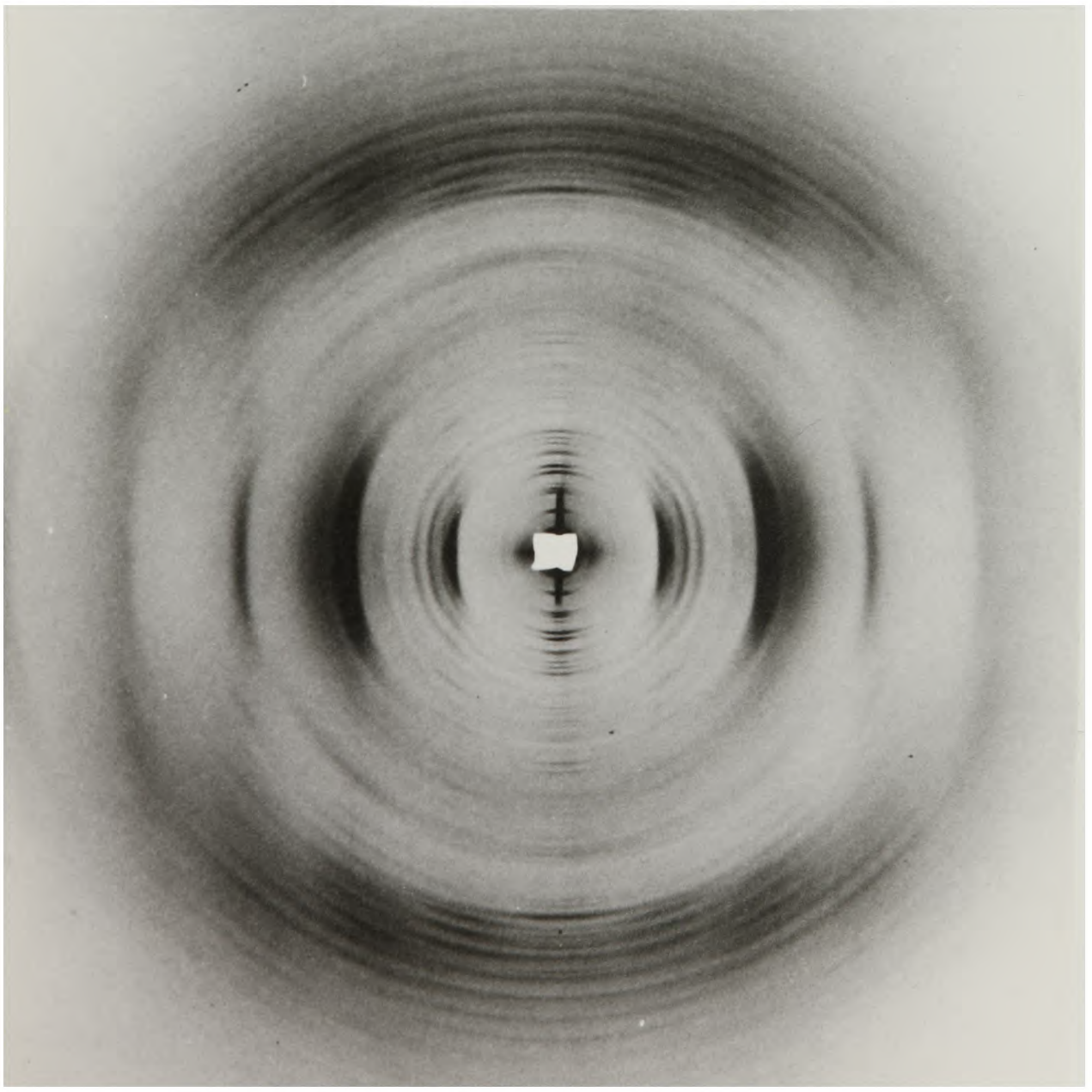

Plate 5.11 The same as 5.10 after drying under room conditions at constant length. Small changes occur near the equator. 80 hour exposure

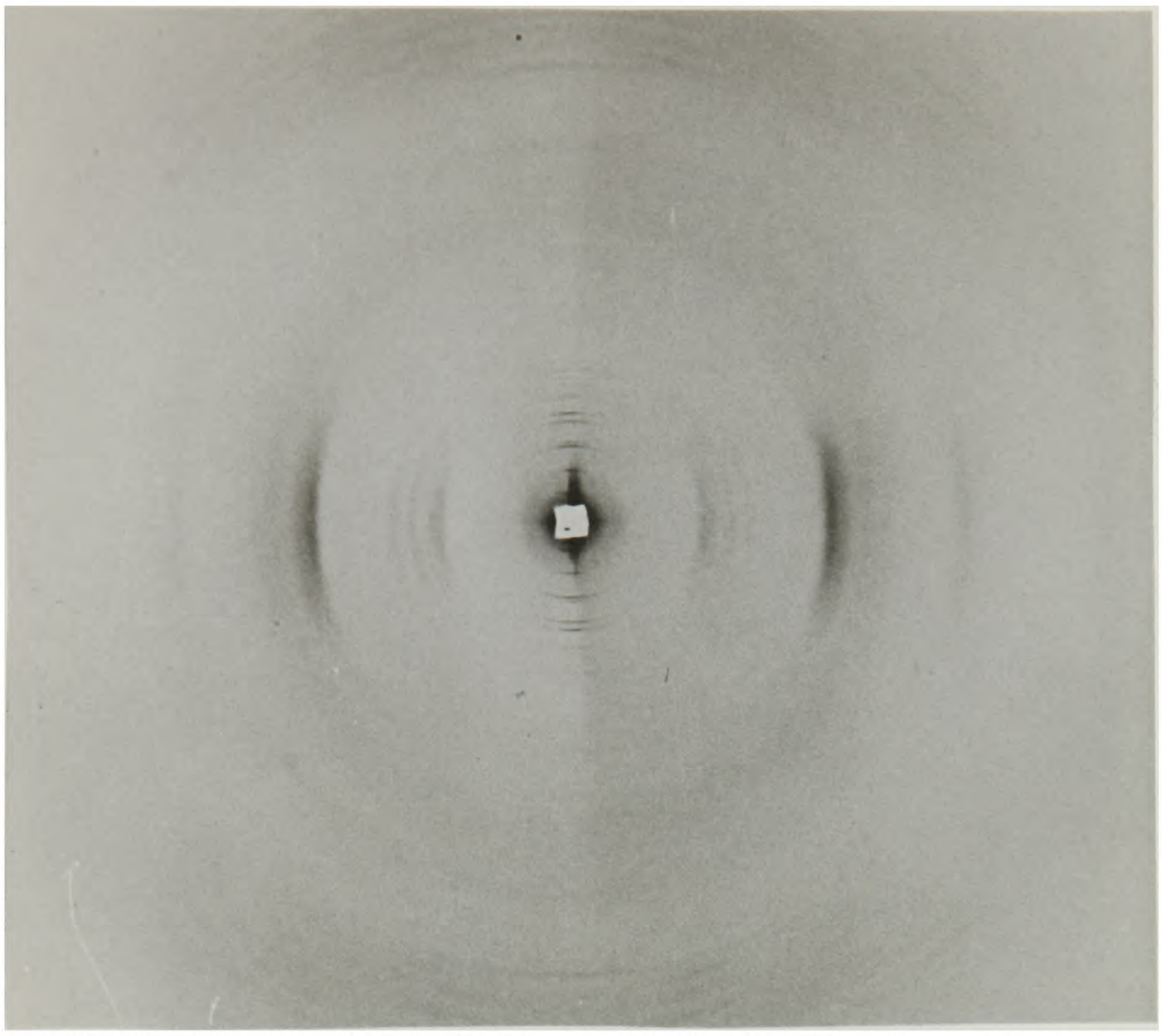

Plate 5.12 Plates 5.12, 5.13, 5.15-5.18. are from the same specimen as plates 5.10-5.11. but four months later. 5.12 is the same as 5.11 except that the specimen is tilted 3° for the 18Å equatorial reflection. 50 hr. exposure. Little deterioration is evident.

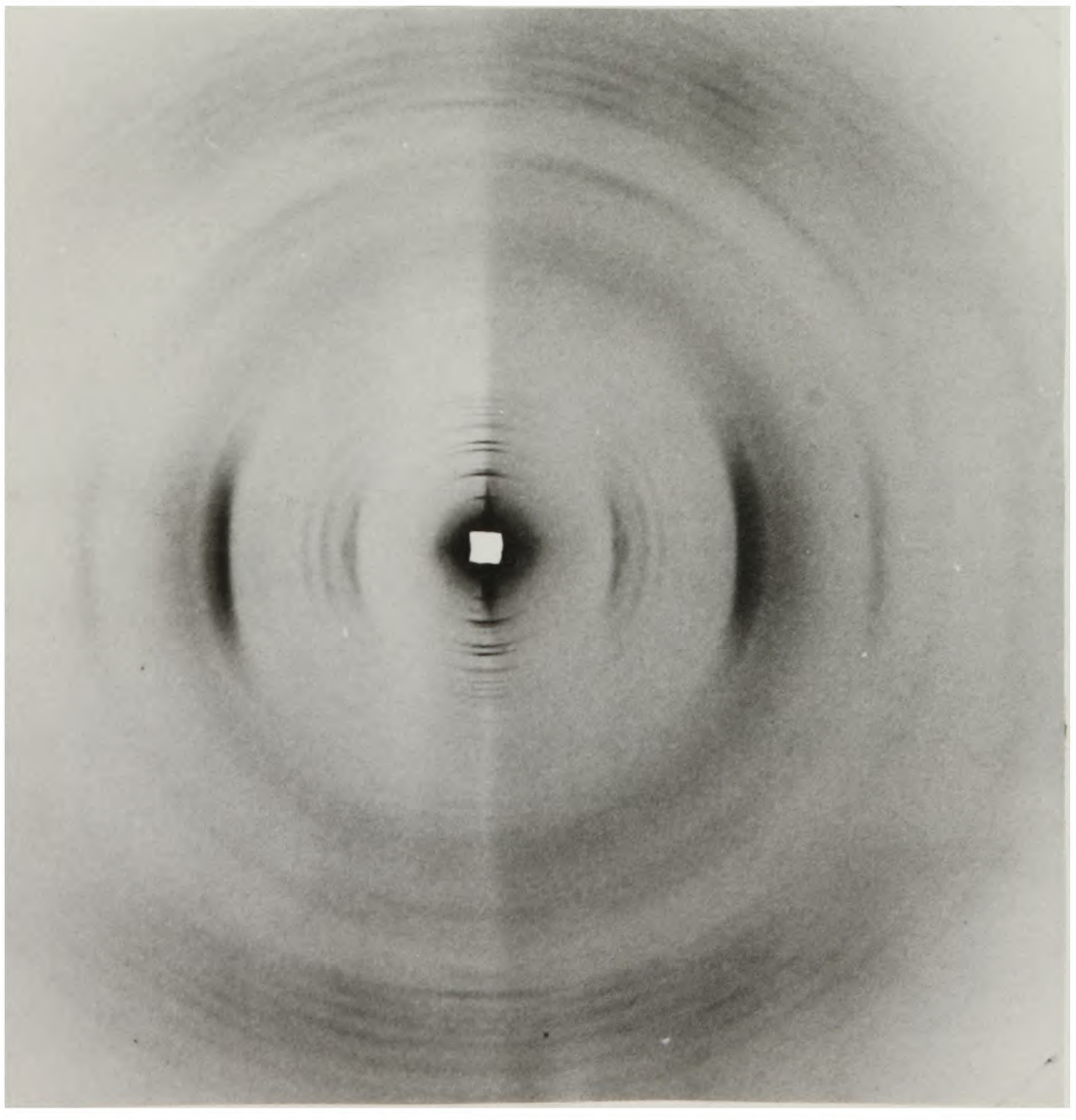

Plate 5.13 X-ray diffraction pattern taken over silica gel from a ribbon from *S.tenuidentata* with the beam in the plane of the ribbon. Changes on drying are most evident in the 18Å equatorial region. 50 hr. exposure.

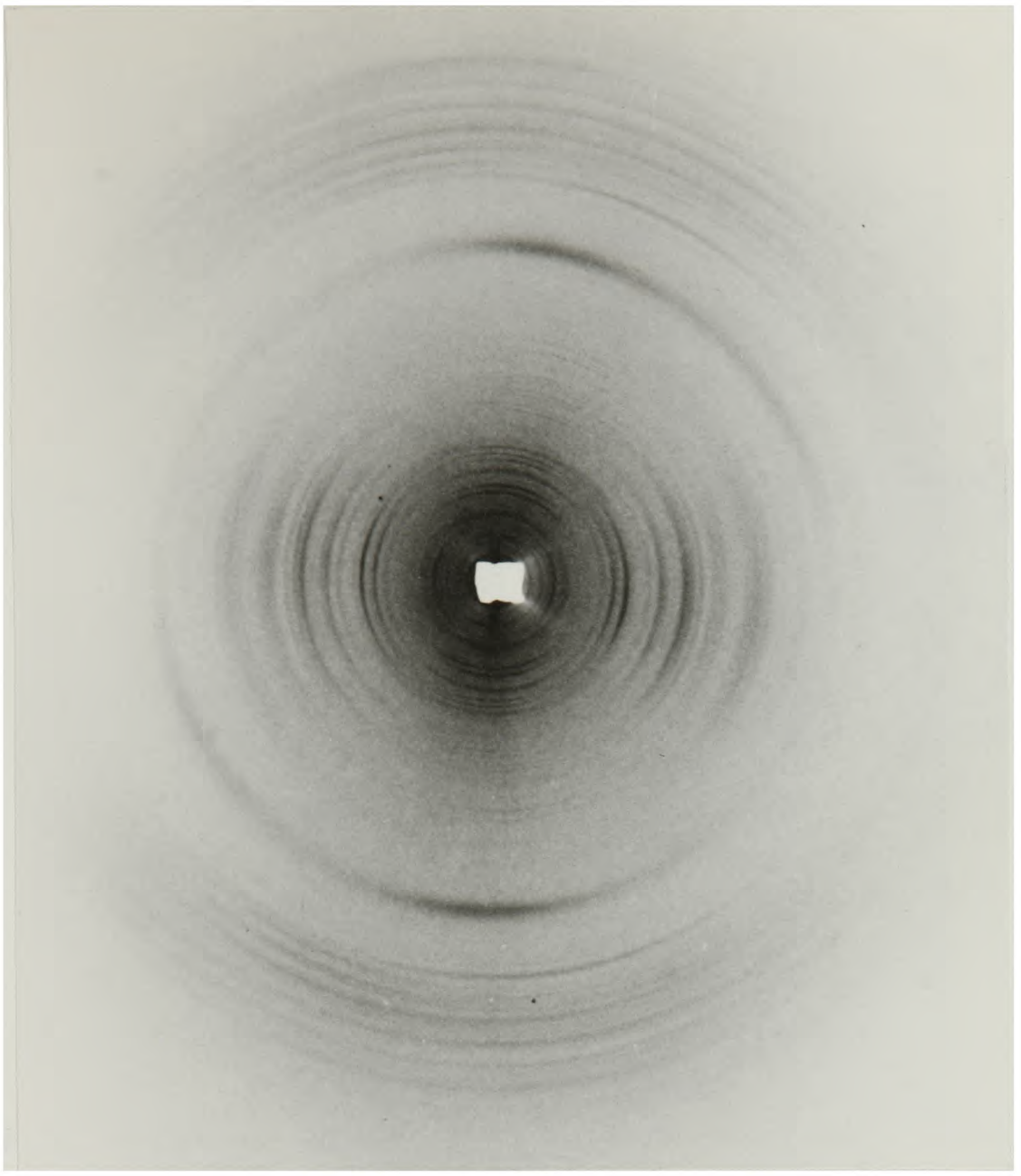

Plate 5.14 X-ray diffraction pattern taken under room conditions of a small selected area in a ribbon from the egg of *S.tenuidentata* with the beam perpendicular to the plane of the ribbon. The specimen was under slight tension. 140 hr. exposure.

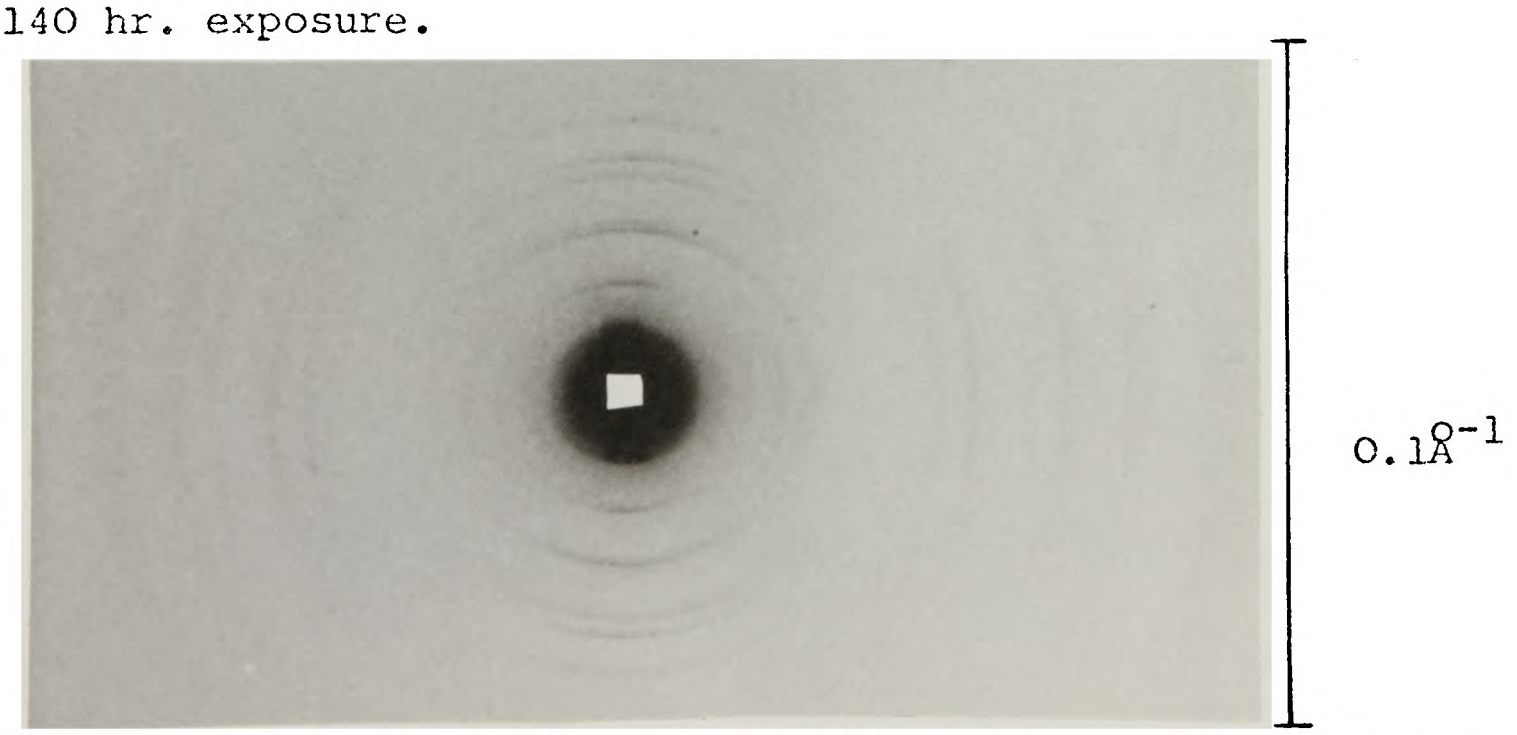

Plate 5.15 X-ray diffraction pattern taken over silica gel of a ribbon from the egg case of *S.tenuidentata* with the beam perpendicular to the plane of the ribbon. 17.5 cm. specimen to film distance. 121 hr. exposure.

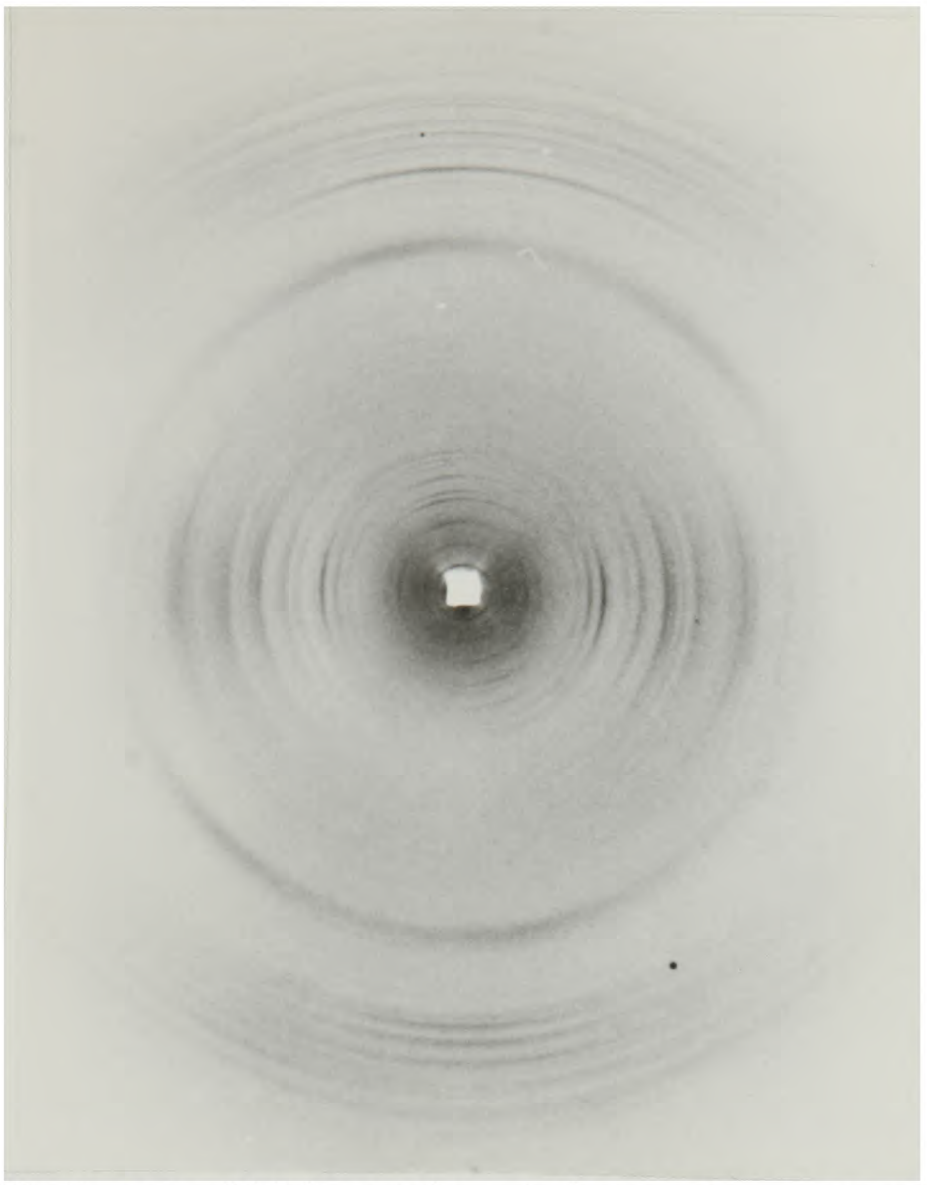

Plate 5.16 X-ray diffraction taken at room conditions from a small selected area (800 x 240 μm) of a specimen from S.tenuidentata The beam is perpendicular to the plane of the ribbon. The pattern is not symmetric about the meridian. 190 hr. exposure.

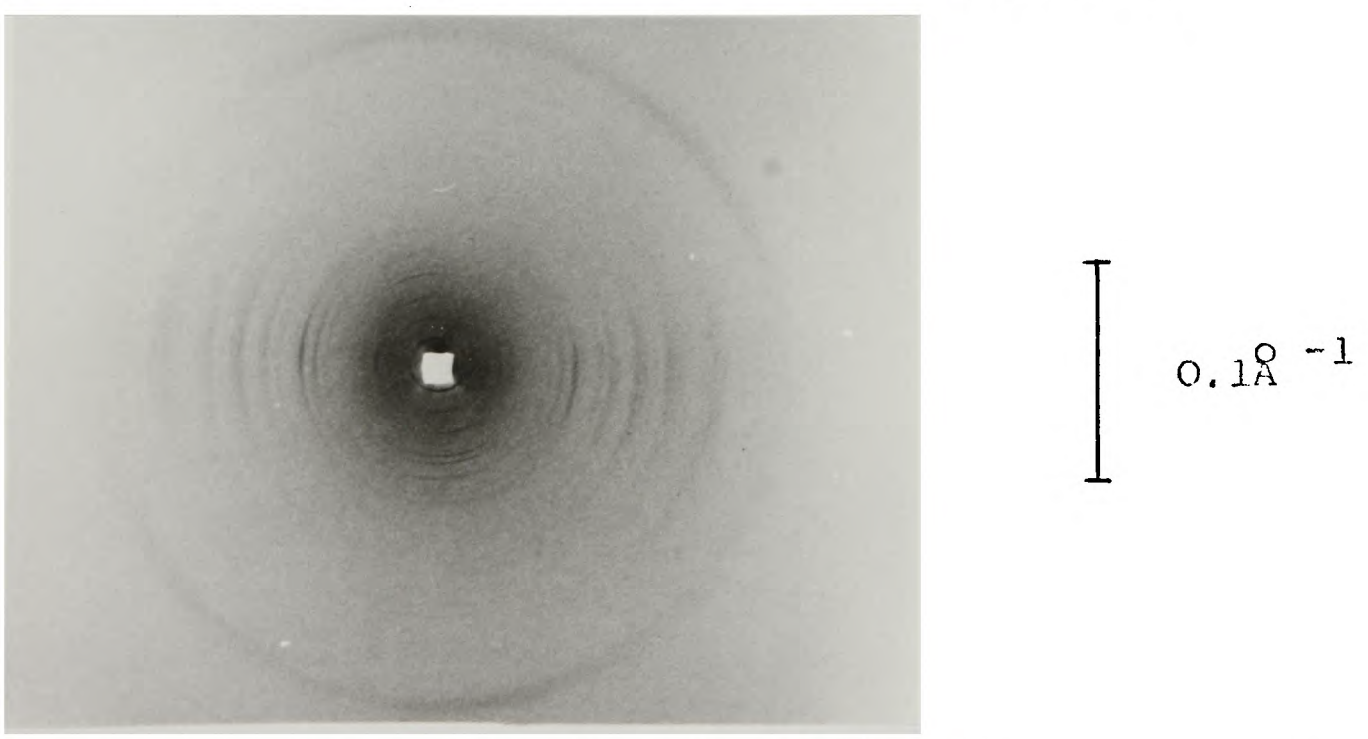

Plate 5.17. The backing film for the diffraction pattern in Plate 5.16, showing the low angle region more clearly.

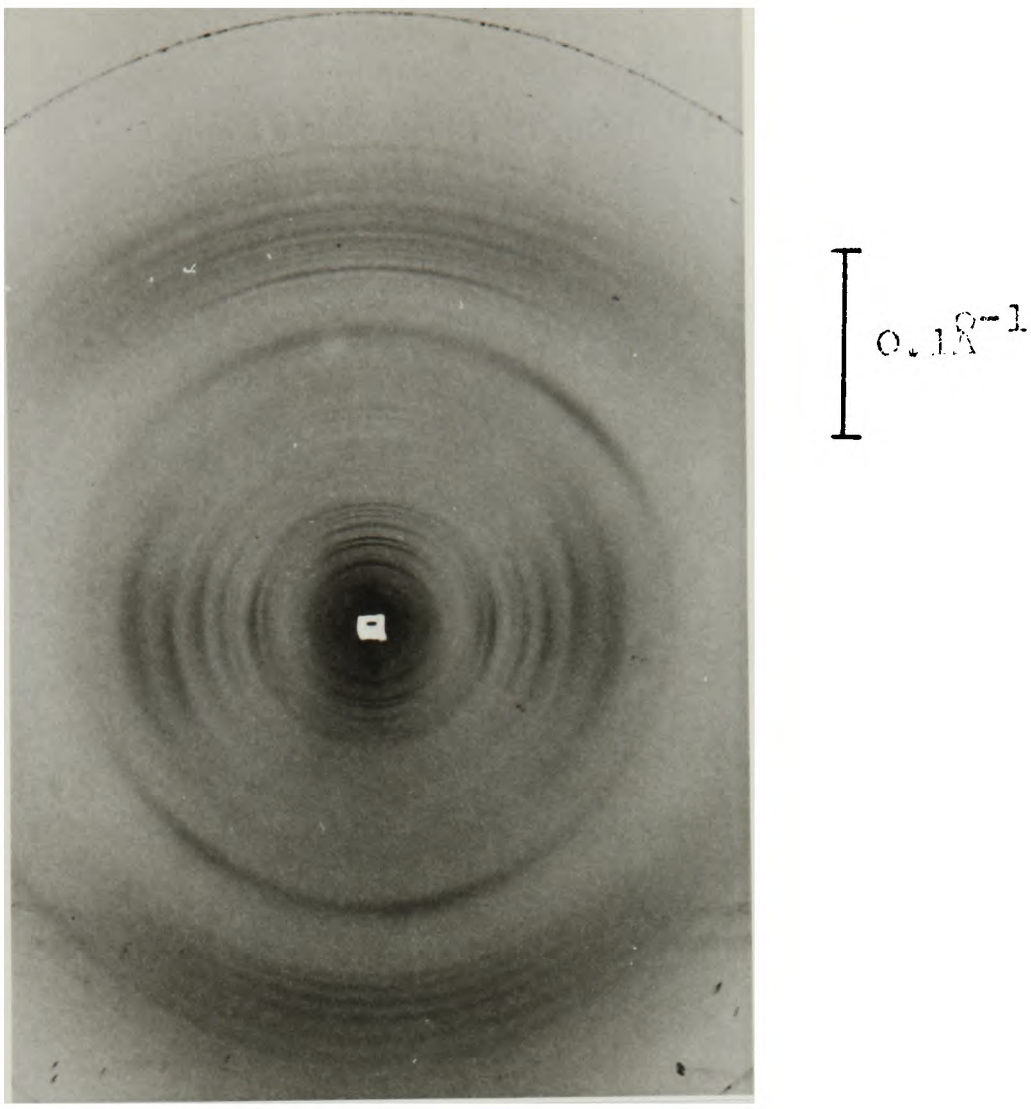

Plate 5.18 X-ray diffraction pattern taken at room conditions of a ribbon from the egg case of *S. tenuidentata*. The specimen is tilted 8.5° from having its plane perpendicular to the beam, so as to observe the 5.12Å meridional reflection. 50 hr. exposure.

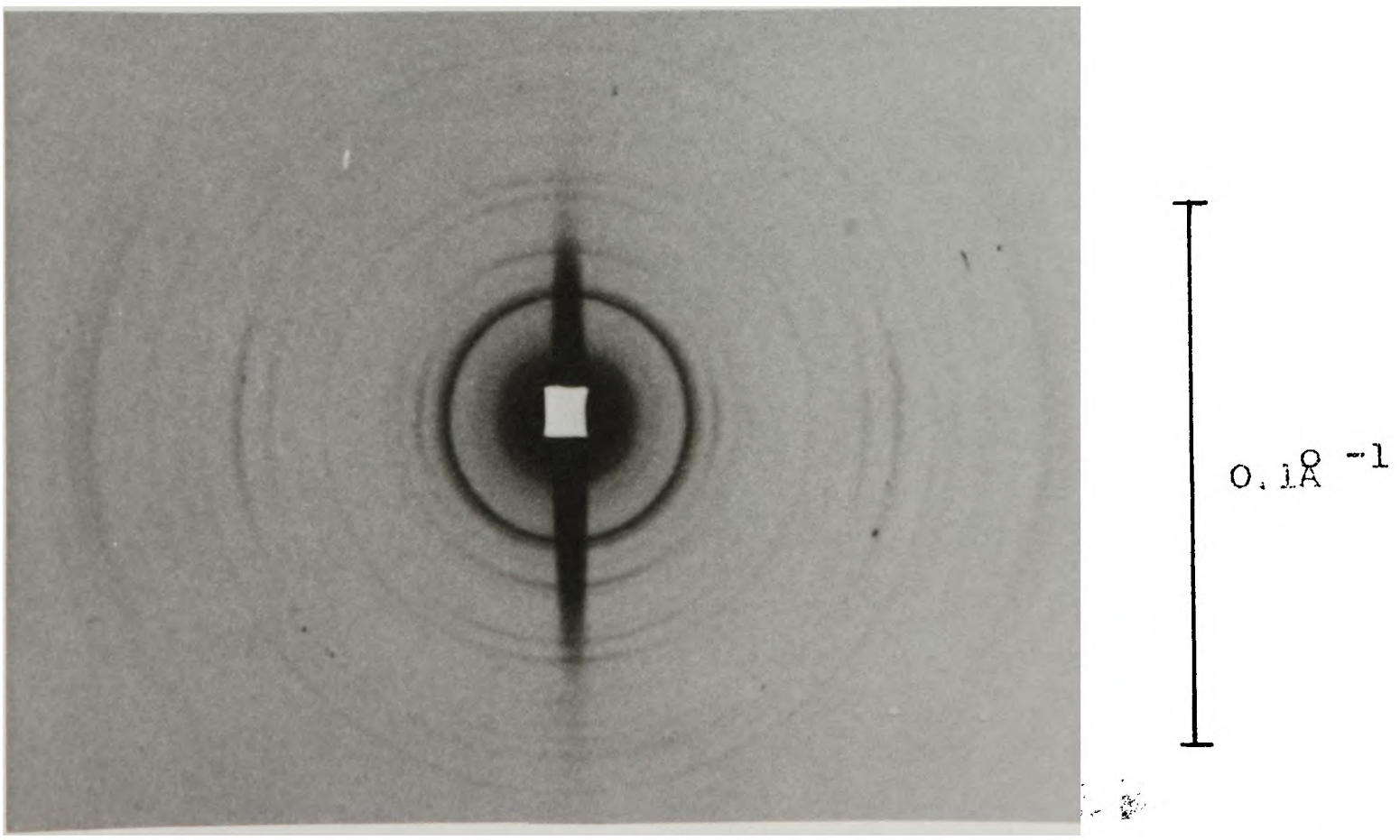

Plate 5.19 X-ray diffraction pattern taken at 100% relative humidity of a ribbon from the egg case of *S.tenuidentata*, showing rings produced by lipid. The beam is perpendicular to the plane of the ribbons. 17.5 cm. specimen to film distance. 22 hr. exposure.

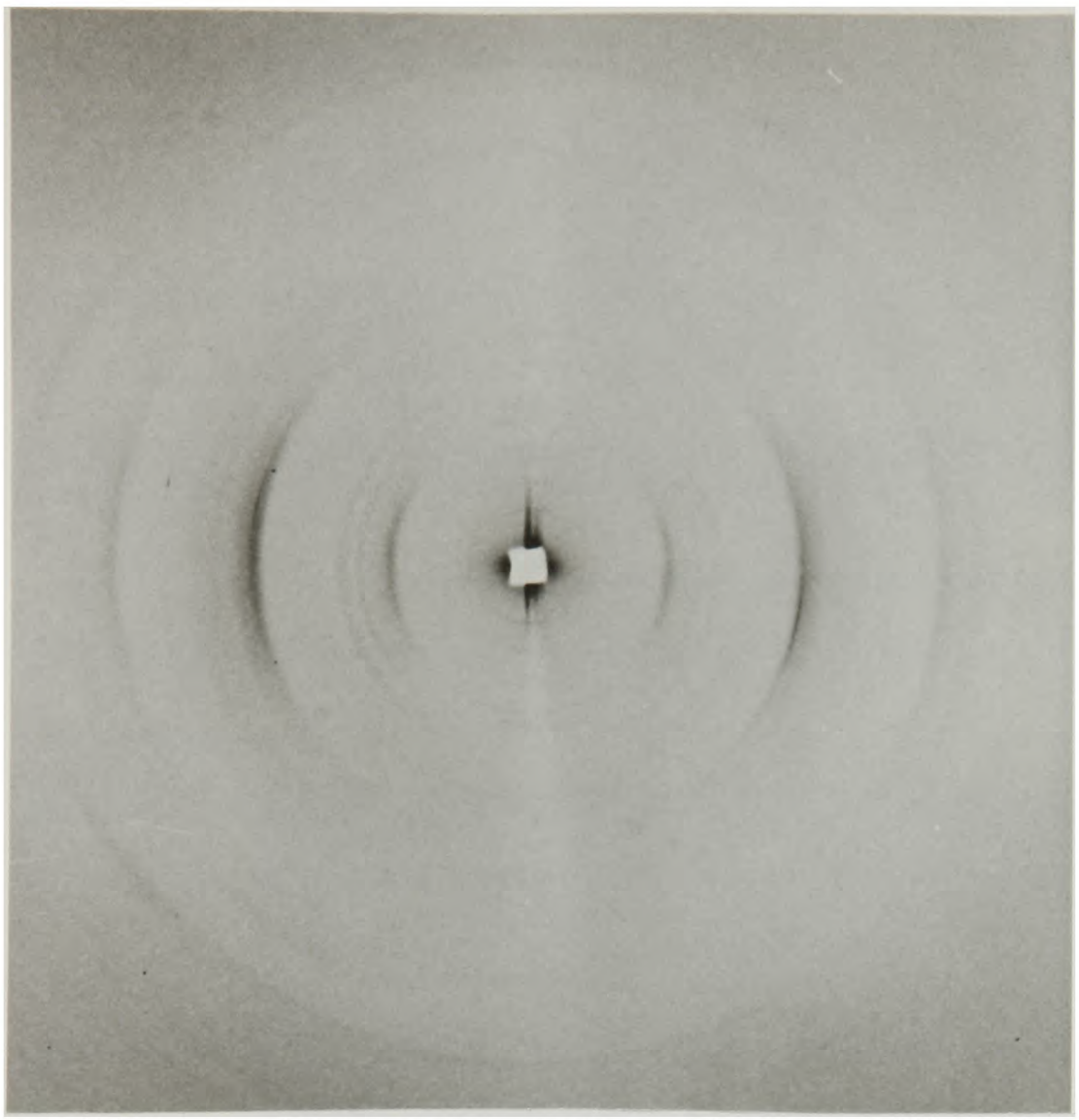

Plate 5.20 X-ray diffraction pattern of a wet ribbon from *S.membranacea*. Beam in the plane of the ribbon. 18 hr. exposure.

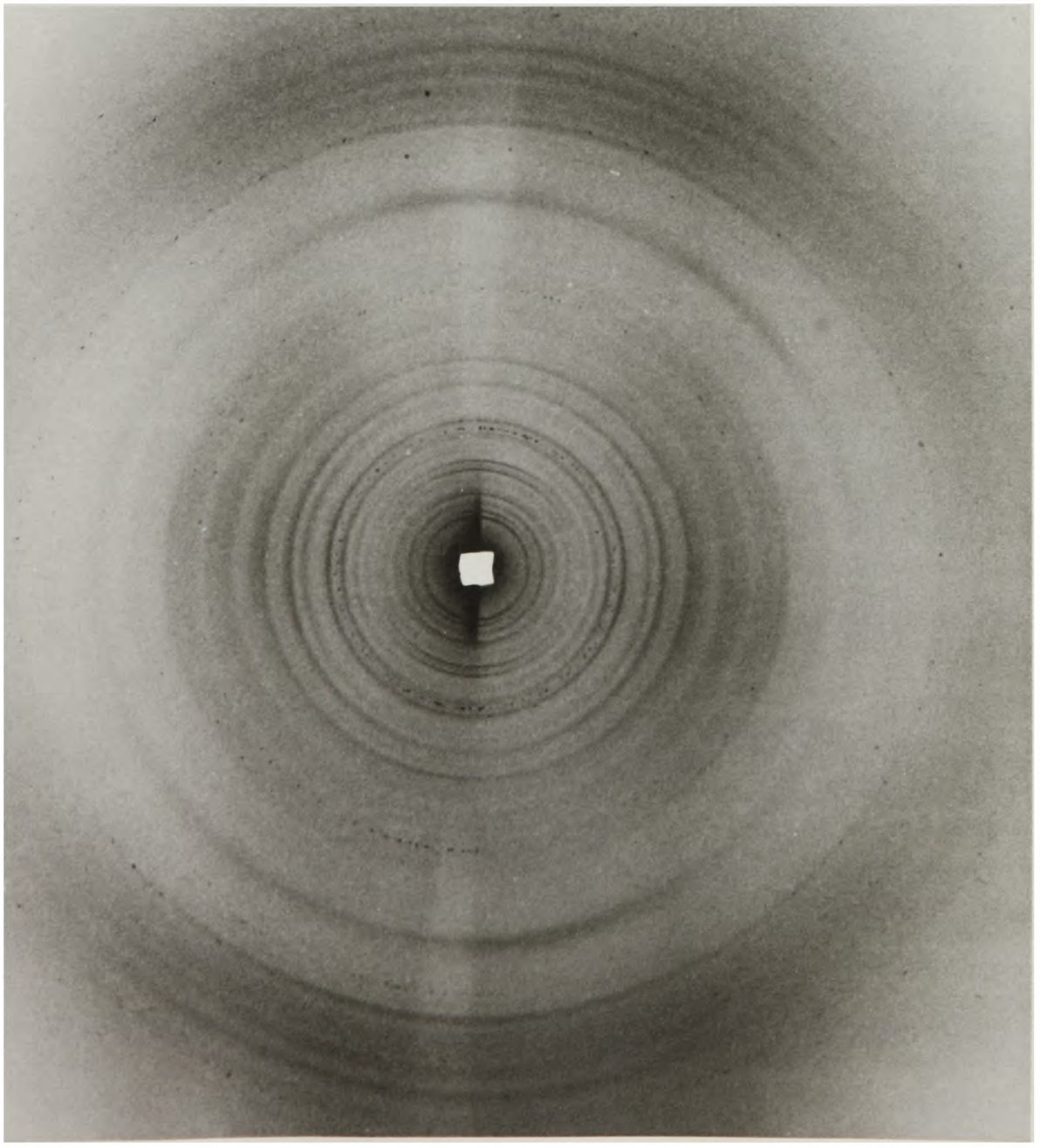

Plate 5.21 X-ray diffraction pattern of a ribbon from *S.membranacea* at room conditions. Beam perpendicular to the plane of the ribbon. 78 hr. exposure

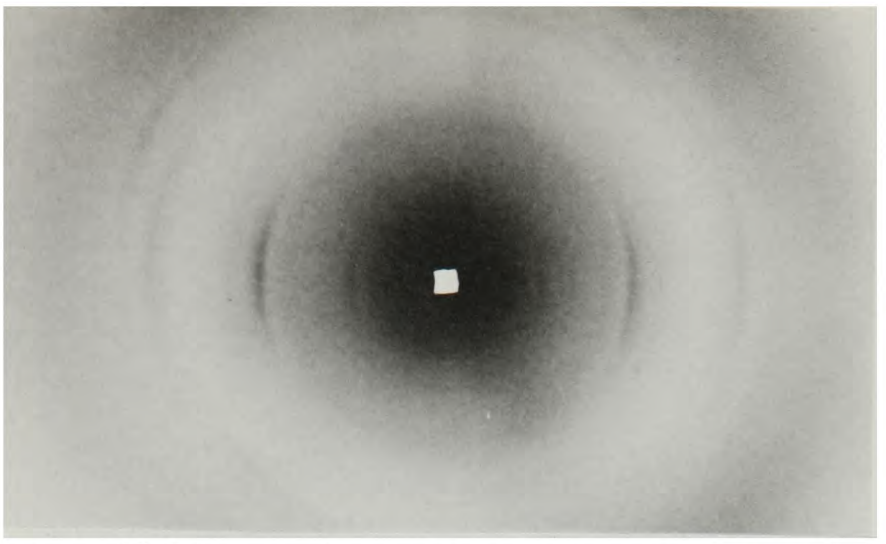

Plate 5.22 X-ray diffraction pattern of a ribbon from the egg case of *S.membramacea* after soaking for 3 months in neutralised 2% phosphotungstic acid. The beam was in the plane of the ribbon. 48 hr. exposure.

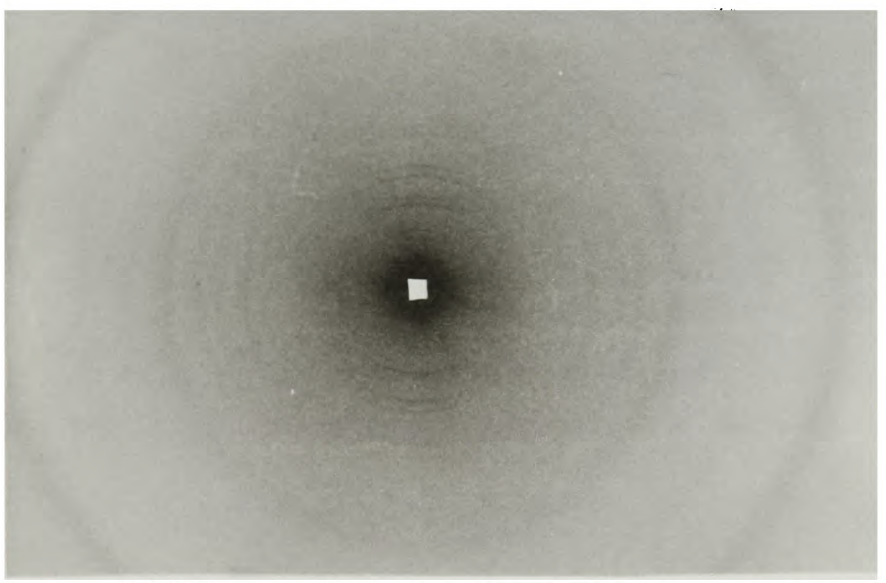

Plate 5.23 X-ray diffraction pattern of a ribbon from *S.membramacea* after soaking in neutral phosphotungstic acid. The beam was perpendicular to the plane of the ribbon. No reflection appears in the 150 Å region. 17.5 cm. specimen film distance. 5 day exposure.

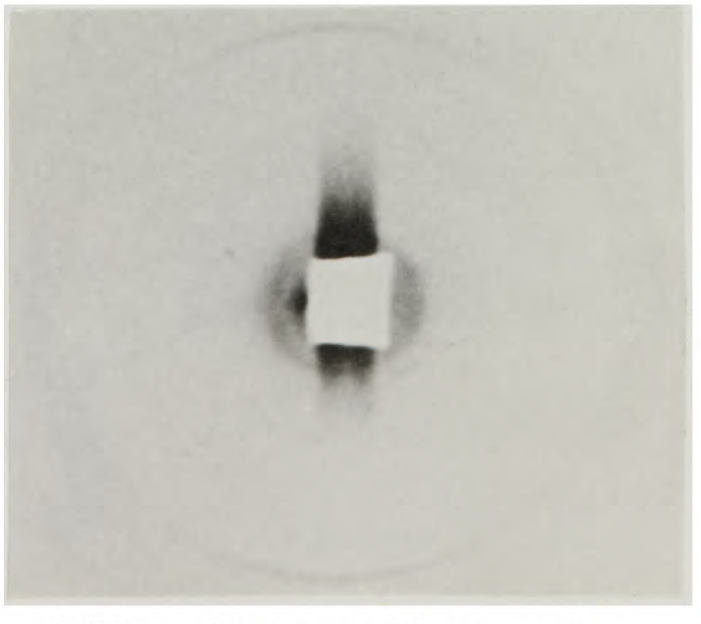

Plate 5.24 X-ray diffraction pattern of a ribbon from *S.membramacea* after soaking for 3 months in 0.5% uranyl acetate solution. The beam was perpendicular to the plane of the ribbon. Low angle reflections at 147 Å are seen. 17.5 cm. specimen film distance.

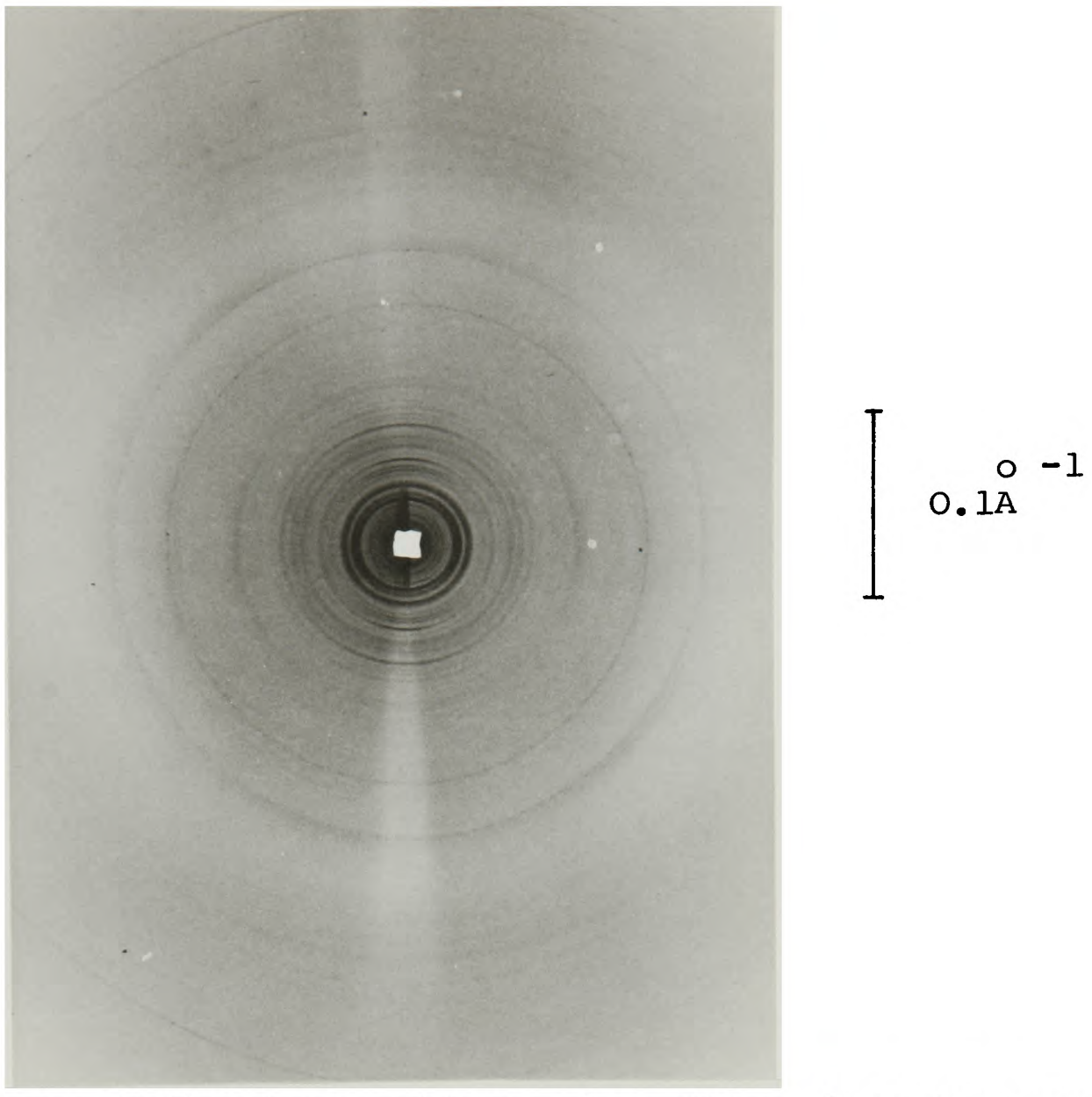

Plate 5.25 X-ray diffraction pattern of a ribbon from the egg case of *S.membramacea* after soaking in 0.5% uranyl acetate solution. The beam was perpendicular to the plane of the ribbon. 72 hr exposure.

Plate 5.26. The same as plate 5.25. 8 hr. exposure.

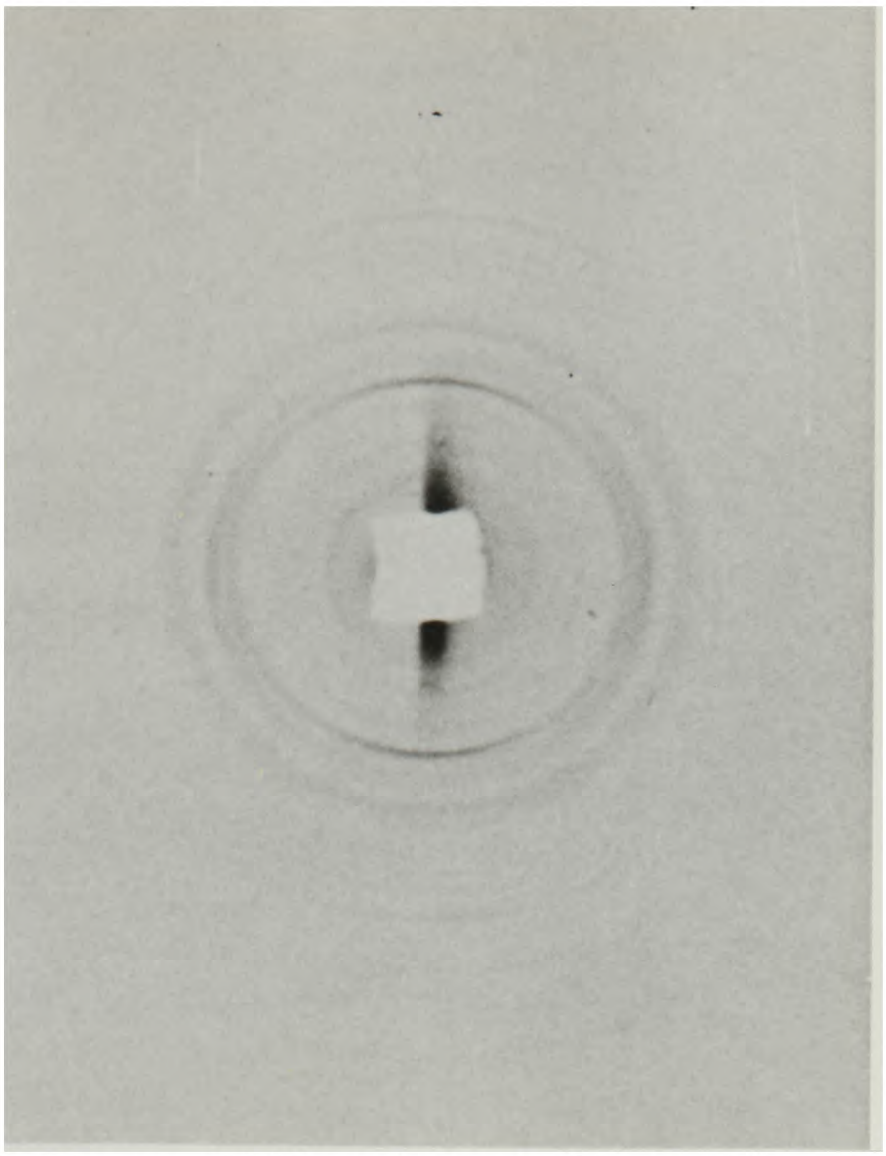

Plate 5.27 X-ray diffraction pattern of a ribbon from the egg case of *S.membramacea* after soaking in 0.5% uranyl acetate solution. The beam was perpendicular to the plane of the ribbon. 17.5 cm. specimen to film distance. 74 hr. exposure.

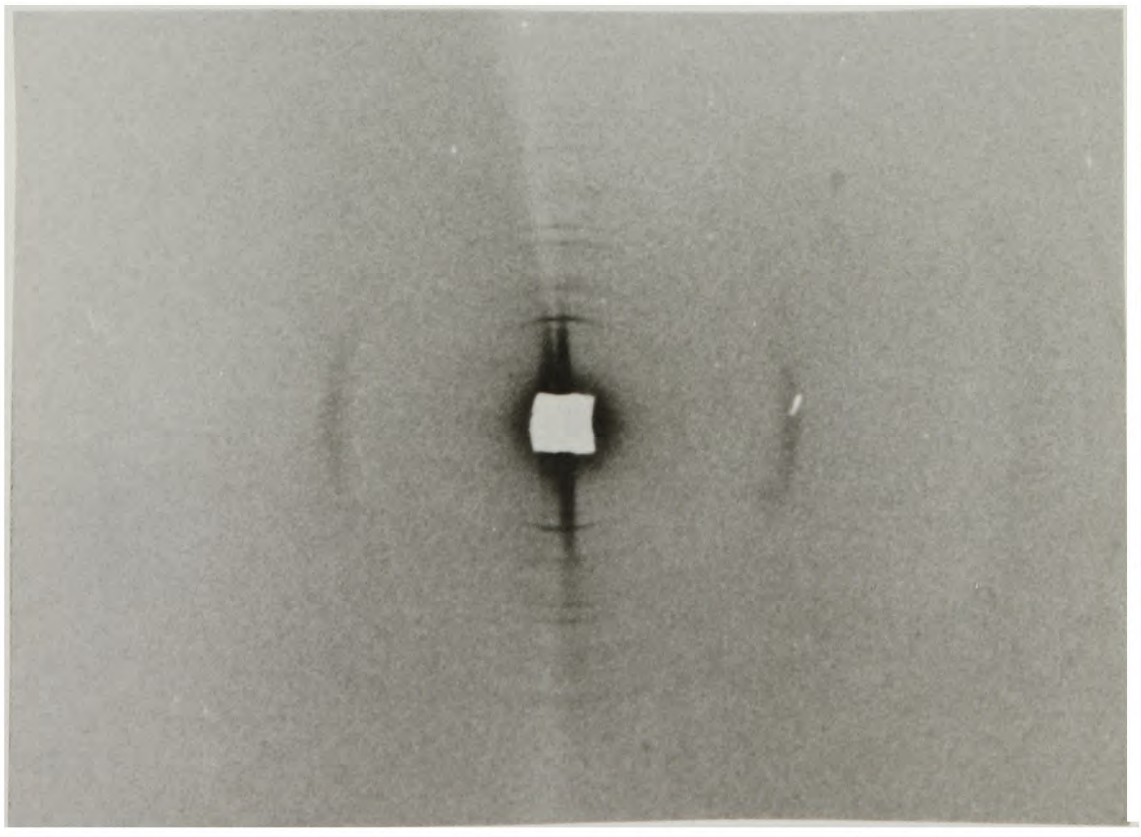

Plate 5.28 X-ray diffraction pattern of a ribbon from the egg case of *S.membramacea* after soaking in 0.5% uranyl acetate solution. The beam was parallel to the plane of the ribbon. 37 hr. exposure.

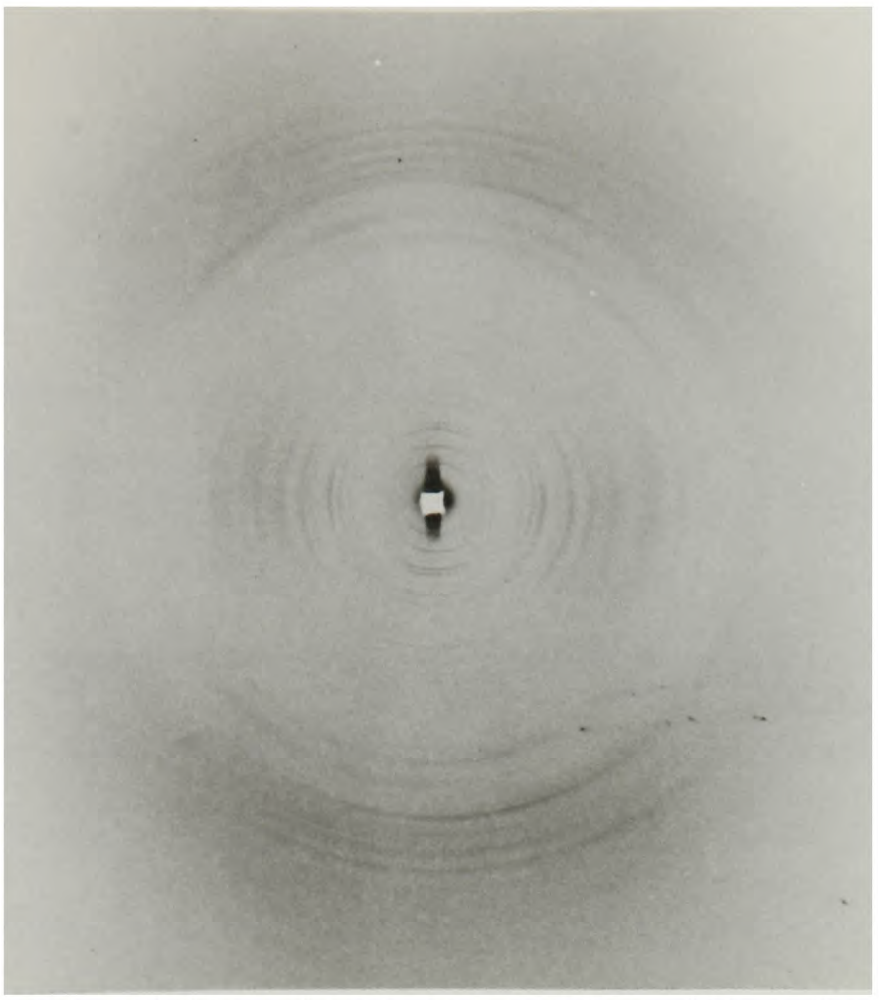

0.1Å $^{-1}$

Plate 5.29 X-ray diffraction pattern of a ribbon from *S.membranacea* after soaking in chlorobenzene and bromobenzene. Beam perpendicular to the ribbon surface. 12 hr. exposure.

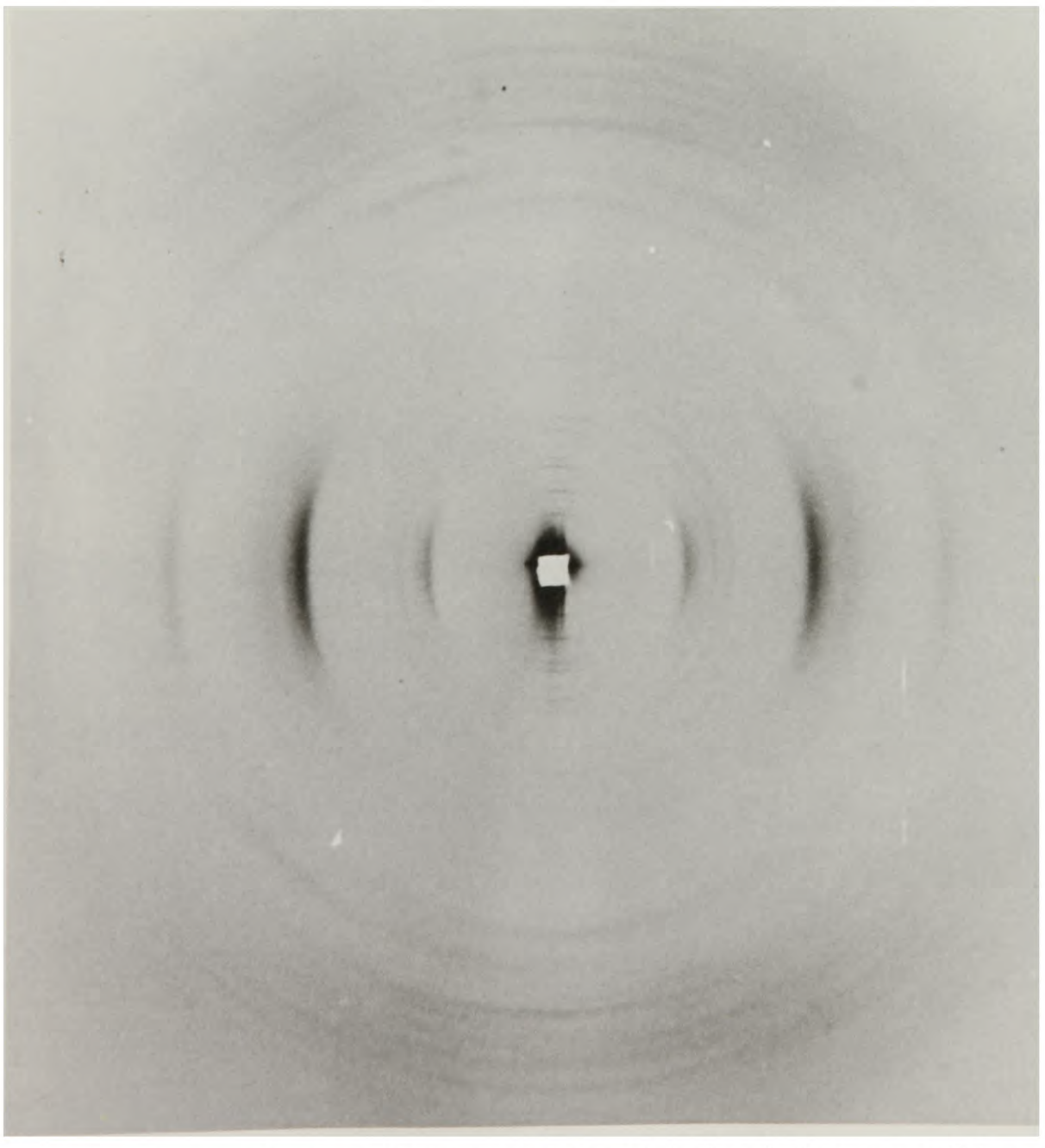

0.1Å $^{-1}$

Plate 5.30 X-ray diffraction pattern obtained from a ribbon from *S.membranacea* after soaking in chlorobenzene and bromobenzene. Beam parallel to the ribbon surface. 15 hr. exposure.

CHAPTER 6

INTERPRETATION AND DISCUSSION

CHAPTER 6

Interpretation and Discussion

In this chapter the work of the earlier chapters is interpreted and discussed. Since the X-ray diffraction patterns and the electron micrographs obtained for S. membramacea and S. tenuidentata were almost identical, the structures are considered to be the same and are discussed together.

6.1. A k.m.e.f structure

Fibres drawn from the gland gave a meridional reflection at 1.49Å and a strong meridional reflectionat 5.18Å. Ribbons gave a weak meridional at 1.485Å and a strong one at 5.12Å. This is characteristic of proteins in the k.m.e.f. group. Another feature common to this class of proteins is intensity in the 10Å equatorial region.

The pattern derived from fibres shows this clearly. It is very similar to that given by α-keratin, where the microfibrils are not packed on a lattice. The reflections superimposed on the smoothly varying region are relatively weak and fairly broad, indicating that most molecules are not packed with any long range order. Reflections streak along the layer lines. The length of the streaks indicatesthat most crystallites present are only a few molecules across.

The equatorial pattern given by ribbons also shows high intensity in the 10Å region, but sampling by the transform of the lattice makes the pattern less obviously of the k.m.e.f. class. Some patterns show a very faint shadow of the fibre pattern, indicating the presence of a little non-crystalline material. There is sampling on a period of 82Å in several regions. This relates to a repeat in the structure of 82Å.

Two helical chains related by a parallel diad axis would give a repeat of half the helix-pitch. On this basis, measurements of the sampling in the 5Å region and the 9Å near equatorial region lead to a pitch of 165 ± 5Å. However, the pitch could vary and thus not bear a simple relation to the period. Proteins of the k.m.e.f. class are generally thought to have a higher pitch about 180Å (Fraser et al., 1965).

6.2 The high angle pattern

The high angle pattern given by the fibres was very weak. It is subject to errors produced by the fibres not being tilted for each reflection, as well as errors derived from the difficulty in seeing the reflections. However, they appear to be consistent with a two stranded coiled-coil of pitch about 165Å, since many of the reflections in the meridional region are orders of 165/16Å = 10.3Å. 165Å corresponds closely to 112 residues and 32 turns of the helix, resulting in an approximate 16-fold rotation axis, since both these numbers are multiples of 16. It cannot be said which reflections are truly meridionals, but the strong 1.49Å reflection probably is and this indexes as the seventh order of 10.3Å.

If the reflections that are orders of 10.3Å are meridionals and the others are not, then this is a good system. However, the weakness of the reflections makes meridionals difficult to identify and their width of 2×10^{-2} Å^{-1} results in inaccurate determination of spacings. For this reason, indexing on a repeat of 165/17 = 9.7Å must be considered as a possibility, since many reflections index on this. This would require a 17-fold rotational axis, which would be equivalent to a pitch of about 176Å. As the range of order determined from the reflection width is only 50Å, it is quite possible that some parts of the molecule have this pitch in a

system with a repeat of 82Å. A gradually varying residue rotation is also a possibility, since not all of the molecule need have a symmetry close to that revealed by the strongest reflections. The same arguments apply to the ribbons which give a broad 1.485Å reflection sampled by a large lattice. The reflection at 5.12Å is strong and sharp, indicating that the pitch of the minor helix is better defined than the residue translation. This could be controlled by packing requirements. Even in the fibre pattern, the 5.18Å reflection is substantially more sharply defined than the 1.49Å reflection.

Table 6.1 indexes the high angle meridional and near meridional reflections on a repeat of 9.8Å, corresponding to a 17-fold axis and an 83.5Å repeat, and 10.3Å, corresponding to a 16-fold axis and an 82.5Å repeat.

It seems likely that the pitch of the major helix and the residue translation vary. The pitch of the minor helix is well defined and almost constant.

6.3 Lateral molecular packing

When the thin edge of the ribbon is towards the source, the pattern is sampled at intervals of 18.6 ± 0.1Å, 17.9 ± 0.1Å and 17.5 ± 0.1Å for specimens at 100% relative humidity, room conditions and over silica gel respectively. Very little intensity falls far from these row lines, indicating that this spacing represents a repeat in the structure. It is large enough to allow packing of coiled coil structures. The value estimated for the fibres was 16.8 ± 0.5Å, but this is not inconsistent with these values, considering the problems of measurement.

When the flat face of the ribbon is towards the source, there is a modulation in the equatorial intensity, repeating at 33.0 ± 0.6Å, 32.1 ± 0.6Å and 30.6 ± 0.6Å for specimens at 100% relative humidity, room conditions and over silica gel respectively. A packing scheme for coiled coil structures can easily allow for row lines at 33Å intervals, but no reflections should occur on the equator for odd orders. This is so because the equatorial pattern is the Fourier transform of the electron density after projection on to the equatorial plane. Since a coiled coil is circular in this projection, the projected electron density has a repeat of one coiled coil diameter, corresponding to 16.5Å. However, the structure proposed in fig. 6.1 does have a repeat of 33Å, leading to 33Å row lines. The pattern is so disoriented that off equatorial reflections could be identified as being equatorial. However, it is expected that not all the structure is material arranged on a coiled coil. Gaps or non-coiled-coil material could be responsible for the equatorial modulation.

At this stage in the argument, the simplified structure in fig. 6.1 can be proposed. The stagger between coiled coils in the figure is 41Å (a quarter of the pitch), as proposed by Rudall (1956). The actual stagger probably differs somewhat from this.

6.4 3-Dimensional molecular packing

Sufficient information has now been considered to enable the electron micrographs to be intepreted.

First consider a structure composed of coiled coil structures packed as in fig. 6.1. It is seen that the contours of the surface vary with a repeat of half the pitch. The pattern is identical at intervals

of a quarter of the pitch, but only after a small lateral translation. The way the staining is likely to vary with a repeat of a quarter of the pitch is shown in fig. 6.2. This assumes different negative staining as the contours change from one type to another.

Examination of micrographs showed that structures were continuous across the major striations. These are likely to be coiled coils. The separation between them was about 30Å where the ribbon had been sheared, but for these filaments. Structures between these are considered to be linked non-covalently, allowing easier shearing. This tendency to shear along these striations suggests that molecules are likely to end here. The major line of shear, as marked in fig. 4.1 is likely to be along the molecular axis. Only non-covalent bonds need then be broken. This line passes between identical points separated by about 730Å which is 4.5 times the pitch assumed. The estimated molecular weight of between 50,000 and 55,000 is consistent with an α-helical chain of length about 730Å. The coiled coil would contain two such chains.

The minor striations do not follow the molecular axis. Fig. 6.2 suggests that they are not expected to, but neither are they as expected from this figure. There are fuzzy bands of about 40Å width separated by 80Å, giving a pattern twice the size of that expected. It is seen that 80Å is one ninth of 730Å and it is therefore 0.5 times the pitch assumed. On the basis of fig. 6.2 a pitch somewhat greater than 165Å could maintain the minor striations over this distance, but a change of structure needs to be invoked for the fuzzy band region. It is seen that thesefuzzy bands are not at right angles to the molecular axis, but at about 82° to it. In fig. 4.1 the angle is 81.5°. The dimensions from the micrograph give lateral separations between coiled coils of about

16.5Å. The stagger therefore differs from Rudall's model by about 2.5Å. This does, however, assume that the lateral band represents a constant orientation about the axis. This gives each molecule an identical position with regard to its neighbours. The stagger between adjacent coiled coils becomes 2.5P + 2.5Å, where P is the assumed pitch of 165Å. For optimum packing, the stagger should be $\pm$ (1 $\pm$ 2n). P/4, where n is an integer. If this is to be achieved for a pitch P, then the beginnings of adjacent coiled coils must be rotated about the molecular axis so as to produce a 90 degree difference in their rotational orientations. The lateral striations can be followed and it is seen that, in this model, consecutive groups of three spots are at 90 degrees to each other. Following along the major striations the angle is 180° and the same angle applies between the two ends of the molecules. The system is seen to be consistent.

The remaining problem is the interpretation of the lateral banding. This could represent a change in the structure. Assume that the minor striations show where there is a regular coiled coil structure and the fuzzy bands represent a slightly different structure. This structure would necessarily be described by a parameter the same as the pitch in a regular coiled coil, since the 5.12Å reflection is sharp. However, the residue translation can change since the 1.49Å reflection has a width of $0.02 Å^{-1}$, equivalent to the length of the visible minor striations. Allowing for the extra 2.5Å in the stagger between coiled coils, the pitch for optimum packing is 4 x 2.5Å greater than that expected from the 82.5Å repeat. The optimum pitch becomes 175Å in this region. This is high enough for the striations in fig. 6.2 to be as long as those observed. From poor high angle data, a 17-fold axis is considered a possibility.

This could derive from a pitch of 119 residues corresponding to a pitch of 177Å. Without better high angle data, this remains uncertain. It is also uncertain whether optimum packing is achieved. However, the conditions in the electron microscope are such that the closest packing is expected to be achieved, so the packing is likely to be optimum.

It cannot be shown that the staining pattern has these origins, or indeed that it is uncomplicated by positive staining. However, this explanation is consistent within the limitations of the data.

The structure in the gap region is made difficult to determine by limitations of the data. Generally, there are three densely stained spots in each group, the outer ones being the more dominant. However, fine details, such as those in fig. 6.2, require small quantities of stain to make them visible. Under these conditions, any aggregation of polar groups would be expected to show up with positive staining. Sometimes the central spot cannot be seen. This could be because more stain is present, allowing negative staining to be completely dominant. An alternative explanation might be that positive staining has occurred and that the central spot corresponds to a hole. As the staining time was short and the matrix of protein is dense, the former possibility is considered more likely. Unfortunately, the proximity of the gaps makes the density argument less attractive.

Remembering that the figures given are likely to have errors of about 10Å, we arrive at the structure in fig. 6.3. Each chain in the coiled coil is staggered by about 55Å. A pair of coiled coils interacts as shown with an overlap of 35Å and two gaps of 20Å. The gaps correspond to the outer spots and the overlap region is marked by the central spot. This

indicates that groups are present that stain with uranyl acetate; that is negatively charged groups. The inference is that negatively charged amino acids, such as aspartic acid and glutamic acid are important in defining the stagger between interacting molecules.

X-ray diffraction patterns from specimens held with the thin edge towards the source have most of the intensity close to row lines which are orders of 18Å.

If row lines existed in the equatorial plane at spacings of 36Å, but not along this equator, then they would almost certainly appear as a result of disorientation. Even specimens tilted about the axis showed no evidence of other row lines. This suggests that the structure repeats every 18Å in the direction perpendicular to the electron micrographs of sonicated lamellae. This distance is about correct to allow packing of the coiled-coils proposed.

The existence of the 18Å repeat suggests that the coiled coils pack as in fig. 6.1a. This has different properties in the two perpendicular lateral directions. The different repeat distances in the two directions found from X-ray diffraction and the greater changes with humidity in the 18Å direction support this structure. Materials with differing properties in two perpendicular directions are likely to form sheet structures, such as the lamellae observed.

6.5 Structure and packing of lamellae

The ribbons used for X-ray diffraction work are composed of many lamellae of about 450Å thickness. X-ray diffraction obtains values of 485 ± 3Å, 462 ± 3Å and 452 ± 3Å for material at 100% relative humidity,

at room conditions and over silica gel respectively. The material between the lamellae has a significantly different electron density from them, as indicated by the high intensity of the low orders of the 450Å reflections. When the humidity was changed, the 450Å sampling shifted across the 18Å region. This suggested that the fractional change in the 450Å repeat was greater than that in the 18Å repeat. This probably results from the inter-lamellar material swelling and shrinking more than the lamellae. The very rapid fall off in intensity over the first seven orders of the 450Å reflection and the breadth of these reflections show that the spacing is not regular. The irregularity in the packing of lamellae is clear from plate 4.10, which shows a section through an embedded ribbon. Scattering from regions of regularly packed lamellae would give relatively sharp reflections. At the other extreme, a lamella embedded in the matrix would behave more like an isolated structure of about 450Å thickness. Broad peaks of rapidly decreasing intensity would be produced. The positions of these peaks could differ from the others, since the regular regions probably contain some material between lamellae. Variations in the thickness of lamellae (they taper at the ends in electron micrographs) could cause differences in the positions of reflections. This fits with the low angle region containing broad reflections of decreasing intensity, not separated from each other by clean film.

Examination of most of the diffraction patterns indicates that the meridian and the equator are lines of symmetry. Since the lamellae are asymmetric, this is not expected. It would be produced if both directions of the molecular axis are present in a ribbon. The lamellae could be arranged randomly, but the pattern obtained without a meridional line of symmetry indicates that the same orientation can exist over a 100 μm

thick ribbon. Either the lamellae are randomly arranged in some ribbons and not in others, depending on the conditions, or, what is more likely, the orientation changes after many lamellae. If the latter is correct, random effects, perhaps aided by the conditions of formation, could produce the two orientations present. The existence of small regions looking like the region giving the asymmetric pattern infers random effects. The occurrence of these regions in some egg cases and not in others infers that conditions of formation are important.

Looking at the plane of the ribbon, there is disorientation between lamellae. X-ray diffraction and electron micrographs of embedded ribbons strongly support this.

The continuity of striations through lamellae in the embedded and sectioned ribbons shown in plates 4.1 and 4.12 infers that the 18Å thick sheets pack in register. The similarity of the electron micrographs of embedded ribbons and of sonicated lamellae indicates that very great structural changes do not occur during treatment.

Banding patterns within the sectioned, embedded and stained ribbon are less easily interpreted. The 166Å striation in fig. 4.1 could derive from the edge of the lamella being at an angle to the 133Å striations. The most common pattern is a simple 30Å separation between striations. A possible origin for this is a cut along a major striation, but the period would hardly be maintained over such a distance. It is possible that the 30Å equatorial periodicity could result in a pattern of this form. However, it is surprising that the major striations do not show up. The myosin-like pattern could be produced by sectioning in this direction, but the intense bands are rather far apart to be produced by the major striations. Even though the banding pattern is superficially like that of myosin filaments, myosin seems quite different from this protein.

6.6. Patterson functions

Patterson functions were calculated from the meridional data. This was difficult, owing to the difficulties of identifying true meridional reflections, overlapping reflections and of intensity estimation. However, data from different patterns in which intensities and the reflections present were substantially different (section 5.2.5) gave broadly similar Patterson functions (fig. 6.4). The pattern drops to a low intensity beyond 15Å, so termination effects are likely to be small, but the intensities were multiplied by a function of form exp $(- k l^2)$. k was chosen so as to decrease the intensity of the outermost reflection by a factor of 10. Other factors were tried. A factor of 100 causes a loss of 2 peaks out of 22. A factor of 1 resulted in extra peaks appearing, but these were small and are likely to be produced by termination effects. The peak positions in the Pattersons derived from twodiffraction patterns are recorded in table 6.2. The positions are expressed in units of 0.001 x unit cell of 991Å. It is seen that the two patterns give similar results.

A Patterson function has a mirror plane, so only half the unit cell is shown. It is seen that the two halves of the function also have approximate mirror planes, a consequence of most of the intensity being on even numbered layer lines. This made it reasonable to take the unit cell as 495Å in most of the following analysis. The peaks occur at spacings which are approximately 1/46 of the unit cell; that is 21.5Å. This result is expected from the intensity distribution, which peaks most strongly near and on the 46th layer line. If a Patterson function is calculated out to 30Å resolution, pattern 1 gives a Patterson function with a pronounced periodicity of 1/32 of the unit cell; that is 30.9Å.

This is expected, since most of the intensity then occurs on the 32nd layer line. If k is chosen so that the intensity of the outermost reflection is reduced by a factor of 100, then a period of about 88Å is dominant; a result of three almost equally spaced reflections no longer dominated by the outermost. More useful information could be obtained with a Patterson function from higher resolution data, as indicated by the changes between the above Patterson functions, but good data cannot be obtained at such resolutions.

6.7 Interpretation of Patterson functions

It is possible to fit several solutions to the Patterson function. Examination of the structure in fig. 6.3 suggests a physically meaningful solution. Consider the structure projected on to the molecular axis. Then it is seen that the separation of identical points along a direction parallel to the major striations leads to a projected axial separation of about 89Å. Translation parallel to the other side of the unit cell to an identical point, followed by translation parallel to the major striation to an identical point gives an axial stagger of about 28Å. All possible staggers, S, are all possible sums of these; that is

$$S = ms + nt \qquad (6.1)$$

where s is about 89Å, t is about 28Å and m and n are integers. The Pattersons derived from patterns 1 and 2 have slightly different peaks, but they can both be indexed with the staggers as t = 21.0Å and s = 88.6Å. Expressed in units of one thousandth of the unit cell, these become 21.2 and 89.5. Peaks occur for $|n| \leqslant 6$ and $|m| \leqslant 4$. Beyond these limits, the total number of vectors becomes appreciably smaller.

Disorder would also cause the peak size to become smaller. The largest peaks occur for n = 0, especially when m is small. This is because the second term in (6.1) relates to structures affected by both axial and equatorial disorder. The greater breadth of reflections in the equatorial direction infers more disorder in this direction. Hence terms with n = 0 produce the largest peaks in the Patterson function. There is one exception to the largest peaks occurring for n = 0. This occurs in the Patterson function from pattern 1, and it is the peak for n = 3, m = 0 at 63Å. This peak is also large in the Patterson function from pattern 2. At these resolutions, the gaps can be expected to be responsible for most of the X-ray scattering. Fig. 6.3 shows that the two holes are separated by 55Å. The resolution of the electron micrograph is limited, so that an error of 10Å in the estimate of the separation of two points is as small as can be expected. APatterson function using data out to 15Å, cannot give accuracy better than 15Å. The 10Å error for the electron micrograph is very small, but this material is very stable in the microscope, as can be seen from the micrographs. It is seen that two peaks are expected in the Patterson function at about 60Å. They cannot be resolved, so they will overlap to form a larger peak, as is observed. The full expression for the stagger now becomes

$$S = ms + nt + \ell r \qquad (6.2)$$

where r is about 60Å and ℓ = -1, 0 or 1.

This system is too complex to fit to the Patterson function. However, it can be seen that all peaks can be explained in terms of it. The indexing is in table 6.2. The value of r cannot be easily determined. The breadth of the peak in the Patterson function from pattern 2 is so narrow that r

would be expected to be close to the peak value of 64.4Å. The broader peak in pattern 1 occurs at 62.4Å. Assuming any charge is sliding between coiled coils, we conclude that the most likely value for the centre to centre distance of the two gaps is 65Å. The error, however, is likely to be larger than for the estimate of 55Å obtained from the electron micrograph.

6.8 Origin of approximate unit cells

The equatorial unit cell was difficult to determine. Values such as 463Å were thought possible. From fig. 4.1, it is seen that lines approximately at right angles to the molecular axis could provide periods of about 450Å and about 600Å. All strong reflections indexed on about 310Å and most reflections indexed on 463Å. The cell chosen was 927Å. It is possible that this large cell was a result of there being no true cell. True repeats along lines at small angles to the equator could, through disorientation, result in a cell 927Å being chosen, if 927Å is a common multiple of the true repeats.

The meridional pattern is formed by reciprocal lattice points within about 15 degrees of the molecular axis. When the ribbon is supported with its thin edge towards the source, there is no possibility of telling how far these points are from the molecular axis. With the flat face towards the beam, it would be possible if only one molecular direction were present, but this is not the case. As opposing molecular directions are present, a reflection occurs on both sides of the meridian and arcing often joins the two, perhaps producing a meridional intensity maximum. The angle of arcing is a guide. This varies widely, lending credence to this argument. Some reflections are broader, as if two reflections of very similar spacing have arced and overlapped.

The meridional pattern represents the Fourier transform of the structure projected on to the fibre axis. In this case it represents the Fourier transform of the sum of the structure projected on to all lines within about 15 degrees of the fibre axis, the ones closest to the meridian being weighted most heavily. Fig. 6.3 shows that identical points separated by 495Å occur along lines at an angle of 13° to the major striations and at 8° to the molecular axis. There is another such line at 32 degrees to the major striations and at 11 degrees to the fibre axis. For a line to dominate the pattern, the electron density projected on to it should have variations of large amplitude. In fig. 6.3, the second line would give a very large variation, since the gap regions in adjacent major striations are in register. This situation could change if too much molecular sliding occurs.

It would be an oversimplification to say that the structure projected on to these lines gives the meridional pattern, but these dominate sufficiently for this spacing to be chosen as the best unit cell. The doubling of this cell at higher resolution could indicate that alternate gap regions differ in some way.

The Patterson function is still valid, except that peaks produced by axial staggers between structures separated by a large distance laterally will become broad or non-existent.

6.9 The equatorial pattern

The true equatorial pattern should have a modulation at intervals of 33Å, since the gap regions, when projected on to a line at a small angle to the a axis, give a strong 33Å repeat in electron density within the plane of the ribbon. The packing of coiled-coils superimposed a period of 16.5Å upon this. However, the diffraction from the basic α-helix

results in the 10Å region being the most intense.

6.10 The gap length

Electron microscopy suggests a gap length of 20Å. As the gaps are considered to be dominant in producing the low and medium angle patterns, the pattern should be modulated by the transform of the gap. The position of the first minimum of the modulation is not easy to determine, but, assuming it is the same under all conditions, it is at 11.4 ± 0.7Å (section 5.2.9). If the gaps line up throughout the ribbon, as the evidence suggests then they must scatter as a slit. This would provide an estimate of the gap length of 11.4 ± 0.7Å. If the alignment is imperfect, then this could be an underestimate. Since a disc shaped gap of 13.9A would lead to this estimate, the error is likely to be small. The major source of error is the difficulty of determining the position of the minimum. The value obtained is consistent with the figure obtained from the electron micrographs, especially since effects due to imperfect focusing or optical aberrations would lead to an overestimate from electron micrographs.

The structure close to the gap is uncertain. Electron micrographs show that the lateral bands appear to continue across the overlap region, but this is on the limit of the resolution of the data and must be treated with caution. This does suggest a continuation of the coiled-coil structure into the overlap region. This could fit neatly with a gap length of 7 residues. However, if the gap contains non-α-helical material at the end of the chains, the gap between α-helical material will be greater than that estimated. Such an effect occurs in collagen, where there are teleopeptides at the ends of the triple helical sections; they do not have the triple-helical structure normally associated with the collagen molecule.

The fibre pattern is not sufficiently intense to give a good estimate of

the gap length. A modulation can be seen corresponding to a gap of 26Å, but the minimum is not of zero intensity, suggesting that this is some other effect.

6.11 Primitive Unit Cells

Before the model can be considered reasonable, it must be shown that all the reflections can reasonably be indexed in terms of the primitive unit cell. Since the disorientation is high, a very accurate value for the spacing is required if unambiguous indexing is to be achieved. Unfortunately, such accuracy is only obtained in the region close to the meridian. Using just these reflections, it is found that the reflections can be indexed, but cell dimensions can vary substantially without changing the indexing. The cells fitted to the data have total lengths of gap and molecule in the expected range 742 ± 23Å (viz. 9×82.5Å). The driest material has dimensions closer to those found in electron micrographs, and the areas of the ac plane projections of the cell are smaller for drier specimens. Agents such as water and uranyl acetate cause swelling and molecular sliding. These must occur together unless the gap or the molecule is to become longer. These changes are discussed qualitatively, since the cell dimensions are not sufficiently accurately determined.

Figs. 6.5 and 6.6 show how the molecular length and orientation are related to the unit cell in real space and reciprocal space.

6.11.1 Uranyl acetate treated specimen (S. membramacea)

This specimen (section 5.2.7) gave strong low angle reflections, enabling the meridional reflections to be tested against them. The meridional reflections were indexed on the cell shown in fig. 6.5 according

to the scheme in table 6.4. The weak reflection observed near the meridian could be a first order of a cell double this size in the c direction, but, as it is weak and of uncertain spacing, it is ignored. The cell predicts a low angle 100 reflection at an angle of 21° 10' to the equator at a spacing of 146Å. The strong low angle reflections were found at a spacing of 147Å at an angle of 21° 25' to the equator, well within experimental error. For other reflections, where a strong 100 reflection was not obtained, it proved difficult to analyse data away from the meridian. The presence of two molecular directions and disorientation in regions where reflections were less sharp proved a difficulty for data not on the meridian.

This cell showed the greatest difference from the electron micrographs. The degrees of swelling and molecular sliding were greater than for other conditions. The molecular length and the gap came to 740Å.

6.11.2 A specimen at room conditions (S. tenuidentata)

Several good patterns were obtained, enabling spacings to be accurately determined. The unit cell (fig. 6.5) is close to that found in electron micrographs. The length of the molecule and gap together comes to 734Å. However, the cell parameters are not as well determined as the indexing (table 6.5) suggests, since only a small volume of reciprocal space is represented. Examples of close reflections are seen at higher angles. Overlapping can cause an average value to be found. Where this is probable all likely contributions to the observed reflection are included in table 6.5 and the following tables.

It is seen (fig. 6.7) that most of the reciprocal lattice points within about 15 degrees of the meridian are represented by a reflection falling on

the meridian for a specimen supported with the thin edge towards the source. This pattern contains many well indexed reflections. Other patterns are less well indexed, but they are discussed below.

6.11.3 A specimen over silica gel (S. tenuidentata)

The cell determined for this specimen (fig. 6.5) was the smallest, as expected after dehydration, and it most closely resembled the cell in the electron micrographs. Table 6.6 shows that there are many ambiguities in the indexing. These reflect the problems of overlapping reflections. The length of the molecule and gap is 728Å, not significantly different from the other values.

6.11.4 Specimens at 100% relative humidity

Two different specimens of S. tenuidentata and one of S. membramacea gave similar but different unit cells, as indexed in tables 6.7-6.9. It is not surprising that differences should occur between specimens, since they are cross linked in the egg case and are therefore dependent on the initial conditions.

6.11.5 A specimen treated with chlorobenzene and bromobenzene (S. membramacea)

It was seen in chapter 5 that the unit cell dimensions appeared to be the same as for a specimen at 100% relative humidity. The reflections were indexed on the same cell as that used for the S. membramacea specimen at 100% relative humidity. Table 6.10 shows that the agreement is quite good.

6.11.6 Conclusions

The cell parameters for all cases is given in table 6.11. It appears that swelling and molecular sliding is stimulated by a polar environment, uranyl acetate being more effective than water. It seems likely that polar interactions are being weakened, reflecting their importance in the structure. The similarity in the effects of the chlorobenzene and bromobenzene mixture and water is surprising. Possibly, the mixture is kept in the structure by dipolar interactions, the greater molecular mass compensating for the lower dipole moment, as compared with water.

6.12 Other material present

It is known that material is present between the k.m.e.f. sheets. As most reflections index well, it is thought that few medium angle reflections are given by the inter-lamellar material. It is noticed that some reflections index poorly. The reflection at about 24.7Å is the most noticeable of these. These reflections could well derive from the second component.

It is known that small crystals are present in the egg cases, as seen by the presence of granular rings on X-ray diffraction patterns. Examination under the optical microscope reveals small crystals of various sizes of the order of 10 μm. They could easily be the calcium citrate crystals found by Parker and Rudall (1955), but the diffraction rings do not correspond to the commonest forms of this substance. The crystals are found on the surfaces of sheet like structures, but they are not uniformly distributed between egg cases or within an egg case. The presence of a soluble substance is suggested by the condensation of water on a ribbon at high humidities; that is when the vapour pressure

of the water is higher than the saturated vapour pressure of the solution on the ribbon. Calcium citrate may not be sufficiently soluble to produce the observed effect, so another salt may be responsible.

There is a likelihood of lipid being present (section 5.2.4.6). This was not always present and, when it was, the amount varied. The sampling of the lipid reflection by the 450Å row lines suggested that the lipid was intimately associated with the protein. The width of the sampled reflection inferred crystallites of dimensions at least 400Å at right angles to the lamellae. Perhaps the lipid forms ordered structures on the edges of the lamellae.

6.13 Larger unit cells

The presence of a number of weak reflections which could not be indexed could derive from a larger unit cell or a second component. Examination of the structure in fig. 6.3 shows that the cell is probably larger. Irrespective of the relative rotation between coiled-coil units, there is a repeat of 1/9 of the length of the molecule and gap. Since the coiled coil has a diad axis, the length contains 4•5 repeats of what is probably the average pitch. Assuming the two chains are of equal length, the two ends of the coiled coil are oriented at 180 degrees to each other. The cell will at least be doubled in the c direction to account for this. This was also suggested by the diffraction patterns from the specimen stained with uranyl acetate. This is consistent with a 90 degree relative orientation between adjacent coiled coils. The stagger of 2•5 times the average pitch combined with a 90 degree rotational difference between the termini of adjacent coiled coils leads to packing as proposed (section

6.4). The rotational difference between consecutive overlap regions along the c axis of the primitive unit cell becomes 180 degrees, and along the a axis becomes 90 degrees, leading to a doubling of the unit cell in the a direction. The stagger between adjacent coiled coils must change as conditions change; the unit cell changes its dimensions, leading to molecular sliding. However, the packing remains close to the optimum and has some of the essential features proposed by Rudall (1956).

6.14 The structure of the fibres

The similarity between the structure of the fibres and that of the ribbons is not proven. Since the fibres were produced without the contents of the right colleterial gland and the calcium citrate gland being added, not all the material is present, so differences in structure can be expected. Pulling fibres results in rapid drying, which would be expected to inhibit the formation of regular structures. However, when it is considered that the left gland produces most of the material, similar structures in the ribbons and the fibres may be found.

The discussion of sections 6.1, 6.2 and 6.3 shows that the structure is very similar as regards lateral packing and a coiled coil structure, but the meridional diffraction pattern remains to be indexed. Unfortunately this pattern is very weak, so data are not available. The pattern obtained shows streaks crossing the meridian. Owing to the small crystallite size, reflections close to the meridian form streaks crossing the meridian. Since fibres are rotationally disoriented around the fibre axis, there are always reflections on both sides of the meridian which form streaks centred on the meridian. Fortunately the disorientation is small.

The meridional information cannot give the dimensions of the primitive unit cell. A two dimensional unit cell, as used to describe the electron micrographs, needs at least three pieces of information to define it. This is provided where reflections arc across the meridian, since terms in a^2, c^2 and a.c are required to define the distance in reciprocal space. In this case only the components of the reciprocal lattice points projected on to the axis are required. This depends only on a and c as seen from fig. 6.8.

Information can be obtained. Fig. 6.8 shows how L, the length of the molecule and gap together, is related to distances a and c, the angle marked δ, and the angle between c and the molecular axis α. This diagram follows directly from fig. 6.3, and provides the relationships

$$\sin \alpha = \frac{2a}{L}$$

$$\cos \alpha = \frac{7c + 2a \tan \delta}{L}$$

$$\therefore \cos \alpha = \frac{7c}{L} + \sin\alpha \tan \delta$$

The diagram of the reciprocal unit cell shows that the distance projected on to the fibre axis by a reciprocal lattice point is

$$P_{h\ell} = \ell . \frac{1}{c} \cos \alpha + h \frac{1}{a} \sin \alpha .$$

where h and ℓ are constants. This becomes

$$P_{h\ell} = \ell \left(\frac{7}{L} + \frac{\sin\alpha \tan \delta}{c}\right) + h \frac{2}{L}$$

δ is a small angle below 5°, so the distance becomes approximately M/L, where M is a constant. The fibre axis is more closely parallel to the c* axis than the a* axis, so many consecutive points along the a* axis will not give reflections on the meridian. As δ is small and $P_{h\ell} \simeq M/L$, then the diffraction pattern is likely to index along the meridian on a cell

It would be hoped that data would be obtained from regions far from the meridian, but the random orientation of crystallites about the fibre axis leads to intensities being too low.

The best indexing was achieved on a unit cell of 1435Å, but this value is not certain. As a number which is close to a multiple of L, it is possible to relate this to the structure, unlike the other possible indexing schemes. It also gave the best indexing as indicated by the standard errors between observed and calculated values. On this basis, this unit cell is thought to be correct.

If the value is correct, then the gap regions must have virtually disappeared, possibly at the expense of a greater overlap. 1435Å is 2L which requires the cell size to be doubled in the c direction. This is expected (section 6.13), but it is surprising that it is detected here, unless the structure has changed a little. It is possible that information away from the hℓ plane appeared on the meridian more here than for the ribbons. The ribbons were much more disoriented in the ac plane which would lead to most of the meridional data coming from points in the hℓ plane. If the unit cell is 2c, but c in projection on to the ac plane, then this result is explained.

The structure of the fibres is less certain than that of the ribbons, owing to the poorer diffraction patterns obtained.

6.15 Summary of the solution

The ribbons from the egg case contain lamellae of size about 10 μm x 1 μm and thickness close to 460Å, depending on the conditions. These lamellae pack into ribbons or sometimes sheets which form the outer

case of the ootheca. A ribbon is typically of the order of 10 mm x 1 mm. x 0.1 mm., but it can be subdivided until it can no longer be handled. The lamellae are arranged in the ribbon with the long axes approximately parallel to the long axis of the ribbon and their planes approximately in the plane of the ribbon. Disorientations between lamellae of 10 degrees or more are general.

The structure of a lamella repeats through its thickness at intervals of about 18Å, depending on the conditions. The structure of this 18Å thick sheet is shown in fig. 6.3. The packing between sheets differs from that proposed by Rudall (1956) (fig. 6.1), but within the sheet, it is very similar. Coiled coil structures pack parallel in such a way as to allow a close packing as suggested by Rudall (1956). This requires a stagger of a quarter of the pitch between coiled coils.

The structure has a repeat along the fibre axis of 82.5Å which probably relates to an average pitch of 165Å. It seemed likely that this pitch varied. Some evidence suggested the presence of a pitch of about 175Å, closer to that expected for a coiled coil. The width of the 1.5Å reflection indicated that this residue translation was only maintained for a distance of about 50Å, even though the pitch appeared to be maintained for a greater distance. This leads to there being 50Å lengths of coiled coil of supercoil pitch 175Å. The rest of the 82.5Å repeat is probably helical material with a pitch very close to that in the α-helix, but with changes in the residue translation and the supercoil pitch; this region would show as the fuzzy bands on the electron micrographs.

The stagger between adjacent coiled coils is 2.5 x 165Å. With the appropriate azimuthal rotations, the major striations become lines of overlap regions between every other coiled coil, each region being

rotated by 180° from the one before, if Rudall's optimum packing is to be achieved. Adjacent major striations then have overlap regions rotated about the fibre axis 90 degrees from each other. When the orientations of overlap regions are considered, the unit cell is doubled along both sides, but for most purposes the unit cell is about 95Å x 140Å and contains one coiled coil of total length, including the gap, of about 740Å (9 x 82.5Å) which is 4.5 times the average pitch. Since the unit cell changes with conditions, packing cannot always be precisely like that proposed by Rudall (1956) but it is likely to be close. The probability of variations in the pitch also makes the packing less regular.

The coiled coil structures themselves have appreciable α-helical structure. The molecular weights estimated are consistent with a molecular length of about 720Å, assuming the molecule contains two chains which dissociate in SDS, as is expected for non-covalently linked protein chains. The gap length estimated is about 15Å and the stagger between the two chains in a coiled coil is estimated to be 55Å (the error in this is likely to be up to 15Å).

Electron microscopy of the stained lamellae revealed that the overlap region was usually stained even with negative staining, inferring the presence of negatively charged amino acids in the overlap region. The amino acid composition of the ribbons given in chapter 1 is consistent with a structure that is largely α-helical, containing small quantities of helix-disrupting residues and large amounts of acidic amino acids.

6.16 Further work

Before much work can be directed towards improving the model, better diffraction patterns are required. For this, a more suitable species of praying mantis must be found. Only after an exhaustive survey of egg

cases from different species, would it be worth while developing a colony of insects. The colony used for this work took nearly six months to mature after hatching. Better data would allow more accurate intensities and positions to be obtained for the reflections and a more quantitative analysis could be carried out.

It should be possible to use the information so far derived from the data to index more of the off-meridional data, but this task is not easy. This would allow unit cells to be determined more accurately. It is doubtful if intensities and indexing could be made accurate enough to elucidate more clearly the overlap region. It is hoped that measurement of the low angle reflections in terms of polar coordinates can give values of the reciprocal lattice spacing s which are accurate enough to index the reflections. Even then, this is dependent on the unit cells already found. However, an extension to regions farther from the meridian should increase the accuracy of cell dimensions determined.

The possibility of producing artificial forms of the protein has not been fully explored. Some material is likely to remain for this when R. Pau completes the determination of accurate molecular weights and amino acid compositions.

6.17 General discussion

The conclusions drawn from this work may have a bearing on more general problems. In this section, no general principles are established, but the existence of such principles is assumed.

6.17.1 k-m-e f structures

It has been established that this protein contains an appreciable

amount of protein with a coiled-coil α-helical structure, confirming Rudall's (1956) assignment of this protein to the k-m-e-f class. There are no indications that the lateral packing of the coiled-coils differs greatly from that in other proteins of the k-m-e-f class. It is probable that regular α-helical structure extends for distances of only 50Å. This situation is almost identical to that in α-keratin, where the structure extends for about 60Å (Fraser and MacRae, 1973b). In the praying mantis egg case protein, the other structure appears to be a helix of a very similar pitch but the residue translation differs. This region is uncertain without more data. In α-keratin there are indications that the regions between the α-helical sections are less regular (Fraser et al., 1972).

The gap length and the stagger between the two chains are small. This is probably typical for the k-m-e-f class. In tropomyosin the stagger is thought to be 14 residues (Hodges et al., 1973), which is about a third of that in this protein. The small size of the stagger can be related to the existence of a two chain unit (section 6.18.2).

6.1.7.2 Sheets and microfibrils

The coiled-coil structure has a small stagger between chains. A stagger which is a smaller fraction of the molecular length could lead to a microfibrillar structure as in collagen (Smith, 1968). If after a few molecules, the sheet can curl up to place the last molecule along the same line as the first, then microfibrils can be constructed. In this case, it would take about 14 molecules before this could be done. The most stable arrangement is then a small overlap with the next coiled coil. The supercoiling is a means by which chains can be stabilised in pairs.

The lateral packing is different in two perpendicular directions, a prerequisite for the development of a sheet structure. With this model, packing in the plane of the sheet allows good molecular interlocking in the manner proposed by Rudall (1956). The smaller amount of swelling at high humidities in this direction implies that the coiled coils interact more strongly. This suggests that the greater extent of the lattice in the plane of the sheet results from stronger interactions between the subunits (coiled coils). Another expected property of a plane sheet is that the two surfaces should be identical. If this is not the case, the sheet may be expected to be curved or even to form a structure like that of a Swiss roll, as is possibly the case for paramyosin (section 1.5.4.1). Examination of the 18Å thick sheet shows that this is the case. The molecular length is 4.5 times the pitch. By this mechanism, consecutive molecules are rotated about the fibre axis 180 degrees from each other. This allows the same structures to be present on either side of the sheet without restricting the range of possible sequences for this purpose. Control of the length to $\frac{1}{2}(2n + 1)$ times the average pitch, where n is an integer, is much more easily achieved by genetic selection than are many changes in the sequence.

Microfibrillar structures, such as the two chain coiled coil can themselves aggregate into microfibrils. α-keratin, which forms microfibrils from α-helical coiled coils (Fraser and MacRae, 1973b) and collagen which forms microfibrils from three chain units (Smith, 1968) are examples of this. The most stable structure appears to involve supercoiling of the microfibril in both these cases (for collagen see Miller and Parry, 1973).

Eventually, microfibrils generally form a lattice. If the lattice is not very similar in two perpendicular directions at right angles to the fibrils, then sheet structures are expected to be formed. Sheets can then pack parallel to each other. α-keratin is an example where the microfibrils do not form a regular lattice, but are embedded in a matrix (Fraser et al., 1972). There is a pseudo-hexagonal packing in α-keratin, but not a regular lattice.

6.1.7.3 The amino acid composition

The amino acid composition (table 1.3) is similar to that of the α-helical muscle proteins. However the content of the helix-disrupting residues, proline, glycine and cysteine is higher. These could be found in non-α-helical regions; proline certainly is. The higher content of glycine and alanine than in the muscle proteins could indicate an evolutionary link with the other silks.

The differences between the amino acid compositions and molecular weights of proteins of the k-m-e-f group makes it impossible to regard them as one protein. They are a group of different proteins.

It appeared that negatively charged groups were dominant on the surface of the lamellae as seen from the good positive staining of lamellae achieved with uranyl acetate. They appeared particularly important in the overlap region. It would be expected that hydrophobic residues would dominate in intermolecular interactions, since they prefer to interact with each other rather than with water. However, two hydrophobic surfaces would define a molecular stagger by steric effects rather than any other. The introduction of positively and negatively charged groups

allows the two chains to have sequences which strongly favour one particular stagger. When the overlap region is short a high concentration of charged groups is expected. Where the overlap region is the greater part of the molecular length, then the charged groups can be more scattered, allowing the system to utilize the stabilising effect of hydrophobic interactions in an aqueous environment.

Since the material swells anisotropically, swelling coincides with molecular sliding. Swelling occurs most readily in the presence of water or uranyl acetate. Both these agents are polar and therefore tend to disrupt polar interactions. This also infers the importance of polar interactions in defining molecular staggers.

Table 6.1

The high angle meridional and near meridional pattern given by the fibres

Observed spacing* Å	Order of 167/17 Å	Calculated spacing Å	Order of 165/16 Å	Calculated spacing Å
11.09				
10.81				
9.82	1	9.80		
9.08				
8.62				
5.38				
5.18			2	5.15
4.95	2	4.90		
4.78				
4.57				
3.20	3	3.27		
3.06				
2.49	4	2.45	4	2.58
2.13			5	2.06
1.93	5	1.96		
1.65	6	1.63	6	1.72
1.49			7	1.47
1.37	7	1.40		
1.30			8	1.29
1.18	8	1.22		
1.17				
≠1.14	9	1.09	9	1.14

*Exposure times given would not reveal weak reflections beyond about 8 A

≠Reflection on the edge of the film, giving a less reliable estimate of its position.

Table 6.2

Peaks in the Patterson function at 15 Å resolution from two similar diffraction patterns and indexing on the scheme chosen

Peak positions		Possible indexing								
Pattern 1	Pattern 2	n	m	Calc. pos.	n	m	Calc. pos.	n	m	Calc pos
Å x1000/991										
0	0	0	0	0						
23		±1	0	21.2						
	27	-3	1	25.9						
46		±2	0	42.4	-2	1	47.1			
65.5	63	3	0	63.6	-1	1	68.3			
90	89	0	1	89.5	-4	2	94.2	±4	0	84.8
109.5	109	±5	0	106	1	1	110.7			
127.5	128	±6	0	127.2	2	1	131.9			
142		0	4	142	-6	3	141.3			
152	153	3	1	153.1	-1	2	157.8			
173	175.5	4	1	174.3	0	2	179			
191	192	5	1	195.5	2	3	189.1	6	2	193.8
218	218	2	2	221.4	5	2	215			
238	240	3	2	242.6	4	2	236.2	0	3	231.5

Table 6.3

Patterson function from pattern 1 out to 30 Å resolution

Peak position	Intervals of 1/32 of unit cell
0	0
32	31.2
62	62.5
93	93.7
126	125.0
156	156.2
186	187.5
220	218.7
250	250.0

Table 6.4

Indexing of the meridional pattern of the uranyl acetate treated specimen (S.membramacea)

Indexing		Spacing Å		Reciprocal spacing $Å^{-1} \times 10^6$	
h	ℓ	Observed	Calc.	Observed	Calc.
0	1	97.5	98.6	1026	1015
1	1	78.9	80.3	1268	1245
-	-	53.9	-	1854	-
1	2	46.1	46.2	2169	2166
2	2	40.8	40.2	2452	2490
-	-	36.2	-	2763	-
1	3	31.6	31.8	3170	3145
2	3	29.2	29.6	3430	3383
3	3	26.6	26.8	3760	3735
0	4	24.5	24.6	4089	4060
2	4	23.5	23.1	4262	4331
3	4	21.8	21.7	4591	4616
3	6	15.5	15.4	6447	6497

Table 6.5

Indexing of the meridional pattern from two specimens from S.tenuidentata at room conditions

Indexing		Spacing Å		Reciprocal spacing $Å^{-1} \times 10^6$	
h	ℓ	Observed	Calc.	Observed	Calc.
1	1	80.97	80.84	1235	1237
1	2	45.15	45.25	2215	2210
1	3	30.81	30.65	3245	3262
2	3	29.01	29.29	3447	3415
3	3	27.10	26.94	3689	3711
4	3	24.66	24.32	4055	4112
1	4	23.23	23.18	4305	4314
3	4	21.54	21.57	4642	4636
4	4	20.24	20.21	4939	4948
5	4	18.76	18.74	5330	5337
0	5	}18.47{	18.49	} 5414 {	5409
1	5		18.54		5393
2	5	18.13	18.18	5516	5500
3	5	17.72	17.81	5642	5617
4	5	17.00	17.05	5882	5865
5	5	16.21	16.17	6171	6185
2	6	15.40	15.37	6496	6506
4	6	14.64	14.64	6831	6829
5	6	14.05	14.09	7113	7096
1	7	13.28	13.27	7532	7534
0	7	} 13.23 {	13.21	} 7560 {	7572
2	7		13.22		7564
7	6	12.93	12.82	7735	7800
1	7	} 12.99 {	13.03	} 7696 {	7677
3	7		13.04		7663
5	7	12.44	12.43	8036	8049
6	7	11.99	12.01	8336	8329

Table 6.6

Indexing of the meridional pattern from the specimen over silica gel (S.tenuidentata)

Indexing		Spacing Å		Reciprocal spacing $Å^{-1} \times 10^6$	
h	ℓ	Observed	Calc.	Observed	Calc.
1	1	78.74	80.26	1270	1246
1	2	44.80	44.78	2232	2231
2	2	39.89	40.13	2507	2492
3	2	34.36	34.35	2910	2911
0	3	30.63	30.49	3264	3280
1	3		30.44		3285
4	2	29.38	29.14	3404	3431
2	3		29.04		3444
3	3	26.70	26.75	3745	3738
4	3	23.60	24.17	4237	4137
0	4	23.05	22.87	4338	4372
1	4		22.94		4359
5	3	21.44	21.68	4665	4613
3	4		21.39		4674
4	4	20.13	20.07	4968	4983
3	5	17.72	17.64	5642	5669
6	4	17.00	17.17	5884	5822
4	5		16.91		5912
5	5	16.14	16.06	6196	6229
6	5	15.16	15.13	6594	6610
0	6		15.25		6559
1	6		15.33		6525
2	6		15.22		6570
8	5	13.22	13.30	7567	7521
1	7		13.14		7612
9	5	12.47	12.44	8021	8034

Table 6.7

Indexing of the meridional pattern from a specimen of S.tenuidentata at 100% relative humidity

Indexing		Spacing Å		Reciprocal spacing $Å^{-1} \times 10^6$	
h	ℓ	Observed	Calc.	Observed	Calc.
1	1	78.86	79.11	1268	1264
1	2	44.91	45.03	2227	2221
1	3	30.79	30.78	3247	3248
2	3	28.91	28.88	3459	3462
-	-	24.72	-	4045	-
1	4	23.05	23.32	4338	4288
3	4	21.39	21.22	4675	4713

Table 6.8

Indexing of the meridional pattern from a second specimen *S.tenuidentata* at 100% relative humidity

Indexing		Spacing Å		Reciprocal spacing $Å^{-1}$ 10^6	
h	ℓ	Observed	Calc.	Observed	Calc.
$\bar{1}$	1	78.00	77.82	1282*	1285
0	1	96.62	93.28	1035	1072
1	1	83.54	81.37	1197	1229
1	2	45.72	45.23	2187	2211
1	3	30.71	30.76	3256	3251
2	3	29.39	29.30	3402	3413
4	3	24.68	24.70	4051	4048
2	4	22.56	22.60	4432	4423
3	4	21.62	21.61	4626	4629
6	3	20.33	20.17	4921	4957
4	4		20.35		4915
5	4	19.04	18.98	5253	5268
2	5	18.24	18.33	5483	5456
6	4	17.76	17.62	5628	5675
3	5		17.80		5618
4	5	17.07	17.09	5857	5851
8	4	15.26	15.13	6569	6609
2	6		15.38		6502
3	6		15.07		6634

*Reflection observed well off the meridian at about the correct position for the $\bar{1}01$ reflection

Table 6.9

Indexing of the meridional pattern from a specimen from S.membramacea at 100% relative humidity

Indexing		Spacing Å		Reciprocal spacing $Å^{-1} \times 10^6$	
h	ℓ	Observed	Calc.	Observed	Calc.
0	1	100.3	95.33	997	1049
1	2	45.46	45.43	2199	2202
2	2	40.49	40.03	2470	2498
1	3	30.87	31.10	3239	3215
1	4	23.36	23.61	4280	4246
3	4	21.36	21.47	4683	4659
3	5	17.70	17.80	5650	5619
4	7	12.85	12.79	7788	7820

Table 6.10

Indexing of the meridional pattern from a specimen from S.membramacea after treatment with chlorobenzene and bromobenzene

Indexing		Spacing Å		Reciprocal spacing $Å^{-1}$ 10^6	
h	ℓ	Observed	Calc.	Observed	Calc.
0	1	96.06	95.33	1041	1049
1	1	80.26	80.06	1246	1249
1	2	44.36	45.43	2254	2202
2	2	40.49	40.03	2470	2498
3	2	34.91	34.18	2865	2927
1	3	31.03	31.10	3223	3215
4	2	28.91	29.06	3459	3441
2	3		29.21		3424
3	3	26.70	26.69	3745	3747
–	–	25.72	–	4045	–
1	4	23.30	23.55	4291	4246
2	4	22.39	22.70	4466	4405
3	4	21.37	21.47	4679	4659
5	4	18.60	18.52	5375	5399
2	5		18.48		5411
4	5	16.92	16.95	5909	5901
5	5	16.15	16.02	6195	6245
2	6	15.48	15.55	6459	6432

Table 6.11

Parameters of the unit cells

Conditions	Sp.	a Å	c Å	β	ℓ Å	α	table
Uranyl acetate	M	145.9	98.62	87°56'	739.9	23°14'	6.4
Room	T	139.4	92.94	95°44'	733.6	22°22'	6.5
Silica gel	T	139.1	92.00	95°57'	728.2	22°28'	6.6
100% R.H.	T	144.7	94.52	90°	722.1Å	23°37'	6.7
100% R.H.	T	152.5	93.37	92°51'	734.9	24°31'	6.8
100% R.H.	M	145.9	95.33	90°24'	730.3	24°16'	6.9
Chloro- and bromobenzene	M	145.9	95.33	90°24'	730.3	24°16'	6.10
E.M.(fig.4.1)	T	134	94	98°	730	21°	-

M S.membramacea

T S.tenuidentata

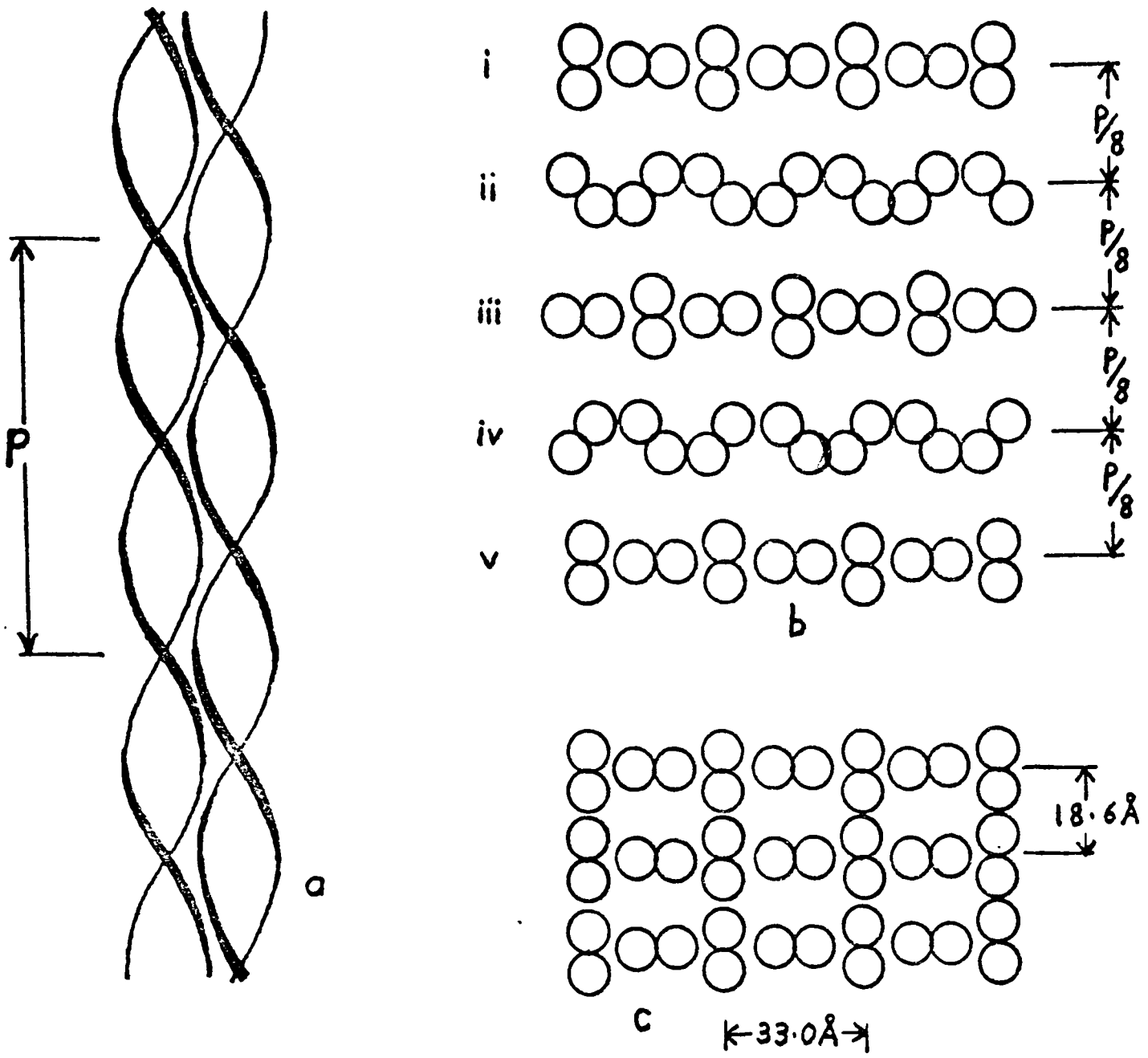

Fig.6.1 Packing of coiled coils. 6.1a shows two coiled coils of pitch, P, and relative stagger P/4 packed as suggested by K.M.Rudall. 6.1 b shows sections through a layer of such coiled coils at axial intervals of P/8. 6.1c shows the packing of layers in the model proposed in this thesis. The dimensions are for wet specimens.

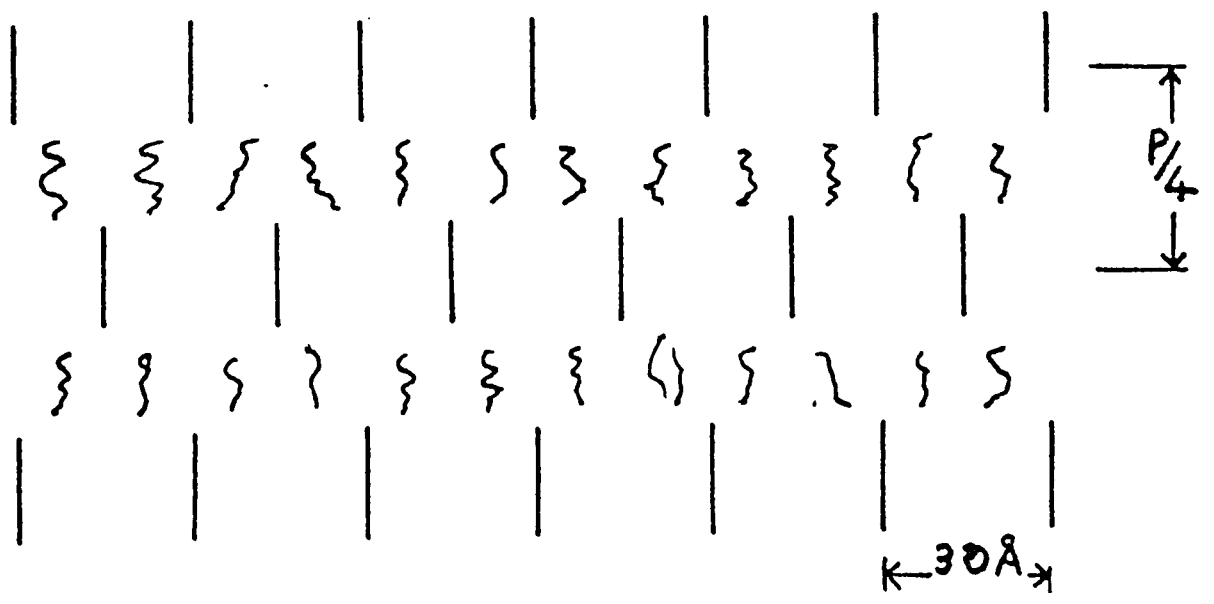

Fig. 6.2 Possible negative staining where either sections i, iii and v in fig. 6.1 have a well defined stain pattern or else ii and iv do. All lines on the diagram represent stain.

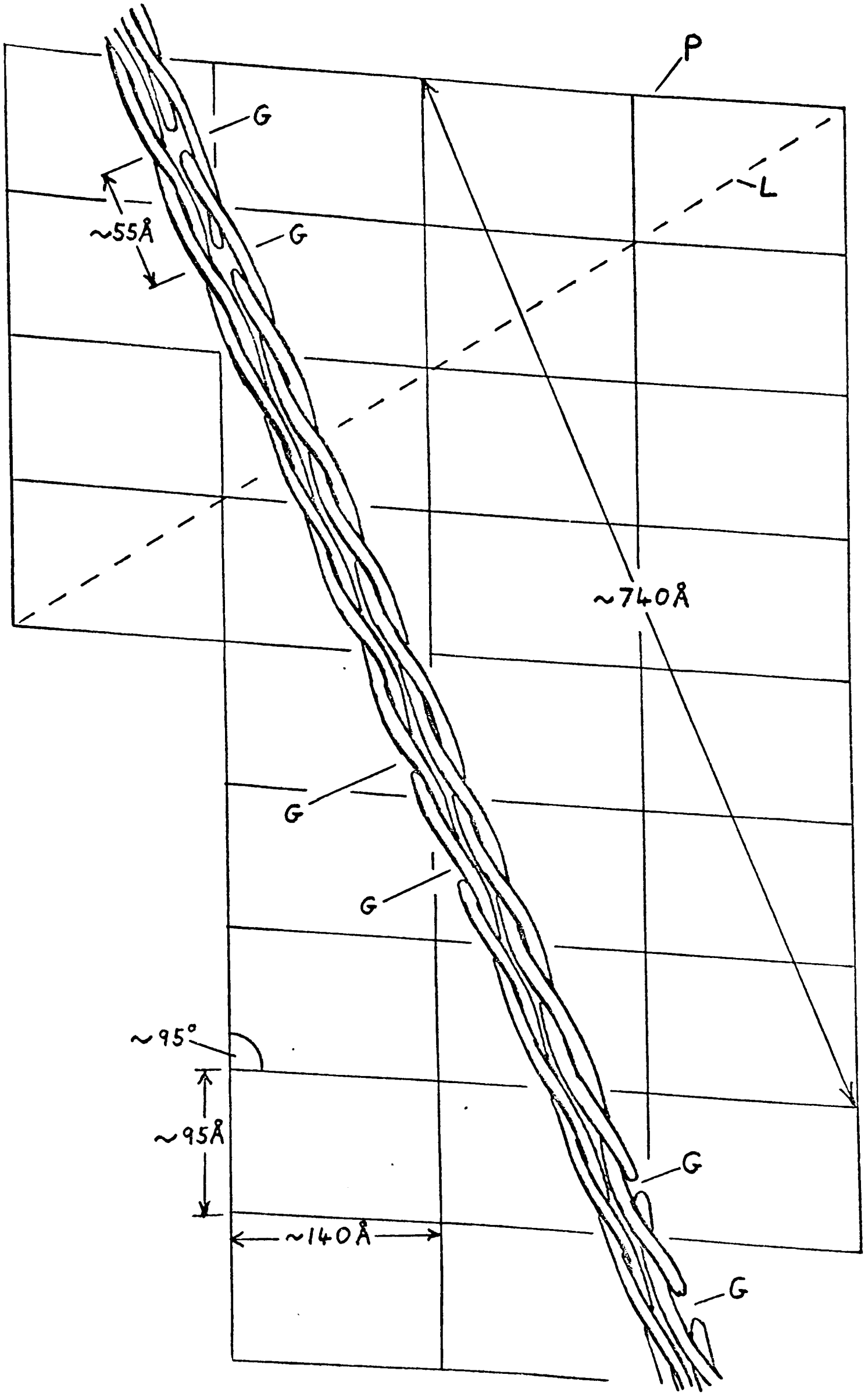

Fig. 6.3 Idealised packing of coiled coils. The probable variations in pitch and deviations from regularity are not marked. G, gap of length ~ 15Å; L, line of fuzzy bands, probably representing a rather different structure at 80 Å intervals.

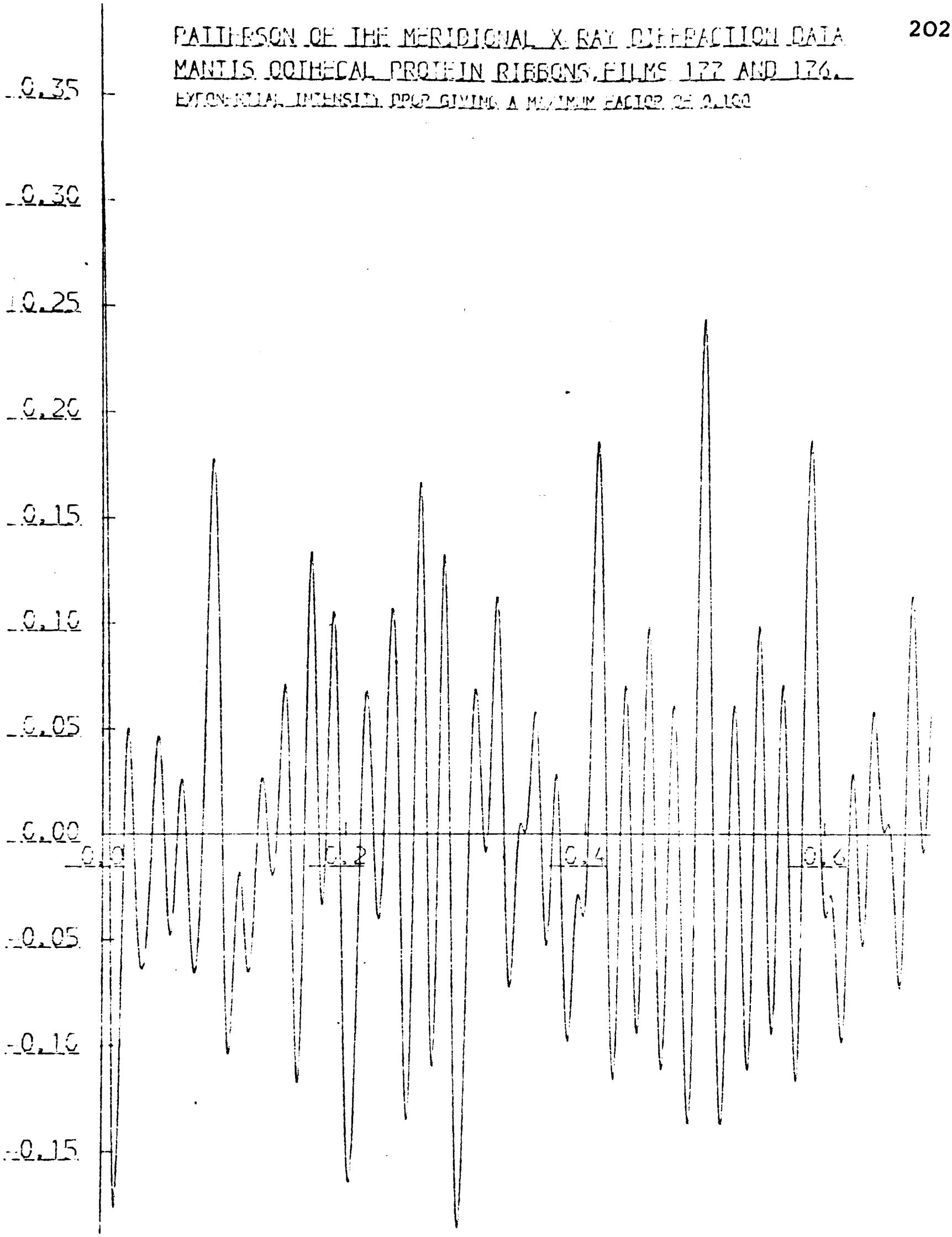

Fig. 6.4 Patterson function of the meridional X-ray diffraction pattern out to 16Å resolution for a specimen from *S.tenuidentata* at room conditions. The horizontal axis is calibrated in fractions of the 991Å unit cell. The pattern is symmetric about 0.5 on the horizontal axis. The 000 reflection was not included.

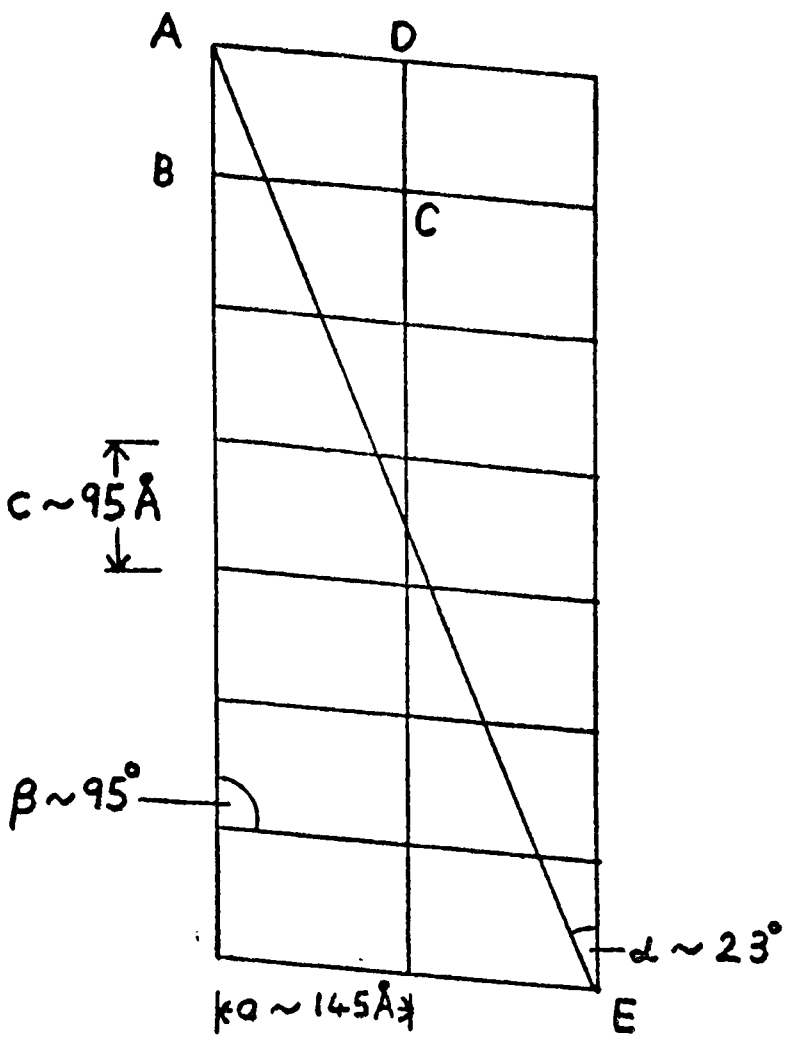

Fig. 6.5 Diagram defining symbols used to define the unit cell and the molecular axis, AE. The molecular length, AE=ℓ

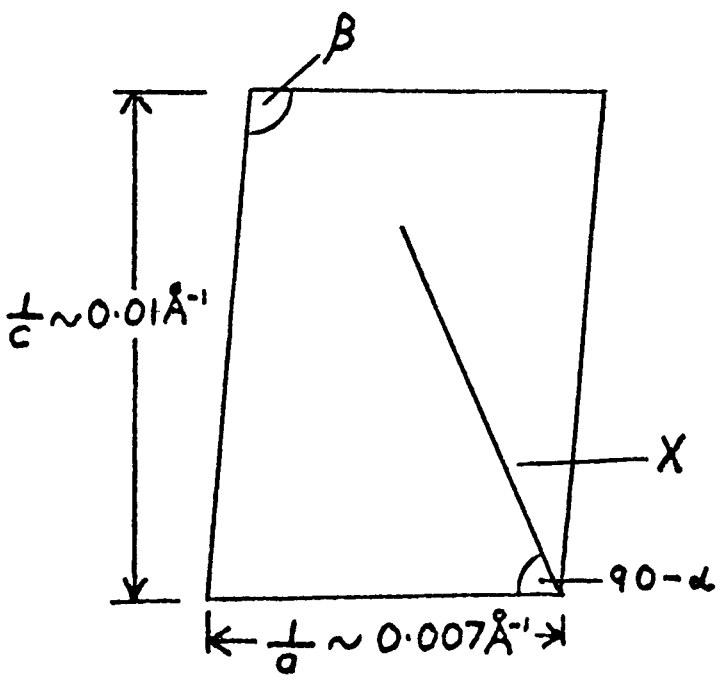

Fig. 6.6 The unit cell in reciprocal space. X, the molecular axis.

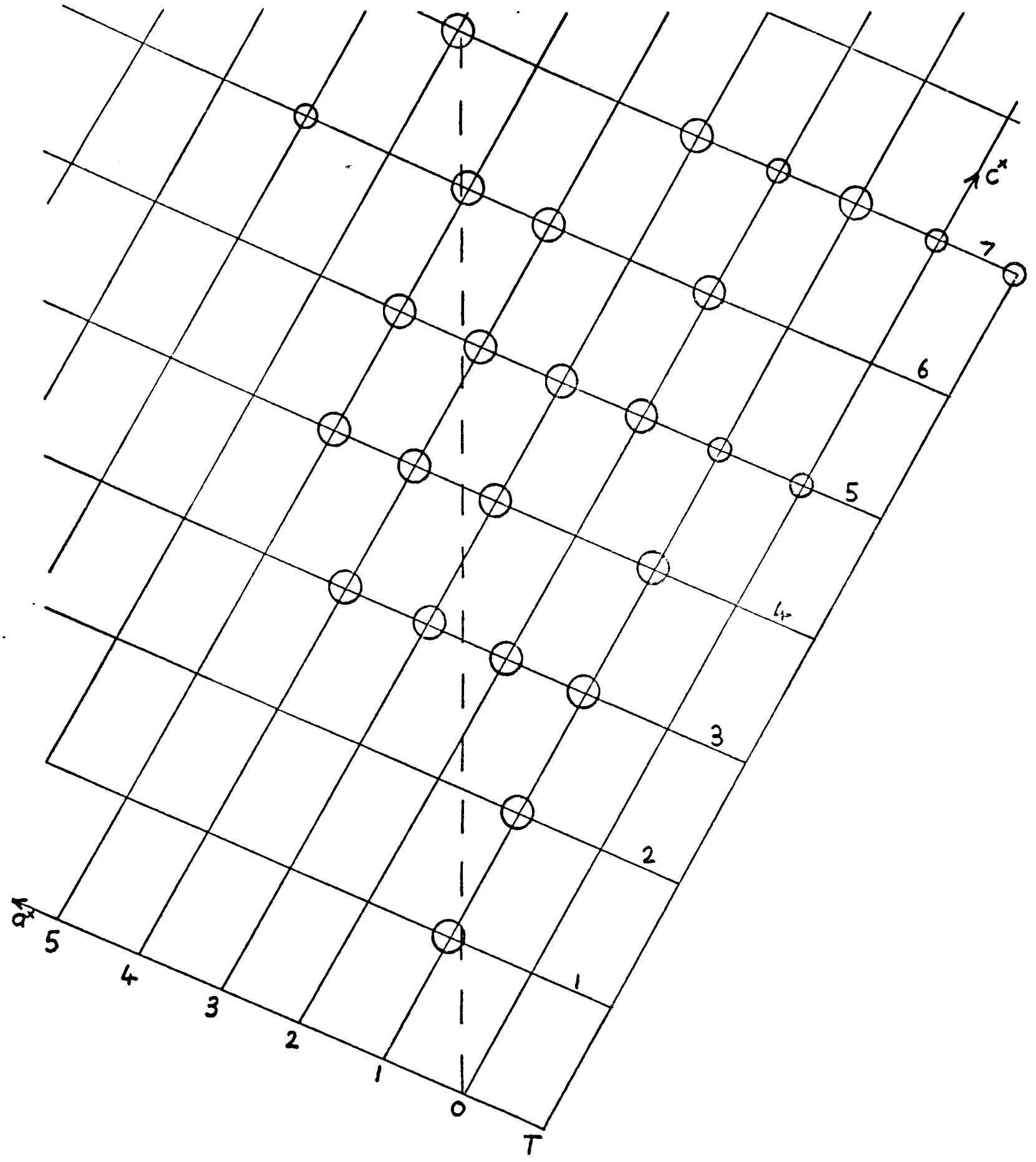

Fig. 6.7 Reciprocal lattice for dry ribbons from *S.tenuidentata*. The dotted line is the direction of the axis of the ribbon. The circles are reflections falling on the meridian of diffraction patterns - a result of disorientation. The small circles mark reflections where indexing is ambiguous.

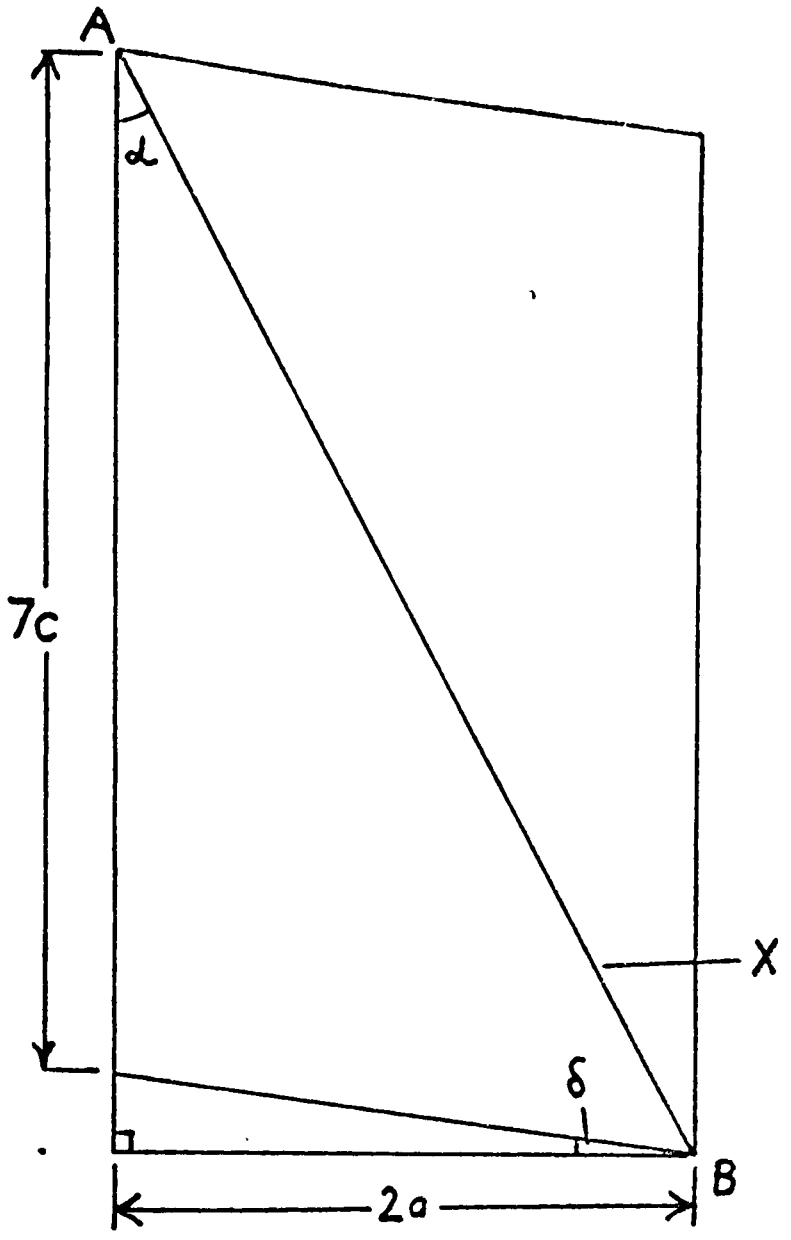

Real space

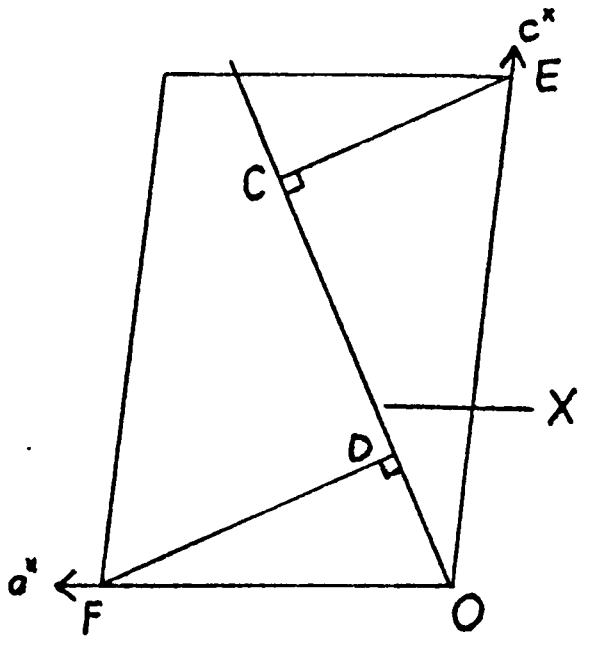

Reciprocal space

Fig. 6.8 (See also fig. 6.5) Diagram illustrating the derivation of relationships needed for the interpretation of the X-ray diffraction patterns from fibres drawn from the gland of *S.membramacea*.
For convenience of calculation, the distance 2a is measured perpendicular to the c axis of the unit cell. AB= molecular length = ℓ; X, direction of the molecular axis; CO and DO are the distances EO and FO after projection on to the molecular axis.

APPENDIX I

ANALYSIS OF X-RAY DIFFRACTION DATA

I.I Estimation of Reciprocal Lattice Parameters

I.I.I The Reciprocal Lattice Spacing, ρ

I.I.2 The Component of the Reciprocal Lattice along the fibre, ζ

I.I.3 The Equatorial Component ξ

I.2 Analysis of errors

I.2.I Errors in ρ

I.2.2 Errors in ζ

I.2.3 Errors in ξ

I.3 Calibration

APPENDIX I

Analysis of X-Ray Diffraction Data

The diffraction patterns from the praying mantis egg case ribbons presented problems for measurement. Owing to disorientation, measurement errors were large, which is serious for such a large unit cell. It was necessary to have some idea of the errors. Random errors are easily estimated, but systematic errors must be estimated from a knowledge of the experimental arrangement.

The formulae used to evaluate reciprocal lattice coordinates are equivalent to those used by other workers. They are widely stated (Fraser and MacRae, 1973a, for example). Errors in these coordinates are expressed in terms of measured parameters and evaluated - a standard technique.

Diffraction patterns were calibrated by covering the specimen with aluminium powder and making measuements on the rings of the powder diffraction pattern.

The methods of this appendix were incorporated in a computer programme.

I.1. Estimate of reciprocal lattice parameters

I.1.1. The reciprocal lattice spacing, ρ

The mathematical symbols used are defined on the diagram of the arrangement of the specimen and film (fig. I.1) From the diagram, OD = $2r=D$, CA = x, AB = y, specimen tilt in the horizontal plane = β, $\angle COA = \mu$, $\angle AOD = \chi - \beta$, $\angle AOB = \chi$, $\angle COB = 2\theta$. It is clear from Fig.I.1 that

$$\chi = \frac{y}{2r} \qquad \text{(I.1)}$$

and

$$\tan \mu = \frac{x}{2r} \sec (\chi - \beta) \qquad \text{(I.2)}$$

Simple trigonometry leads to the relationship

$$\cos 2\theta = \cos \mu \cos \chi \qquad \text{(I.3)}$$

From Bragg's Law,

$$\rho = \frac{1}{d} = \frac{2}{\lambda} (\sin^2\theta)^{\frac{1}{2}}$$

which becomes $\rho = \frac{\sqrt{2}}{\lambda} (1 - \cos \mu \cos \chi)^{\frac{1}{2}}$ (I.4)

I.1.2. The component of the reciprocal lattice along the fibre 3.

Several equivalent formulae can be derived. The most useful for the analysis of errors is

$$3 = \frac{1}{\lambda} (H \cos \beta + A \sin \beta) \qquad \text{(I.5)}$$

where $A = 1 - \cos \mu \cos \chi$ (I.6)

and $$H = \frac{\sin (\frac{Y}{D}) \cos (\frac{Y}{D} - \beta)}{(\frac{x}{D})^2 + \cos^2 (\frac{Y}{D} - \beta)} \qquad \text{(I.7)}$$

A has already been evaluated in finding ρ. This can be found using standard trigonometry.

I.1.3 The equatorial component ξ

By Pythagoras' theorem,

$$\xi = \sqrt{\rho^2 - 3^2} \qquad \text{(I.8)}$$

I.2 Analysis of errors

The standard errors are calculated from the standard errors

of the measured quantitities. The errors in x and y are calculated from the measurements on the position of the reflection. The error in D is estimated using measurements on the calibration curve. The error in β was estimated from a knowledge of the particular experimental conditions. The standard errors in x, y and D could be reduced by taking more measurements. However, the errors may not be random, since properties of the eye affect the measurements. It is wise to regard the estimated errors as a minimum value. In the following the standard error in a parameter f is δf.

I.2.1. Errors in ρ

$$\rho = \rho\ (x,y,D,\beta\ ) \tag{I.9}$$

$$(\delta\rho)^2 = \left(\frac{\partial\rho}{\partial x}\right)^2 (\delta x)^2 + \left(\frac{\partial\rho}{\partial y}\right)^2 (\delta y)^2 + \left(\frac{\partial\rho}{\partial D}\right)^2 (\delta D)^2 + \left(\frac{\partial\rho}{\partial\beta}\right)^2 (\delta\beta)^2 \tag{I.10}$$

Equation (I.10) is the solution except for evaluating the partial differentials. The major steps in this are set out below. From equations I.1, I.2, and I.4, we find,

$$\rho = \frac{\sqrt{2}}{\lambda}\left\{1 - \left[\frac{D^2\cos^2\left(\frac{Y}{D} - \beta\right)}{D^2\cos^2\left(\frac{Y}{D} - \beta\right) + x^2}\right]^{\frac{1}{2}} \cos\frac{Y}{D}\right\}^{\frac{1}{2}}$$

$$= \frac{\sqrt{2}}{\lambda}\left\{1 - \frac{D\cos\left(\frac{Y}{D}\right)\cos\left(\frac{Y}{D} - \beta\right)}{\sqrt{x^2 + D^2\cos^2\left(\frac{Y}{D} - \beta\right)}}\right\}^{\frac{1}{2}}$$

Replacing the numerator and denominator by E and F,

$$\rho = \frac{\sqrt{2}}{\lambda}\left\{1 - \frac{E}{F}\right\}^{\frac{1}{2}}$$

Replacing F by $\sqrt{G}$,

$$\rho = \frac{\sqrt{2}}{\lambda}\left\{1 - \frac{E}{\sqrt{G}}\right\}^{\frac{1}{2}}$$

$$\rho = \frac{\sqrt{2}}{\lambda} A^{\frac{1}{2}}$$

where A, E, F are functions of x, y, β and D.

Let f be x, y, β or D.

$$\frac{\partial \rho}{\partial f} = \frac{\partial \rho}{\partial A} \left\{ \frac{\partial A}{\partial E} \frac{\partial E}{\partial f} + \frac{\partial A}{\partial F} \frac{\partial F}{\partial f} \right\}$$

$$\frac{\partial \rho}{\partial A} = \frac{\sqrt{2}}{\lambda} \frac{1}{2} A^{-\frac{1}{2}}$$

$$\frac{\partial A}{\partial E} = -\frac{1}{F}$$

$$\frac{\partial A}{\partial F} = \frac{E}{F^2}$$

$$\frac{\partial E}{\partial x} = 0$$

$$\frac{\partial E}{\partial y} = -\left\{ \sin\left(\frac{Y}{D}\right) \cos\left(\frac{Y}{D} - \beta\right) + \sin\left(\frac{Y}{D} - \beta\right) \left(\frac{1}{D}\right) \cos\left(\frac{Y}{D}\right) \right\}$$

$$\frac{\partial E}{\partial D} = \cos\left(\frac{Y}{D}\right) \cos\left(\frac{Y}{D} - \beta\right) + \frac{Y}{D} \cos\left(\frac{Y}{D} - \beta\right) \sin\left(\frac{Y}{D}\right) + \frac{Y}{D} \cos\left(\frac{Y}{D}\right) \sin\left(\frac{Y}{D} - \beta\right)$$

$$\frac{\partial E}{\partial \beta} = D \cos\left(\frac{Y}{D}\right) \sin\left(\frac{Y}{D} - \beta\right)$$

$$\frac{\partial F}{\partial f} = \frac{\partial F}{\partial G} \frac{\partial G}{\partial f}$$

$$\frac{\partial F}{\partial G} = \frac{1}{2F}$$

$$\frac{\partial G}{\partial x} = 2x$$

$$\frac{\partial G}{\partial y} = -2D \cos\left(\frac{Y}{D} - \beta\right) \sin\left(\frac{Y}{D} - \beta\right)$$

$$\frac{\partial G}{\partial D} = 2D \cos^2\left(\frac{Y}{D} - \beta\right) + 2y \cos\left(\frac{Y}{D} - \beta\right) \sin\left(\frac{Y}{D} - \beta\right)$$

$$\frac{\partial G}{\partial \beta} = 2D^2 \cos\left(\frac{Y}{D} - \beta\right) \sin\left(\frac{Y}{D} - \beta\right)$$

The above equations relate the original partial derivatives to measurements. A computer programme is simply written by taking the equations in reverse order.

I.2.2. Errors in $\mathfrak{Z}$

$$\mathfrak{Z} = \frac{1}{\lambda} \{ H \cos \beta + A \sin \beta, \} \qquad (I.5)$$

where H and A are defined in section I.1.2. The error is found from

$$(\delta \mathfrak{Z})^2 = \left(\frac{\partial \mathfrak{Z}}{\partial x}\right)^2 (\delta x)^2 + \left(\frac{\partial \mathfrak{Z}}{\partial y}\right)^2 (\delta y)^2 + \left(\frac{\partial \mathfrak{Z}}{\partial D}\right)^2 (\delta D)^2 + \left(\frac{\partial \mathfrak{Z}}{\partial \beta}\right)^2 (\delta \beta)^2$$

For f = x, y or D

$$\frac{\partial \mathfrak{Z}}{\partial f} = \frac{1}{\lambda} \left\{\frac{\partial H}{\partial f} \cos \beta + \frac{\partial A}{\partial f} \sin \beta \right\}$$

$$\frac{\partial \mathfrak{Z}}{\partial \beta} = \frac{1}{\lambda} \{- H \sin \beta + \cos \beta \frac{\partial H}{\partial \beta} + A \cos \beta + \sin \beta \frac{\partial A}{\partial \beta}\}$$

$\frac{\partial A}{\partial f}$ has been determined in section I.2.1.

$$H = \frac{D \sin \left(\frac{Y}{D}\right) \cos \left(\frac{Y}{D} - \beta\right)}{\sqrt{x^2 + D^2 \cos^2 \left(\frac{Y}{D} - \beta\right)}}$$

Replacing the numerator and denominator by P and F

$$H = \frac{P}{F}$$

$$\frac{\partial H}{\partial f} = \frac{\partial H}{\partial P} \frac{\partial P}{\partial f} + \frac{\partial H}{\partial F} \frac{\partial F}{\partial f}$$

$\frac{\partial F}{\partial f}$ has been determined in section I.2.1.

$$\frac{\partial P}{\partial x} = 0$$

$$\frac{\partial P}{\partial y} = \cos\left(\frac{Y}{D}\right) \cos\left(\frac{Y}{D} - \beta\right) - \sin \left(\frac{Y}{D}\right) \sin \left(\frac{Y}{D} - \beta\right)$$

$$\frac{\partial P}{\partial D} = \sin \left(\frac{Y}{D}\right) \cos \left(\frac{Y}{D} - \beta\right) - \frac{Y}{D} \cos \left(\frac{Y}{D} - \beta\right) \cos \frac{Y}{D} + \frac{Y}{D} \sin \frac{Y}{D} \sin\left(\frac{Y}{D} - \beta\right)$$

$$\frac{\partial P}{\partial \beta} = D\sin\left(\frac{Y}{D}\right) \sin\left(\frac{Y}{D} - \beta\right)$$

$$\frac{\partial H}{\partial P} = \frac{1}{F}$$

$$\frac{\partial H}{\partial F} = \frac{-P}{F^2}$$

These equations relate the partial derivatives to the measurements. A programme can be written by taking the equations in reverse order.

I.2.3 Errors in ξ

$$\xi^2 = \rho^2 - \zeta^2 = Q$$

$$\frac{\partial \xi}{\partial f} = \frac{\partial \xi}{\partial Q} \frac{\partial Q}{\partial F}$$

$$\frac{\partial \xi}{\partial Q} = \frac{1}{2\sqrt{Q}} = \frac{1}{2\xi}$$

$$\frac{\partial Q}{\partial f} = \frac{\partial Q}{\partial \rho} \frac{\partial \rho}{\partial f} + \frac{\partial Q}{\partial \zeta} \frac{\partial \zeta}{\partial f}$$

$$\frac{\partial Q}{\partial \rho} = 2\rho$$

$$\frac{\partial Q}{\partial \zeta} = =2\zeta$$

$$\therefore \frac{\partial \xi}{\partial f} = \frac{1}{\xi}\left(\rho \frac{\partial \rho}{\partial f} + \zeta \frac{\partial \zeta}{\partial f}\right)$$

This enables the derivatives $\frac{\partial \xi}{\partial x}$, $\frac{\partial \xi}{\partial y}$, $\frac{\partial \xi}{\partial D}$ and $\frac{\partial \xi}{\partial \beta}$ to be evaluated in terms of derivatives already determined. The standard error is found from

$$(\delta\xi)^2 = \left(\frac{\partial \xi}{\partial x}\right)^2 (\delta x)^2 + \left(\frac{\partial \xi}{\partial y}\right)^2 (\delta y)^2 + \left(\frac{\partial \xi}{\partial D}\right)^2 (\delta D)^2 + \left(\frac{\partial \xi}{\partial \beta}\right)^2 (\delta\beta)^2$$

I.3 Calibration

The specimen was covered with aluminium powder. This produces powder diffraction rings on the film. Measurement of the extreme values of y were taken a number of times, so as to supply an estimate of the error. From the known spacing, 2.33307Å, for the first diffraction ring, the diffraction angle 2θ could be calculated. In this case, $2\theta = \chi$. It was then simple to calculate the specimen film distance and its standard error.

Appendix II

X-Ray Diffraction Data

This appendix is devoted to a record of the measurements made, including those not used in the body of the thesis. Most of the additional data presented here is of rather a poor quality and difficult to interpret. The film numbers recorded with the data refer to the original films. For the purposes of the thesis, this appendix is of little relevance, but it could be useful to future workers.

The errors calculated are standard errors estimated as described in appendix I. It must be remembered that specimens were not tilted for each reflection. The high degree of disorientation present means that information from an appreciable area in reciprocal space can occur at one point on the film. Besides complicating the analysis, this means that the specimen need not be precisely set for a particular reflection. Sufficient information is given in the following tables to enable the surface in reciprocal space corresponding to a perfectly oriented specimen to be found.

The data recorded are not always complete. Sometimes the pattern made it very difficult to obtain complete information about all the reflections. On other occasions, not all measurements were necessary to obtain the required information. It is sometimes noted that a reflection was measured on only one side of the centre of the film. This was occasionally necessary where the background radiation was not uniform. Some specimens were supported vertically so as to use the direction with the best focusing for the equatorial region.

The tables are recorded in the order given in the table below. The following abbreviations are used :-

T - S. tenuidentata

M - S. membramacea

R - ribbon

F - fibres

R.H. - relative humidity

room - room conditions

S.G. - silica gel

C & B - chlorobenzene & bromobenzene

UA - uranyl acetate

PTA - phosphotungstic acid (neutralised)

F - flat face towards the source

E - thin edge towards the source

Film No.	Specimen	Conditions & treatment	Specimen orientation	Specimen tilt (deg)	Specimen-film distance (cm.)	Notes
3	TR	100% R.H.	F.	O	17.5	
84	TR	100% R.H.	E	O	11	
174	TR	100% R.H.	E	O	11	
178)	TR					
177)	TR	room	E	O	11	
176)	TR					
183	TR	room	F	O	11	Handed pattern
187	TR	room	F	O	11	Specimen vertical
188	TR	100% R.H.	F	8.5	11	ditto
190	TR	room	F	O	11	
200	TR	S.G.	F	O	11	
203	TR	S.G.	E	O	11	
92	TR	100% R.H.	E	O	64.7	
193	MR	C & B	F	O	11	
194	MR	C & B	E	O	11	
197	MR	100% R.H.	E	O	11	
199	MR	UA	E	O	11	
201	MR	UA	F	O	17.5	
204	MR	UA	F	O	17.5	
205	MR	PTA	E	O	11	
208	MR	UA	F	O	11	
213	MR	PTA	F	O	11	
214	MF	room	-	O	11	
217	MF	room	-	8.5	11	
219	MF	room	-	31	11	

To simplify the presentation, certain abbreviations are used. They are :-

VVS - very very strong
VS - very strong
S - strong
MS - medium strong
M - medium
MW - medium weak
W - weak
VW - very weak
VVW - very very weak

M - meridional
E - equatorial
NE - near equatorial
NM - near meridional
EC - equatorial component
MC - meridional component
? - description uncertain

Film No. 3. Egg case stored for 9 months in liquid nitrogen. Specimen held under tension at 100% R.H. viewed at right angles to the ribbon face. Cylindrical film. 17.5 cm. specimen to film distance. S. membramacea.

			$A^{o-1} \times 10^5$					
			ρ		ζ		ξ	
Description	Position	Intensity	Value	Error	Value	Error	Value	Error
	-	S	1286	10	822	8	989	10
Measured as M	M or NM	W	1035	7	1035	7	0	-
	M	S	1197	14	1197	14	0	-
	NE	MW	1705	15	583	11	1602	15
Broad Lipid?	E	MW	2256	15	0	-	2256	15
Same Reflection. split?	NE	MW	2312	15	5049	103	2256	15
	M	VS	2187	13	2187	13	0	-
	NM	MW	3221	18	3028	17	1098	8
NE?	NE	VW	2932	17	5158	102	2886	16
			$\rho \times 10^5$		$\zeta \times 10^5$		$\xi \times 10^5$	
	M	W	3256	19	3255	19	0	-
	M	VS	3402	20	3401	20	0	-
Split?		W	3401	43	2017	61	2738	25
Possible splitting)		W	3366	31	1503	21	3012	40
of above reflection)		W	3416	27	2310	25	2517	57

Description	Position	Intensity	ρ Value	ρ Error	ζ Value	ζ Error	ξ Value	ξ Error
Possibly NE Diffuse.	E	W	3377	22	0	-	3377	22
Split?	NE	W	4002	30	3792	14	3923	32
One side only Split? α 2?	M	VW	3511	21	3510	21	0	-
	M	S	4051	25	4049	25	0	-
	NM	S	4013	33	3870	32	1062	27
	NM	S	4323	31	4092	29	1395	33
One side only	M	VW	4432	30	4430	30	0	-
	M	VS	4626	27	4623	27	0	-
One side only α 2?	M	VW	4727	28	4724	29	0	-
	M	MW	4921	29	4917	29	0	-
	NM	MW	4935	38	4778	28	1235	102
	M	MW	5253	30	5248	30	0	-
	NM	MW	5250	33	5072	31	1354	30
	NM	MW	5395	37	5345	37	727	53
	NM	MW	5437	37	5345	37	996	30
	M	VW	5483	32	5478	32	0	-
Possibly split	NE	W	5248	40	1851	60	4911	33
	E	S	5739	33	0	-	5739	33
	NE	W	5938	46	2916	51	5172	38
	NE	W	5973	35	942	22	5899	35
?	E	VW	6044	34	0	-	6044	34
	M	MW	5628	32	5623	32	0	-
	M	M	5857	33	5851	34	0	-
Granular ring. Salt crystals?	-	M	6052	34	-	-	-	-
	M	M	6128	36	6121	37	0	-
	NM	M	6155	39	6045	36	1160	75
Granular ring. Salt crystals?			6415	37				
	M	M	6496	37	6488	37	0	-
	NM	M	6569	39	6391	37	1519	39
	E	S	6367	36	0	-	6367	36

Measurements on three reflections suggested a splitting into reflections at 7 deg. 13 min. ± 24 mins. to each other.

Angles were measured at the centre of the pattern.

Film No. 84. The specimen had been held under slight tension at 100% R.H. for several weeks. During this time it was soaked for about 30 minutes in acetone. This removed most of the lipid. The pattern was obtained at room conditions. The specimen was supported with the thin edge towards the source. 11 cm. specimen to film distance.

S. teniudentata.

			$\rho \times 10^5$		A^{o-1} $\beta \times 10^5$		$\xi \times 10^5$	
Description	Po sition	Intensity	Value	Error	Value	Error	Value	Error
	M	S	1231	6	1231	6	0	-
One side only	NM	VW	1689	18	1613	18	501	119
	M	S	2220	7	2220	7	0	-
Measured as NM	M or NM	VW	2844	9	2833	9	254	16
	NM	VW	3014	16	2712	10	1316	29
Diffuse	E	W	1561	10	0	-	1561	10
Diffuse	E	W	1363	20	0	-	1363	20
Diffuse	E	W	1118	5	0	-	1118	5
Row line streak Hard to measure	E	W	859	4	0	-	859	4
Very arced Probably lipid	E	W	2156	9	0	-	2156	9
Very arced Probably lipid Samples?	E	W	2408	8	0	-	2408	8
	E		2554	9	0	-	2554	9
One side only Artifact?	E	W	2909	19	0	-	2909	19
Hard to measure	E	W	5094	20	0	-	5094	20
One side only	E	W	4856	20	0	-	4856	20

Description	Position	Intensity	ρ Value	ρ Error	3 Value	3 Error	ξ Value	ξ Error
Hard to measure	NE		5120	18	1080	17	5005	17
Hard to measure	NE		4498	25	2195	12	3926	27
Hard to measure	NE		4914	19	2183	12	4403	19
	M	S	3273	10	3272	10	0	-
Sharp	M	S	3446	11	3444	11	0	-
	M	W	3703	11	3702	11	0	-
	M	W	4057	14	4055	14	0	-
	M	S	4309	13	4307	13	0	-
	M	S	4656	14	4653	14	0	-
Measured as NM	M or NM	W	4954	16	4945	16	285	57
	NM	VW	4964	16	4930	16	578	32
Possibly NM	M	VW	5310	16	5306	16	0	-
Same reflection Measured as NM	NM	W	5266	15	5247	16	454	44
	M	VW	5414	16	5409	16	0	-
Possibly NM	M		5516	16	5511	16	0	-
Same reflection Measured as NM	NM		5513	16	5474	16	652	37
Broad	E	S	5661	17	0	-	5661	17
Poorly resolved	E		5514	18	0	-	5514	18
Sampled	NE		5788	21	1273	17	5646	20
Sampled	NE		5725	20	1922	19	5392	19
	M	W	5685	17	5679	17	0	-
MC measured	M & NM		5903	18	5897	18	0	-
Hard to measure Artifact?	M		6174	18	6167	19	0	-

Description	Position	Intensity	ℓ Value	ℓ Error	ℨ Value	ℨ Error	ξ Value	ξ Error
Measured as M	M & or NM		6533	19	6525	20	0	-
Artifact?	NM		6537	19	6525	20	393	96
Layer line	M & 2 NM's		6842	20	6833	21	-	-
Better NM above			6844	20	6833	21	383	112
			6823	33	6370	31	2444	44
			6890	22	6700	23	1608	32
			6842	22	6791	22	835	56
			7101	62	5972	40	3843	95
Layer line streak	NM		7696	24	7683	25	-	-
Layer line streak	NM		7533	23	7520	24	-	-
	M	W	7113	21	7102	22	0	-
Measured as M	M or NM		8387	24	8369	26	0	-
	NM		8409	24	8369	26	828	98
Blurred	M		7561	23	7548	24	0	-
Blurred	M		7735	23	7721	24	0	-
Broad	M		8670	59	8655	60	0	-
	M		9116	27	9093	29	0	-
	M		9330	27	9306	29	671	162
Blurred	M	VW	9635	33	9609	35	7151	168
	M	VVW	9920	31	9891	34	0	-
Measured as M	M & or NM		10120	29	10089	32	0	-
Blurred	M		10577	33	10541	36	0	-
Blurred	M		10811	31	10774	35	0	-
Measured as M	M & or NM	M	11294	34	11251	37	0	-
Measured as M	M & or NM	S	11781	36	11733	40	0	-
Broad	M	W	13002	38	12936	43	13021	2259
Blurred	M	W	14033	41	13951	48	0	-
Blurred	M	W	13847	41	13768	48	0	-
	M	W	15336	44	15228	54	0	-
	M	W	15739	45	15623	55	0	-
	M	W	16151	46	16026	57	0	-

Description	Position	Intensity	ρ Value	ρ Error	3 Value	3 Error	ξ Value	ξ Error
One side only	M	W	16304	47	16175	58	0	-
	M	W	16560	48	16424	59	0	-
	M	VVW	16951	48	16806	61	0	-
	M	VVW	17661	51	17497	65	0	-
Measured as M	M or NM	W	18553	54	18363	70	0	-
	M	MW	18876	54	18675	71	0	-
	M	MW	18923	54	18672	71	0	-
	M		19232	55	19020	73	0	-
	NM		19333	56	19011	73	3515	282
	M	S	19469	56	19249	74	0	-
	NM	S	19550	58	19241	74	3458	305
Probably M & NM	M		19607	56	19382	75	0	-
Probably M & NM	M		20120	59	19877	78	0	-
	M	W	20525	59	20266	80	0	-
	M	VW	20806	59	20538	81	0	-
	M		21123	60	20842	83	0	-
MC measured	NM	VW	21348	61	21058	85	-	-
	M	S	21630	62	21328	87	0	-
	M	W	22387	64	22051	91	0	-
Measured as M	M or NM		22701	66	22351	93	0	-
	M	W	23298	68	22919	97	0	-
	M	W	23455	69	23069	99	0	-
Measured as M	M & NM		23724	67	23325	99	0	-
Ring			24351	70	-	-	-	-
	M	W	24719	72	24268	107	0	-
	M		25953	75	25429	115	0	-
Sampled	E	S	5670	17	0	-	5670	17
	E		6052	22	-	-	6052	22
	NE	S	5779	18	1304	11	5630	18
	NE		6049	60	2507	134	5505	20

Description	Position	Intensity	ζ Value	ζ Error	ζ^3 Value	ζ^3 Error	ζ_{223} Value	ζ_{223} Error
Broad	E		6947	25	0	-	6947	25
	E	W	7182	22	0	-	7182	22
	E		7659	23	0	-	7659	23
	E	W	7874	23	0	-	7874	23
	E	W	8584	26	0	-	8584	26
	NE		6702	43	3753	57	5553	33
	NE		7287	-	4500	-	5731	-
			8221	28	6154	25	5450	67
			8829	34	6784	34	5647	31
			10601	38	9009	37	5588	45
		W	11588	49	9880	47	6054	63
		W	12510	67	11107	72	5758	64
		W	13501	55	12184	51	5816	213
		W	16509	71	15419	68	5899	165
		W	18773	91	17465	78	6885	236
		MS	19876	119	18415	87	7478	319
Poorly Resolved			19497	129	18884	115	4854	388
			19563	131	19120	87	4141	620
			21007	310	19656	309	7411	269
			21832	428	20417	415	7732	420
			22836	288	21914	277	6422	423
			23637	319	22646	302	6773	496
	E		11085	32	0	-	11085	32
	E		11739	33	0	-	11739	33
	E		12670	37	0	-	12670	37
			17707	496	13489	538	11470	383
			19746	376	15903	360	11705	393

Film No. 174. Specimen at 100% R.H. with the thin edge towards the beam. 11 cm. specimen film distance.

S. tenuidentata.

			$A^o - 1$					
			$\rho \times 10^5$		$\zeta \times 10^5$		$\xi \times 10^5$	
Description	Position	Intensity	Value	Error	Value	Error	Value	Error
	M	S	1268	8	1269	8	0	-
	M	S	2221	8	2221	8	0	-
	M	W	3247	22	3246	23	0	-
	M	M	3459	6	3458	6	0	-
	M	M	4045	7	4043	8	0	-
	M	M	4338	8	4336	8	0	-
	M	S	4675	8	4672	9	0	-
	E	S	5461	12	0	-	5461	12
	E	VS	10715	29	0	-	10715	29
	E	S	16143	29	0	-	16143	29
	E	MW	21548	36	0	-	21548	36
	E	M	26837	46	0	-	26837	46

Films Nos. 176, 177, 178. This is a pack of three films in decreasing order of intensity. The specimen is the same as for film 174 after drying under room conditions at constant length. 11 cm. specimen to film distance.

Film No. 178. Axial sampling on the 9Å row line at $\zeta = 0.01376 \pm 0.00045$.

Film No. 177.

			$A^o - 1$					
			$\rho \times 10^5$		$\zeta \times 10^5$		$\xi \times 10^5$	
Description	Position	Intensity	Value	Error	Value	Error	Value	Error
	M	S	19359	35	19143	61	0	-
	M	W	19982	37	19744	64	0	-
	M	W	20409	47	20156	72	0	-
	M	M	20988	38	20712	70	0	-

Description	Position	Intensity	ƒ Value	Error	3 Value	Error	ξ Value	Error
	M	M	21466	41	21170	74	0	-
	M	M	22246	43	21917	78	0	-
	M	M	22621	43	22275	80	0	-
	M	MW	23703	52	23305	90	0	-
	M	MW	24826	45	24369	93	0	-
	M	MW	25833	55	25316	103	0	-
ξ approx-imate			20216	43	19093	68	6646	-
"			21001	43	19870	72	6801	-
"			21883	70	20742	93	6974	-
"			22738	46	21583	82	7157	-
	M	S	1239	8	1239	8	0	-
	M	S	2221	8	2221	8	0	-
	M	M	3217	9	3217	9	0	-
	M	M	3467	10	3465	10	0	-
	M	M	3694	7	3692	7	0	-
	M	VW	4053	10	4051	11	0	-
	M	S	4287	23	4285	23	0	-
	M	VS	4624	11	4621	11	0	-
∠2?	M	VW	4925	9	4921	9	0	-
	E	S	5650	12	0	-	5650	12
	E	VS	11106	24	0	-	11106	24
	E	S	16647	29	0	-	16647	29
	E	W	22223	79	0	-	22223	79
	E	MW	27618	44	0	-	27618	44
Broad	E	W	1927	8	0	-	1927	8
	E	VW	2359	4	0	-	2359	4
	E	VW	2981	9	0	-	2981	9
Row lines NE	EC	S	5650	12	-	-	5750	12
"	EC	S	6086	13	-	-	6086	13
"	EC	M	6926	25	-	-	6926	25
"	EC	M	7685	32	-	-	7685	32
"	EC	S	11148	35	-	-	11149	35
"	EC	M	11799	21	-	-	11799	21
ξ approxi-mate			-	-	1269	8	6700	-

Film 176. Some of these reflections were also measured on film 177.

Description	Position	Intensity	$\rho \times 10^5$ Value	Error	$A^o - 1$ $\beta \times 10^5$ Value	Error	$\xi \times 10^5$ Value	Error
	M	S	1239	8	1239	8	0	-
	M	S	2199	4	2199	4	0	-
	M	M	3217	23	3217	23	0	-
	M	S	3430	6	3429	6	0	-
	M	M	3658	10	3656	10	0	-
	M	W	4053	10	4051	11	0	-
	M	S	4317	11	4314	11	0	-
	M	VS	4632	17	4629	18	0	-
	M	W	4917	12	4914	12	0	-
Broad	M	W	5349	18	5345	19	0	-
	M	W	5606	12	5600	13	0	-
	M	M	5862	18	5856	19	0	-
	M	M	6169	18	6162	19	0	-
Broad	M	MS	6459	20	6450	21	0	-
	M	VW	6821	14	6812	16	0	-
	M	MW	7531	14	7518	16	0	-
	M	W	8036	16	8020	18	0	-
	M	W	8336	21	8318	23	0	-
	M	M	8591	17	8573	20	0	-
	M	VW	8848	22	8827	24	0	-
	M	M	9067	16	9045	20	0	-
	M	M	9308	18	9284	22	0	-
Broad	M	W	9703	19	9676	23	0	-
	M	M	9820	19	9792	23	0	-
	M	M	10068	20	10038	24	0	-
Broad) 2 reflections?)	M	W	10646	19	10610	24	0	-
	M	MS	11267	22	11224	27	0	-
	M	M	11770	21	11722	28	0	-
	M	MW	14155	26	14071	37	0	-
	M	W	13579	28	13505	37	0	-

Description	Position	Intensity	ν Value	ν Error	ν Value	ν Error	ξ Value	ξ Error
	M	MW	13988	50	13906	56	0	-
	M	M	15233	28	15128	42	0	-
	M	M	15626	29	15512	43	0	-
	M	M	16077	30	15953	45	0	-
	M	MW	16477	42	16344	55	0	-
	M	W	17613	44	17451	60	0	-
	M	W	18136	68	17958	79	0	-
	M	MW	18499	38	18310	59	0	-
	M	M	18833	36	18634	59	0	-
Diffuse	M	S	19398	39	19180	63	0	-
	M	M	20036	40	19796	67	0	-
	M	M	20427	48	20172	73	0	-
	M	MS	21035	39	20757	70	0	-
Diffuse	M	MS	21541	43	21242	75	0	-
	M	MS	22307	51	21975	83	0	-
Diffuse	M	MS	22604	43	22259	80	0	-
Diffuse	M	MS	23634	44	23239	86	0	-
Diffuse	M	MS	24743	63	24289	101	0	-
Diffuse	M	MS	25836	50	25319	101	0	-
ξ approxi-mate		S	-	-	1380	9	5700	-
" sharp			-	-	2720	48	5700	-
" diffuse		M	-	-	3805	16	5700	-
" diffuse		M	-	-	4815	19	5700	-
" sharp		W	-	-	6117	26	5700	-
" diffuse		M	-	-	7025	22	5700	-
"		M	-	-	8308	41	5700	-
" diffuse		MS	-	-	9104	55	5700	-
"		W	-	-	9956	33	5700	-
	M	S	20172	39	19031	66	0	-
	M	S	20772	81	19630	98	0	-
	M	S	21681	50	20531	79	0	-
	M	S	22985	46	21812	83	0	-
		W	13454	31	7249	30	11334	40
		W	14121	38	8367	44	11375	63
		W	14770	40	9367	46	11420	71
		W	15954	57	11047	70	11511	129

Description	Position	Intensity	ℓ Value	Error	3 Value	Error	ξ Value	Error
Broad		MS	16282	66	11487	83	11539	160
		M	18013	55	13692	67	11705	132
		M	18722	50	14549	63	11783	116
		M	19674	52	15669	68	11898	127
Sharp		MS	20586	50	16712	68	12020	120
		MS	21490	56	17724	79	12152	151
		MS	22635	126	18977	147	12338	423
		MS	23362	54	19759	85	12466	151
		MS	24456	57	20915	93	12676	174
		W	25432	63	21929	103	12881	207
ξ approximate Broad		3rd, 4th & 5th row lines of 17A°	-	-	7301	109	-	-
"		2nd, 3rd, 4th and 5th row lines	-	-	10191	85	-	-
Diffuse	E	W	1912	22	0	-	1912	22
	E	VW	2381	22	0	-	2381	22
	E	W	3032	16	0	-	3032	16

Film No. 183. Specimen held with the flat face towards the beam under room conditions. S. tenuidentata. This is the pattern without a meridional line of symmetry 11 cm. specimen to film distance.

Description	Position	Intensity	$\rho \times 10^5$ Value	Error	A^{o-1} $\zeta \times 10^5$ Value	Error	$\xi \times 10^5$ Value	Error
Reflections along a line at 18° to fibre axis		VS	1246	2	1184	2	387	14
		S	2220	4	2111	4	687	25
		MW	4657	8	4446	9	1385	55
"		MS	3216	6	3071	6	954	38
"		MS	4303	8	4107	8	1283	50
"		M	5335	10	5068	10	1668	59
"		W	5913	12	5614	13	1855	75
"		W	6221	13	5906	13	1953	78
"		W	6528	13	6197	14	2052	81
"		W	8333	16	7902	18	2646	99
"		W	8643	17	8192	19	2754	102
	NE	MS	1761	50	650	5	1637	54
	E	MS	2330	4	0	-	2330	4
	E	MS	2983	14	0	-	2983	14
	E	MW	3597	8	0	-	3597	8
3 approximate	NE	MW	5381	42	1461	-	5179	43
	E	M	5928	12	0	-	5928	12
	E	S	6579	14	0	-	6579	14
	E	W	6977	19	0	-	6977	19
3 approximate	NE	W	7754	14	1456	-	7616	15
	E	MS	8276	21	0	-	8276	21
Perhaps NE	E	W	8549	15	0	-	8549	15
	E	MS	9460	18	0	-	9460	18
	E	M	9903	19	0	-	9903	19
3 approximate	NE	MW	10384	21	2172	-	10154	21
	E	M	10869	26	0	-	10869	26

Description	Position	Intensity	ƒ Value	Error	3 Value	Error	ξ 230 Value	Error
3 approxi-mate	NE	MS	13191	25	2873	-	12874	25
	E	M	12453	27	0	-	12453	27
	E	M	13518	28	0	-	13518	28
	E	W	14227	38	0	-	14227	38
	E	W	14947	27	0	-	14947	27
	M?	MS	4673	10	4670	11	0	-
	M	MW	6167	32	6160	32	0	-
	M	W	17564	35	17403	54	0	-
	M	W	17840	44	17671	60	0	-
	M	W	18130	33	17953	55	0	-
	M	MW	18493	37	18305	58	0	-
	M	MW	18841	37	18642	60	0	-
	M	VS	19378	35	19161	61	0	-
	M	VW	19813	36	19581	63	0	-
	M	W	20059	39	19818	66	0	-
	M	M	20392	37	20139	66	0	-
	M	W	20739	38	20473	68	0	-
	M	MS	20956	41	20682	71	0	-
	M	M	21506	42	21209	74	0	-
	M	MW	21896	49	21583	80	0	-
	M	MS	22229	43	21900	79	0	-
	M	MW	22474	41	22135	78	0	-
	M	VW	22719	43	22369	81	0	-
	M	M	23527	45	23138	86	0	-
	M	M	24060	43	23644	88	0	-
	M	M	25744	48	25233	100	0	-
	M	MW	26763	48	26188	106	0	-
Maxima of)	E		4682	8	0	-	4682	8
of intensity)	E		6427	12	0	-	6427	12
modula-)	E		9310	17	0	-	9310	17
tions)	E		12995	23	0	-	12995	23
"	M		21000	38	20723	70	0	-
"	M		22272	40	21942	77	0	-
"	M		23657	43	23261	85	0	-
"	M		24752	45	24298	92	0	-

Description	Position	Intensity	ρ Value	ρ Error	ʒ Value	ʒ Error	ξ Value	ξ Error
"	M		25787	46	25273	99	0	-
"	M		26878	48	26296	107	0	-
Measured as M	M or NM		30224	54	29394	132	0	-
"	M or NM		31648	56	30693	144	0	-
"	M or NM		34257	61	33043	167	0	-
"	M or NM		35387	63	34047	177	0	-

Film No. 187. Fibre axis vertical. Specimen under room conditions with the flat face towards the beam. 11 cm. specimen to film distance. S. tenuidentata.

A^{o-1}

Description	Position	Intensity	$\rho \times 10^5$ Value	$\rho \times 10^5$ Error	$\zeta \times 10^5$ Value	$\zeta \times 10^5$ Error	$\xi \times 10^5$ Value	$\xi \times 10^5$ Error
	NE		1249	18	762	1	989	22
	NE		1817	7	763	2	1649	8
Equatorial)	M		-	-	-	-	2264	22
components)	MS		-	-	-	-	2997	9
of E and NE)	W		-	-	-	-	3604	7
reflections)	MS		-	-	-	-	5403	18
"	S		-	-	-	-	5944	12
"	VS		-	-	-	-	6586	13
"	MW		-	-	-	-	7744	18
"	M		-	-	-	-	8289	18.
"	MS		-	-	-	-	9422	21
" α 2?	MW		-	-	-	-	9835	31
"	MW		-	-	-	-	10306	28
"	MS		-	-	-	-	10870	29
"	MW		-	-	-	-	12485	34
"	MS		-	-	-	-	12988	33
"	M		-	-	-	-	13491	37
"	W		-	-	-	-	14157	38
"	W		-	-	-	-	14850	40

Film No. 188. Fibre axis vertical. Specimen at 100% R.H. with the flat face towards the source. 11 cm. specimen to film distance. S. tenuidentata.

Description Position and Intensity	ξ $A^{o-1} \times 10^5$ Value	Error
Equatorial components of	5681	11
strong equatorial and	6381	13
near equatorial	8609	18
reflections	9190	20

Film No. 190. Specimen under room conditions with the specimen tilted about an axis at right angles to the fibre axis by 8.5^o from the position with the flat face towards the source. 11 cm. specimen to film distance. S. tenuidentata.

			$\rho \times 10^5$		A^{o-1} $\zeta \times 10^5$		$\xi \times 10^5$	
Description	Position	Intensity	Value	Error	Value	Error	Value	Error
	M	VW	17680	49	17679	46	0	-
	M	W	18188	56	18188	51	0	-
	M	W	18566	48	18566	44	0	-
	M	W	18957	51	18957	46	0	-
	M	VS	19494	49	19494	45	0	-
	M	M	20160	60	20160	55	0	-
	M	M	20479	58	20478	53	0	-
	M	M	20913	59	20911	53	0	-
	M	MS	21159	53	21156	48	0	-
Broad	M	M	21607	52	21603	47	0	-
Sharp	M	M	22330	53	22323	48	0	-
Broad	M	M	22763	63	22754	57	0	-
Broad	M	M	23715	55	23700	51	0	-
	M	M	24262	62	24243	58	0	-
	M	M	24881	71	24856	65	0	-
Salt rings		W	26045	58	-	-	-	-
"		VW	30025	63	-	-	-	-
"		VS	33153	68	-	-	-	-
"		M	40322	78	-	-	-	-
"		M	44121	83	-	-	-	-

Film No. 200. Specimen over silica gel with the flat face towards the source. 11 cm. specimen to film distance. S. tenuidentata. The pattern gives an equatorial line and a meridional line close to which most intensity falls. They are at about 87 degrees to each other.

Description	Position	Intensity	$\rho \times 10^5$ Value	Error	A^{o-1} $\zeta \times 10^5$ Value	Error	$\xi \times 10^5$ Value	Error
		W	1375	18	839	23	1090	14
	M	S	1257	6	1256	6	0	-
	M	S	2221	15	2221	15	0	-
Wide arc	M	S	3259	10	3258	10	0	-
	M	M	3394	10	3393	10	0	-
MC measured	NM	MW	-	-	4235	12	-	-
	M	S	4654	16	4651	16	0	-
Broad	M	W	5340	24	5335	24	0	-
	M	W	5882	17	5876	18	0	-
	M	W	6202	20	6194	21	0	-
EC measured	NE	W	-	-	-	-	1154	6
	NE	W	-	-	-	-	1683	7
	E	W	2456	7	0	-	2456	7
	E	M	3062	10	0	-	3062	10
Very broad)	E		3543	43	0	-	3543	43
2 reflections?)								
	E	MS	6238	67	0	-	6238	67
	E	S	6779	19	0	-	6779	19
	E	W	7117	22	0	-	7117	22
	E	W	7885	24	0	-	7885	24
	E	M	8450	26	0	-	8450	26
Sharp	E	W	6117	50	0	-	6117	50
Sharp	E	W	6859	28	0	-	6859	28
Broad	M	M	7436	24	0	-	7436	24

Film 203. Specimen held over silica gel with the thin edge towards the beam. 11 cm. specimen to film distance.
S. tenuidentata.

Description	Position	Intensity	$\rho \times 10^5$ Value	Error	A^{o-1} 3×10^5 Value	Error	$\xi \times 10^5$ Value	Error
	M	S	1283	9	1283	9	0	-
	M	S	2243	10	2243	10	0	-
	M	VW	2507	11	2506	11	0	-
	M	VW	2910	15	2909	15	0	-
	M	S	3269	21	3268	21	0	-
	M	MS	3415	21	3414	21	0	-
	M	M	3745	18	3743	19	0	-
	M	MS	4338	20	4336	20	0	-
	M	S	4677	23	4674	24	0	-
	M	VW	4968	22	4965	23	0	-
Broad 2)	M	M	5357	25	5352	25	0	-
reflections?)								
	M	W	5642	25	5637	26	0	-
	M	M	5884	28	5878	28	0	-
	M	MW	6191	29	6184	29	0	-
Broad	M	MW	5950	27	5944	27	0	-
	M	W	6594	33	6586	34	0	-
	M	W	7567	35	7555	36	0	-
	M	W	8021	42	8006	43	0	-
	M	W	8687	42	8667	43	0	-
	M	VW	8599	42	8580	43	0	-
	M	W	10032	48	10002	49	0	-
	M	VW	10748	57	10711	58	0	-
	M	W	11274	59	11231	61	0	-
	M	W	11726	55	11680	57	0	-
Broad	M	S	19432	87	19213	99	0	-
	M	W	20098	103	19856	113	0	-
	M	W	20417	92	20163	104	0	-
	M	MW	20938	96	20664	110	0	-
	M	M	21610	97	21309	112	0	-

Description	Position	Intensity	ƒ Value	ƒ Error	ʒ Value	ʒ Error	ξ Value	ξ Error
Broad	M	M	22700	102	22351	119	0	-
	M	W	24855	125	24395	144	0	-
	M	W	26020	136	25492	157	0	-
ξ approximate		S	-	-	1387	17	5800	-
"		MW	-	-	2613	48	5800	-
"		MW	-	-	3755	94	5800	-
"		W	-	-	4843	41	5800	-
"		W	-	-	5973	34	5800	-
"		MW	-	-	6987	34	5800	-
"		W	-	-	8544	44	5800	-
"		W	-	-	9210	110	5800	-
" Broad		S	-	-	19129	135	5800	-
" "		S	-	-	19852	107	5800	-
" "		S	-	-	20157	109	5800	-
Row lines measured)		VS	-	-	-	-	5752	27
from E and NE)		VS	-	-	-	-	6202	29
reflections)		W	-	-	-	-	6753	59
"		M	-	-	-	-	7114	39
"		MW	-	-	-	-	7844	45
" Broad		VW	-	-	-	-	8583	48
" Broad, Perhaps) 2 row lines)		VW	-	-	-	-	9832	66
"		VVW	-	-	-	-	10687	48
"		VS	-	-	-	-	11368	51
" Blur		W	-	-	-	-	12018	57
" Blur		W	-	-	-	-	12932	67
"		M	-	-	-	-	17041	73
"		W	-	-	-	-	22638	95
Maximum in the) intensity)			24145	119	7641	149	22904	121
Modulation on the) 3rd and 4th row) lines of 17A°)								

Film No. 92. Specimen from S. tenuidentata, at 100% R.H. Thin edge of the ribbon towards the source. Specimen to film distance 64.7 cm.

Position	Intensity	$\xi \times 10^5$ A^{o-1}
E	VVS	1982
E	M	4013
E	VVW	6496

Film No. 193. Specimen after soaking in a mixture of chlorobenzene and bromobenzene. The pattern was obtained with the flat face towards the beam. 11 cm. specimen to film distance. S. membramacea.

			$\rho \times 10^5$ A^{o-1}		3×10^5 A^{o-1}		$\xi \times 10^5$ A^{o-1}	
Description	Position	Intensity	Value	Error	Value	Error	Value	Error
M and NM measured)		W	1041	29	1041	29	0	-
as M. NM's could)		W	1246	15	1246	15	0	-
not be clearly)		S	2236	8	2236	8	0	-
identified owing)		M	2477	30	2477	30	0	-
to disorientation)		W	2858	16	2858	16	0	-
"		S	3225	6	3224	6	0	-
"		W	3745	10	3743	10	0	-
"		S	4295	8	4292	8	0	-
"	α 2?	W	4448	11	4446	11	0	-
"		S	4690	17	4687	17	0	-
"		W	5386	24	5381	24	0	-
"		S	5906	11	5900	12	0	-
"		W	6177	13	6170	14	0	-
"		M	6462	12	6454	13	0	-
"		S	9118	27	9096	29	0	-
		M	2256	30	1807	35	1350	15
		M	2949	25	1807	35	2331	15
		W	3638	20	1806	35	3158	10
		W	4407	37	1804	35	4021	37

Description	Position	Intensity	ρ Value	ρ Error	ζ Value	ζ Error	ξ^{237} Value	ξ^{237} Error
ζ measurement doubtful		M	5505	17	1802	35	5202	12
	E	MS	5984	24	0	-	5984	24
	E	S	6586	19	0	-	6586	19
Poor ζ Measurement)	E & or NE	VS	8290	59	1794	36	8093	60
	E	M	9739	33	0	-	9739	33
	E	M	10893	24	0	-	10893	24
Blur	E	W	12877	28	0	-	12877	28
Blur	E	W	15005	76	0	-	15005	76

Film 194. Specimen of S. membramacea after soaking in a mixture of chlorobenzene and bromobenzene. It was supported with the thin edge of the ribbon towards the source. 11 cm. specimen to film distance.

Description	Position	Intensity	$\rho \times 10^5$ A^{o-1} Value	Error	$\zeta \times 10^5$ A^{o-1} Value	Error	$\xi \times 10^5$ A^{o-1} Value	Error
	M	M	1165	52	1165	52	0	-
	M	S	2272	15	2272	15	0	-
	M	MW	2463	15	2462	15	0	-
	M	W	2873	5	2872	5	0	-
	M	MS	3220	20	3219	20	0	-
	M	W	4580	11	4577	11	0	-
	M	S	4287	11	4285	11	0	-
	M	W	4485	17	4482	17	0	-
	M	S	4669	11	4665	12	0	-
	M	W	5364	10	5359	10	0	-
	M	MS	5913	13	5907	14	0	-
	M	W	6213	18	6206	19	0	-
	M	M	6455	14	6448	15	0	-
	M	S	9118	27	9096	29	0	-
	M	S	19374	35	19157	61	0	-
	M	W	20446	43	20190	70	0	-
	M	MS	21422	41	21129	73	0	-
	M	MS	22535	43	22193	80	0	-

Description	Position	Intensity	ρ Value	ρ Error	ζ Value	ζ Error	ξ Value	ξ Error
ξ estimated		S	-	-	1582	20	5700	-
" diffuse		M	-	-	18207	89	5700	-
" sharp		M	-	-	18845	78	5700	-
"		M	-	-	19695	89	5700	-
"		M	-	-	20480	76	5700	-
"		M	-	-	21404	114	5700	-
Equatorial components of E and NE reflections		S	-	-	-	-	5715	18
"		MW	-	-	-	-	6180	18
"		M	-	-	-	-	6984	14
"			-	-	-	-	7550	35
"		VS	-	-	-	-	11212	21
"		W	-	-	-	-	11853	60
" Blur		W	-	-	-	-	13481	24
"		S	-	-	-	-	16719	32
"		W	-	-	-	-	22444	39

Film No. 197. Specimen of S. membramacea supported with the thin edge towards the source at 100% R.H. Specimen film distance 11 cm.

Description	Position	Intensity	$\rho \times 10^5$ Value	$\rho \times 10^5$ Error	$\zeta \times 10^5$ (A^{o-1}) Value	$\zeta \times 10^5$ Error	$\xi \times 10^5$ Value	$\xi \times 10^5$ Error
	M	W	997	29	997	29	0	-
	M	S	2199	30	2199	30	0	-
	M	M	2470	9	2470	9	0	-
	M	W	2770	5	2770	5	0	-
	M	M	3239	30	3238	30	0	-
	M	M	4280	17	4278	17	0	-
	M	MW	4683	11	4680	12	0	-
	M	S	5650	13	5644	13	0	-
	M	W	6076	22	6069	22	0	-
	M	W	7788	35	7774	35	0	-
	M	W	9047	35	9025	37	0	-
	M	W	10581	49	10546	51	0	-

Film No. 201. Specimen from S. membramacea after soaking for 3 months in 0.5% uranyl acetate solution with the flat face of the ribbon towards the source. 17.5 cm. specimen to film distance.

Reflections on lines at an angle of 21 deg. 26 ± 5 min. from the equator. A direct measurement of ζ gives = 0.00680 ± 0.00003.

Film No. 204. Specimen from S. membramacea after soaking for 3 months in 0.5% uranyl acetate solution. Supported with the flat face of the ribbon towards the source. 17.5 cm. specimen to film distance.

			$\zeta \times 10^5$		A^{o-1} $\zeta \times 10^5$		$\xi \times 10^5$	
Description	Position	Intensity	Value	Error	Value	Error	Value	Error
Hard to measure			1680	49	1330	14	1025	79
Same row line) 3 approximate)			1090	74	370	-	1025	79
Intensity enhanced) by the treatment)								
	E	M	3363	11	0	-	3363	11
"	E	VS	2985	23	0	-	2985	23
"	E	S	2713	12	0	-	2713	12

Film 205. Specimen from S. membramacea after soaking for 3 months in 2% phosphotungstic acid (PTA) neutralised with sodium hydroxide. The specimen was supported with the thin edge of the ribbon towards the source. 11 cm. specimen to film distance.

			$\zeta \times 10^5$		$\zeta \times 10^5$		$\xi \times 10^5$	
Description	Position	Intensity	Value	Error	Value	Error	Value	Error
	M	M	2770	15	2770	16	0	-
	M	S	3181	16	3180	16	0	-
	M	S	4273	23	4270	23	0	-
	M	S	4646	8	4643	9	0	-
	E	S	5664	13	0	-	5664	13
	M	MW	1906	3	1905	3	0	-

Description	Position	Intensity	ρ Value	ρ Error	ζ Value	ζ Error	ξ Value	ξ Error
Row lines measured)		S	-	-	-	-	5374	38
from E and NE)		M	-	-	-	-	6564	14
reflections)								
		M	-	-	-	-	7288	15
		VS	-	-	-	-	10685	66
"		MW	-	-	-	-	11154	37
"		W	-	-	-	-	12143	38
"		W	-	-	-	-	12970	67
"		W	-	-	-	-	14293	67
"		S	-	-	-	-	15991	48
"	Blur	W	-	-	-	-	17216	40
"		W	-	-	-	-	21411	46
"		M	-	-	-	-	26656	50

Film 199. Specimen of S. membramacea after soaking for 3 months in 0.5% uranyl acetate solution. The ribbon was supported with the thin edge towards the source. 11 cm. specimen to film distance.

Description	Position	Intensity	$\rho \times 10^5$ Value	$\rho \times 10^5$ Error	$\zeta \times 10^5$ Value	$\zeta \times 10^5$ Error	$\xi \times 10^5$ Value	$\xi \times 10^5$ Error
					A^{o-1}			
Intensity)	M	VS	2455	9	2455	9	0	-
enhanced by)								
the treatment)								
	M	W	2206	8	2206	8	0	-
	M	W	2763	37	2763	37	0	-
	M	M	3181	30	3180	30	0	-
	M	MW	3430	6	3429	6	0	-
	M	VW	3760	52	3759	52	0	-
	M	M	4089	16	4087	17	0	-
	M	MS	4258	11	4256	11	0	-
	M	S	4610	11	4607	11	0	-
	M	M	6455	38	6448	39	0	-
Intensity)	E	S	5272	38	0	-	5272	38
enhanced by)								
the treatment)								
ζ and ξ								
approximate	E	W	10580	42	0	-	10580	42
			5331	37	7890	41	5272	38

Description	Position	Intensity	f Value	Error	3 Value	Error	ξ^{241} Value	Error
	E	VS	11070	29	0	-	11070	29
	E	W	6078	45	0	-	6078	45
	E	M	6890	12	0	-	6890	12
	E	MW	7618	45	0	-	7619	45

Film No. 208. Specimen from S. membramacea after soaking for 3 months in 0.5% uranyl acetate solution with the flat face of the ribbon towards the source. 11 cm. specimen film distance.

Description	Position	Intensity	$f \times 10^5$ Value	Error	A^{o-1} 3×10^5 Value	Error	$\xi \times 10^5$ Value	Error
	M	W	1026	15	1026	15	0	-
	M	MS	1269	8	1269	8	0	-
	M	W	1854	22	1854	22	0	-
	M	MS	2133	8	2133	8	0	-
	M	VS	2448	4	2448	4	0	-
	M	S	3159	9	3158	9	0	-
	M	MS	4009	23	4007	23	0	-
	M	MS	4265	17	4263	17	0	-
	M	S	4573	8	4570	9	0	-
		MS	1593	18	1378	3	799	37
		S	1345	10	645	15	1180	8
		MS	1949	9	645	15	1839	8
		S	2446	6	645	15	2359	4
	E	VS	2908	9	0	-	2908	9
		MS	3164	22	927	10	3025	23
	E	M	3500	16	3500	16	0	-
		MW	4800	19	2091	39	4321	39
	M	W	4120	10	0	-	4120	10

Film No. 213. Specimen from S. membramacea after soaking for 3 months in 2% phosphotungstic acid (PTA) neutralised with sodium hydroxide. The specimen is supported with the flat face of the ribbon towards the source. Specimen to film distance 11 cm.

			$\rho \times 10^5$		A^{o-1} $\zeta \times 10^5$		$\xi \times 10^5$	
Description	Position	Intensity	Value	Error	Value	Error	Value	Error
	M	MW	1057	19	1057	19	0	-
	M	MW	1243	19	1243	19	0	-
	M	MW	1929	10	1929	10	0	-
	M	M	2216	3	2216	3	0	-
	M	MW	2462	5	2461	5	0	-
	M	S	3176	6	3175	6	0	-
	M	MW	3825	6	3823	7	0	-
	M	S	4246	5	4244	5	0	-
	M	S	4617	5	4614	6	0	-
	M	MW	5318	33	5312	33	0	-
	M	M	5822	11	5816	12	0	-
Row lines)								
measured from)		MW	-	-	-	-	2410	10
E and NE reflections)								
"		M	-	-	-	-	3048	10
"		W	-	-	-	-	3612	37
"		W	-	-	-	-	4895	6
"		MW	-	-	-	-	5425	15
"		M	-	-	-	-	5976	15
"		MS	-	-	-	-	6572	14
"		W	-	-	-	-	7721	61
"		MW	-	-	-	-	8286	20

Film No. 214. Fibres drawn from the gland of S. membramacea. 11 cm. specimen to film distance. The following table also refers to this film.

Description	Position	Intensity	$\rho \times 10^5$ Value	Error	A^{o-1} 3×10^5 Value	Error	$\xi \times 10^5$ Value	Error
Layer line streaks measured on meridian		M	5862	30	5856	30	0	-
"		MW	5196	25	5191	25	0	-
"		MW	4712	23	4709	23	0	-
"		MW	4170	20	4168	20	0	-
"		MW	3796	17	3795	17	0	-
"		VW	3349	17	3348	17	0	-
"		VVW	2998	53	2997	53	0	-
"		W	2382	13	2382	13	0	-
"		MW	1913	11	1913	11	0	-
"	Blur	MW	6111	31	6104	32	0	-
"		VW	7026	39	7016	39	0	-
"		VW	7699	36	7686	36	0	-
"		W	9044	47	9022	48	0	-
"	Blur	W	9278	48	9254	49	0	-
"	Broad	W	10213	66	10182	67	0	-
"		VW	11046	60	11006	62	0	-
"		VW	11645	92	11598	92	0	-
	E or NE	S	6416	35	0	-	6416	35
	E & NE	S	9304	60	0	-	9304	60
Broad 2 reflections?		S	11986	58	0	-	11986	58
Layer line; also samples other row lines		S	9429	42	1471	26	9313	42
1 or 2 layer lines sampling row lines		VW	10419	51	4605	49	9347	46
Layer line sampling row lines		W	9902	46	3320	32	9329	44
"		VW	9652	44	2508	31	9320	43

Film No. 214 (as above). More accurate measurements and extra measurements in the low angle region. The measurements were made using a Nikon shadowgraph. The reflections are all layer line streaks from meridional and near meridional reflections.

Description, position and intensity	A^{o-1} $\mathfrak{Z} \times 10^5$ Value	Error
Fine	253	17
"	428	17
"	774	17
"	977	17
More intense and broader	1275	24
"	613	4
	1877	9
	2418	21
	2790	21
	3290	22
	3840	26
	4188	25
	4713	22
	5235	25
	5853	27

Film No. 217. Fibres drawn from the gland of S. membramacea. 11 cm. specimen to film distance. The fibre axis was tilted 8.5^o away from being at right angles to the X-ray beam.

Description	Position	Intensity	$\mathfrak{f} \times 10^5$ Value	Error	$\mathfrak{Z} \times 10^5$ Value	Error	$\mathfrak{E} \times 10^5$ Value	Error
	M	W	18598	82	18598	75	0	-
	M	S	19317	41	19317	38	0	-
	M	W	20216	53	20216	48	0	-
	M	W	20930	53	20928	48	0	-
	M	VW	21899	45	21894	41	0	-
Very broad			22623	119	20401	45	9779	307
	E		12340	38	0	-	12330	38
	E		9498	30	0	-	9498	30
	E		6365	20	0	-	6365	20

Film No. 219. Fibres drawn from the gland of S. membranacea. 11 cm. specimen film distance. Fibre axis tilted as before but by 31°.

Description	Position	Intensity	$\rho \times 10^5$ Value	Error	$\zeta \times 10^5$ Value	Error	$\xi \times 10^5$ Value	Error
	M		67132	275	67132	275	0	-
			21480	98	19989	151	7864	364
The remaining reflections	)		31295	142	29920	177		
are all weak. They are	)		32706	173	31374	184		
all measured on the	)		40130	196	39102	177		
meridian, but they	)		46849	329	46159	173		
may not be	)		51791	223	51349	128		
meridional	)		60790	324	60702	60		
"			72850	290	72741	89		
"			77393	301	77024	161		
"			86481	319	84958	333		
"			87352	320	85663	352		
" Broad			90344	324	87994	420		

APPENDIX III

STATISTICAL IDEAS AND PROTEIN STRUCTURE

APPENDIX III

Statistical Ideas and Protein Structure

This work is not part of the main thesis and has not yet been developed fully. For this reason, the survey of the literature and the ramifications of the arguments are more limited than in the main thesis. This appendix concentrates on the development and illustration of techniques rather than properties of the proteins concerned. The particular statistical test required depends on the numbers and distributions, so some methods may need to be varied.

III.1. Introduction

Fibrous proteins are generally built of long uniform molecules and the variations along these molecules are often periodic in nature. This makes statistical ideas very useful in the analysis of periodic variations and interactions. The number of periods of a certain repeating property in a molecular length is often so great that periodicities can be identified without necessarily recognising the property which is significant in the periodicity. The number of interactions between adjacent molecules is so great that precise energy calculations, which are almost impossible, are not necessary. However, if the number of residues is small, the amino acids may well have to be grouped according to properties in order to obtain significant results. There are many ways of doing this; for example, by charge, size and hydrophilicity.

III.2 Regularities in Sequence

It is to be expected that all fibrous proteins contain certain regularities in the sequence which relate to the structure. Sometimes the relevant property of the regularly spaced amino acids is easy to identify and may be simply hydrophobicity. Often the property is less general and harder to identify - in some cases only one amino acid is suitable. To overcome this problem, it is suggested that regularly spaced amino acid positions should be taken for investigation of the population of amino acids. If certain amino acids repeat significantly more often than would be expected for a system with no periodicities, then that periodicity is probably important for the protein. It then remains to identify the relevant property of the amino acids present and relate it to the higher levels of structure.

III.2.1. The Residue Distribution.

A method also useful for less regular patterns is given below. A protein chain has 1000 residues and 10 of these are a particular amino acid to be investigated. It is proposed that this amino acid preferentially occurs at the twelve sites shown in Fig. III.1. Each site contains five amino acid positions and 7 of the 10 amino acids occur at those sites. The probability of seven or more occurring at these sites for randomly distributed residues is

$$\sum_{i=7}^{10} \frac{10!}{i!\,(10-i)!} \left(1-\frac{60}{1000}\right)^{10-i} \left(\frac{60}{1000}\right)^{i} \qquad \text{(III.1)}$$

as given by the binomial distribution. This can be used to test for preferential inclusion or exclusion of particular

residues. Care must be taken since a periodicity in one residue can impose peridicities on other residues. The regular glycine distribution in collagen increases the probability of finding non-glycine residues at the other positions. For this reason, a high level of significance is desired. If the relevant property of the amino acid can be identified, the hypothesis can be set up to include all residues with that property and, if the hypothesis is correct, a higher significance is likely to be obtained. Carrying out this procedure for individual amino acids is a method of arriving at a hypothesis concerning the necessary properties.

It may be found that only one amino acid position is important at each site. This is likely to be true for residues controlling interactions between rapidly rotating structures. At higher levels of structure, more positions may be important. For example, two adjacent residues oriented the same way could make up such a site. These could be separated by several residue positions along the molecule.

The sites chosen may or may not be separated by regular intervals. The separation could be determined as an integral or non-integral number of residues, for example a 28Å periodicity could be examined as easily as a 28 residue periodicity.

In general terms, for a chain of length A residues including r residues of interest , the probability of the residues occurring n or more times at a out of a total of A amino acid positions along the chain is

$$N = \sum_{i=n}^{r} \frac{r\,!}{i!\,(r-i)\,!} \left(1 - \frac{a}{A}\right)^{r-i} \left(\frac{a}{A}\right)^{i} \qquad \text{(III.2)}$$

The most probable value is

$$N_p = \frac{r\ a}{A} \qquad \text{(III.3)}$$

with a standard error of

$$\sqrt{(1 - \frac{a}{A})\ \ (\frac{a}{A})\ \ (\frac{1}{r})} \qquad \text{(III.4)}$$

This technique has been applied to the collagen sequence as described below.

III.2.2 Regular Periodicities

Sometimes it is not possible to produce a hypothesis, but the same method could still be used to test for periodicities by using a χ^2 test. Assuming a random distribution of residues the expected total, E, for a particular residue occuring at specified sites can be found. This can be compared with the observed value, O, by

$$\chi^2 = \sum_{\text{all residues}} \frac{(O - E)^2}{E} \qquad \text{(III.4)}$$

A high value of χ^2 indicates that a significant pattern is present. Reference to a text on statistics will provide tables of χ^2 and appropriate modifications which are sometimes necessary in the above formula.

In tropomyosin below, the positioning of the first site strongly affects the likelihood of finding a significant periodicity. To overcome this, site 1 could be fixed at one end of the molecule and χ^2 could be calculated. Then, staggering one residue at a time, other values of χ^2 could be calculated until all possibilities had been covered. In the case of a periodicity of seven residues, seven values would be

calculated. The variation of χ^2 over these values would show the importance of the periodicity at different residue positions, which would be interesting for tropomyosin. A total χ^2, χ^2_p, for the periodicity could be calculated

$$\chi^2_p = \sum_{\text{all positions}} \chi^2 \qquad \text{(III.5)}$$

A graph of χ^2_p plotted against periodicity would have peaks at important periodicities in the sequence.

III.2.3. Separations between Residues

A similar property that can be investigated is the separation between like residues. There are grounds for believing that similar separations occur throughout a sequence. Obviously, regular periodicities would also show up if this property was searched for. The method used in applying this search to tropomyosin has resemblances to methods involving nearest neighbour distributions, as described later. The work done on tropomyosin illustrates this method and is described in Section III.

III.2.4 Nearest Neighbours

Sometimes certain groups occur near other ones much more than expected for a random system. In the case of tropomyosin, the nearest residue may be three residues along the chain, owing to the rapid rotation of the α-helix. Where proximity, rather than a fixed separation, is the important factor, it is better to investigate the nearest neighbour distribution than the predominant separations.

Each group having the property of interest is compared in turn with the nearest neighbour of interest and the separation

is recorded. It may, for example, be of interest to compare each lysine with the nearest lysine, or each group of one charge, with the nearest group of the opposite charge.

As an example consider the nearest negatively charged neighbour to each positively charged group. If a proportion p of all groups is negatively charged, the probability of the nearest negatively charged group being n residues away from a randomly chosen positively charged group is P where

$$P = p\,(1 - p)^{n-1} \qquad \text{(III.6)}$$

This distribution is shown in fig. III.2. If proximity is important, a distribution more akin to the dotted lines in fig (III.3) is obtained. If a certain separation is favoured a peak is obtained, otherwise the probability is higher for small separations.

III.3 The Tropomyosin sequence

About half of the sequence has been published (Hodges and Smillie, 1970, 1972, a,b, Hodges et al, 1973). It is clear from the published sequence that the hydrophobic residues are regularly arranged at positions II and V in a repeat of seven along the molecule. This arrangement was postulated by Crick (1953a,b) for a two stranded coiled coil structure making two turns per seven residues with respect to the major helix of the coiled coil. The hydrophobic groups lie along the line of contact between the two strands.

The work done below was carried out on a provisional 146 residue sequence at the C-terminal end received prior to

publication. The sequence is tabulated in table III.1

Since only a short section of sequence was available only some illustrative calculations were performed. The significance of most results was low, so only the more significant results are noted.

When the full sequence is available, the calculations will give results of greater significance. The second chain will then be added with the stagger of 14 residues which leads to good interlocking between the chains in a coiled coil with a hydrophobic core (Hodges et al, 1973).

III.3.1. Muscle

The structure and function of muscle has been reviewed (Huxley, 1971). Contraction of muscle occurs when the thick and thin filaments slide between each other. The thick filaments contain myosin. Myosin is a fibrous protein with a globular head that makes contact with the thin filaments repeatedly during contraction. The thin filament is a two stranded coil of F actin with tropomyosin running in the grooves on either side. Troponin is also present. F actin is a chain of globular subunits estimated by electron microscopy to be 55Å axially, 35 Å radially and 50 Å tangentially (Moore et al, 1970). The two strands are staggered by 27.5 Å giving a periodicity in axial projection of 27.5 Å .

III.3.2. The Separation between Residues

The work is preliminary so only separations by multiples of seven were considered, although other separations would be very likely to produce interesting results. If separations

expressed in angstroms are to be investigated, then the nearest residue could be considered. The tropomyosin work does not indicate the definition of the separations, but if calculations were carried out at every separation, not just multiples of seven residues, and the fraction of comparisons producing identical groups was plotted, then the width of the peaks would indicate the definition of the separations. It seems likely that residues stabilising the most rapidly coiling structures will give rise to the best defined separations and periodicities. Owing to the rapid rotation of the chain, separations relating to interactions between larger structures could produce peaks separated by several residues. In the case of tropomyosin, a three residue translation brings the residue orientation to only 50 degrees from the starting position and a seven residue translation produces a similar angle.

It is also possible to consider separations approximating to certain values, which need not necessarily correspond to an integral number of residues. If several residues are considered for each comparison, a higher level of significance will be obtained for some situations.

The following comparisons are categorised according to their relation to the structure.

III.3.3. Stabilisation of the Coiled Coil.

Each residue was considered in turn and when it was identical with a residue separated from it by a multiple of seven this was recorded. The first residue was compared with twenty others, the eighth with nineteen and every residue was so compared until the 134th was reached. The same method was used for each of the other columns in table III.1. The number

and proportion of times the residues compared are identical for the various columns is shown in table III.2. The standard errors stated assume that the comparisons made are a random sample from the molecular chain and are taken as $\sqrt{n}$ where n events are counted.

The lowest total corresponds to group VII, which is on the outside of the coiled-coil model proposed by Crick (1953a,b). The next lowest total occurs for Group IV which corresponds to residues away from the line of contact between the chains. The mainly hydrophobic groups, II and V, both have high totals; these are found on the inside of the coiled coil. Groups I, III and VI, which are mainly hydrophilic, have high totals, which seems to indicate that they are instrumental along with groups II and V, in the stabilisation of the coiled coil, since a repeat of seven is a fundamental property of the structure.

Groups VII and IV, which have low totals, probably control interactions with actin, troponin and perhaps myosin.These interactions are likely to be controlled by periodicities which are not necessarily multiples of seven, in which case residues from different columns of the sequence table could contribute to one periodicity. Such periodicities may be less well defined, since these control interactions between more slowly coiling structures. It might be thought that these interactions are more polar than those within the coiled coil, but hydrophobic interactions are still important.

If groups following and preceding the hydrophobic residues form a barrier between a hydrophobic environment and a hydrophilic one, this could have a stabilising effect. Glutamine and its acid have a short paraffin chain and a hydrophilic

terminus to the residue, so the high incidence of one or the other in these positions is not surprising.Lysine could fulfil a similar role for interactions between larger structures, where a longer paraffin chain is required.

The highly hydrophobic nature of groups III and VI emphasises the importance of these in coiled-coil interactions. It may be expected that tightly coiled structures will be stabilised by fewer of the large hydrophobic residues, such as tyrosine and phenylalanine. Interactions between such structures could be expected to be in part by means of hydrophylic residues. This view is supported by the ability of three stranded collagen molecules or dimers of paramyosin to exist intact and separated in an aqueous environment.

III.3.4. Other interactions

Comparisons were also made for fixed separations between residues.. Tests were carried out for each of the seven groups. A separation by 14 residues, for example, was found by comparing every pair of residues separated by this amount and recording the fraction of the comparisons finding identical residues. Taking the seven groups together the most significant separations were 28, 35, 56, 77, 84 and 112 residues.

The 28, 56, 84 and 112 residue repeats indicate a 28 residue periodicity. Hodges et al (1973) found that the 14 residue stagger was achieved by matching a small hydrophobic residue in one chain with a large hydrophobic residue in the other chain. For perfect matching, a large hydrophobic residue would have a small hydrophobic residue 14 residues on either side.

This leads to large hydrophobics being on a 28 residue repeat and the small residues being on another 28 residue repeat displaced 14 residues from the first.Groups II and V in table III.1 show this to be the case. The sequence down column II is (Ile or Leu, Leu, Ala, X)$_n$, with a few exceptions. The 28 residue repeat is also significant in Groups I, III and VI, perhaps indicating a relationship between the structure of the core and that of the periphery of the coiled coil.

The 77 residue separation corresponds to 110 Å measured along the thin filament or 114Å along the coiled tropomyosin molecule. It may relate to the 27.5Å or the 55Å repeat along the thin filament, which could be found directly by a fuller analysis of this type. In this case it could correspond to 28Å periodicity seen as lightly stained bands in electron micrographs of *in vitro* aggregates of tropomyosin (Caspar *et al*., 1969; Parry and Squire, 1973). Hydrophobic residues away from the coiled coil axis occur at 28Å intervals. (A.Miller, (personal communication); Parry, 1974).

The 35 residue separation and the 49 and 63 residue separations in group I require more information before their origin can be identified. Charged residues appear to be involved, but significance is low.

III.3.5 A three dimensional approach

A one dimensional study only gives limited information, but perhaps sufficient to commence a three dimensional study. Knowing the α-helix has 3.5 residues per turn, the sequence has been arranged in fig. III.3 to make the angular and spatial arrangements more apparent. As yet, only one chain is represented.

III.3.6 Distortions of the coiled coil

Certain residues may cause distortions: non-hydrophobic groups in positions II and V; glycine, tyrosine, asparagine, serine, proline and cysteine (Finkelstein and Ptitsyn, 1971); and also aspartic acid (Kotelchuck and Scheraga, 1968, 1969, Lewis et al, 1970).

In position II, such residues occur on a period of 28 residues. Table III.4 is the same as table III.3 with only these residues recorded. Hydrophobic groups not in positions III and VI are likely to form intermolecular interactions not disruptive to the coiled coil, so these are not included, except for those listed above.

The arrangement of these residues is similar to that of the hydropbobic residues, which probably interact with actin, so they may relate to small distortions of the coiled coil allowing a stronger interaction with actin. Most of these residues not near the hydrophobic residues are arginine, lysine, glutamine and glutamic acid, which may be speculated as being present at the interface between protein and the aqueous environemnt, thus playing a twin role by means of a hydrophobic paraffin chain and a polar part. The helix propensity of the residues recorded was determined in a very different system.

The residues (table III.4) are arranged in a band of gradually decreasing pitch as it becomes farther from the C terminus. The residues also tend to lie on the dotted lines. The dotted lines are about 180° apart around the α-helix. The significance of this awaits the full sequence.

III.3.7 Interactions with the actin helix

Large hydrophobic residues and most hydrophobic residues away from the coiled coil axis probably contribute to interactions with actin. These residues and the positively charged residues are arranged on related patterns. The large hydrophobic residues, tyrosine and phenylalanine, hydrophobic residues not in positions II and V, and positively charged residues are recorded in table III.5

The hydrophobic residues lie near a helix on the surface of the α-helix. At angles of about 90° around the α-helix from this line are found the positively charged groups, mainly lysine, but their positions are less well defined. The hydrophobic residues have a tendency to cluster on a repeat that may be 55Å, which relates to the actin structure.

The pitch of the F-actin helix has been estimated as 700Å (Huxley, 1963) and the screw sense has been determined as right-handed (Depue and Rice, 1965). The screw sense in the thin filaments of insect flight muscle is right handed (Reedy, 1968). The pitch in muscle has been estimated as being between 698Å and 812Å, depending on the muscle and the experimentalists. (Fraser and MacRae, 1973 a).

The repeat distance of the line linking the hydrophobics may be close to 110Å. A tropomyosin pitch of 186Å would be 180Å after projection on to the thin filaments. To interact with the actin helix, the line of hydrophobics should go once round the α-helix in 140Å. The discrepancy may disappear when the full sequence, the two chains and the pitch of tropomyosin can be considered together. The two helices of opposite hands

(a coiled coil is left handed) rotate towards each other. The pitches of the actin and tropomyosin helices are P_A and P_T (P_T is the pitch projected on to the axis of the thin filament). The line of hydrophobic residues passes once round the α-helix in distance R. Then

$$\frac{R}{P_A} = \frac{P_T - R}{P_T} \qquad \text{(III.7)}$$

The axis of the tropomyosin molecule is inclined to that of the thin filament, so in practice the coiled coil of period P_T rotates more rapidly than expected from this formula , as the value of 110Å rather than 140Å suggests.

The lines of positively charged groups on either side of the line of hydrophobic residues are mainly lysine. Perhaps lysine fulfils a similar role to glutamic acid. The long paraffin chains could interact with the line of hydrophobic residues and the polar parts with the aqueous environment. tropomyosin moves in the groove of the actin helix (Parry and Squire, 1973). Lysine has a high temperature factor (Kendrew, 1962) inferring the flexibility required for movement.

III.3.8 Further work.

With the full sequence, the second chain will be included and the analysis will be more quantitative. If the overlap between coiled coils can be established, a long chain of molecules can be analysed with greater thoroughness.

III.3.9 General speculation

The core of the coiled coil is very hydrophobic. This is

probably a general feature for small structures, as evidenced by their stability in aqueous environments, in particular acidic and basic ones. It seems likely that tightly coiled three chain structures, such as the collagen molecule, are stabilised by small and medium sized hydrophobic amino acids; whereas the data on tropomyosin are consistent with only the largest ones being excluded from the core.

Most hydrophobic residues not on the coiled coil axis fall on a line enabling easy interaction with the actin helix. This is produced by preferential exclusion of these groups from surfaces in an aqueous environment. These could control azimuthal relationships between interacting structures, but there is no reason to suppose that they are more important than polar residues, in controlling axial register. These hydrophobic amino acids may be larger than those on the coiled-coil axis. As the periodicities are less well defined, in part a consequence of the rapidly coiling α-helices not presenting residues at the correct angle at the required intervals and in part the greater area over which interactions may occur, larger residues may well be preferred.

There are many glutamines or glutamic acid residues bordering the hydrophobic core indicating that hydrophilic groups with hydrophobic chains are an important stabilising factor at the interface between hydrophobic and hydrophilic regions. The stabilising groups are more likely to be the acid, since interactions with water would then be stronger. It would be predicted that interactions between larger structures would use residues with longer paraffin chains, such as lysine. It is clear that lysine is preferentially arranged on lines 90^{o} around the α-helix

on either side of the line of hydrophobics controlling interactions with actin.

An interesting observation is that groups generally considered to disrupt an α-helical or a coiled-coil structure are arranged in a helical band around the coiled-coil bearing some relation to the line of contact with the actin helix.

These observations are useful in deciding how to group residues to give high significance in the techniques proposed and used.

III.4. The collagen sequence

III.4.1. Regularities

Collagen has not been studied in the same way as tropomyosin, but a number of regularities in the positions of specific groups were noted by a colleague. Statistical tests were performed using the methods of section III.2.1. Testing significance is not easy, since a regularity may be imposed by the presence of other regularities. For example, the glycine periodicity excludes phenylalanine from a third of the residue positions.

As an example of the techniques used on tropomyosin, observe the separation between phenylalanine residues. They occur at positions 23, 92, 167, 233, 317, 404, 464, 503, 632, 791, 932 in the sequence as published by Hulmes et al (1973). Staggers that are multiples of about D = 234 residues are found. Positions 233, 464 and 932 are described approximately by

$$j = D - 3,$$

where j is an integer. Assuming other positions differ from

these by submultiples of D, the others are best described by

$$kD - (3/11)\,D-3$$

for positions 167, 404 and 632;

$$\ell D - (7/11)D - 3$$

for positions 92 and 791

$$\ell D - (1/6)\,D - 3$$

for position 503 and

$$mD - (1/9)\,D - 3$$

for position 23, where k, ℓ, m and n are integers. This indicates that separations of 21, 26, 39 and 234 residues may be important, but only further analysis can show this.

The regularity of phenylalanine suggests that only one residue is suitable for certain functions as stated in section III.2. If the analysis of section III.3 had grouped all hydrophobic amino acids together, important features of tropomyosin would have been missed. It is clear that the techniques described in section III.2 could be very powerful if applied to collagen.

III.4.2. General speculations

From the analysis of tropomyosin, it was suggested that glutamic acid plays an important part in the stabilisation of rapidly coiling structures. The difference between the two non-glycine positions in the collagen sequence is likely to relate to the structure of the triple helix, so the distribution of glutamic acid residues was investigated. For the sequence $(Gly\text{-}X\text{-}Y)_1$

it was found that position X contained 38 residues and position Y 6 residues. This indicates that the role of glutamic acid could be similar to that in tropomyosin.

Here glutamic acid residues were concentrated close to the line of hydrophobics stabilising the coiled coil, suggesting that the hydrophobic paraffin chain and the hydrophilic charged terminus enabled it to make stabilising interactions with both the hydrophobic amino acids and the aqueous environment. The equivalent role in collagen would be the stabilisation of the interactions between collagen molecules. There was a suggestion that lysine performed a similar role for the interaction between actin and tropomyosin. This is more likely to be equivalent to interactions between microfibrils. The larger size of the structures may require the longer paraffin chain possessed by lysine.

The suggestion that small hydrophobic amino acids stabilise tightly coiled structures is supported by the glycine periodicity in collagen. Positions X and Y are well away from the axis of the triple helix so they must also contribute to inter-molecular interactions.

III.4.3 Interactions

Analysis of the interactions between long fibrous protein molecules is made possible by the statistical features described in section III.1 . These techniques are explained by reference to collagen.

III.4.3.1. Proposals for Investigation.

When the collagen sequence determined by various workers

was collated by Hulmes et al (1973) colleagues discovered that complex scoring schemes were of no avail. A colleague and I agreed that polar interactions could be scored equally. Moreover his view that polar groups controlled the interaction was worth testing. It seemed reasonable to count the interactions made between two collagen α1chains. A program was written to count the number of interactions made between two chains as they were staggered by different amounts. Applying the central limit theorem to the distribution of residue-residue interaction energies (see section III 4.3.4), it is found that the interaction energy and the number of interactions maximise together.

To investigate the importance of polar interactions, the number of interactions between unlike charges and the number between like charges were found. The latter was subtracted from the former to obtain a number representing the interaction. Since like charges repel and do not make contact, the effect of like charges is much less. If this was followed up, they would have been treated separately from other interactions. As one molecule interacts with others along most or all of its length, it was considered that an appropriate normalisation was needed. Counting interactions with other molecules would require assumptions regarding the staggers between more than one molecule, so only two interacting molecules were considered. Instead, the number of interactions was divided by the number of residues compared at that stagger.

Ir appeared likely that a stagger of D (668$\mathring{A}$ ± 2$\mathring{A}$. Wray, 1972; Miller and Parry, 1973) occurred between collagen molecules,

(that is between triple helices), since it fitted the Hodge-Petruska model. On this basis, the graph of the number of interacting residues as plotted in fig. III.3 was the predicted result of the analysis, the dips occurring because like interactions were considered. If only like interactions are considered, then the dips disappear, leaving peaks at D and 3D. Fig. III.3 also illustrates diagrammatically how the peak at 3D is produced. The presence of this peak does not necessarily indicate that a 3D stagger is important in vivo.

Interactions between unlike charges were given a score of 1 and between like charges a score of -1, all others being scored zero. It was decided to plot the results using the graph-plotting package available on the ICL 1906A computer. A colleague suggested an extension to include opposing residues plus one either side. This is reasonable since side chains are quite long, and the main chains are thought to be staggered by one residue within the molecule. As it was a trial program, interactions between more greatly separated residues were not counted. The importance of these must be tested by observing their effect on the results. A colleague used this method.The output revealed peaks at multiples of D - a significant event, since it was the first time sequence had been related to structure in proteins, except for local interactions.

The method introduces several useful techniques. These are: counting interactions instead of making approximate energy calculations; considering residues with a selected property; staggering chains to find the favourable interactions; and plotting the results in a form showing these directly.

III.4.3.2 Further investigations

The method has been well illustrated by work carried out by Hulmes et al (1973). This section is devoted to a discussion of their work.

III.4.3.2.1. Analysis

Hulmes et al (1973) used the method for interactions between positively charged amino acids (lysine, hydroxylysine and arginine) and negatively charged ones (glutamic acid and aspartic acid). They used the same method for interactions between amino acids with a large hydrophobic side chain (valine, methionine, isoleucine, leucine and phenylalanine). Repulsions between like charges were considered, but apparently not separately from other interactions. Simple energy calculations were also made by giving different scores to different interactions, but counting the interactions gave better results.

Best results were obtained when residues several positions to either side of the opposing residues were considered. The optimum range being $\pm$ 3 for charge interactions and $\pm$ 2 for hydrophobic interactions. The way this was done is illustrated in Fig. III.4

Statistical significance was investigated by generating 20 random sequences of the residues in the real sequence so as to maintain the real distribution between positions in the triplet Gly-X-Y.

The analyses were performed without the normalisation procedure in the original program.

III.4.3.2.2. Results

The results are shown in fig. III.5 for the charged inter-

actions, hydrophobic interactions and total interactions. All groups show sharp peaks at intervals corresponding to staggers of OD, 1D, 2D, 3D, and 4D, where D = 234 $\pm$ 1 residues. No regularity was found for random sequences. The peaks at D are 3 to 3.5 standard deviations from the mean for random sequences.

If a second interacting molecule translated 5D from the first is considered, the peaks at multiples of D become approximately equivalent, except for those at OD which are two to three times higher than those at 1D. For charged residues, the high peak at OD is attributed to an observed tendency of negative and positive charges to be close together, suggesting that intra-molecular charge interactions are an important factor. The hydrophobic interaction curve shows fine structure with an apparent period of D/11. Inspection shows there are two patterns of opposite phase, each with a period 2D/11, and each modulated by a pattern with a period of 2D (see fig. III.6). Frequency analysis shows strong spacings at 21 residues (D/11), and at 39 and 47 residues which is consistent with a period of 2D/11 sampled by the fifth and sixth orders of D. Most amino acids with large hydrophobic side chains contribute to this structure. They often occur on a pattern with intervals of 2D/11 and D/11. This fine structure was not found for charged residues.

The values for D of 234 $\pm$ 1 residues and 668 $\pm$ 2Å correspond to a residue translation of 2.855 $\pm$ 0.02Å, close to the value of 2.91 $\pm$ 0.01Å obtained by X-ray diffraction measurements. The D/11 interval is 21 residues and the pitch, P, of the chain supercoil is approximately 30 residues, so the simple relationship D/11 = 2 P/3 may apply.

III.4.3.3. Discussion

Hulmes et al (1973) were mainly interested in finding the D repeat and succeeded in doing so. This section speculates on how the method can be extended.

III 4.3.3.1 Analysis

It would have been interesting to see results from different groups of amino acids. Amino acids with short side chains- glycine, alanine, valine, serine,threonine, cysteine and proline - are likely to be involved in intramolecular interactions, which are likely to be very well defined and perhaps only opposing residues need be considered. This should enable the stagger (probably one or two residues) between the $\alpha 1$ chains to be determined. Information may also be obtained relating to the amino acids remaining for inter-chain interactions.

20 random sequences are not needed to investigate significance. In the analysis of the significance of the peaks at multples of D, it was stated that the deviation from the mean determined for a random sequence was 3.5 standard deviations indicating a confidence level of 0.1%. The level is much less than this if one peak is considered alone, as there are many staggers at which it can occur. If the regular periodicity of these peaks is considered, then the confidence level becomes much higher. The interesting feature is not the difference between the number of interactions at a peak and the number for a random sequence. It is the difference between the number at the peaks and the number between the peaks. This relates to staggers between interacting molecules and can be analysed by elementary statistics for a randomly distributed variable. When the main peaks have been considered, these can

be subtracted from the curve before the other peaks are analysed.

III 4.3.3.2 Results

Approximately equivalent peaks were obtained at all multiples of D, compared with the predicted peaks at D and 3D (See section III 4.3.1.). The four peaks are equivalent because amino acids of opposite charge are often paired, allowing interactions between charged groups to occur at all multiples of D. This has been investigated further (Doyle et al, 1974)*. Since the arguments in section III. 4.3.1 suggest that a simple system would produce peaks at 1D and 3D, it may be expected that the structure requires an interaction at 2D or 4D. The microfibril structure proposed by Smith (1968), although defined by a 1D stagger alone, does have an interaction at 4D. Since this interaction is only for a small fraction of the molecular length, it is surprising that the peaks are as significant as those at 1D and 3D (The significance of the peak at 4D is difficult to estimate, owing to the small number of residues available for interaction.). This could result from the extra peaks being defined by a pairing of charges. Further work (Doyle et al., 1974)* supports the greater importance of the 1D stagger.

The pairing of groups of opposite charge was attributed to intra-molecular interactions, and the high peak at OD is attributed to this. Measurements from the curve for charge interactions (fig.III.5) indicate that the peak at OD would become only a little higher than those at multiples of D after normalising as suggested in section III 4.3.1. This means that the pairing occurs almost exclusively for residues involved

*See appendix VI.

in interactions at multiples of D. This makes it unlikely that pairing is to allow intra-molecular bonding and a requirement for interactions occurring at multiples of D seems the most probable explanation.

The lesser definition in the curve for charged interactions derives from the higher background, the peak height remaining the same as for hydrophobic interactions. The peak height indicates that the interactions are probably equally important and the higher background relates to interactions with an aqueous environment. As hydrophobic groups are confined to non-aqueous environments, charged interactions in their vicinity are likely to be produced by largely hydrophobic amino acids such as lysine.

The fine structure in the hydrophobic curve is expected. If the small hydrophobic amino acids, which are more likely to stabilise the molecule, had been included, the molecular structure would have been more apparent in this. The structure remaining probably relates to inter-molecular interactions. It indicates that collagen molecules are coiled so as to present groups for inter-molecular interactions only at specified intervals. A repeated separation distance between large hydrophobic residues would appear as a peak in the interaction curve. If the molecules are packed so as to present some hydrophobic groups to an aqueous environment, these are likely to be shielded by long, flexible amino acids, such as lysine. The structure of the interaction curve is also evident in the arrangement of phenylalanine (see section III.4.1). The other patterns in the distribution of hydrophobic groups also probably

relate to intermolecular interactions.

The fine structure is unlikely to relate to possible in vivo staggers between molecules, since interactions at staggers of D are a controlling factor. For this reason, a direct analysis of the sequence, as applied to tropomyosin, would be a more appropriate means of investigation.

The relationships between the molecular structure and the pitch are changed if the microfibril is supercoiled. Assuming the fine structure comes from intra-microfibrillar interactions, the pitch of interest is that in the coordinate frame rotating with the supercoiling microfibril. If the supercoil has a hand opposite to that in the molecule and the pitch is 700 Å, then a molecular pitch of about 28.5 residues is required in the frame rotating with the supercoil, if the experimentally determined pitch is correct.

III 4.3.4. The statistical bases

The method has been illustrated. It is now possible to appreciate the statistical basis.

III 4.3.4.1 The energy distribution

When two molecules interact, the interaction energies between pairs of amino acids follow a distribution which is well behaved. The range of energies relates to the interacting groups, their environment and relative translation. For such a distribution, the mean energy is fairly well defined, as seen from the central limit theorem. The variance of the means determined for different molecular staggers is 1/n, where n is

the number of interactions counted, so it is an advantage to compare structures with many amino acids. The mean is directly related to the number of interactions as used in the analysis.

At a stagger corresponding to an important interaction, the energy could change, owing to specific residues being involved in interactions, but it is very unlikely that the number of interactions would not change. If the mean of the energy distribution is unchanged, the interaction energy is directly related to the number of interactions.

III 4.3.4.2 Significance of Peak Heights

The peaks in the interaction curve are superimposed upon a background level. This background is produced by unspecific interactions with solvent, irregular interactions between protein molecules and interactions which cannot occur because the amino acids are displaced too far azimuthally. At a peak the number of contributing interactions is greater than the deviation from the background level, since there are few amino acids left to contribute to the background. If it is assumed that the fraction of residues contributing to the background is constant after subtraction of the peaks, then several relationships are obtained. For a peak maximum of N interactions and a background of height n, the peak height is

$$P = N - n \qquad \text{(III.8)}$$

and the number of interactions is

$$I = (N-n) + N/(T-1) \qquad \text{(III.9)}$$

where T is the total number of amino acids tested for interactions

and is found from

$$T = A - S \qquad \text{(III.10)}$$

where

A is the number of amino acids in the chain and S is the relative stagger of the molecules.

The background level beneath the peak is

$$B = n - N(T-1) \qquad \text{(III.11)}$$

so the standard error of the number of interactions is

$$E = \sqrt{I} + \sqrt{B} \qquad \text{(III.12)}$$

This applies to a peak height at one stagger. If a peak appears, the confidence levels must allow for the fact that it could have occurred at any other stagger.

The parameter which must be minimised is the fractional standard error

$$E_F = E / I \qquad \text{(III.13)}$$
$$= \frac{1}{\sqrt{I}} + \frac{\sqrt{B}}{I}$$

To increase the significance, residues interacting with those translated several positions along the chain have been included. As the range is increased, B increases increasingly rapidly and I increases decreasingly rapidly so that a minimum value for E_F is reached for a particular range. The correct range can be found from the interaction curves determined with different ranges.

III 4.3.5 Three dimensional inferences

This analysis shows how the optimum staggers between molecules can be determined. This can lead to certain restrictions on protein structure. Once this has been done, use of the methods applied to tropomysoin could lead to angular relationships. These

could be fed back into the interactions analysis. Starting with the molecular structure the method may be capable of being extended step by step up to the structure of the collagen fibril.

Examination of the fine structure of the hydrophobic interaction curve gives information on the three dimensional structure. Calculations on part of the sequence suggest that the curve may differ in the overlap region (five stranded) and the gap region (four stranded). A five stranded structure of pitch 30 residues would lead to intermolecular interactions at intervals of 30 n $\pm$ 9 residues, where n is an integer. (Fig.III.7) A whole number of turns corresponds to 30 residues, whereas 9 residues corresponds to a turn of 108^{o}, the internal angle of a pentagon. Angles of (360 n $\pm$ 108) degrees are expected. (A colleague performed the same analysis on all the sequence together. His arguments and conclusions were identical). This neatly fits in with a 30 residue pitch, since the three chains are thought to be staggered by one residue from each other. The angle of 120^{o} between each of the three chains would lead to there being a third of the pitch between points where adjacent chains can make an interaction with the adjacent microfibril. Combined with the stagger of one residue, this leads to there being 9 residues between points where the sequence performs a similar role. Since one chain has similar interactions at a separation of 9 residues, the system is efficient. The interaction curves for both the whole sequence and the overlap regions gives peaks at 21 residues and 39 residues supporting this, whereas the gap region gives 21 and 42 residues. Before a different structure is proposed for this region, the calculations must be checked

using the whole sequence.

III.5. The future

The preliminary work on tropomyosin provides hope that three dimensional protein structures can be derived from the sequences of fibrous proteins. This can be tested for the full sequence of tropomyosin and for collagen.

The one dimensional work on collagen shows how molecular staggers can be estimated - an important first step in three dimensional work. Applied to tropomyosin, this is likely to reveal the molecular stagger, thought to be 14 residues. The overlap between coiled coils is too short to obtain an accurate value for this in this way. Fine structure relating to the interaction with actin will be present. Owing to the lesser definition of the interacting edge than between the small diameter collagen molecules, and owing to the lower number of residues in the sequence, the fine structure may be close to the noise level of the interaction curve. Any peaks other than that at 14 residues will be very interesting.

TABLES FOR APPENDIX III

Table		VII	I	II	III	IV	V	VI
III.1	1	Lys	Glx	Ile	Glx	Glx	Ile	Glx
	2	Lys	Glx	Leu	Lys	Glx(Glu)	Ala	Lys
	3	His	Ile	Ala	Glx(Glu)	Asx(Asp)	Ala	Asp
	4	Arg	Lys	Tyr	Glx	Glx	Val	Ala
	5	Arg	Lys	Leu	Val	Ile	Ile or Leu	Glx
	6	Gly or Ser	Glx or Asx	Leu	Glx	Arg	Ser or Ala	Glx
	7	Glx	Arg	Ala	Glx	Val or Leu	Ala or Ser	Glx
	8	Ser or Gly	Lys	CMC(Cys)	Gly or Ala	Asx or Glx	Leu	Glx
	9	Glx	Glx	Leu	Lys	Lys, Ile or Thr	Val	Thr
	10	Asn	Asx	Leu	Lys	Ser	Leu	Glx
	11	Ala	Val or Glx	Ala	Glx	Lys	Tyr	Ser
	12	Glx	Lys	Glx	Asx	Lys	Tyr	Glx
	13	Glx	Glx	Ile	Lys	Leu or Val	Leu	Ser
	14	Asx	Lys	Leu	Lys	Glx	Ala	Glx
	15	Thr	Arg	Ala	Glx	Phe	Ala	Glx
	16	Arg	Ser	Val	Thr or Ala	Lys	Leu	Glx
	17	Lys	Ser	Ile	Asx	Asx	Leu	Glx
	18	Asx	Glx	Val or Leu	Tyr	Ala	Glx	Lys
	19	Leu	Lys	Tyr	Lys	Ala	Ile	Ser
	20	Glx(Glu) Glx(Glu)		Leu	Asx(Asp)	His	Ala	Leu
	21	Asn	Asp	Hser (Met)	Thr	Ser	Ile	COOH

The provisional sequence for the 146 residues of tropomyosin at the C terminal end. The brackets indicate the form published by Hodges et al (1973) when the 137 residues at the C terminal end were published.

Glx = Glutamine or glutamic acid

Asx = Asparagine or aspartic acid.

TABLE III.2

	VII	I	II	III	IV	V	VI	Total
Total	18	39	39	41	23	43	59	262
Proportion	0.09	0.19	0.19	0.20	0.11	0.21	0.31	0.18
S.E.	0.02	0.03	0.03	0.03	0.02	0.03	0.04	0.01

The number and proportion of groups producing identical comparisons within the seven groups of the sequence.

TABLE III.3

Arrangements of residues by position and angle

	III	VII	IV	I	V	II	VI	III	VII	IV
1		Lys		Glx		Ile			Lys	
1	Glx		Glx		Ile		Glx	Glx		Glx
2		Lys		Glx		Leu			Lys	
2	Lys		Glx		Ala		Lys	Lys		Glx
3		His		Ile		Ala			His	
3	Glx		Asx		Ala		Asp	Glx		Asx
4		Arg		Lys		Tyr			Arg	
4	Glx		Glx		Val		Ala	Glx		Glx
5		Arg		Lys		Leu			Arg	
5	Val		Ile		Ile or Leu		Glx	Val		Ile
6		Gly or SER		Glx or Asx		Leu			Gly or Ser	
6	Glx		Arg		Ser or Ala		Glx	Glx		Arg
7		Glx		Arg		Ala			Glx	
7	Glx		Val or Leu		Ala or Ser		Glx	Glx		Val or Leu
8		Ser or Gly		Lys		Cys			Ser or Gly	
8	Gly or Ala		Asx or Glx		Leu		Glx	Gly or Ala		Asx or Glx
9		Glx		Glx		Leu			Glx	
9	Lys		Lys, Ile, Thr		Val		Thr	Lys		Lys, Ile Thr
10		Asn		Asx		Leu			Asn	
10	Lys		Ser		Leu		Glx	Lys		Ser
11		Ala		Val or Glx		Ala			Ala	
11	Glx		Lys		Tyr		Ser	Glx		Lys
12		Glx		Lys		Glx			Glx	
12	Asx		Lys		Tyr		Glx	Asx		Lys
13		Glx		Glx		Ile			Glx	
13	Lys		Leu or Val		Leu		Ser	Lys		Leu or Val
14		Asx		Lys		Leu			Asx	
14	Lys		Glx		Ala		Glx	Lys		Glx
15		Thr		Arg		Ala			Thr	
15	Glx		Phe		Ala		Glx	Glx		Phe

TABLE III.3 (cont'd)

	III	VII	IV	I	V	II	VI	III	CII	IV
16		Arg		Ser		Val			Arg	
16	Thr or Ala		Lys		Leu		Glx	Thr or Ala		Lys
17		Lys		Ser		Ile			Lys	
17	Asx		Asx		Leu		Glx	Asx		Asx
18		Asx		Glx		Val or Leu			Asx	
18	Tyr		Ala		Glx		Lys	Tyr		Ala
19		Leu		Lys		Tyr			Leu	
19	Lys		Ala		Ile		Ser	Lys		Ala
20		Glx		Glx		Leu			Glx	
20	Asx		His		Ala		Leu	Asx		His
21		Asn		Asp		Met		Thr	Asn	
21	Thr		Ser		Ile		COOH			Ser

TABLE III.4
Arrangement of coiled coil disrupting residues

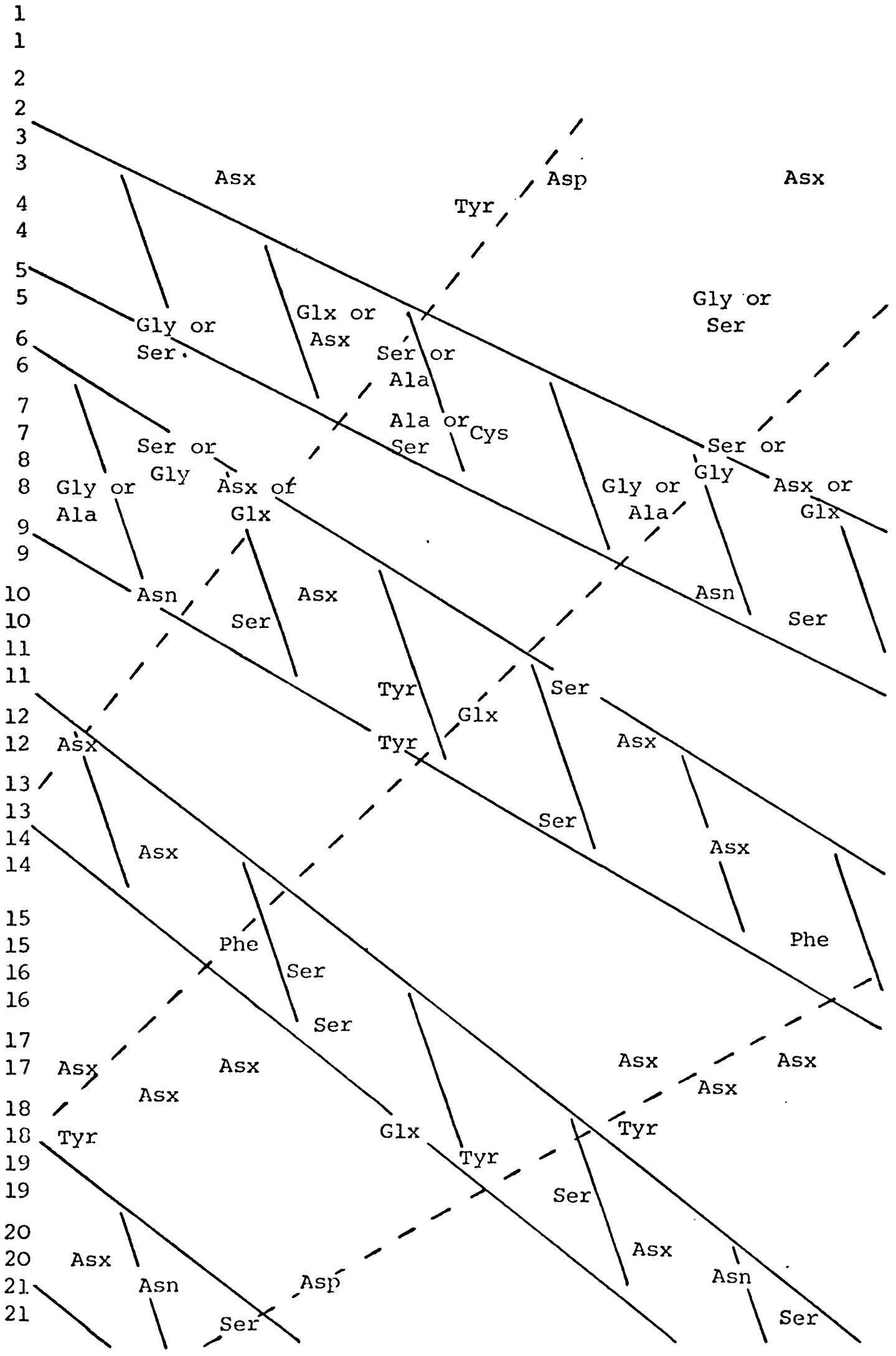

TABLE III.5

Arrangement of positive and hydrophobic residues

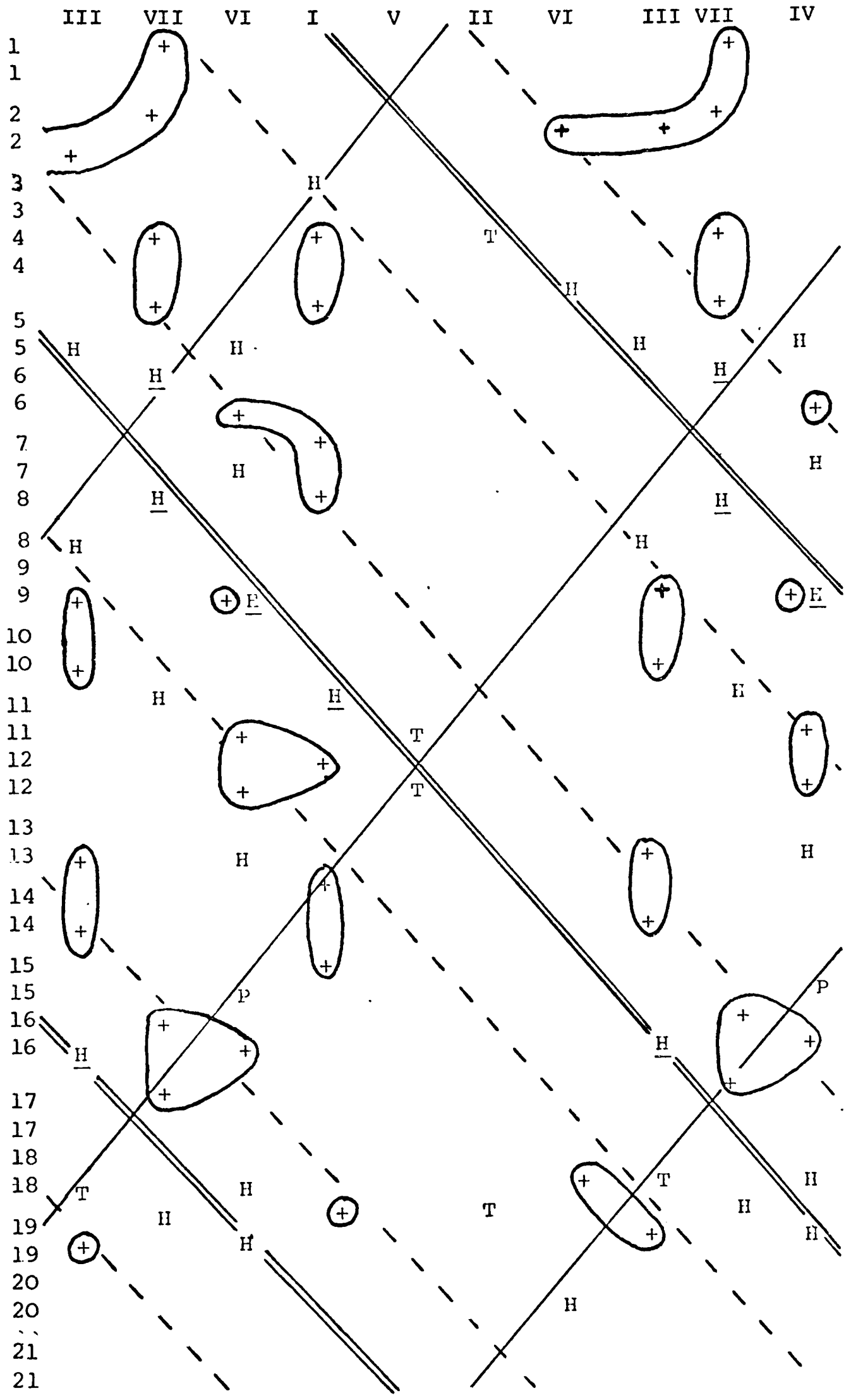

Table III.5

Legend

═══ Line of hydrophobics making contact with the actin helix.

—— line of hydrophobics

--------- lines of positively charged residues

— — — — lines of positively charged residues

+ positively charged residue

H hydrophobic residue

H̲ residues that are sometimes hydrophobic

T tyrosine (large hydrophobic)

P phenylalanine (large hydrophobic)

Fig. III.1 A hypothetical distribution of residue positions favouring certain amino acids. Positions 1 and 1000 are marked. P, protein chain; S, a site containing 5 residue positions.

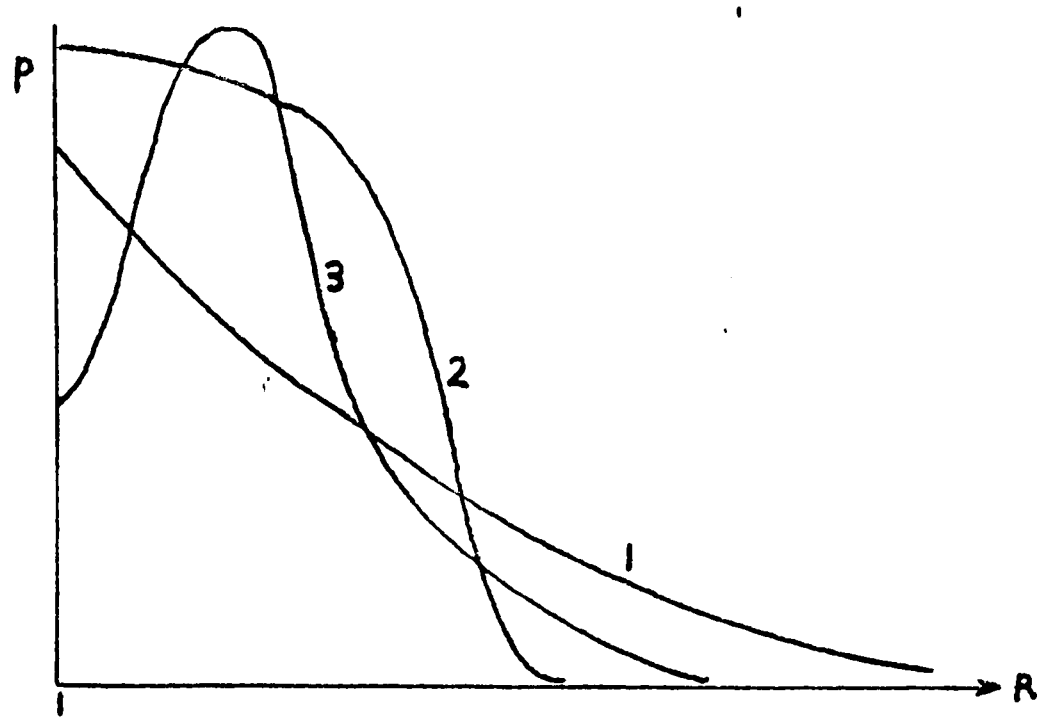

Fig. III.2 The nearest neighbour distribution of residues is a histogram which approximates to these curves in the case of: 1, a random distribution; 2, close proximity being favoured; 3, separations close to a certain small value being favoured.

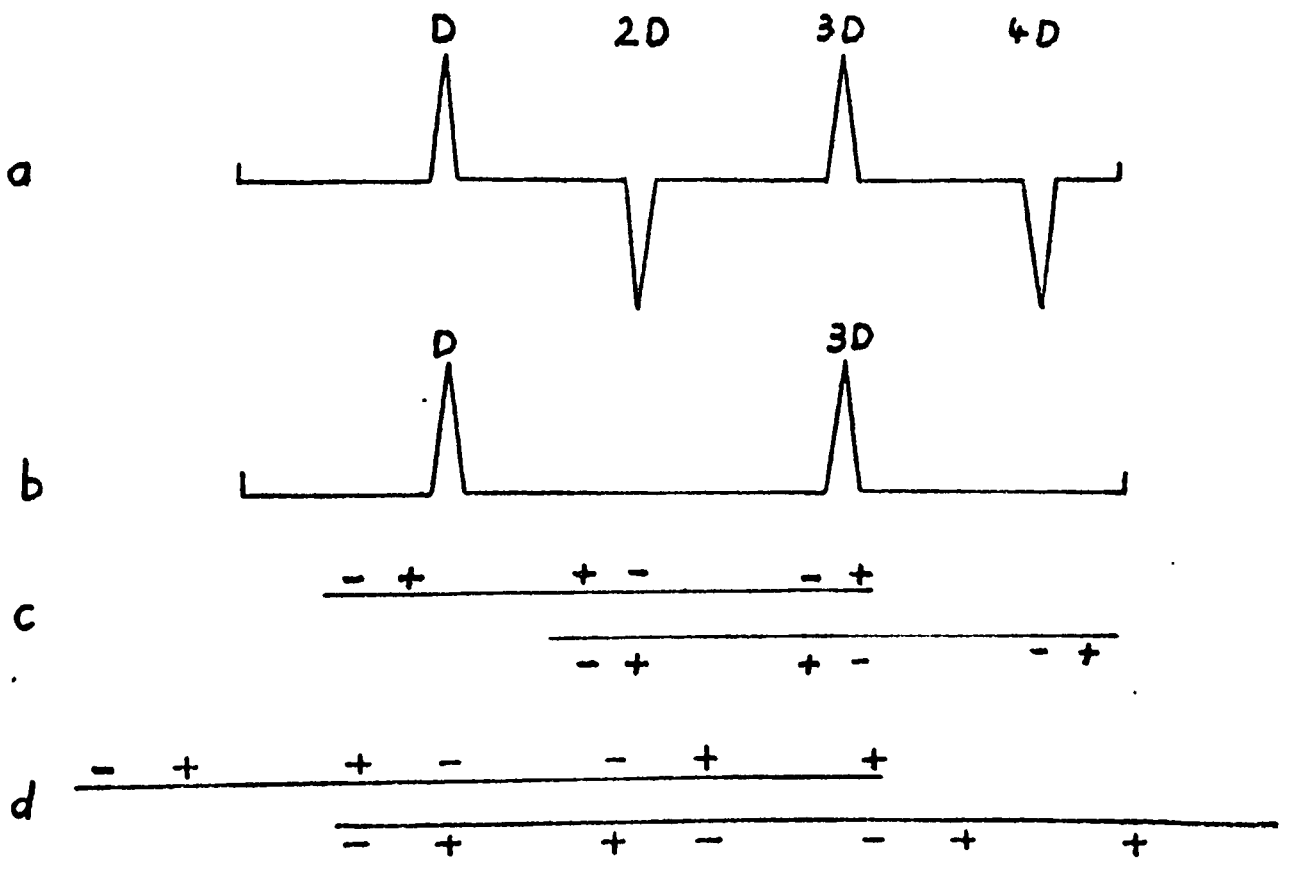

Fig. III.3 Idealised interaction curves for collagen predicted for: a), charge interactions; and b, interactions between opposite charges. Illustration of possible charge interactions where two interacting chains are staggered by c) D, and d), 2D.

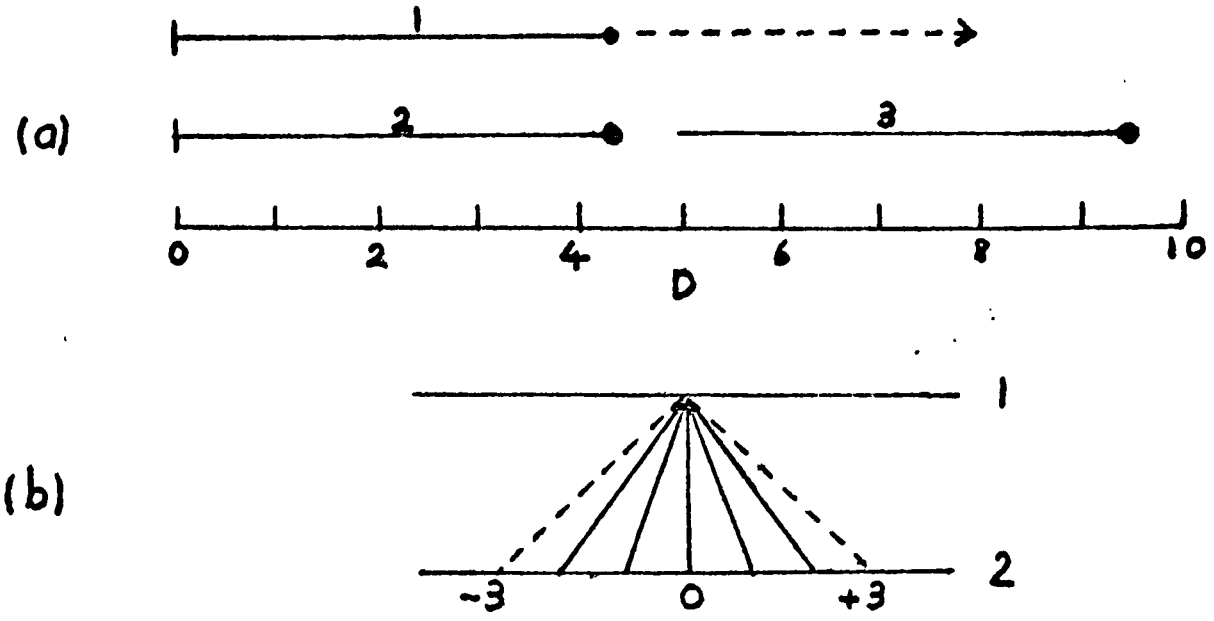

Fig. III.4 An illustration of the method used to count molecular interactions (a) The interactions were counted as all possible staggers as molecules 1 was moved past molecule 2. In some cases, the additional interactions that would occur as molecule 1 overlaps molecule 3 were included. (b) an interaction was counted if two residues in opposite chains were within ± 2 (Hydrophobic) or ± 3 (charged) residues apart. (From Hulmes et al. 1973)

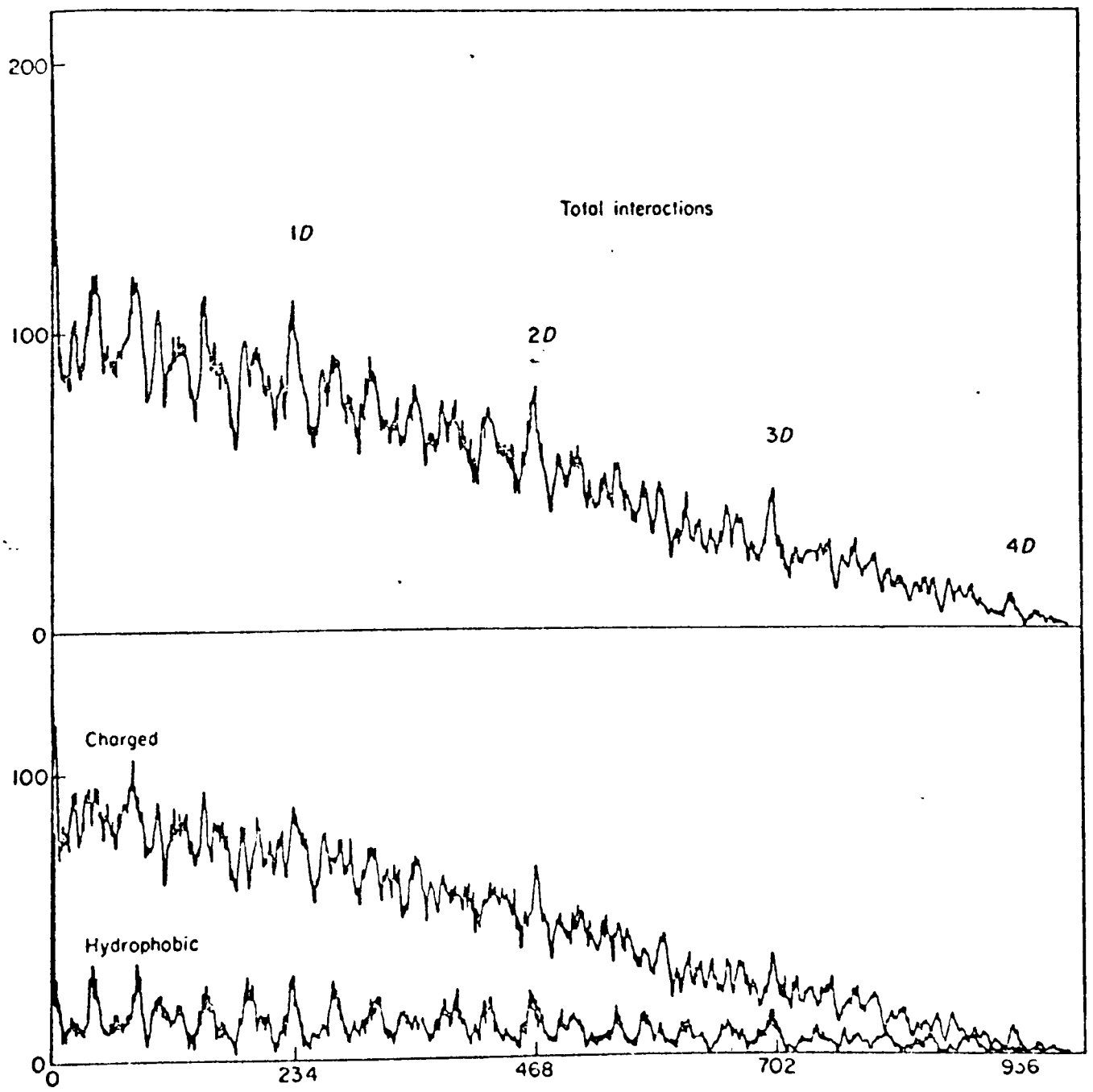

Fig.III.5 A computer plot of the number of hydrophobic and charge interactions and their total between two collagen molecules (on the ordinate) as a function of the stagger between them. The stagger (on the abscissa) is measured in residues. The D intervals are marked. (From Hulmes et al. 1973)

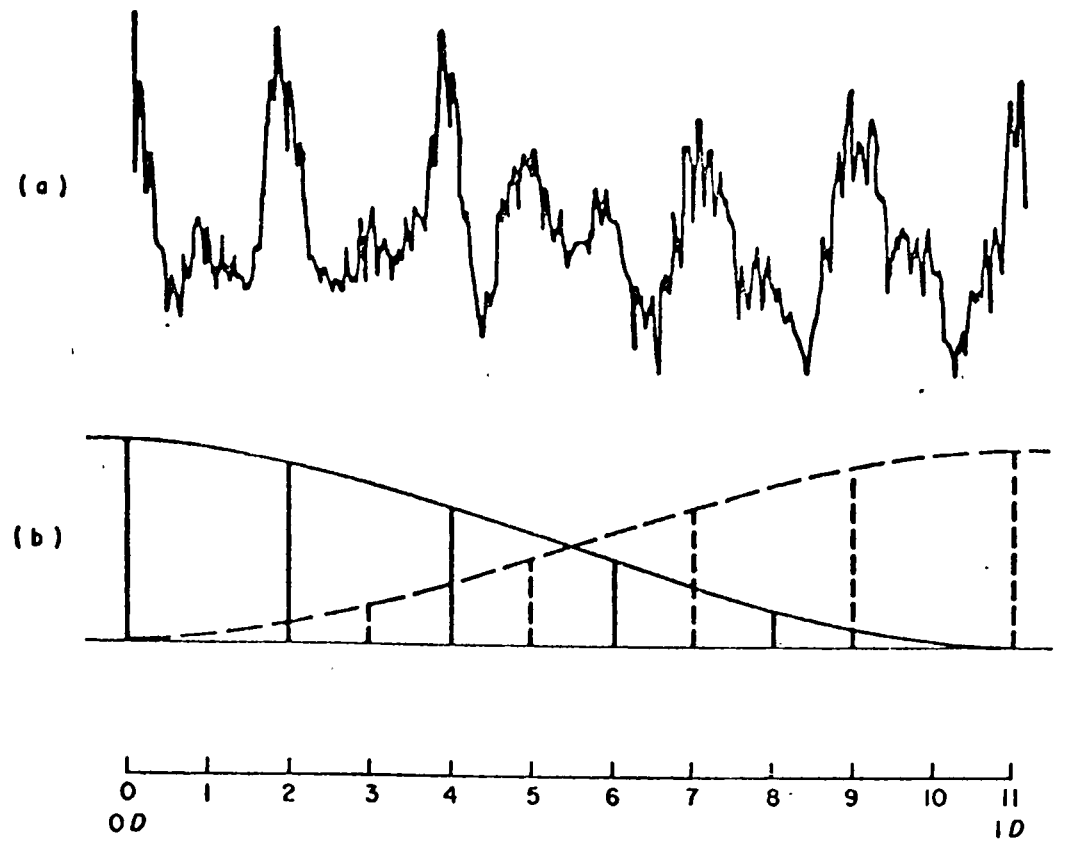

Fig. III.6(a) An enlarged portion (0-234 residues) of the hydrophobic interaction curve in Fig. 4 (b) An idealised representation of the curve showing the pattern of which it is composed. (From Hulmes et al, 1973)

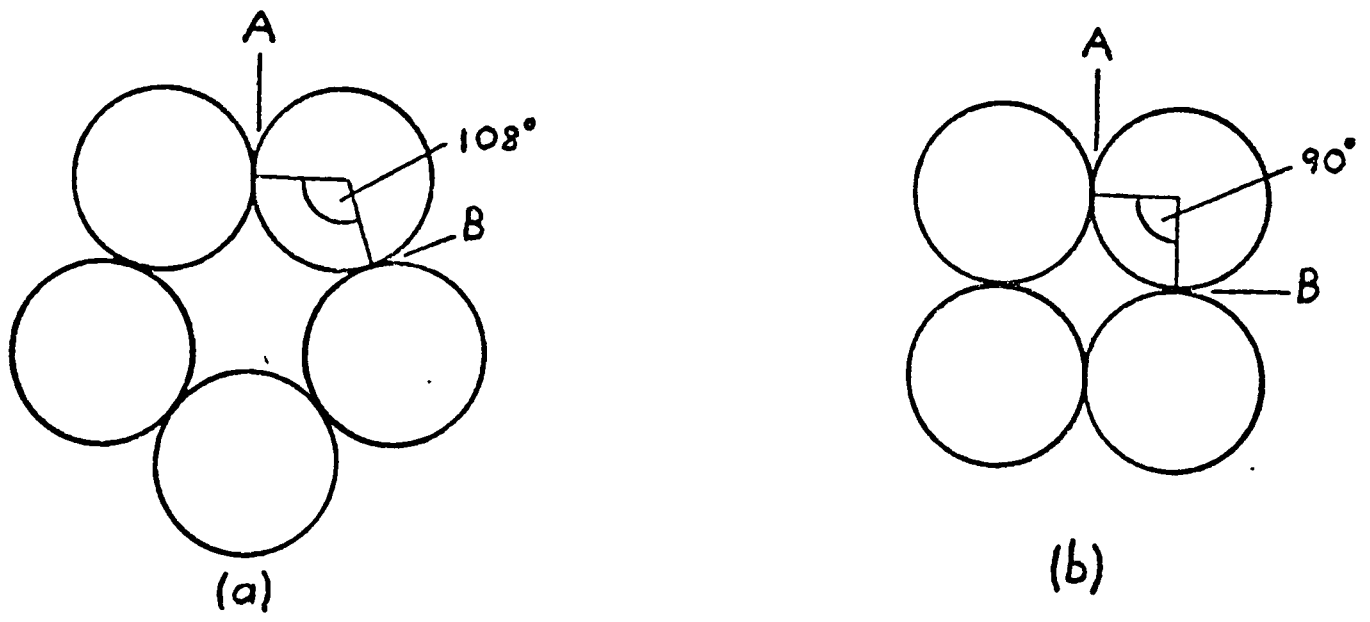

Fig. III.7(a) An illustration of how interactions between coiled structures packed pentagonally are separated by $nP \pm \frac{108}{360} P = nP \pm \frac{3}{10} P$ where P is the pitch, measured axially. Each circle represents the three stranded collagen molecule. Interactions take place at A and B. (b) shows how a four stranded unit leads to a separation of $nP \pm \frac{90}{360} P = nP \pm \frac{1}{4} P$.

APPENDIX IV

Studies on Synthetic Polypeptides

Attempts were made to produce oriented films and fibres of two synthetic sequential polyheptapeptides synthesised by Cowell and Jones (1972). The sequences were

$(Leu\text{-}Glu\text{-}Lys\text{-}Ala\text{-}Glu\text{-}Ser\text{-}Gly)_n$ I

and

$(Leu\text{-}Glu\text{-}Lys\text{-}Ala\text{-}Glu\text{-}Ala\text{-}Gly)_n$ II

These sequences are of the form $(H\text{-}X\text{-}X\text{-}H\text{-}X\text{-}X\text{-}X)_n$ where H is a hydrophobic residue. This form was suggested by Crick (1953b) as a possible basis for an α-helical coiled coil structure.

Great effort failed to produce oriented arrangements of these molecules. Fibres could not be drawn and films could not be stroked from solutions of the polypeptides in many common laboratory reagents, including chloroform, acetone, benzene, dimethyl formamide, water, formic acid and acetic acid. The protein was rather insoluble in all but strong solutions of the acids, so no viscous solutions or gels were produced.

Later chemical work indicated α-helix contents of 40% for for polymer (I) and 20% for polymer (II) (Cowell and Jones, 1972), which explains why orientation was not achieved. For ease of orientation, the protein needs a high axial ratio and therefore a high molecular weight. The number and weight average molecular weights were 6,000 and 11,000 respectively for polymer (I), and 3,000 and 6,000 respectively for polymer (II), (Cowell and Jones, 1972), which are very low values.

In the case of (I), which has contiguous serine and glycine residues, the low α-helix content could be attributed to these residues not favouring α-helix formation (Goldsack, 1969). More likely, the molecular weights were too low. A study on $(Tyr\text{-}Ala\text{-}Glu)_n$ found that the critical molecular weight for the onset of α-helix formation was about 5,000 (Schechter et al, 1971)

The only X-ray diffraction pattern obtained was the powder pattern of (I) shown in plate IV.1. Measurements to the centres of the broad rings gave spacings of 10.9Å and 21.1Å . Perhaps a small proportion of the material formed order regions. An α-helical structure with an axial repeat of 14 residues could produce rings at 21Å and 10.5Å. The lateral spacing between α-helices could result in a 10.5 Å ring or even a 21Å ring if alternate α-helices were arranged differently.

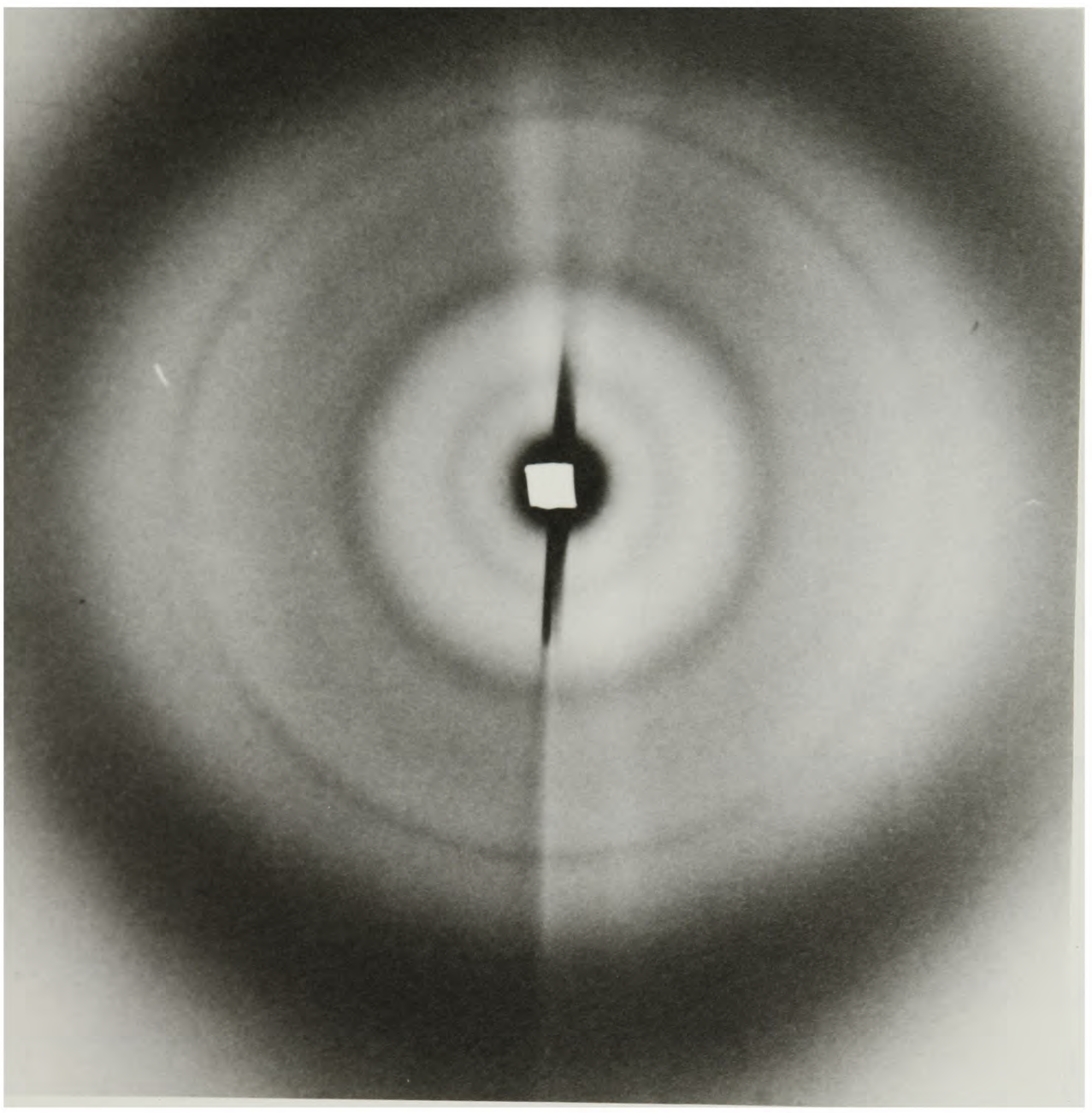

Plate IV. 1 X-ray diffraction pattern from a powder of the synthetic sequential polyheptapeptide, (Leu-Glu-Lys-Ala-Glu-Ser-Gly)

APPENDIX V

The Praying Mantis

A colony of *Sphodromantis membramacea* was raised from an egg case sent by Dr. W. Kenchington. This replaced a colony of *S.tenuidentata* which had been kept earlier. An adult female *S.membramacea* is shown in plate 5.1, together with egg cases. Plate 5.2 shows egg cases of both *S.tenuidentata* and *S. membramacea*.

By keeping the insects in a large cage with many resting places and giving them a surplus of food, cannibalism was not too serious. Young insects were fed on drosophila, but, as they grew, they were given flies and cockroaches. They grew faster at 24^{o}C than at room temperatures.

Collection of fresh egg cases was made easier by reversing the hours of light and darkness, since they much more often produced egg cases at night. A tendency for several insects to produce at the same time was observed, but this was not examined for statistical significance.

An interesting observation was that a newly hatched insect could recognise, catch and eat drosophila without parental assistance. This observation opens up questions on developmental neurobiology and the genetic transferance of knowledge.

APPENDIX VI

Origins and Implications of the D Stagger in Collagen

This appendix concerns a paper by Doyle et al.(1974) currently in press. It is based on a criticism of the interpretation of the importance of pairs of opposite charges given by Hulmes et al. (1973). (See section III.4.3).

The required interaction curves were suggested and colleagues calculated them using the methods of section III.4.3. The results indicated that the paired charges did lead to interactions favouring the D stagger in collagen.

The origins of the D periodicity in the interaction curve have interesting implications for evolution. A colleague investigated whether a D or 2D periodicity in the sequence could have resulted from gene duplication. No evidence for this was found.

The arguments are presented in the paper which continues the appendix.

ORIGINS AND IMPLICATIONS OF THE D STAGGER IN COLLAGEN

Barbara B. Doyle, David W.L. Hukins, David J.S. Hulmes,
Andrew Miller, Christopher J. Rattew[1] and John Woodhead-Galloway

Laboratory of Molecular Biophysics
Department of Zoology
South Parks Road, Oxford OX1 3PS

Summary Although the distribution of hydrophobic residues in the α1 chain collagen sequence has a D ≈ 670 Å periodicity, it is dipoles formed by 100 residues occurring in pairs of unlike charge which are responsible for the 1D stagger between molecules. Sheet models based on the Hodge-Petruska model for the axially projected collagen structure require interactions specifying 1D and 4D staggers. We found no evidence for interactions specifying a strong 4D stagger and, therefore, favour the Smith microfibril model which is specified by 1D stagger interactions alone. Two hydroxylysine residues, 234 residues apart, may form a covalent cross-link stabilising the 1D stagger. Gene duplication does not appear to be responsible for the periodicity in the sequence.

Introduction The D ≈ 670 Å periodicity of collagen fibres is caused by parallel molecules of length 4.4D having an axial translation, or stagger, of nD with respect to each other, where n is an integer (1). It has been shown (2) that the distribution of charged and large hydrophobic residues in the triple-helical region, for the available α1 chain sequence, is responsible for favourable interactions at 0D, 1D, 2D, 3D and 4D staggers, where D = 234 ± 1 residue translations.[2] We shall show that the 1D stagger is specified by charged residues occurring close together in the sequence in pairs of opposite charge. Consideration of possible covalent cross-links, subsequently formed between molecules,

---

1. Present address: Department of Biophysics, University of London King's College, 26-29 Drury Lane, London WC2B 5RL.

2. Comparison of observed and computer generated electron micrographs yielded D = 232 ± 0.5 residue translations (3). Walton (4,5) obtained D = 233 ± 1 by methods similar to those of refs. 2 and 3. X-ray diffraction suggests D = 234 ± 2 (6).

provides further evidence for a 1D stagger between adjacent molecules. The 1D stagger has important implications for the formation of a collagen microfibril (7). Surprisingly we shall show that the pseudo D period in the sequence, which determines this 1D stagger (8), is not a result of gene duplication.

Hydrophobic interactions Hydrophobic residues alone lead to favourable interactions for integral staggers of D with, of course, the maximum possible number of hydrophobic interactions occurring at 0D (2) (see fig. 1a). For anti-parallel molecules, however, the most stable interactions do not occur at integral D staggers (9).

Electrostatic interactions In general any distribution of charged residues would tend to destabilise a 0D stagger, which would maximise repulsions between like charges, but would not necessarily stabilise any D stagger. We have examined the sequence to see if any particular aspect of its distribution of charged residues would favour an integral D stagger.

The triple-helical region of the α1 chain sequence (2) contains 87 positively and 73 negatively charged residues. Of these 100 occur in pairs so that a positively and a negatively charged residue are separated by $\leqslant 2$ uncharged residues (Table 1), as has been mentioned previously (2). The remaining 60 unpaired charges are implicated in the formation of fibrous long spacing (FLS) collagen (9) but they do not specify a D periodicity.

Fig.2 shows that the most stable interaction between parallel molecules, when only the paired charge residues are considered, occurs for molecules staggered by 1D. We may consider the paired charged residues to form dipoles and fig.1b shows that this idea aids our understanding of how paired charges specify a 1D stagger.

Pairs of residues of opposite charge were previously unsuspected of having any special importance for the interactions of collagen, or any other protein, molecules and may prove to be of more general importance.

Cross-links After the triple helical collagen molecules have assembled into a fibril,under the influence of hydrophobic and electrostatic interactions, the fibril is stabilised by the formation of covalent cross-links involving lysine and hydroxylysíne (10).
Two of the four hydroxylysine residues in the sequence (at positions 681 and 915) are 234 residues apart, suggesting that their function is to form cross-links which stabilise the 1D stagger between adjacent molecules. Furthermore 4 of the 32 lysine residues occur in pairs 234 residues apart, while 10 occur in pairs which are 234 $\pm$ 3 residues apart.

Implications for Smith's microfibril If adjacent molecules in the most general axially projected collagen fibril model, with parallel molecules related by staggers of nD (1), are related by a 1D stagger then the familiar Hodge-Petruska model is produced (11, 12).
We have found the source, in the α1 chain sequence, of interactions leading specifically to a 1D stagger and have identified residues which might form a cross-link stabilising this stagger. Therefore we prefer the Hodge-Petruska model to the other schemes, in which adjacent molecules would be related by other specific nD staggers. (see ref. 6).

The Hodge-Petruska, or indeed any other, model for the axially projected structure of the collagen fibril does not directly lead to a three-dimensional model. Staggered molecules could form sheets but Smith (7) suggested that a sheet with a width of five molecules was

rolled into a cylinder (fig. 3). Evidence for (but not proof of) this cylinder, or microfibril, was provided by X-ray diffraction (13) and electron microscopy (6, 14, 15). Further evidence is provided by the results described here.

A simple sheet model like that of fig.3 requires two kinds of interactions for its integrity: one kind specifies a 1D stagger while the other specifies a 4D stagger. (Other sheet models also require at least two kinds of interactions). Although we have found the source of a strong 1D stagger we have found no such evidence for a comparably strong 4D stagger. However if this sheet is rolled into a cylinder the molecules become sub-units on a five-fold helix which can be specified solely by one interaction between successive residues: the 1D stagger. Once the microfibril has assembled the resulting 4D stagger may be stabilised by specific cross-links but only the interactions responsible for the 1D stagger are necessary for self-assembly.

Genetic implications We have investigated how a collagen molecule with the D periodic interactions, which we have observed, could have evolved. At first sight the obvious mechanism would be by successive duplication of a gene corresponding to a length D of sequence. We investigated this possibility by translating the sequence past itself, one residue at a time, counting the number of homologies; thus we did not allow for the possibility of deletions since we were searching for the source of an exact periodicity produced by duplication of an entire D segment with glycine as every third residue (see ref. 16). At no position, other of course than OD, did the number of identical residues exceed 15% (if gene duplication were responsible we might expect

about 50% homology - ref. 17). Furthermore when amino acids related by a single base change in their codons were considered to be homologous, this value did not exceed 30%. We conclude that there is no evidence in the sequence for the D periodicity being caused primarily by gene duplication.[3]

Upon further consideration we can see that gene duplication is unlikely to be responsible for a 1D periodicity because the 1D stagger is specified by interactions between unlike charged residues. Gene duplication, although ideal for specifying the distribution of hydrophobic residues, would not produce oppositely charged residues at corresponding positions in consecutive D periods. Once the observed periodicity was established in a 2D length it is conceivable that the periodicity of the entire sequence could have been achieved by gene duplication. However, we found no evidence for this possibility and can only conclude that whatever mechanism is responsible for the 1D periodicity, within a 2D period, is probably responsible for the periodicity of the entire sequence.

In conclusion we are beginning to understand how the collagen sequence is responsible for the self-assembly of molecules into fibrils but not how this periodic sequence evolved.

---

3. Similar conclusions were reached by C.J. MacLean and K.A.Piez (2).

Acknowledgements This work is part of the programme of the Medical Research Council Research Group in Molecular Biophysics, University of Oxford. B.B.D. is a Helen May Whitney Fellow and J. W.-G. is supported by the Arthritis and Rheumatism Council.

References

1. Cox, R.W., Grant, R.A. and Horne, R.W. (1967) J.Roy.Microscop. Soc. 87, 123-142.
2. Hulmes, D.J.S., Miller, A., Parry, D.A.D., Piez, K.A. and Woodhead-Galloway, J. (1973) J.Mol.Biol. 79, 137-148.
3. Chapman, J.A. and Hardcastle, R.A. (1974) Connective Tissue Res. in press.
4. Walton, A.G. (1973) in "Preprints of the Vth Annual Biomaterials Symposium", Hulbert, S.F. (ed.), Section 7, p.1, Clemson University, South Carolina.
5. Walton, A.G. (1974) J.Biomed.Matls.Res. in press.
6. Doyle, B.B., Hulmes, D.J.S., Miller, A., Parry D.A.D., Piez, K.A. and Woodhead-Galloway, J. (1974) Proc.Roy.Soc.Lond. Ser.B., 186, 67-74.
7. Smith, J.W. (1968) Nature, 219, 157-158.
8. Doyle, B.B., Hulmes, D.J.S., Miller, A., Parry, D.A.D., Piez, K.A. and Woodhead-Galloway, J. (1974) Proc.Roy.Soc.Lond.Ser.B., in press.
9. Doyle, B.B., Hukins, D.W.L., Hulmes, D.J.S., Miller, A. and Woodhead-Galloway, J. (1974) J.Mol.Biol. submitted for publication.
10. Tanzer, M.L. (1973) Science, 180, 561-566.
11. Schmitt, F.O., Gross, J. and Highberger, J.H. (1955) Exp. Cell Res.Suppl. 3, 326-334.
12. Hodge, A.J. and Petruska, J.A. (1963) in "Aspects of Protein Structure" Ramachandran, G.N. (ed.), pp.289-300, Academic Press, New York.
13. Miller, A. and Wray, J.S. (1971) Nature, 230, 437-439.
14. Smith, J.W. and Frame, J. (1969) J.Cell Sci. 4, 421-436.
15. Bouteille, M. and Pease, D.C. (1971) J.Ultrastructure Res. 35 314-338.
16. Needleman, S.B. and Wunsch, C.D. (1970) J.Mol.Biol. 48, 443-453.
17. Yudkin, M.and Offord, R. (1973) "Comprehensible Biochemistry", pp. 467-470, Longman, London.

Table 1 Positions of paired charged residues classified according to the direction of the resulting dipole

1. Dipoles pointing towards C terminus

Arg-Asp	144-146	567-569	845-846	989-992	
Arg-Glu	183-186	192-194	294-296	729-731	737-740
	833-834	855-857	885-887		
Lys-Asp	50-53	264-266	434-435	531-533	564-566
	573-576	581-582	654-656	852-854	881-884
	971-972				
Lys-Glu	108-110	174-176	270-272	645-647	722-723

2. Dipoles pointing towards N terminus

Asp-Arg	384-386	620-621			
Glu-Arg	131-132	308-309	332-333	347-350	419-420
	452-453	500-501	506-507	554-555	788-789
	812-813				
Asp-Lys	96-99	372-374	602-603		
Glu-Lys	56-59	288-290	413-416	476-479	752-753
	800-803				

Figure Captions

Fig. 1 Schematic diagram showing how (a) hydrophobic residues and (b) dipoles can specify D staggers. Any apparently random, but asymmetric, distribution of hydrophobic residues (crosses) which was, at least roughly, repeated in every D period would lead to a D periodicity in the interactions of parallel, but not anti-parallel, molecules. Pairing of unlike charged residues to form dipoles (arrows) can stabilise 1D and 3D staggers if the dipoles point in opposite directions in successive D periods, since parallel dipoles have a destabilising influence while anti-parallel dipoles contribute to stability. In practice, no peak corresponding to a 3D stagger appears above the noise level of fig.2. This figure does not show the actual distribution of hydrophobic residues or dipoles.

Fig.2 Interactions between dipoles on two parallel molecules as a function of the stagger between them. Dipoles consist of unlike charged residues separated by less than three residues. Anti-parallel dipoles within a range of $\pm$ 3 residues, score +1; parallel dipoles score -1. The ordinate is the total score and the abscissa is measured in residues. The 1D peak has a height corresponding to 11 stabilising dipole-dipole interactions: since the minimum number of dipoles pointing in either direction is 22 this represents 50% of the maximum possible stability.

Fig.3 Hodge-Petruska model for the axially projected collagen structure. A sheet model based on this structure requires two kinds of interactions between molecules: one kind (between molecules like P and Q) leads to a 1D stagger, while the other (between molecules like P and R) leads to a 4D stagger.

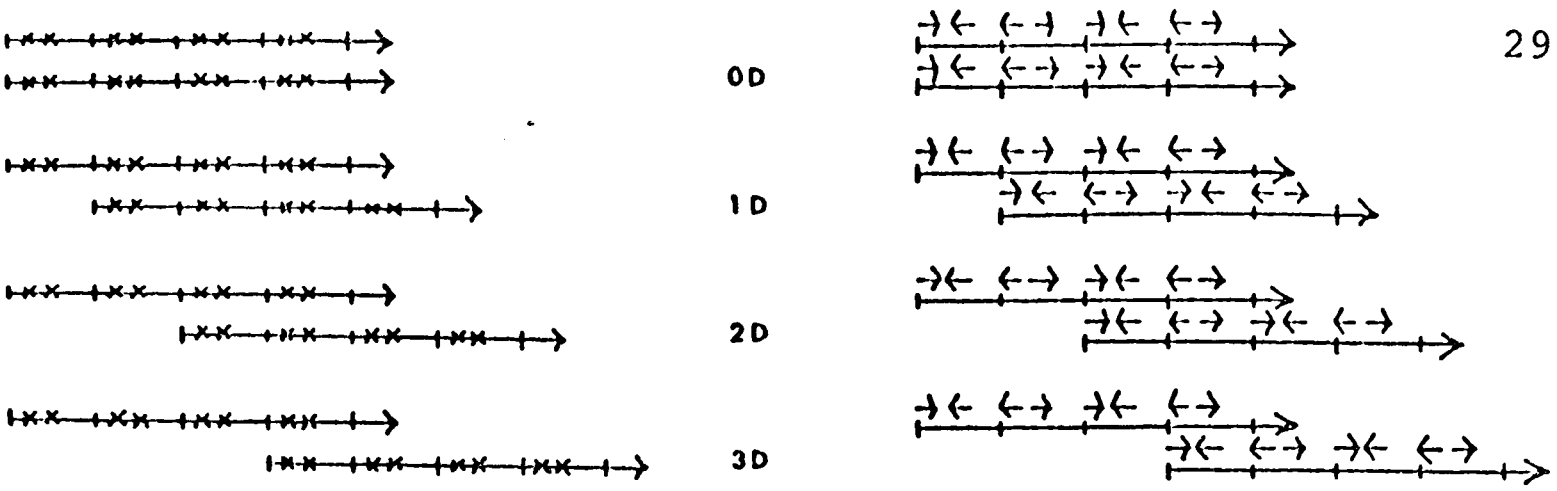

a HYDROPHOBIC

b DIPOLES

FIG.1

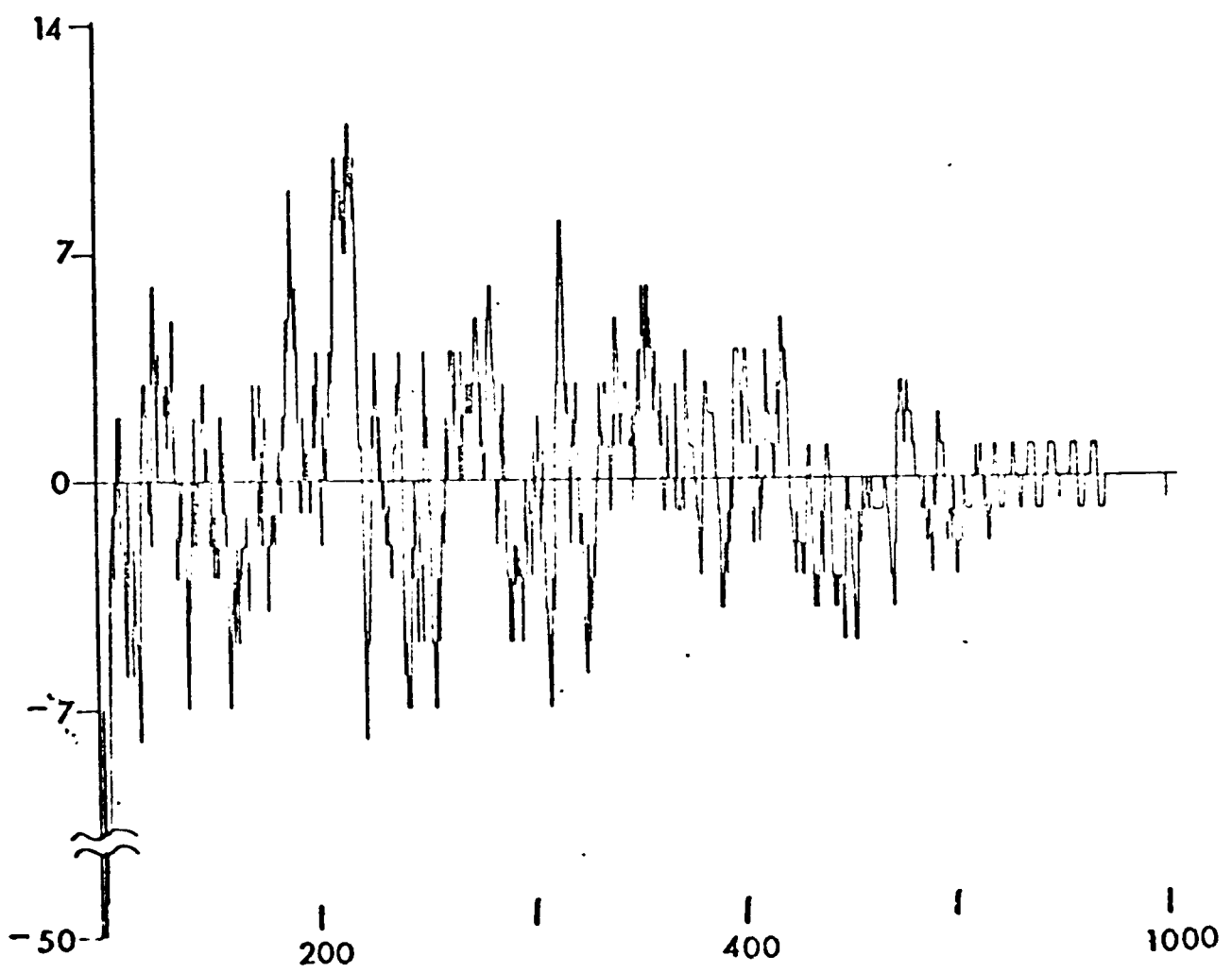

FIG.2

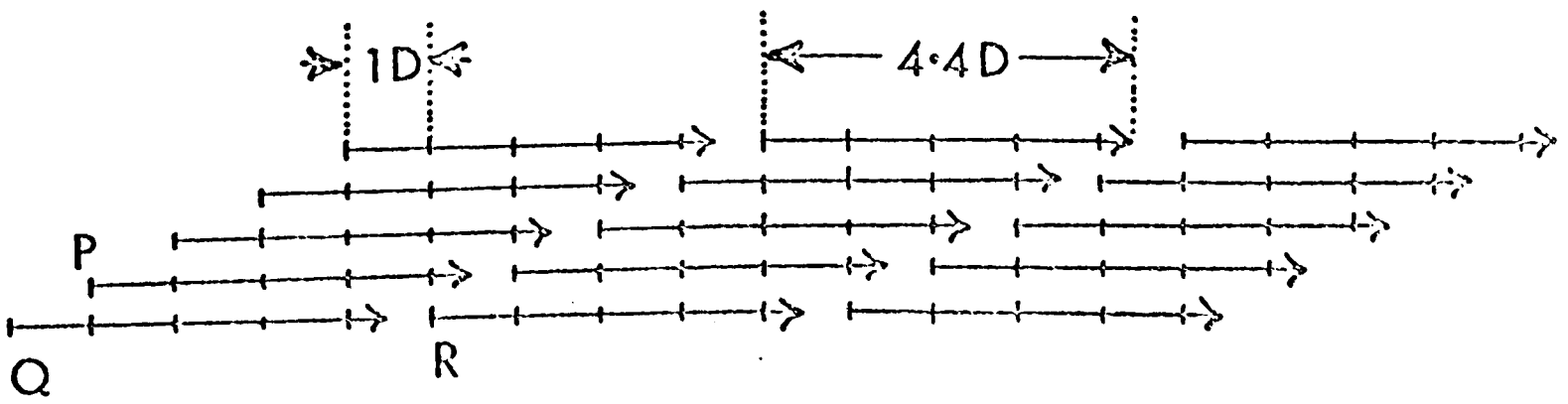

FIG. 3

REFERENCES

ARNOTT, S. (1968). In "Symposium on Fibrous Proteins, Australia 1967" (W.G. Crewther, ed.), p 26. Butterworths, London.

ARNOTT, S., and WONACOTT, A. J. (1966a). Polymer 7, 157.

ARNOTT, S., and WONACOTT, A. J. (1966b). J. Mol.Biol. 21, 371.

ARNOTT, S., and DOVER, S.D. (1967). J. Mol.Biol. 30, 209.

ASTBURY, W. T. (1947). Proc. Roy. Soc. Ser. B 134, 303.

ASTBURY, W. T., REED, R., and SPARK, L. C. (1948). Biochem. J. 43, 282.

ATKINS, E. D. T. (1967). J. Mol. Biol. 24, 139.

BACON, G. E., and LOWDE R. D. (1948). Acta Crystallogr. 1, 303.

BAILEY, K. (1948). Biochem. J. 43, 271.

BAMFORD, C. H., HANBY, W. E., and HAPPEY, F. (1951). Proc. Roy. Soc. Ser A 205, 30.

BEAR, R. S., and SELBY, C. C. (1956). J. Biophys. Biochem. Cytol. 2,55.

BLEANEY, B. I., and BLEANEY, B. (1965). "Electricity and Magnetism", ch 10. Oxford Univ. Press, Oxford.

BROWN, L., and TROTTER, I.F. (1956). Trans. Faraday Soc. 52, 537.

BRUNET, P. C. J., and KENT, P. W. (1955). Proc. Roy. Soc. Ser. B 144, 259.

BURNSTOCK, G. (1970). In "Smooth Muscle" (E. Bülbring, A. F. Brading, A. W. Jones, and T. Tomita, eds.), p. 1. Arnold, London.

CASPAR, D.L.D., COHEN, C., and LONGLEY, W. (1967). J.Mol.Biol. 41, 87.

COCHRAN, W., CRICK, F. H. C., and VAND, V. (1952). Acta Crystallogr. 5, 581.

COHEN, C. (1966). In "Principles of Biomolecular Organisation" (G. E. W. Wolstenholme and M. O'Conner, eds.), p. 101, Churchill, London.

COHEN, C. and SZENT-GYÖRGYI, A. G. (1957). J. Amer. Chem. Soc. 79, 248.

COHEN, C., and SZENT-GYÖRGYI, A. G. (1960). Int. Congr. Biochem. 4th. 8, 108. Pergamon, Oxford.

COHEN, C., and HOLMES, K. C. (1963). J. Mol. Biol. 6, 423.

COHEN, C., SZENT-GYÖRGYI, A. G., and KENDRICK-JONES, J. (1971a). J. Mol. Biol. 56, 223.

COHEN, C., CASPAR, D. L. D., PARRY, D. A. D., and LUCAS, R. M. (1971b). Sympos. Quant. Biol. 36, 205.

COMPTON, A. H. (1923). Phil. Mag. 45, 1121.

COMPTON, A. H., and ALLISON, S. K. (1935). "X-rays in Theory and Experiment", p. 745. Van Nostrand, New York.

COOKE, P. H., and FAY, F. S. (1972). Exp. Cell Res. 71, 265.

CORFIELD, M. C., FLETCHER, J. C., ROBSON, A. (1968). In "Symposium on Fibrous Proteins, Australia 1967 "W. G. Crewther, ed.), p. 289. Butterworths, London.

COWELL, R. D., and JONES, J. H. (1972). J. Chem. Soc. (C), 1814.

CREWTHER, W. G., DOBB, M. G., DOWLING, L. M., and HARRAP, B. S. (1968). In "Symposium on Fibrous Proteins, Australia 1967"(W.G. Crewther ed.), p. 329. Butterworths, London.

CREWTHER, W. G., and DOWLING, L. M. (1971). Appl. Polym. Symp. No. 18, 1.

CRICK, F. H. C. (1952). Nature (London) 170, 882.

CRICK, F. H. C. (1953a). Acta Crystallogr. 6, 685.

CRICK, F. H. C. (1953b). Acta Crystallogr. 6, 689.

DARWIN, C. G. (1914). Phil. Mag. 27, 315 and 675.

DEPUE, R. H. and RICE, R. V. (1965). J. Mol. Biol. 12, 302.

de WOLFF, P. M. (1950). Appl. Sci. Res., B1, p. 119.

DICKERSON, R. E. (1964). In "The Proteins" (H. Neurath, ed.), Vol. II, p. 603. Academic Press, New York.

DICKERSON, R. E., and GEIS , I. (1969). "The Structure and Action of Proteins". Harper and Row, New York.

DOYLE, B. B., HUKINS, D. W. L., HULMES, D. J. S., MILLER, A., RATTEW-, C.J., and WOODHEAD-GALLOWAY, J. (1974). Biochem. Biophys. Res. Commun.

EHRENBERG, W. (1949). J. Opt. Soc. Amer. 39, 746.

ELLIOTT, A. (1967). In "Poly-d-Amino Acids" (G. D. Fasman ed.), p. 1. Dekker, New York.

ELLIOTT, A. (1971). Phil. Trans. Roy. Soc. London Ser. B 261, 197.

ELLIOTT, A., and MALCOLM, B. R. (1958). Proc. Roy. Soc. Ser. A 249, 30.

ELLIOTT, A., LOWY, J., PARRY, D. A. D., and VIBERT, P. J. (1968). Nature (London) 218, 656.

ELLIOTT, A., and LOWY, J. (1970). J. Mol. Biol. 53, 181.

ELLIOTT, G. F. (1963). Acta Crystallogr. 16, A 81.

ELLIOTT, G. F. (1964). J. Mol. Biol. 10, 89.

FASMAN, G. D. (1967). "Poly-α-Amino Acids". Dekker, New York.

FEYNMAN, R. P., LEIGHTON, R. B., and SANDS, M. (1964). "The Feynman Lectures on Physics", Vol. II, ch. 38. Addison Wesley, Reading Massachusetts.

FILSHIE, B. K., and ROGERS, G. E. (1961). J. Mol. Biol. 3, 784.

FINKELSTEIN, A. V., and PTITSYN, O.B. (1971). J. Mol. Biol. 62, 613.

FLOWER, N. E., and KENCHINGTON, W. (1967). J. Roy. Microscop. Soc. 86, 297.

FLOWER, N. E., GEDDES, A. J., and RUDALL, K. M. (1969). J. Ult. Res. 26, 262.

FOURNET, G. (1951). Thèse Université de Paris. (Reference quoted by Witz, 1969).

FRANKS, A. (1955). Proc. Phys. Soc. B 68, 1054.

FRANKS, A. (1958). Br. J. Appl. Phys. 9, 349.

FRANKS, A. (1973). Physics Bulletin, 24, 426.

FRASER, R. D. B., MACRAE, T. P., and MILLER, A. (1964). J. Mol. Biol. 10, 147.

FRASER, R. D. B., MACRAE, T. P., and MILLER, A. (1965). J. Mol. Biol. 14, 432.

FRASER, R. D. B., MACRAE, T. P., PARRY, D. A. D., and SUZUKI, E. (1971). Polymer 12, 35.

FRASER, R. D. B., MACRAE, T. P., and ROGERS, G. E. (1972). "Keratins - Their Composition, Structure and Biosynthesis". Thomas, Springfield, Illinois.

FRASER, R. D. B., and MACRAE, T. P. (1973a). "Conformation in Fibrous Proteins". Academic Press, New York.

FRASER, R. D. B., and MACRAE, T. P. (1973b). Polymer 14, 61.

GEDDES, A. J., PARKER, K. D., ATKINS, E. D. T., and BEIGHTON, E. (1968). J. Mol. Biol. 32, 343.

GOLDSACK, D. E. (1969). Biopolymers 7, 299.

GUINIER, A. (1946). Comptes Rendus Acad. Sci. (Paris) 223, 31.

GUINIER, A. (1963). "X-Ray Diffraction". W. H. Freeman and Co., San Francisco.

GUINIER, A., FOURNET, G., WALKER, C. B., and YUDOWITCH, K. L. (1955). "Small Angle Scattering of X-Rays". Chapman and Hall, London.

HALL, C. E., JAKUS, M. A., and SCHMITT, F. O. (1945). J. Appl. Phys. 16, 459.

HANSON, J., and LOWY, J. (1963). J. Mol. Biol. 6, 46.

HANSON, J., and LOWY, J. (1964a). In "Biochemistry of Muscle Contraction" (J. Gergely, ed.), p. 141. Little, Brown, Boston, Massachusetts.

HANSON, J., and LOWY, J. (1964b). In "Biochemistry of Muscle Contraction" (J. Gergely, ed.), p. 400. Little, Brown, Boston, Massachusetts.

HANSON, J., O'BRIEN, E. J., and BENNETT, P. M. (1971). J. Mol. Biol. 58, 865.

HAPPEY, F. (1950). Nature (London), 166, 396.

HARRISON, R. G., LOWEY, S., and COHEN, C. (1971). J. Mol. Biol. 59, 531.

HODGES, R. S., and SMILLIE, L. B. (1970). Biochem. Biophys. Res. Commun. 41, 987.

HODGES, R. S., and SMILLIE, L. B. (1972a). Can. J. Biochem. 50, 312.

HODGES, R. S., and SMILLIE, L. B. (1972b). Can. J. Biochem. 50, 330.

HODGES, R. S., SODER, J., SMILLIE, L. B., and JURASEK, L. (1973). Sympos. Quant. Biol. 37, 299.

HOLMES, K. C., and BLOW D. M. (1965). In "Methods of Biochemical Analysis" (D. Glick, ed.), Vol. 13, p. 113. Wiley (Interscience), New York.

HOLTZER, A., LOWEY, S., and SCHUSTER, T. M. (1962). In "Symposium on the Molecular Basis of Neoplasia." (R. W. Cumley, et al., eds.), p. 259. University of Texas Press, Austin, Texas.

HOLTZER, A., CLARK, R., and LOWEY, S. (1965). Biochemistry 4, 2401.

HOSKEN, R., MOSS, B. A., O'DONNELL, I. J., and THOMPSON, E. O. P. (1968). Aust. J. Biol. Sci. 21, 593.

HUGGINS, M. L. (1952). J. Amer. Chem. Soc. 74, 3963.

HULMES, D. J. S., MILLER, A., PARRY, D. A. D., PIEZ, K. A., WOODHEAD-GALLOWAY, J. (1973). J. Mol. Biol. 79, 137.

HUSZAR, G., and ELZINGER, M. (1971). Biochemistry 10, 229.

HUXLEY, H. E. (1963). J. Mol. Biol. 7, 281.

HUXLEY, H. E. (1971). Proc. Roy. Soc. Ser. B 178, 131.

HUXLEY, H. E., and BROWN, W. (1967). J. Mol. Biol. 30, 383.

JAMES, R. W. (1948). "The Optical Principles of the Diffraction of X-Rays". Bell, London.

JEFFREY, P. D. (1972). J. Textile Inst. 63, 91.

JOHANN, H. H. (1931). Z. Phys. 69, 185.

JOHANSSON, T. (1933). Z. Phys. 82, 507.

KENCHINGTON, W., and FLOWER, N. E. (1969). J. Microsc. 89, 263.

KENDREW, J. C. (1962). Brookhaven Symp. Biol. 15, 216.

KENDREW, J. C., DICKERSON, R. E., STRANDBERG, B. E., HART, R. G., DAVIES, D. R., PHILLIPS, D. C., and SHORE, V. C. (1960). Nature (London) 185, 422.

KIESSIG, H. (1931). Ann. Phys. Lpz. 10, 715 and 769.

KING, M. V., and YOUNG, M. (1972). J. Mol. Biol. 63, 539.

KLUG, A., CRICK, F. H. C., and WYCKOFF, H. W. (1958). Acta. Crystallogr. 11, 199.

KOTELCHUCK, D., and SCHERAGA, H. A. (1968). Proc. Nat. Acad. Sci. U.S. 61, 1163.

KOTELCHUCK, D., and SCHERAGA, H. A. (1969). Proc. Nat. Acad. Sci. U.S. 62, 14.

LANG, A. R. (1956). Acta Crystallogr. 9, 436.

LANGRIDGE, R., WILSON, H. R., HOOPER, C. W., WILKINS, M. H. F., and HAMILTON, L. D. (1960). J. Mol. Biol. 2, 19.

LEWIS, P. N., GŌ, N., GŌ, M., KOTELCHUCK, D., and SCHERAGA, H.A. (1970). Proc. Nat. Acad. Sci. U.S. 65, 810.

LINDSEY, K. (1973). Quoted by Franks (1973) as being in preparation.

LOWEY, S. (1971). In "Subunits in Biological Systems". (S.N. Timasheff and G. D. Fasman, eds.), Part A, p. 201. Dekker, New York.

LOWEY, S., KUCERA, J., and HOLTZER, A. (1963). J. Mol. Biol. 7, 234.

LOWEY, S., SLAYTER, H, S., WEEDS, A. G., and BAKER, H. (1969). J. Mol. Biol. 42, 1.

LOWY, J., and SMALL, J. V. (1970). Nature (London) 227, 46.

LOWY, J., VIBERT, P. J., HASELGROVE, J. C., and POULSEN, F. R. (1973). Phil. Trans. Roy. Soc. Ser. B 265, 193.

LUCAS, F., SHAW, J. T. B., and SMITH, S. G. (1958). Advan. Protein Chem. 13, 207.

LUCAS, F., and RUDALL, K. M. (1968). In "Comprehensive Biochemistry" (M. Florkin and E. H. Stotz, eds.), Vol. 26B, 475. Elsevier, Amsterdam.

MCCUBBIN, W. D., and KAY, C. M. (1968). Biochim. Biophys. Acta. 154, 239.

MILLARD, A., and RUDALL, K. M. (1962). In "Fifth International Congress for Electron Microscopy". Academic Press, New York.

MILLER, A., and WRAY, J. S. (1971). Nature (London) 230, 437.

MILLER, A., and PARRY, D. A. D. (1973). J. Mol. Biol. 75, 441.

MOORE, P. B., HUXLEY, H. E., and DEROSIER, D. J. (1970). J. Mol. Biol. 50, 279.

NEVILLE, A. C., and LUKE, B. M. (1971). J. Cell Sci. 8, 93.

O'DONNELL, I. J. (1969). Aust. J. Biol. Sci. 22, 471.

OLANDER, J. (1971). Biochemistry 10, 601.

OLANDER, J., EMERSON, M. F., and HOLTZER, A. (1967). J. Amer. Chem. Soc. 89, 3058.

OOI, T., and FUJIME-HIGASHI, S. (1971). Advan. Biophys. 2, 113.

PARDON, J. F. (1967). Acta Crystallogr. 23, 937.

PARKER, K. D., and RUDALL, K. M. (1955). Biochem. Biophys. Acta. 17, 287.

PARRY, D. A. D. (1974). Biochem. Biophys. Res. Commun. 57, 216.

PARRY, D. A. D., and SUZUKI, E. (1969). Biopolymers 7, 189.

PARRY, D. A. D., and SQUIRE, J. M. (1973). J. Mol. Biol. 75, 33.

PAULING, L., and COREY, R. B. (1951). Proc. Nat. Acad. Sci. U.S. 37, 241.

PAULING, L., and COREY, R. B. (1953). Nature (London). 171, 59.

PEISER, M. S., ROOKSBY, H. P., WILSON, A. J. C. (1960). In "X-Ray Diffraction by Polycrystalline Materials" (H. S. Peiser, H. P. Rooksby and A. J. C. Wilson, eds.), ch. 2. Inst. of Phys., London.

PERUTZ, M. F. (1951a). Rep. Progr. Chem. 48, 361.

PERUTZ, M. F. (1951b). Nature (London) 168, 653.

PRINS, J. A. (1928). Z. Phys. 47, 479.

RAINFORD, P., and RICE, R. V. (1970). Biopolymers 9, 1.

RAMACHANDRAN, G. N. (1960). Proc. Indian Acad. Sci. A 52, 240.

RAMSDEN, W. (1938). Nature (London) 142, 1120

REEDY, M. K. (1968). J. Mol. Biol. 31, 155.

REEDY, M. K., HOLMES, K. C., TREGEAR, R. T. (1965). Nature (London) 207, 1276.

RENNINGER, M. (1956). Z. Kristallogr. 107, 464.

RICE, R. V., MCMANUS, G. M., DEVINE, C. E., and SOMLYO, A. P. (1971). Nature (London) New Biol. 231, 242.

RIDDIFORD, L. M. (1966). J. Biol. Chem. 241. 2792.

RIESER, W. M., JR. (1957). J. Opt. Soc. Amer. 47, 987.

ROGERS, G. E. (1959). Ann. N.Y. Acad. Sci. 83, 378.

ROWE, A. J. (1964). Proc. Roy. Soc. Ser. B 160, 437.

RUDALL, K. M. (1956). In "Lectures on the Scientific Basis of Medicine". Vol. 5, p. 217. British Postgraduate Med. Fed., Univ. of London.

RUDALL, K. M. (1962). In "Comparative Biochemistry". (M. Florkin and H. S. Mason, eds.), Vol. 4, p. 397. Academic Press, New York.

RUDALL, K. M. (1968). In "Treatise on Collagen" (B. S. Gould, ed), Vol. 2, Part A, p. 83. Academic Press, New York.

RUDALL, K. M., and KENCHINGTON, W. (1971). Annu. Rev. Entomol. 16, 73.

SAKISAKA, Y. (1927). Jap. J. Phys. 4, 171.

SAKISAKA, Y. (1930). Proc. Math. Phys. Soc. Japan 12, 189.

SANDSTRÖM, A. E. (1957). "Experimental Methods in X-Ray Spectroscopy". Encyclopaedia of Physics. Vol. 30, "X-Rays". (S. Flügge, ed.). Springer, Berlin.

SCHECHTER, B., SCHECHTER, J., RAMACHANDRAN, J., CONWAY-JACOBS, A., and SELA, M. (1971). European J. Biochem. 20, 301.

SEIFTER, S., and GALLOP, P.M. (1966). In "The Proteins". (H. Neurath, ed.), 2nd ed., Vol. 4, 153. Academic Press, New York.

SIMMONS, N. S., COHEN, C., SZENT-GYÖRGYI, A. G., WETLAUFER, O. B., BLOUT, E. R. (1961). J. Amer. Chem. Soc. 83, 4766.

SLAYTER, E. M. (1969). In "Physical Principles and Techniques of Protein Chemistry". (S. J. Leach, ed.), Part A, p. 1. Academic Press, New York.

SMITH, J. W. (1968). Nature (London) 219, 157.

SOMLYO, A. P., SOMLYO, A. V., DEVINE, C. E., and RICE, R. V. (1971a). Nature (London) New Biol. 231, 243.

SOMLYO, A. P., DEVINE, C. E., and SOMLYO, A. V. (1971b). Nature (London). New Biol. 233, 218.

SQUIRE, J. M. (1971). Nature (London) 233, 457.

STAY, B., and ROTH, L. M. (1962). Ann. Entomol. Soc. Amer. 55, 124.

SUGETA, H., and MIYAZAWA, T. (1967). Biopolymers 5, 673.

SZENT-GYÖRGYI, A. G., COHEN, C., and PHILPOTT, D. E. (1960). J. Mol. Biol. 2, 133.

SZENT-GYÖRGYI, A. G., COHEN, C., and KENDRICK-JONES, J. (1971). J. Mol. Biol. 56, 239.

THOMPSON, E. O. P., and O'DONNELL I. J. (1965). Aust. J. Biol. Sci. 18, 1207.

TSAO, T. C., BAILEY, K., and ADAIR, G. S. (1951). Proc. Roy. Soc. Ser. A 235, 189.

VAINSHTEIN, B. K. (1966). "Diffraction of X-rays by Chain Molecules". Elsevier, Amsterdam.

WARWICKER, J. O. (1960). J. Mol. Biol. 2, 350.

WEBER, K., and OSBORN, M. (1969). J. Biol. Chem. 244, 4406.

WHITE, J. E. (1950). J. Appl. Phys. 21, 855.

WHITTAKER, E. J. W. (1955). Acta Crystallogr. 8, 571.

WILSDORF, H. (1951). Naturwissenschaften 38, 250.

WILSON, H. R. (1966). "Diffraction of X-rays by Proteins, Nucleic Acids and Viruses". Edward Arnold, London.

WITZ, J. (1969). Acta Crystallogr. A 25, 30.

WOODS, E. F. (1967). J. Biol. Chem. 242, 2859.

WOODS, E. F. (1969). Biochem. J. 113, 39.

WOOLFSON, M. M. (1970). "An Introduction to X-ray Crystallography". Cambridge Univ. Press, London.

YUDKIN, M., and OFFORD, R. (1971). "A Guidebook to Biochemistry". Cambridge Univ. Press, London.

YUDKIN, M., and OFFORD, R. (1973). "Comprehensible Biochemistry". Longmans, London.